MIXED OLEIC ACID STEALTH LIPOSOMES FOR ANTICANCER DRUGS DELIVERY

VICIT RIZAL EH SUK

FACULTY OF SCIENCE
UNIVERSITY OF MALAYA
KUALA LUMPUR

2018

MIXED OLEIC ACID STEALTH LIPOSOMES FOR ANTICANCER DRUGS DELIVERY

VICIT RIZAL EH SUK

THESIS SUBMITTED IN FULFILMENT OF THE REQUIREMENTS FOR THE DEGREE OF DOCTOR OF PHILOSOPHY

DEPARTMENT OF CHEMISTRY
FACULTY OF SCIENCE
UNIVERSITY OF MALAYA
KUALA LUMPUR

2018

UNIVERSITY OF MALAYA
ORIGINAL LITERARY WORK DECLARATION

Name of Candidate: **VICIT RIZAL EH SUK**

Matric No: **SHC120021**

Name of Degree: **DOCTOR OF PHILOSOPHY**

Title of Project Paper/Research Report/Dissertation/Thesis ("this Work"):

MIXED OLEIC ACID STEALTH LIPOSOMES FOR ANTICANCER DRUGS DELIVERY

Field of Study: **COLLOID CHEMISTRY**

I do solemnly and sincerely declare that:

(1) I am the sole author/writer of this Work;
(2) This Work is original;
(3) Any use of any work in which copyright exists was done by way of fair dealing and for permitted purposes and any excerpt or extract from, or reference to or reproduction of any copyright work has been disclosed expressly and sufficiently and the title of the Work and its authorship have been acknowledged in this Work;
(4) I do not have any actual knowledge nor do I ought reasonably to know that the making of this work constitutes an infringement of any copyright work;
(5) I hereby assign all and every rights in the copyright to this Work to the University of Malaya ("UM"), who henceforth shall be owner of the copyright in this Work and that any reproduction or use in any form or by any means whatsoever is prohibited without the written consent of UM having been first had and obtained;
(6) I am fully aware that if in the course of making this Work I have infringed any copyright whether intentionally or otherwise, I may be subject to legal action or any other action as may be determined by UM.

Candidate's Signature   Date:

Subscribed and solemnly declared before,

Witness's Signature   Date:

Name:

Designation:

MIXED OLEIC ACID STEALTH LIPOSOMES FOR

ANTICANCER DRUGS DELIVERY

ABSTRACT

Liposomal drug Nano carrier from phospholipids has been widely explored and proven to be the preferred formulation for liposomal chemotherapy despite their high cost. Fatty acids are the best alternative to the conventional phospholipids liposomes attributed to their amphiphilic structure, ease of preparation, economical, and easily available. However, the lack of interest among researchers in exploring fatty acid liposomes for chemotherapy could be due to their low encapsulation efficiency of active ingredients, unstable, high-clearance in the blood system, and potentially causing cell lysis. This study focused on using mixed monounsaturated C-18 fatty acid, soy lecithin, and erucic acid for liposomal anticancer Nano carrier in chemotherapy. Erucic acid, with 22 alkyl carbon chain, expected to enhance liposomes stability, reduce the size, and increase encapsulation efficiency of active ingredients. The incorporation of the strongly proven biocompatible stealth material from PEGylated lipid, 1,2-dioleoyl-sn-glycero-3-phosphoethanolamide-N-[methoxy (polyethylene glycol)-2000 (DOPEPEG2000) improved stability and prolong the lifetime of liposomes. The pH equilibrium curves for all lipids were obtained by titrating oleic acid, soy lecithin, or erucic acid against 0.05 mol dm^{-3} hydrochloric acid to define the region where liposomes were mostly presence. Liposomes were prepared by employing the thin lipid hydration technique followed by pH adjustment to produce the desired liposome regime. The thin layer of lipid was hydrated with saline phosphate buffered (PBS) at the concentration higher than their critical vesicle concentration (CVC). The optical polarizing microscope (OPM) displayed the presence of liposomes through their unique birefringence property while the micrograph high resolution-transmission electron microscope (HR-TEM) established that the liposomes had the circular silhouette with

the size ranging from 100 to 600 nm. These findings were supported by the data obtained from the dynamic light scattering measurements with the lowest surface charge of mixed oleic acid-erucic acid liposomes around -90 mV. The encapsulation efficiency of different anticancer drugs namely folinic acid, doxorubicin, methotrexate, and irinotecan were above 60% while more than 20% of the anticancer drugs were released after 24 hours showing a slow released property which was very useful for inhibiting the proliferations of cancer cells. Fabrication of fatty acid liposomes may potentially be beneficial for manufacturing the novel biomimetic system for drug delivery vehicles.

Keywords: liposomes, oleic acid, log P, anticancer drug, *in vitro* release

LIPOSOM CAMPURAN ASID OLIK TERHINDAR BAGI PENGHANTARAN UBATAN ANTIBARAH

ABSTRAK

Liposom pembawa nano ubatan daripada fosfolipid telah diselidik secara meluas dan menjadi bahan kegemaran untuk menghasilkan liposom bagi kegunaan kemoterapi meskipun harganya yang tinggi. Asid lemak merupakan pilihan terbaik bagi menggantikan fosfolipid berikutan strukturnya yang amfifilik, memerlukan cara penyediaan yang mudah, berpatutan, dan mudah diperolehi. Walaubagaimanapun, penerokaannya untuk kegunaan kemoterapi kurang mendapat minat dikalangan para penyelidik berikutan tahap kecekapan pengkapsulan dan kestabilan yang rendah serta mudah disingkirkan di dalam sistem darah seterusnya menyebabkan lisis pada sel. Penyelidikan ini adalah bertumpukan kepada penggunaan campuran asid lemak tepu mono C-18, lesitin soya, dan asid erusik bagi menghasilkan liposom pembawa nano ubatan antibarah untuk kegunaan semasa kemoterapi. Erusik asid yang mempunyai 22 karbon alkil dirantaiannya dijangka berupaya meningkatkan kestabilan, mengurangkan saiz dan meningkatkan kecekapan pengkapsulan bahan aktif. Bahan pelindung iaitu lipid bersauh PEG seperti 1,2-dioleoil-sn-glisero-3-fosfoetanolamida-N-[metoksi (polietilena glikol)-2000 (DOPEPEG2000) telah digunakan untuk meningkatkan kestabilan dan memanjangkan jangkahayat liposom. Lengkung keseimbangan pH telah diperolehi dengan mentitrat asid olik, lesitin soya, dan asid erusik terhadap 0.05 mol dm^{-3} asid hidroklorik bagi menentukan kawasan liposom berkepadatan tinggi. Liposom disediakan dengan menggunakan kaedah penghidratan lapisan nipis lipid dan seterusnya bacaan pH daripada larutan diselaraskan ke nilai yang dikehendaki. Lapisan nipis lipid yang berkepekatan lebih tinggi daripada kepekatan genting vesikelnya (CVC) kemudian dihidrat dengan larutan penimbal fosfat bergaram (PBS). Mikroskop pengutuban optikal (OPM) digunakan untuk menentukan kehadiran

liposom melalui sifat dwibiasannya manakala mikroskop penghantaran elektron beresolusi tinggi (HR-TEM) memaparkan yang liposom adalah berbentuk bulat dan mempunyai saiz diantara 100 ke 600 nm. Ini adalah selari dengan data yang diperolehi dengan menggunakan teknik penyerakan cahaya dinamik manakala caj permukaan yang paling rendah telah diperolehi daripada liposom campuran asid olik - asid erusik iaitu - 90 mV. Nilai kecekapan pengkapsulan bagi pelbagai ubat antibarah seperti asid folinik, doksorubisin, metotreksat, dan irinotekan adalah melebihi 60% manakala lebih 20% daripada ubatan antibarah dibebaskan selepas 24 jam menunjukkan ciri-ciri pembebasan perlahan yang sangat berguna bagi menghalang pertumbuhan sel barah. Penghasilan liposom asid lemak ini adalah sangat bermanfaat bagi penghasilan sistem pengangkutan ubatan mimikan bio.

Kata kunci: liposom, asid olik, log P, ubatan antibarah, pembebasan *in vitro*

TABLE OF CONTENTS

LIST OF FIGURES

LIST OF TABLES

LIST OF SYMBOLS AND ABBREVIATIONS

3-D	Three Dimension
A	Absorbance of the solution
AEM	Analytical Electron Microscopy
A_{min}	Minimum surface area per surfactant molecule,
b	Path length in cm
c	Concentration of the absorber.
CMC	Critical Micelle Concentration
CVC	Critical Vesicle Concentration
DLS	Dynamic Light Scattering
DMEM	Dulbecco's Modified Eagle Medium
DOPEPEG2000	1,2-Dioleoyl-Sn-Glycerol-3-Phosphoethanolamide-N-[Methoxy(Polyethyleneglycol)-2000]
DSC	Differential Scanning Calorimetry
EE	Encapsulation Efficiency
FTIR	Fourier Transform Infra-Red Spectroscopy
HCl	Hydrochloric Acid
HIV	Human Immunodeficiency Virus
HPV	Human Papillomaviruses
HR-TEM	High Resolution-Transmission Electron Microscopy
IR	Infra-Red
K_B	Boltzmann's constant, and
LUV	Large Unilamellar Vesicles
MLV	Multilamellar Vesicles
MTT	3-[4,5-Dimethylthiazol-2-Yl]-2,5-Diphenyltetrazolium Bromide
MVV	Multi Vesicular Vesicles
MWCO	Molecular Weight Cut Off
NaOH	Sodium Hydroxide
OPM	Optical Polarizing Microscope
P	Power of radiation passing through cells containing solvent
P_0	Power of radiation passing through cells containing analyte
PBS	Phosphate Buffered Saline
pK_a	Negative base-10 logarithm of the acid dissociation constant (K_a) of a solution

R	Universal gas constant, 8.314 Nm mol^{-1} K^{-1}
STEM	Scanning Transmission Electron Microscope
SUPAC	Scale-Up and Post Approval Changes
Surfactant	Surface Active Agent
SUV	Small Unilamellar Vesicles
T	Absolute thermodynamic temperature, 303 K
Tc	Gel-Liquid crystal transition temperature
U.S.FDA	The United States of America Food and Drug Administration
U_E	Electrophoretic mobility
USA	The United States of America
UV	Ultraviolet
Γ	Maximum adsorption density
γ	Surface tension
ε	Molar absorptivity
ζ	Zeta potential
η	Dynamic viscosity of the solvent
Π	Interfacial pressure

LIST OF APPENDICES

CHAPTER 1: INTRODUCTION

1.1   Cancer in the World

Cancer can be explained as an uncontrolled proliferation of cells in the body (Martinez-Pastor & Mostoslavsky, 2012) disregarding of normal cell division and potentially invade or spread to other parts of the body. In 2012, 14.1 million of new cancer cases and 8.2 million cancer deaths (Bray & Shield, 2017) were reported globally. World Health Organization estimated the new cases of cancer would increase up to 21.4 million cases in 2030 (Beaglehole et al., 2011). The common sites of new cancer cases reported are lung, breast, cervix, prostrate, colorectum, stomach, liver, and oesophagus.

Beaglehole and co-workers reported that more than 2.6 million cancer cases per year were recognized to be the controllable causes (Beaglehole et al., 2011). The major risk factors are such as the use of tobacco, consumption of alcohol, unhealthy diets, and physical inactivity. De Martel and co-worker added that the infectious agents such as *Helicobacter pylori*, human papillomaviruses (HPV), and hepatitis B and C viruses contributed about two millions of new cancer cases in 2008 (de Martel et al., 2012). Occupational carcinogenic (asbestos, aromatic amines, benzidine, benzene) and environmental factors (radiation, chemical pollution) were also explained to be the cause of cancer (Vineis & Wild, 2014).

The growth of cancer cells is divided into four numerical stage and scientifically classified as stage I for the case where cancer is relatively small, stage II for cancer cells that spread into lymph nodes close to the tumour, stage III for the cancer cells that spread into surrounding tissues, and stage IV for the cancer cells that spread to other organs. Cancer staging is one of the most important parameters that usually used to indicate prognosis, to assess the treatment results, to evaluate the similarities between

different cases, to diagnose the cancer trends, and to design a suitable therapy to treat cancer (Dollinger et al., 2002).

1.2 Cancer Therapies

1.2.1 Surgery

Surgery is the oldest local treatment for removing of cancer tissues (Dollinger et al., 2002). However, the development of the anaesthetic and tissue histochemical techniques in the nineteenth century that significantly improve the treatment of cancer that leads to the development of medical oncology.
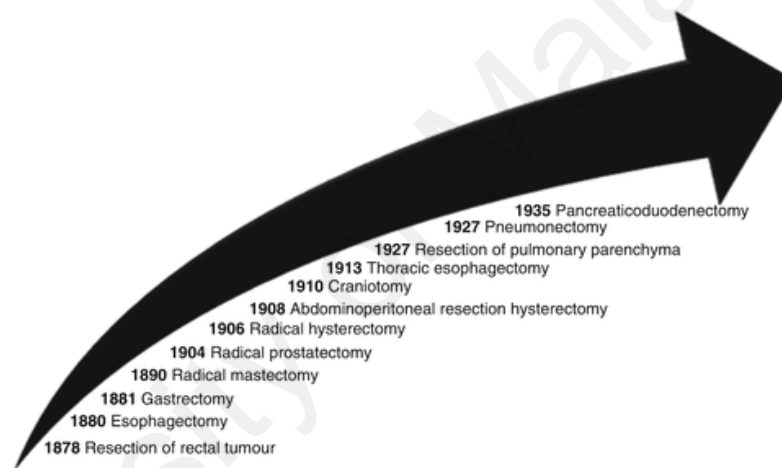
Figure 1.1: A timeline is representing the breakthroughs in oncology (Bae et al., 2013). Reprinted permission granted by Springer.

Figure 1.1 displays the successful journey of surgical resection in order to remove the benign tumour before developing cancer, remove primary and metastatic tumours, relieve side-symptoms, or investigate the stage of tumours (Bae et al., 2013). Since then, various multidisciplinary fields such as surgeons, pathologists, radiologists, epidemiologists, and psychologists were merged to optimize through the surgical resection regarding cancer stage and adjusted during treatment for changes in patient status. The common side effects of the surgical procedure are bleeding, blood clots, damage to nearby tissues and organs, renal failure (Merkow et al., 2013), infections as well as the reaction of anaesthesia (Dollinger et al., 2002; Buckley et al., 2014).

2

Surgical resection is proven to be the most effective treatment to eliminate cancerous cells then increase the survival rates and prevent recurrence (Wu, 2013). However, surgery only does not successfully cure cancer that has been spread or metastases to another part of the body.

1.2.2 Radiotherapy

In the case when surgical resection is impossible, or cancer has been spread, radiation therapy is used independently or combined with the surgery. Since the discovery of X-rays by Wilhelm Röntgen in 1895 (Röntgen, 1896; Bae et al., 2013), electron beams, high energy X-rays, and isotopes had been widely used to kill the cancer through the ionization reaction that destroy the chromosomes and DNA of cancer cells so that they cannot divide (Dollinger et al., 2002).

Radiotherapy can be done externally and internally depending on the biology of the cancer cells, possible complications to the patients and the radiation sources. The external radiation source can be high and low energy radiation, orthovoltage equipment, megavoltage equipment, or stereotactic radiosurgery. Generally, the filament is heated at high temperature to emit the electrons that hit the tungsten target and finally produce the X-rays of high energy up to 1000 kV. In internal radiation technique, radioactive sources such as strontium 89 and iodine 113 are delivered via injection or implanted at cancer cells. These radioactive sources were then producing high radiations that kill the cancer cells.

Many researchers had been reported the successful result in killing the cancerous cells by using the radiation treatment such as oesophageal cancer (Chun et al., 2017), vulvar cancer (Vorbeck et al., 2017), head and neck cancer (Yom, 2015), and lung cancer (Dan & Williams, 2017). However, the main concern is the ionizing radiation that indiscriminate will affects the survival of noncancerous cells (Bae et al., 2013).

Also, it is reported that the patients treated with radiation showed many side effects such as skin erythema, peeling skin, nausea, diarrhoea, and inflammation.

1.2.3   Chemotherapy

Chemotherapy is the use of chemical compounds that have anti-cancer activities to control the growth of tumours, relief pain, kill the cancer cells, and cure cancer (Dollinger et al., 2002). It is prescribed in the metastasis cases where the cancerous cells had diffused to the other parts of the body (Heshmat & Eltawil, 2017). The use of the chemical compounds to treat the cancer cell was first reported by Louis Goodman and Alfred Gilman in 1942 by using nitrogen mustard to treat non-Hodgkin lymphoma (Gilman, 1963; Goodman et al., 1984; Bae et al., 2013). Since then, a broad range of chemical compounds has been used to interrupt the growth of cancer at different stages of a cell cycle, for example antimetabolites will attack during the cell division while alkaloids prevent the formation of the chromosome. Every year, the development of the technology to synthesize anticancer molecules adds the new drug to the list.

Delivery of chemotherapeutic agents to the circulatory systems can be performed using various routes such as oral (Gupta et al., 2017), intra-arterial through artery at head, neck, liver or pelvis (Lewis & Bloomston, 2016), intraperitoneal through abdominal cavity (Sun et al., 2016), and intravenous (Wacker, 2013; Vlasova et al., 2014; Feng et al., 2016). Sometimes, these chemotherapeutic agents were combined to improve efficacy, reduce side effects, and prevent drug resistance. There are four visible results that can be observed after chemotherapy, which is "complete remission" for the case where the tumour entirely disappears, "partial remission" where half of the tumour is shrunken, "stabilization" where the tumour is neither shrinks or grows, or "progression" where the tumour grows (Dollinger et al., 2002).

As the chemotherapy is effectively inhibiting the cancerous cells, this treatment is also affecting other rapidly growing cells in the body, such as hair follicles, nails, and the cells in the gastrointestinal tracks. The immediate side effect such as nausea and vomiting are normally reported in post chemotherapy patients, where it can be found up to 96% of patients underwent chemotherapy (Hosseini et al., 2016). Some chemotherapy drugs can cause the damage to organs such as heart, lung, or kidney, and may lead to another cancer due to the cell mutation during chemotherapy (Dollinger et al., 2002).

1.3   Nanocarriers System for Chemotherapy

Since the idea of adjuvant chemotherapy was introduced in the early 1970s (Bae et al., 2013), the treatment of cancer showed a synergizing effect in curing various cancers. Even though this combinational mechanism is successful in treating numerous cancer, it still caused more than 14.5 million deaths worldwide in 2014 (Heshmat & Eltawil, 2017) due to insufficient delivery of chemotherapeutic drugs to the tumour target tissue or due to severe and harmful toxic effects on normal cells (Andresen et al., 2005). Many carriers, such as molecular conjugates and colloidal particulates (Immordino et al., 2006), had been explored in the attempt to deliver the chemotherapeutic drugs to the targeted tumours and hence improve the therapeutic effect of the treatment.

The traditional chemotherapeutic drugs have a limited therapeutic effect where even relatively small changes in drug disposition may lead to a lower drug activity or extreme toxicities. Furthermore, the response to the chemotherapy is varied regarding the genes involved in drug metabolism, body size, the ratio of fat to total mass, and abnormalities in liver or kidneys functions.
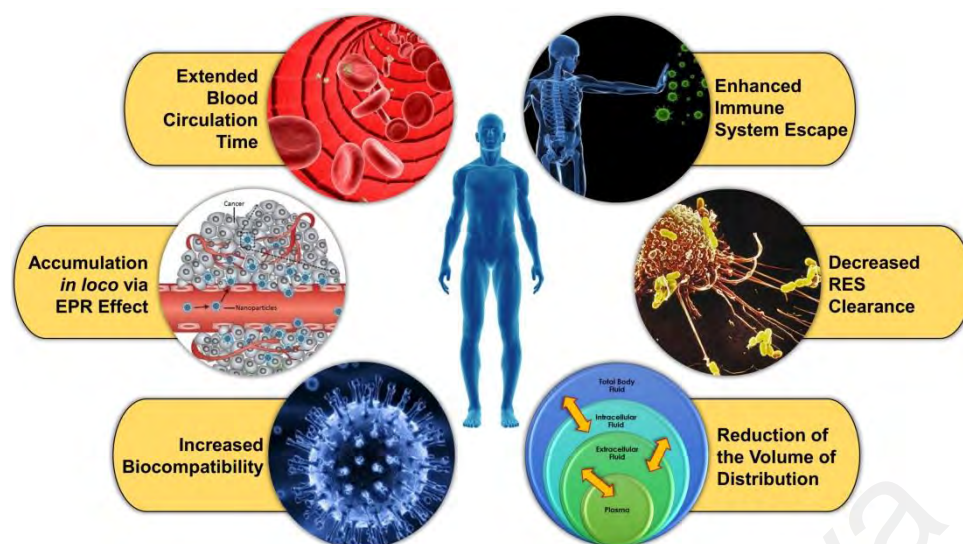
Figure 1.2: Major benefits of nanocarriers for chemotherapy delivery (Giodini et al., 2017). Abbreviation: RES: reticuloendothelial system, EPR: enhanced permeability and retention. Reprinted permission granted by Elsevier.

The advancement in the pharmaceutical technology allows the scientists to deliver the innovative chemotherapeutic drugs to the specific tissues by incorporating in the nanocarriers (Giodini et al., 2017). It is proven that the nanocarriers exhibit a significant improvement in carrying the chemotherapeutic drugs and strongly accumulate at the targeted tissues so that specific toxicity which is different from the toxicity of the pure compound can be increased (Wacker, 2013). Figure 1.2 exhibits the general benefits achieved in the application of nanocarrier systems for delivering chemotherapeutic drugs. Giodini and co-workers reported that the use of nanocarriers successfully enhanced permeability and retention effect of therapeutic agents at the designated site of action (Giodini et al., 2017).

Various nanocarriers with dimensions up to 1000 nm has been explored, such as niosomes, Nano spheres, erythrocytes, polymeric conjugates, and micelles (Cagel et al., 2017), however, liposomes gained the most interest from the researchers due to their composition, which makes them biocompatible and biodegradable, when introduce into the body. Liposomes were firstly proposed as nanocarriers in cancer treatment by Gregoriadis and co-workers in 1974 (Gregoriadis et al., 1974; Andresen et al., 2005)

due to the controllable size from microscale to nanoscale (Immordino et al., 2006; Sala et al., 2017), and their ability to encapsulate both hydrophilic and hydrophobic chemotherapeutic drugs, which protected them from oxidation and degradation (Lasic, 1998). Liposomes are also reported to improve the therapeutic efficacies by stabilizing chemotherapeutic drugs, overcoming obstacles to cellular and tissue uptake, and improving bio-distribution of chemotherapeutic drugs at the designated target gland, organ, or system (Sercombe et al., 2015). In the 1980s, the Liposome Company successfully developed the egg phosphatidylcholine/cholesterol liposomes encapsulating doxorubicin with citrate complex and marketed it as Myocet® to be used as a first line treatment of metastatic breast cancer in adult women (Swenson et al., 2001).

Since then, many pharmaceutical companies competitively studied the liposomes as a promising carrier for chemotherapeutically active compounds. However, some of the major drawback for liposomes to be used in pharmaceutics is the instability of liposomes especially in the circulatory system, where they are degraded by the reticuloendothelial system (RES). It was documented that particle size, surface charge, and liposome composition had a strong influence on the stability of liposomes (Giodini et al., 2017). The low encapsulation efficiency is reported as a result of the inconsistence chemotherapeutic drug load (Andresen et al., 2005). This is directly affecting the release of chemotherapeutically active compounds to the targeted site. Also, the complexity of production process as well as high cost of manufacture and materials (Wacker, 2013) limit the commercialization of liposomes encapsulating chemotherapeutic drugs.

1.4   Objectives

Over the past few decades, liposomes have gained extensive interest as a carrier system for chemotherapeutic drugs, due to their biocompatibility, low toxicity, lack of immune system activation, and targeted delivery of bioactive compounds to the site of action. Liposomes are formulated using phospholipids. In this study, stealth fatty acid liposomes are prepared with the aim to achieve these following objectives:

i.   To prepare and characterize stealth oleic acid liposomes

ii. To encapsulate and evaluate cytotoxicity of various log P anticancer drugs towards human lung cancer cells

iii. To study the *in vitro* release and the mechanism of release of anticancer drugs from stealth oleic acid liposomes

CHAPTER 2: LITERATURE REVIEW

2.1 Liposomes

Since the discovery of liposomes in 1964 (Bangham & Horne, 1964), liposomal technologies was evolved from only in the biological membranes (Lasic, 1998) study to various multidisciplinary including physics and mathematics (Wang et al., 2008), biochemistry (Anabousi et al., 2006; Boakye et al., 2015; Sun et al., 2015), colloid science (Chen & Szostak, 2004; Chia & Misran, 2013; Fameau et al., 2014), and cosmetic sciences (Himeno et al., 2017; Wang et al., 2017). The applications of liposomes are based on their colloidal properties such as surface charge, size, microencapsulation, membrane mechanical strength, surface properties, leakage rate, fusogenic activity, or interaction with particular cells (Lasic, 1998).
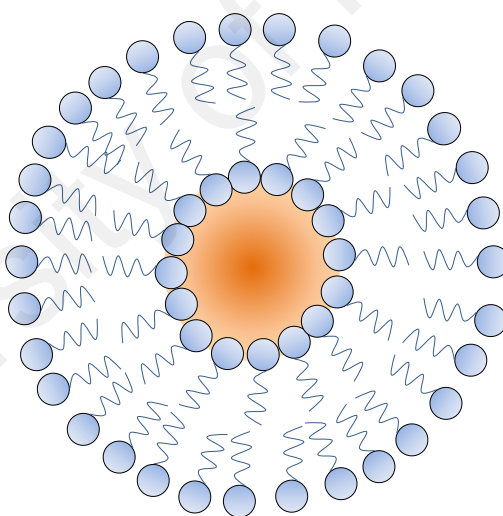
Figure 2.1: Schematic diagrams of liposomes.

Liposomes are self-assembled spherical particles (Lasic, 1998), that compose of one or more lipid bilayers (Gulati et al., 1998; Hudiyanti et al., 2014) entrapping their aqueous dispersion medium (Mufamadi et al., 2011) as illustrated in Figure 2.1. Liposomes are formed naturally and synthetically from amphiphilic molecules (Gulati et al., 1998; Lasic, 1998; Gregoriadis, 2016), such as natural phospholipids or lipids (Ge et al., 2003; Hudiyanti et al., 2014; Zhao et al., 2015) for instance 1,2-distearoryl-sn-

glycero-3-phosphatidyl choline (DSPC) (Moussa et al., 2017), phosphatidylcholine (Dwiastuti et al., 2016; Guo & Kim, 2016), phosphatidylserine (Takayama et al., 2013) and fatty acid (Kanicky & Shah, 2002; Morigaki et al., 2003; Ahmad et al., 2014). These amphiphilic molecules pose a polar and non-polar property according to their symmetry and distribution of their electronic clouds, which can self-orientate to form the ordered structures depending on their hydrophobic-hydrophilic interaction and aqueous environment. Micelles form when the hydrophilic section is greater than the hydrophobic section, while reverse micelles form when the hydrophilic section is smaller than the hydrophobic section. At an excess concentration, long-range order liquid crystalline phases, such as lamellar, hexagonal, and cubic structures, are formed, which later can be dispersed to form liposomes, hexasomes and cubosomes, as shown in Figure 2.2.

Liposomes can be classified regarding the size and structure of the liposomes, which range from 0.025 to 2.5 μm (Akbarzadeh et al., 2013). Generally, liposomes can be classified by their size and number of bilayers, which is unilamellar and multilamellar liposomes. Unilamellar liposomes are spherical vesicles entrapping aqueous solution and bounded by a single bilayer of an amphiphilic lipid or a mixture of such lipids. Unilamellar liposomes can be divided into small unilamellar vesicles (SUV) and large unilamellar vesicles (LUV). Differently, multi vesicular vesicles (MVV) and multilamellar vesicles (MLV) have an onion structure entrapping smaller liposomes inside the body of liposomes separated by layers of water. Different type of liposomes can be achieved by using different techniques of preparation.
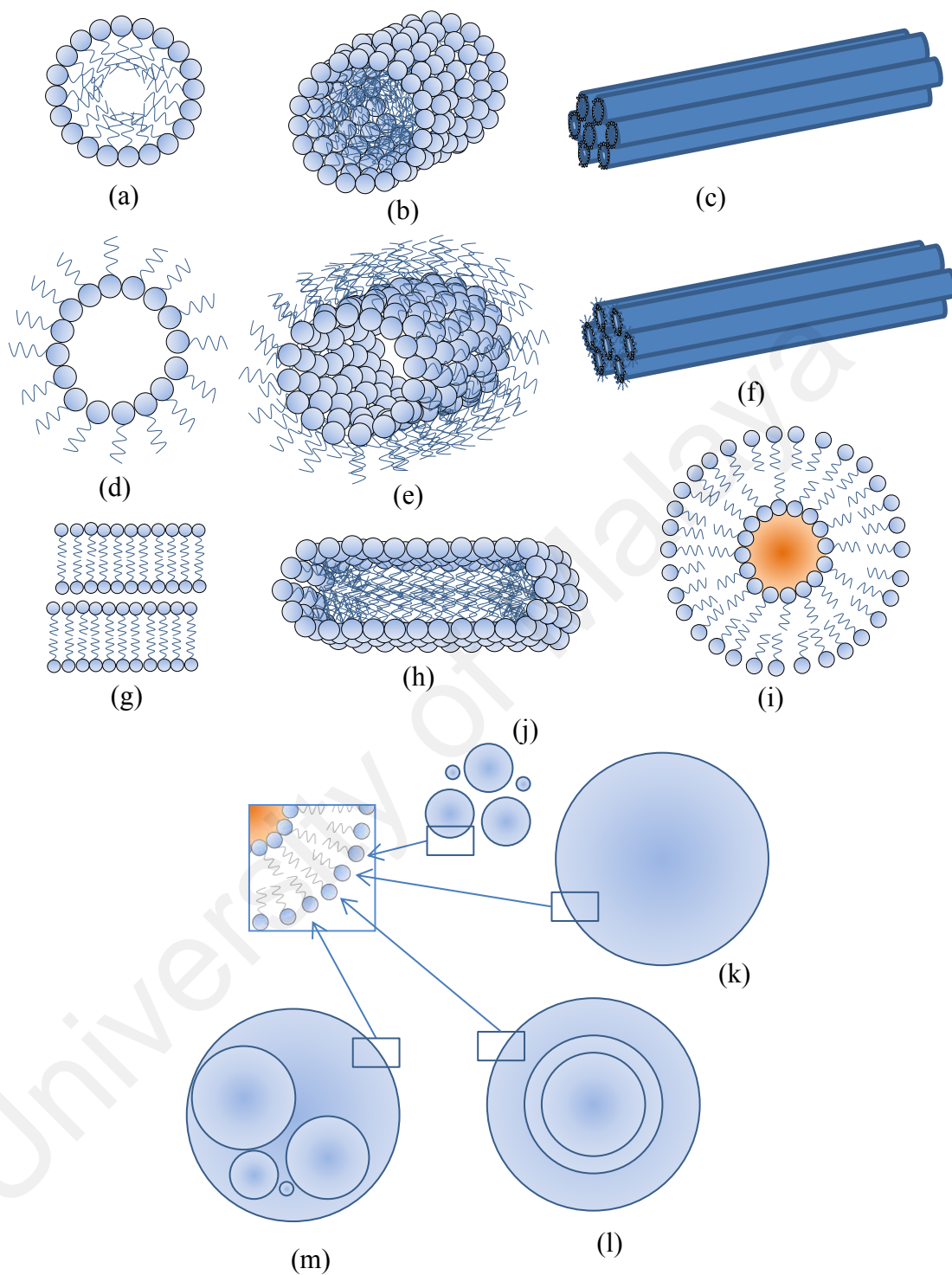
Figure 2.2: Self aggregation of amphiphilic molecules forming (a) micelles, (b) prolate micelles, (c) hexagonal phase micelles, (d) inverse micelles, (e) prolate inverse micelles, (f) hexagonal phase inverse micelles, (g) lamellar phase, (h) oblate micelles, (i) liposomes, (j) small unilamellar liposomes, (k) large unilamellar liposomes, (l) multi lamellar liposomes, and (m) multi vesicular liposomes.

2.2 Methods of Liposomes Preparation

The features of liposomes, for instance size, lamellarity, and encapsulation efficiency, are mostly controlled by their preparation mechanism (Cortesi, 1999). Generally, preparation of liposomes involves multi-steps, which start with the preparation of amphiphilic lipid molecules (Dua et al., 2012), and hydration of lipid films followed by sizing of liposomes (Hamilton & Guo, 1984; Riaz, 1996; Akbarzadeh et al., 2013; Gregoriadis, 2016).
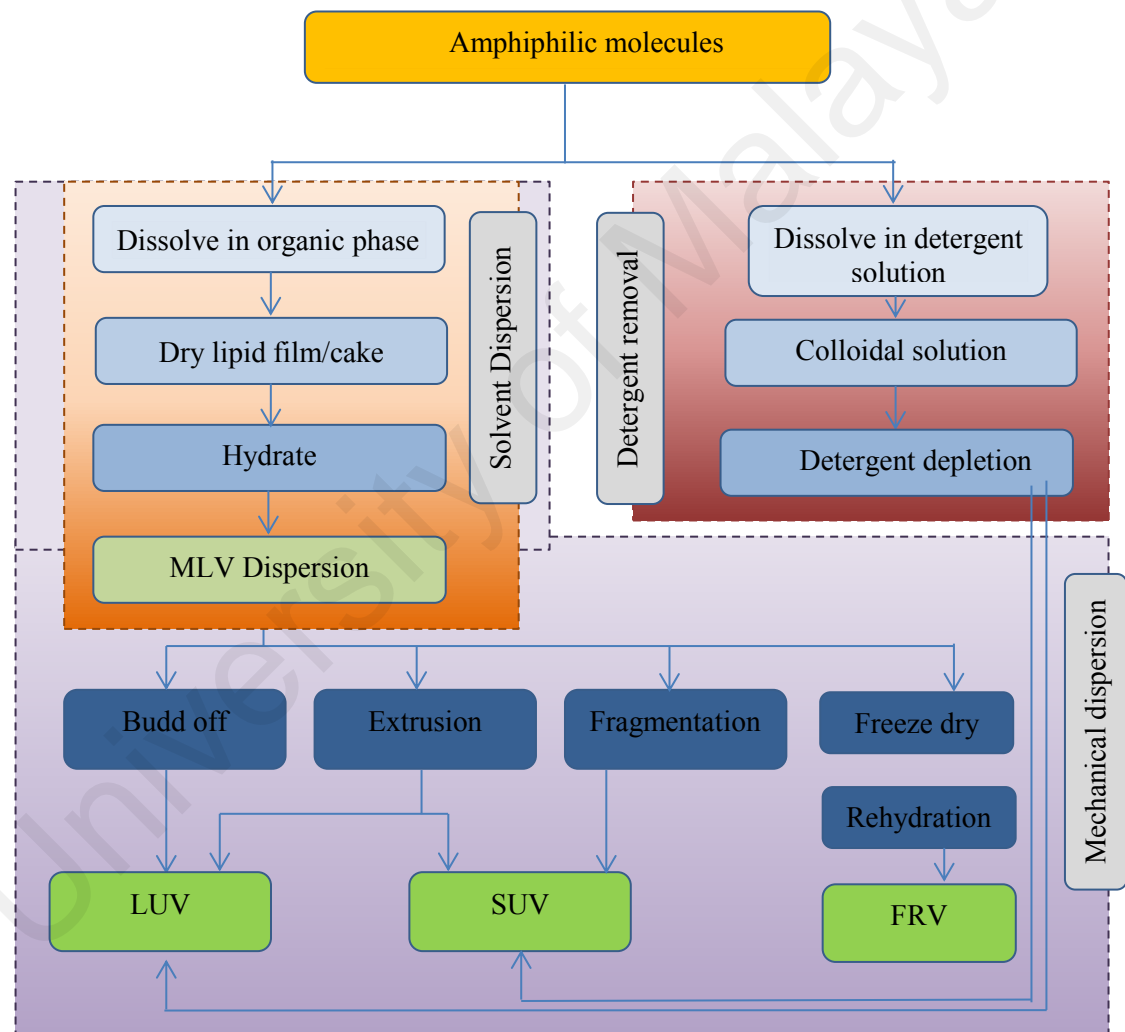
Figure 2.3: General preparation methods of liposomes, which produce different types of liposomes, such as the multi lamellar vesicles (MLV), large unilamellar vesicles (LUV), a small unilamellar vesicle (SUV), and freeze drying rehydration vesicles (FRV).

Lipids are firstly dissolved in an organic solvent, such as chloroform, methanol, or mixture of both chloroform and ethanol, to produce a homogenous solution of lipids (Dua et al., 2012). The solvents are then removed from the mixture by using a dry nitrogen or argon flow or by employing a rotary evaporator, producing the thin films or cakes of lipids. The hydration of lipids step can be divided into solvent dispersion technique, detergent removal technique, and mechanical dispersion technique as shown in Figure 2.3. The different mechanism can be employed in order to obtain the differently desired liposomes. Liposomes can be produced by hydrating the thin lipids film or cakes that result in the formation of myelin from the swelling of liquid crystalline bilayers (Torchilin & Weissig, 2003). The exposed hydrophobic edges will rearrange in order to reduce the energy where liposomes are spontaneously formed either in the structure of multi lamellar vesicles (MLV), large unilamellar vesicles (LUV), a small unilamellar vesicle (SUV), or freeze drying rehydration vesicles (FRV). These liposomes then undergo resizing process until the desired size is achieved.

2.2.1 Solvent Dispersion Method

During the solvent dispersion method, an aqueous phase containing active ingredients is introduced to the lipids, which were previously dissolved in an organic solvent. Lipids molecules will spontaneously reorganize after the organic solvent is discarded from the mixture which later will form the liposomes (Cortesi, 1999). Miscibility of organic solvent with aqueous phase will determine whether the liposomal system forms either in the monophasic or diphasic system.

In the monophasic system, an organic solvent that is used is miscible with the aqueous phase of lipid, such as ethanol, as described as ethanolic injection method. The lipid in the ethanol solution is rapidly introduced to the excess hydration medium

producing SUVs within the range of 30-100 nm in a short time (Dua et al., 2012; Sala et al., 2017).

The situation when the organic solvent is immiscible with the aqueous is known as the biphasic system, where lipid will rearrange as a monolayer across the interface of an aqueous medium and an organic solvent. This system can be achieved by either ether injection or reverse phase evaporation method. In the ether injection method, the lipid is dissolved in diethyl ether, or ether/methanol mixture, which is gently injected into the aqueous solution containing the active ingredients, followed by removal of solvent until liposomes with a size of 70-190 nm are formed spontaneously. In reverse phase evaporation method, lipid in the organic solvent (diethyl ether, isopropyl ether, or the combination of isopropyl ether and chloroform) and aqueous buffer are mixed and sonicated to produce water in oil emulsion. Liposomes are formed during the removal of the solvent.

However, the drawbacks of the solvent dispersion method are the heterogeneity of liposomes formed, degradation of active ingredients by organic solvents, the formation of the azeotrope with water, and low encapsulation efficiency of active ingredients especially for hydrophilic compounds (Cortesi, 1999).

2.2.2 Detergent Depletion Method

Detergent depletion method was first proposed to incorporate protein into the phospholipids bilayers (Patil & Jadhav, 2014) and now widely used to prepared LUV liposomes due to the mildness to the protein that is sensitive towards any physical or solvent treatments. In this method, the lipid is solubilized with surfactant micelles such as from sodium cholate, alkyl(thio)glucosides and alkyl-oxypolyethylenes in the aqueous phase (Torchilin & Weissig, 2003). Removal of detergent through dilution, dialysis, gel filtration, or adsorption/binding leads to the formation of homogeneous

LUV liposomes. Commercially available devices that normally employed in the removal of surfactants are such as Lipoprep, which uses the dialysis technique, Sephadex G-259 using gel filtration, and Bio-Beads SM-210 and Amberlite XAD-2 bead to bind with the excess surfactant (Dua et al., 2012). However, the primary concern of this technique was the surfactant residue in the solution which could result in toxicity to the cells (Mozafari, 2005).

2.2.3   Mechanical Dispersion Method

Mechanical dispersion technique is the most basic, simple and direct preparation of liposomes, where the lipid is dispersed in an organic solvent such as chloroform, chloroform-methanol mixture, tertiary butanol, or cyclohexane to form a clear, homogeneous mixture (Mozafari, 2005). The solvent was evaporated by using dry nitrogen, argon, or rotary evaporator forming a thin layer film/cake that can be freeze until ready to use.
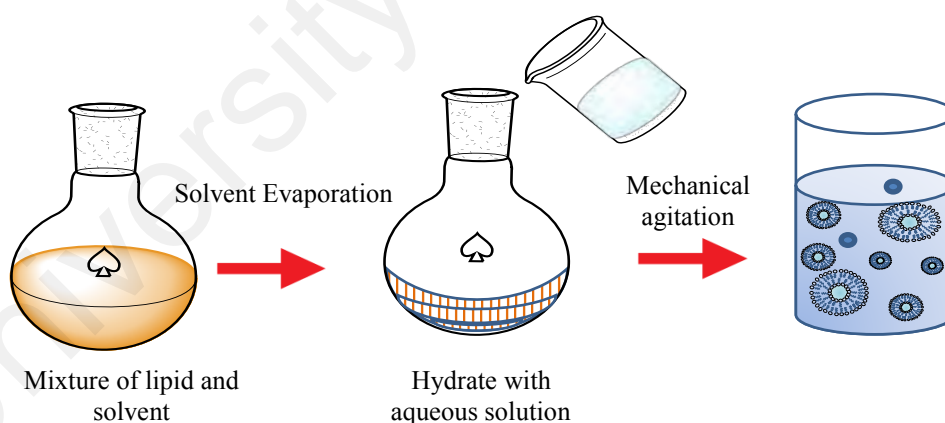
Figure 2.4: Formation of liposomes by thin layer lipid hydration.

The thin layer film/cake is then hydrated by the aqueous solution such as distilled water, buffer solutions, saline, and non-electrolytes such as sugar solutions at a temperature above the gel-liquid crystal transition temperature (T_g) of the lipid (Dua et al., 2012) to form large MLV liposomes as shown in Figure 2.4. Mechanical agitation, such as bud-off (shaking, swirling, pipetting, sonicating or vortexing), extrusion,

15

fragmentation, and freeze drying is needed to break the tubule of lipid and the exposed hydrophobic edge (Torchilin & Weissig, 2003), which later will lead to the development of the unilamellar liposomes. The average size of the liposomes produced using this technique is controlled by the composition and concentration of lipid, temperature, the strength of mechanical agitation such as sonication time and power. Degradation of lipid can be reduced by minimizing the external mechanical agitation.

2.3 Stealth Liposomes

Since the discovery of liposomes, conventional liposomes formulations that generally used in pharmaceutical industry are based on natural phospholipids or lipids, such as 1,2-distearoryl-sn-glycero-3-phosphatidyl choline (DSPC), sphingomyelin, and egg phosphatidylcholine. The conventional lipid-based liposomes encountered many challenges such as metabolite by the process of phagocytosis, instability in plasma, short half-life, and rapidly removed from the blood circulation due to the formulation that containing simply phospholipids (Mufamadi et al., 2011). Furthermore, early degradation of liposomes bilayer leads to the burst released of active ingredients that entrapped within the liposomes, which prevent the active ingredients from successfully delivered to the targeted site. As a result, modification of liposomes surface and membrane is needed to overcome most of the challenges encountered by conventional liposomes technology (Mufamadi et al., 2011).

The first successful modification of liposomes was performed by Allen and Chon in 1987 by using gangliosides and sialic acid derivatives to mimic the erythrocyte membrane (Allen & Martin, 2004; Immordino et al., 2006). Since then, many materials especially polymers have been explored to produce the liposomes that having stealth properties. Hydrophilic polymers showed a promising result due to their flexible chain that inhabits the space neighbouring to the liposome surface ("peri-liposomal layer")

will exclude other macromolecules from this space. Therefore, the liposomes surfaces are hindered from accessed and bonded by blood plasma opsonins, and thus prevent the interactions of macrophages to the liposomes.

Figure 2.5 displays the naturally occurring polymers that extensively used in pharmaceutical and medical applications and being applied in the preparation of stealth liposomes due to their promising properties, such as biodegradability and biocompatibility. Alginate, which is a polysaccharide extracted from seaweed and algae, showed an improvement in stability (Wang et al., 2015; Liu et al., 2016), entrapment efficiency of active ingredients and controlled released properties when being used to coat the liposomes (Bansal et al., 2016). Chitosan was also extensively explored as a material for decorating the membrane of liposomes due to their muco-adhesiveness and non-toxic. Chitosan-based liposomes was successfully prepared by many researchers and showed a higher stability of liposomes even in room temperature, poses a higher encapsulation, slower release properties (Alavi et al., 2017; Li et al., 2017), and improve in skin permeability (Park et al., 2014) as compared to liposomes without chitosan. In addition, dextran which is synthesized from sucrose by lactic-acid bacteria *Leuconostoc mesenteroides* and *Streptococcus mutans* (Bhatia, 2016) is also employed to coat the surface of liposomes (Joshi & Patel, 2012) due to their solubility, biocompatibility, and biodegradability. Many researchers have been reported their success in prolong the life of liposomes even by using a low molecular weight dextran (Menon et al., 2015). Gelatin is another material that is manipulated in the membrane of liposomes due to its wide isoelectric point from positive to negative charge depending on the physiological environment. It has been reported that gelatine-based liposomes membranes showed a linear release of antiviral (Nayak et al., 2017) in addition to the ability to prolong the life of liposomes (Mufamadi et al., 2011).
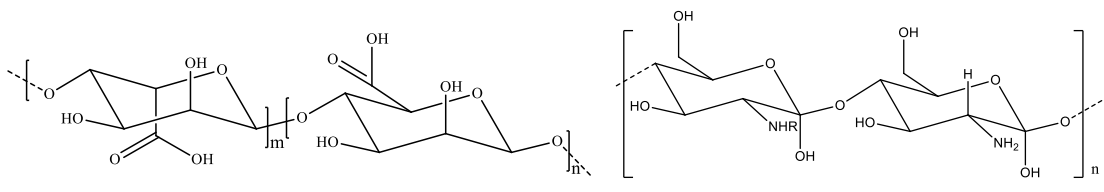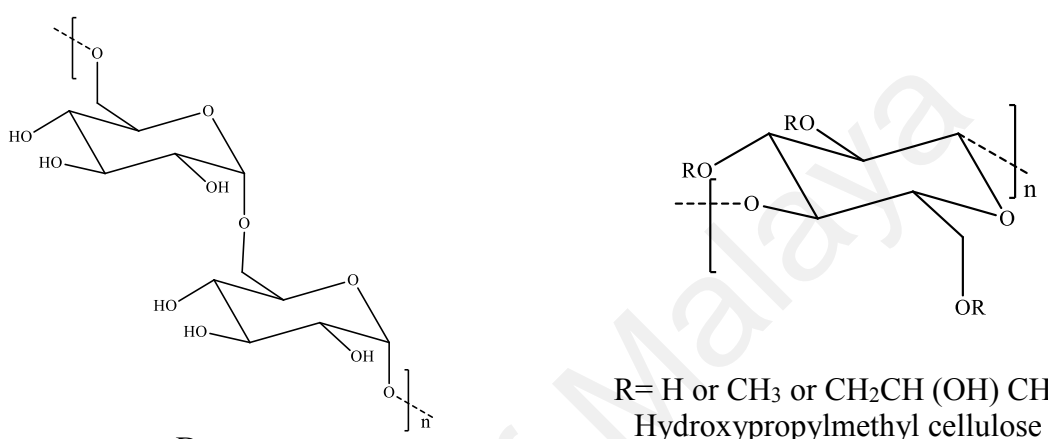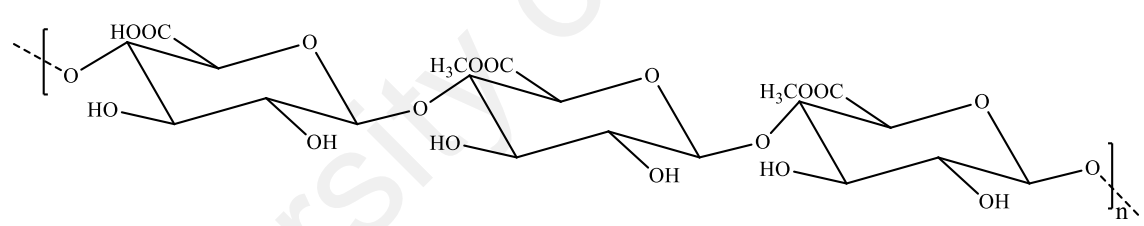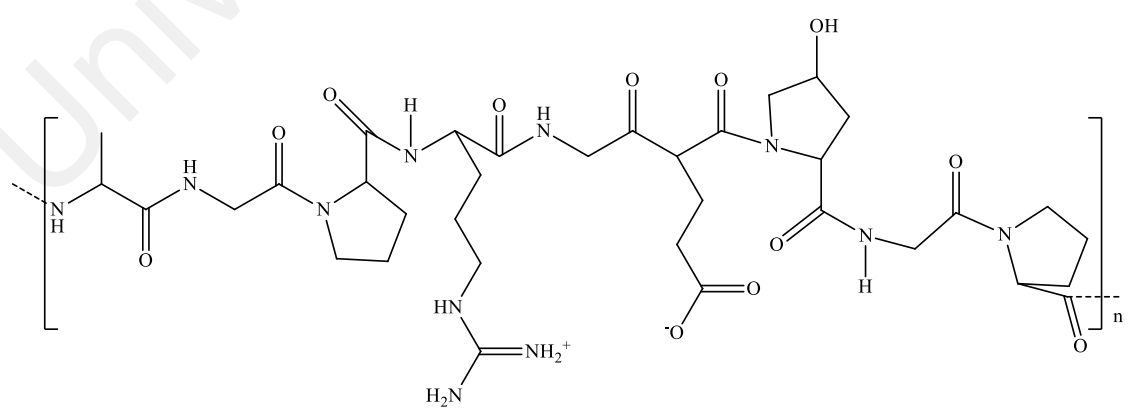
Figure 2.5: Natural materials used to prepare stealth liposomes.
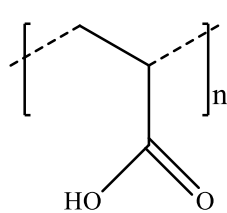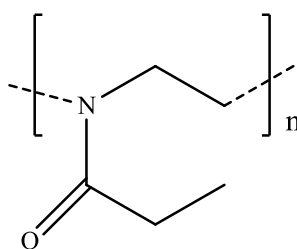
Carbopol   Poly (2-methyl-2-oxazoline)   Polyacrylamide
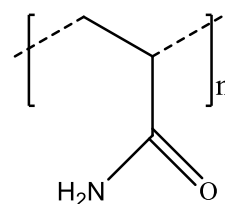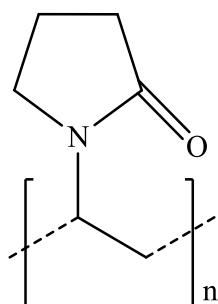
Poly (vinylpyrrolidone)   Poly (glycerol)   Polyvinyl alcohol
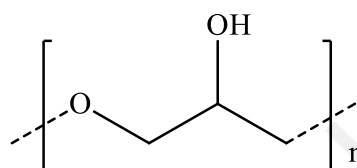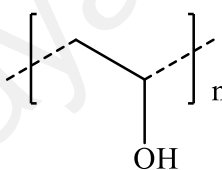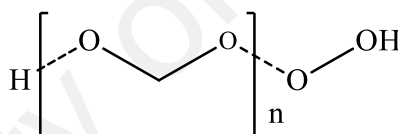
Polyethylene glycol

Figure 2.6: Synthetic materials used to prepare stealth liposomes.

The application of synthetic polymers as presented in Figure 2.6 in the preparation of stealth liposomes was extensively explored due to their outstanding characteristics such as bio-adhesivity, biocompatibility, biodegradability, and low toxicity. Carbopol 980, Carbopol 974NF, and Carbopol 940 are generally used as a pharmaceutical carrier because of their excellent swell-ability in water followed by adherence to the intestinal mucus resulted from the formation of hydrogen bridges at their carboxylic groups (Mufamadi et al., 2011). In the release study of curcumin by Berginc and coworkers, liposomes coated with carbopol displayed a slower release properties and rose in bio adhesiveness as compared to non-coated liposomes (Berginc et al., 2014). This was

agreeable with the result reported by the researchers from Gifu Pharmaceutical University that carbopol promoted the adhesive percentage of carbopol coated liposomes on the surface of the intestines (Takeuchi et al., 2003). Another hydrophilic synthetic polymer that is broadly used in the formulation of stealth liposomes was polyvinyl alcohol (PVA) due to its low protein adsorption, water soluble, non-toxic, as well as chemical resistance. Many researchers have been reported the ability of PVA to enhance the viscosity, stability and release of active ingredients from PVA-coated liposomes (Mufamadi et al., 2011). In addition to that, liposomes coated with PVA were reported to have an improved penetration through monolayer that suggested a better delivery system (Zasada et al., 2015).

Polyethylene glycol (PEG) is the most reported material to be grafted to the membrane of liposomes to provide a steric stabilizer hence created the stealth liposomes. This is due to its biocompatibility (Zhang et al., 2012; Hsu et al., 2014), solubility in both aqueous and organic media (Immordino et al., 2006), not alter the mechanism of the therapeutic protein, and biodegradable. However, the most valuable property of PEG is the ability to reduce the uptake of macrophage hence prolongs the presence of liposomes in the blood circulation (Lasic, 1998; Okamoto et al., 2016). Zhang and co-workers have successfully demonstrated that the incorporation of PEG at the membrane of liposomes could reduce the uptake by macrophage up to four folds by using flow cytometry and geometric fluorescence intensity (Zhang et al., 2016). The study by Jøraholmen and team provide another added value to PEG, where incorporation of PEG in liposomes increase the mucoadhesive property of PEGylated liposomes by increasing the penetration of interferon alpha-2b (IFN α-2b) to the to the vaginal epithelium (Jøraholmen et al., 2017).

The manipulation different materials to the liposomal membrane in order to achieve the stealth property can be done by physically adsorbing the polymer onto the surface of the liposomes, by incorporating the stealth materials during preparation, or by covalently anchoring the reactive groups onto the surface of preformed liposomes (Immordino et al., 2006). As a result, active ingredients entrapped in the liposomes are expected to be successfully delivered to the desired site of action.

2.4 Stealth Liposomes for Active Ingredients Delivery

Application of liposomes as the active ingredients delivery is depending on the physicochemical, colloidal appearances such as formulation, size, loading efficiency and the stability of the liposomes, as well as their biological interactions with the cells. Stealth liposomes technology is one of the most used alternatives to develop the liposome-based systems to carry the active ingredients to the targeted sites. Stealth liposomes functionalized with targeting moieties such as antibodies, peptide glycoprotein, oligopeptide, or receptors will ensure the specific targeting properties of the liposomes (Mufamadi et al., 2011).

The delivery of active ingredients to the targeted sites can be achieved by the transfer of liposomal lipids with the lipids of the cell membranes through the process namely lipid exchange (Lasic, 1998), which lead to the released of active ingredients into the targeted sites extracellular fluid and then diffused into the cell (Immordino et al., 2006). Another proposed mechanism is adsorption of the stealth liposomes onto the cells through electrostatic, electrodynamic, van der Waals, hydrophobic insertion, or hydrogen bonding followed by endocytosis where the active ingredients within the stealth liposomes will directly deliver into the cells.

Stealth liposomes can be commercially produced as a suspension, or in a semi-solid form such as a gel, cream, or powder for topical, oral, or sublingual delivery in addition

to the most promising intravenous delivery. Liposomes have been widely used to transport various active ingredients from as simple as nutrients to anticancer drugs. Encapsulation of active ingredients can be achieved by either during the formation of liposomes (passive loading) or after the formation of liposomes (active loading) (Akbarzadeh et al., 2013). Table 2.1 displays the commercially available liposomes encapsulating different active ingredients. Different properties of stealth liposomes will provide varies qualities such as improved drug solubility (amphotericin B, minoxidil), shielding of sensitive molecules (cytosine arabinose, DNA, RNA, antisense oligonucleotides, ribozymes), boosted intracellular uptake (all agents, including antineoplastic agents, antibiotics and antivirals), and altered pharmacokinetics and bio distribution of the encapsulated active ingredient (Lasic, 1998).

Incorporation of vitamins such as vitamin A, C, and E were aimed to overcome the barrier of conventional approach such as effectiveness due to the instability of vitamins, solubility, and barrier properties of skin (Monroig et al., 2007; Marsanasco et al., 2011; Liu et al., 2017). Lypo-Spheric™ and Optimal are among liposomal-based nutrient carriers prepared from phosphatidylethanolamine complex and phosphatidylcholine that are commercially available. Lypo-Spheric™ is marketed as a dietary supplements aiming to deliver the 1000 mg of vitamin C to the cell through intestine without being flush out by the body system. Also, antifungal drug such as amphotericin B was also encapsulated in the hydrogenated soy phosphatidyl choline: cholesterol-distearoylphosphatidyl glycerol liposomes and being marketed in the brand of Ambisome for the treatment of fungi, Cryptococcal meningitis in HIV-infected patients, and the treatment of visceral leishmaniasis.

Table 2.1: Commercially available liposomal products.

Category	Active Ingredient	Brand Name	Use
Nutrient	Vitamin C	Lypo-Spheric™	Protect cells from the damage caused by free radicals, improve immune system
	Glutathione	Optimal	Maintain normal protein structures within the body, neutralizing potentially damaging free radicals throughout the body, support detoxification pathways
Antifungal	Amphotericin B	Ambisome	Treatment of from the species of Aspergillus sp., Candida sp., and/or Cryptococcus sp.
Analgesic	Bupivacaine	Exparel®	Postsurgical analgesia, reduce pain, numb the area around the surgical site
	Morphine Sulfate	Depodur®	Postsurgical analgesia, improved patient mobility
Antivirus	Hepatitis A Vaccine	Epaxal®	Active immunisation against hepatitis A of children from 1 year of age
	Influenza Vaccine	Inflexal® V	Protect children older than 6 months and adults from flu (influenza)
Photodynamic Therapy	Verteporfin	Visudyne®	Treatment of patients with predominantly classic sub foveal choroidal neovascularization
Anticancer	Doxorubicin	Doxil®	Kaposi's sarcoma
	Doxorubicin	Lipodox	Hematological malignancies and many types of carcinoma
	Cytarabine	Depocyt®	Acute myeloid and lymphocytic leukaemia and non-Hodgkin's lymphoma

Analgesic drugs is one of the type of drugs that being considered to be encapsulated in the liposomes in order to overcome the main challenges of conventional analgesic

delivery such as short analgesic coverage, high plasma exposure that related to the increase in the bowel movement, as well as in severe cases of respiratory depression (Hoekman et al., 2014). In the report by Popov and co-workers, analgesic activities of kyotorphin and leu-enkephalin analgesic peptides were prolonged and posed an efficient release when encapsulated in the liposomes (Popov et al., 2013). Stealth liposomes are reported to enhance the delivery of analgesic drugs across the blood–brain barrier that improves in the effectiveness of analgesics (Popov et al., 2013; Hoekman et al., 2014), so that the consumption of analgesic can be significantly reduced (Candiotti et al., 2014). In the market, liposomal base Exparel® and Depodur® encapsulating bupivacaine and morphine respectively are widely used as the delivery of analgesic molecules.

Currently, many anticancer drugs ranging from natural products, alkylating agents, antimetabolites to hormones had been encapsulated in the liposomes as an approach to treat cancerous diseases as shown in Table 2.2 (Raschi et al., 2010). In the cancer treatment, Doxil, Lipodox, and Daunosomes are the common doxorubicin loaded liposomes that being approved by USA Food and Drug Administration (FDA) and Europe Federation to be marketed for the treatment of solid tumour (Immordino et al., 2006; Akbarzadeh et al., 2013). Doxorubicin is an anticancer drug classified in the group of anthracycline, which suspending the growths of the cells by intercalating into the DNA hence kill the rapidly dividing cells including hair, gastrointestinal mucosa, blood cells and tumours (Akbarzadeh et al., 2012; Tacar et al., 2013). Other than reducing the toxicity of anticancer drugs up to 50% (Lasic, 1998), Yang and co-workers showed that liposomes encapsulating doxorubicin improved the uptakes of doxorubicin, induced accumulation in various cancer cells such as human breast adenocarcinoma (MCF-7) cells, human liver hepatocellular carcinoma (HepG2) cells, and human lung carcinoma (A549) cells (Yang et al., 2017). Recently,

an impressive therapeutic discovery showed that the permeation of stealth liposomes encapsulating doxorubicin to the skin was improved to 1.5 folds, while the released of doxorubicin was delayed up to 30% when tested on the rat and porcine skin (Boakye et al., 2015).

Table 2.2: Anticancer drugs and their therapeutic effects.

Class	Anticancer drugs	Therapeutic Effect	Side effects
Natural Product	Curcumin	myeloma, pancreatic, cervix, and colon cancer	N, Dz, and D
	Paclitaxel	Kaposi sarcoma, ovarian, breast, lung, cervical, and pancreatic cancer	H, D, numbness, allergic reaction, and muscle pains
	Irinotecan	colon and small cell lung cancer	D, N, Dz, bone marrow suppression, shortness of breath, and fever
Anthracycline	Doxorubicin	Breast cancer, bladder cancer, Kaposi's sarcoma, and acute lymphocytic leukaemia.	H, N, D, missed menstrual periods, and skin darkening
Alkylating agents	Cisplatin	testicular, ovarian, cervical, breast, bladder, head and neck, oesophageal, and lung cancer	V, bone marrow suppression, and kidney problems
	Ifosfamide	osteosarcoma, small cell lung, bladder, testicular, cervical, and ovarian cancer	H, V, infections, blood in the urine, and kidney problems
Antimetabolites	5fluorouracil	colon, oesophageal, stomach, pancreatic, breast, and cervical cancer	H, inflammation on the skin and mouth, loss of appetite, and low blood cell counts
	Methotrexate	cancer, leukaemia, lymphoma, osteosarcoma, and breast	N, Dz, fever, increased risk of infection, low white blood cell counts
Abbreviation: N= nausea, D= diarrhoea, Dz= dizziness, H= hair loss and V= vomiting			

Curcumin, a compound from the rhizome of turmeric (Menon et al., 2015; Moussa et al., 2017) is one of the natural products that widely used to be entrapped in liposomes for the treatment of cancer due to their impressive antioxidant activity towards multiple myeloma, pancreatic, and colon cancer (Berginc et al., 2014). Saengkrit and

co-worker showed that their liposomal formulation was successfully displayed slow and sustain the release of curcumin for cervical cancer therapy up to 48 hours (Saengkrit et al., 2014). Also, Hassan and co-researchers reported that encapsulation of curcumin in the liposomes improves its intravenous delivery as compared to only liposomes without reducing the therapeutic values of curcumin towards MCF7 breast cancer cells (Hasan et al., 2014).

Anticancer drugs from the metabolites class such as capecitabine, 5fluorouracil, methotrexate, and cytarabine were also being used to encapsulate in the liposomes. In the recent study by Zeb, liposomes encapsulating methotrexate displayed an increase in the skin permeation up to two folds in adjuvant-induced arthritis rat model, which effectively suppressed arthritis as compared to the system without encapsulating in the liposomes (Zeb et al., 2017). Due to the challenge that methotrexate has a limited brain blood barrier penetration, stealth liposomal technique had been explored by Hu and team, which gave out a better brain uptake up to three folds and higher release in plasma reaching ten folds as compared to only methotrexate (Hu et al., 2017).

Generally, encapsulation of various active ingredients in stealth liposomes can improve the encapsulation of active ingredients, reduce the toxicity, and circulation time of liposomes (Akbarzadeh et al., 2013). Furthermore, stealth liposomes enhanced the tolerability of administration and accumulation of active ingredients at sites of action (Lasic, 1998), such as tumours, infections, and inflammations. In most cases, stealth liposomes prolonged the release of therapeutic agent ensure the acute delivery of active ingredient to the targeted site.

2.5   Release of Active Ingredients from Stealth Liposomes

The therapeutic effectiveness of stealth liposomes offered the advantage in prolonging the circulation in the blood or at the targeted tissues and control the release

rate and duration of active ingredients. Many researchers reported that stealth liposomal technology offers a better permeation of active ingredients to the targeted site. In order to understand the permeation and release mechanism of active ingredients across the membrane, kinetic models on the basis of concentration, partition coefficient, and release rate were employed (Jain & Jain, 2016).

Table 2.3: Application of kinetic dissolution models.

Dissolution Models	Application
Zero-order	Active ingredients that do not disaggregate and released slowly or dosage forms of modified release pharmaceutical or matrix tablets with low soluble active ingredient in coated forms/ osmotic systems
First order	Water-soluble active ingredients or active ingredients in the in porous matrices
Higuchi	Active ingredients that constantly and one dimensionally released from the matrix, having smaller particles than the system and the concentration is higher than the solubility of active ingredients
Hixsonñ-Crowell	Active ingredients that release from the changes in the surface area and diameter of the system
Korsmeyer-Peppas	Active ingredients that release from a polymeric system
Baker-Lonsdale	Active ingredients that release from spherical matrices formulations of microcapsules or microspheres
Weibull model	Active ingredients that have a fast and prolonged release profiles
Hopfenberg model	Active ingredients that have biphasic release kinetics and released from the eroding polymers
Gompertz model	Active ingredients that have good solubility and intermediate release rate

In vitro release data is the most important information to predict the effectiveness of *in vivo* release from the stealth liposomes (Siepmann & Siepmann, 2013). The release kinetics of active ingredients especially drugs from stealth liposomes can be quantified using statistical method (multivariate analysis of variance (MANOVA), exploratory data analysis method, and repeated measures design), model independent method (difference factor and a similarity factor), or model dependent method. However, in the

last method, the true correlation between the dependent and independent variables of release is explained which the release mechanism of active ingredients can be studied. Since the fundamental report by Arthur A. Noyes and Willis R. Whitney in 1897 (Noyes & Whitney, 1897; Costa & Lobo, 2001; Siepmann & Siepmann, 2013; Jain & Jain, 2016), many pharmacist and mathematicians had proposed many dissolution models to interpret the release of different formed of active ingredients such as zero order, first order, Higuchi, Korsmeyer-Peppas model, Hixson-Crowell, Baker-Lonsdale model, and Weibull model. Table 2.3 shows various dissolution models that being proposed to explain the release mechanism of active ingredients through the membrane.

The most fitted dissolution model is ruled by the physicochemical properties of active ingredients and the release behaviour. However, in most cases, the structure of liposomes that affect the release of active ingredients will determine the kinetic dissolution model. Figure 2.7 shows the release mechanism of hydrophobic and hydrophilic drugs from liposomes which the released data is explored for preparation of successful liposomal formulation. Koutsoulas and co-workers reported that the release kinetic of terbinafine hydrochloride which is less soluble in water from their liposomal hydrogel was followed Korsmeyer-Peppas model (Koutsoulas et al., 2014). This is due to the polymeric hydrogel that acted as a polymeric barrier protecting the active ingredient from released to the environment. In other impressive findings, stealth liposomes display a zero order model by prolonging the release of a poorly water-soluble lapatinib to more than two weeks (Celia et al., 2014). This is due to the synergistic effect of the active ingredient and the structure of their ultra-stable liposomal formulation.
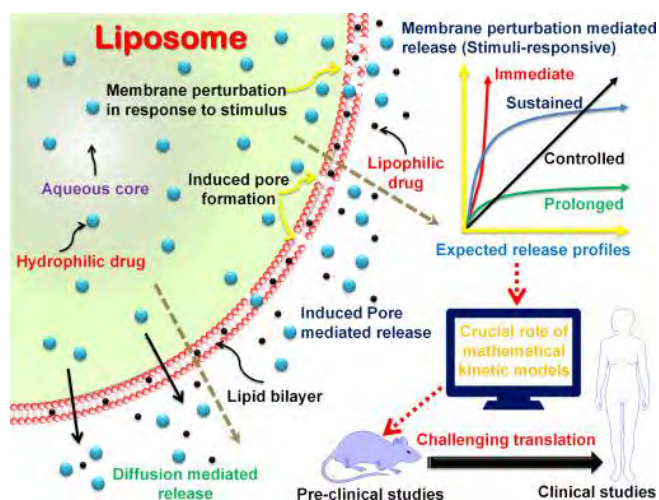
Figure 2.7: The role of mathematical models to translate the release mechanism from liposomes. Reprinted permission granted by Elsevier.

Table 2.4: Software for analysing the kinetic dissolution model (Jain & Jain, 2016).

Software	Developer	User Interface
DDSolver	China Pharmaceutical University, China	Freely available
SigmaPlot™	Systat Software, Inc., USA	Paid
KinetDS	Aleksander Mendyk, Poland	Freely available

Table 2.4 presents the software that can be employed to investigate the release of active ingredients from the stealth liposomes for a better therapeutic and efficacious formulation. This mathematical modelling approach is important to improve the effectiveness of active ingredients and patient compliance, to reduce the administration frequency, and side effects regarding the dosing of the active ingredients (Dash et al., 2010). The understanding in the relationship of active ingredients dissolution and their release geometry from stealth liposomes will provide valuable information for developing stealth liposomes encapsulating active ingredients especially in the critical field such as cancer treatment.

CHAPTER 3: MATERIALS AND METHODS

3.1 Materials

Surfactants, chemicals, and anticancer drugs used in this study are listed in this chapter and used without further purification. All solutions were prepared using deionized water with 18.2 MΩ cm resistivity by Barnstead NANO pure® Diamond™ ultrapure water system. All experiments were carried out at 30±1 °C unless mentioned in the methodology.

3.1.1 Chemicals

Sodium phosphate dibasic dehydrate (Fluka,Germany), sodium phosphate monobasic dihidrate (Fluka, Germany), phosphotungtic acid hydrate (Fluka, Japan), and sodium hydroxide (Fluka, Czech Republic) were purchased from Fluka. Hydrochloric acid with 36.5 to 38% purity (Sigma Aldrich, USA) and phosphate buffered saline tablet (Sigma-Aldrich, Switzerland) were supplied by Sigma-Aldrich. Pharmaceutical grade EMSURE Chloroform (Merck, Germany), microscopy immersion oil (Merck, Germany), and potassium bromide (KBr) (Merck, Germany) for IR spectroscopy were obtained from Merck. MTT (3-[4,5-dimethylthiazol-2-yl]-2,5-diphenyltetrazolium bromide) (Life Technology, USA), DMEM/F-12 (Dulbecco's Modified Eagle Medium/Nutrient Mixture F-12) (Gibco, USA), fetal bovine serum (FBS) (Gibco, USA), and Penicillin-Streptomycin-Glutamine (Gibco, USA) were obtained from Gibco.
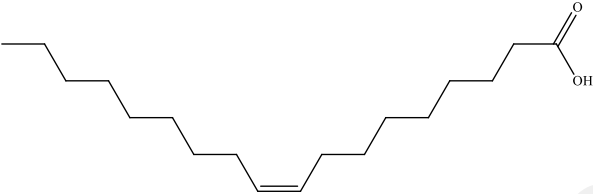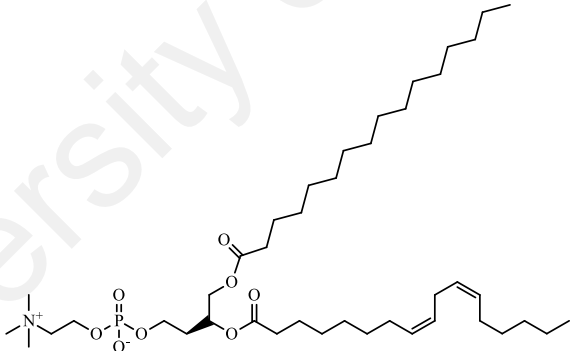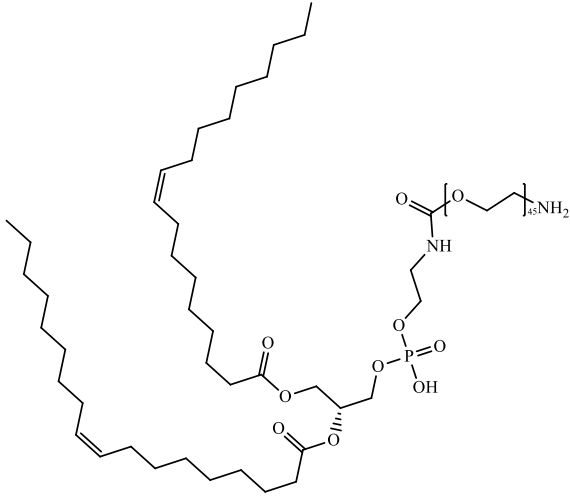
3.1.2 Surfactant

Pharmaceutical grade oleic acid (cis-9-octadecenoic acid) (Fluka, Belgium) and >99% erucic acid (Fluka, Belgium) were purchased from Fluka while L-α-lecithin from soybean (Calbiochem, Germany) which contains 97.1% phosphatidylcholine and 0.35% triglycerides were purchased from Calbiochem. 1,2-dioleoyl-sn-glycerol-3-

phosphoethanolamide-N-[methoxy(polyethyleneglycol)-2000]   (DOPEPEG2000) (Avanti Polar Lipids, USA) was purchased from Avanti Polar Lipids. Table 3.1 shows the list of surfactants used in this research.

Table 3.1: List of surfactants used in the study.

Surfactant	Chemical Structure	Molecular Weight (g mol^{-1})
Oleic acid		282.47
Erucic Acid		338.58
L-α-lecithin		2801.51
DOPEPEG2000		338.58

3.1.3   Anticancer Drugs

Table 3.2 shows the chemical structures of anticancer drugs used in this research. Folinic acid calcium salt hydrate (Fluka, China) was purchased from Fluka. Methotrexate (Cayman, Japan), doxorubicin hydrochloride (Cayman, USA), and irinotecan hydrochloride (Cayman, USA) were produced by Cayman. All anticancer drugs were used without further purification.

Table 3.2: Chemical structure of anticancer drugs.

Anticancer drugs	Molecular Weight (g mol^{-1})	Chemical Structure	Log P*
Folinic acid calcium salt hydrate	511.50		-2.7
Methotrexate	454.44		-0.5
Doxorubicin Hydrochloride	580.99		+0.5
Irinotecan Hydrochloride	623.15		+2.8

*calculated by ChemAxon

3.2   Methodology

3.2.1   Fourier Transform Infra-Red Spectroscopy (FTIR)

Infra-Red (IR) Spectroscopy is one of the most widely used analytical techniques for fundamental research in determining the structure of samples qualitative as well as quantitatively. IR spectroscopy is known for its versatility due to the ability to analyse various samples ranging from solid, liquid, gas, pastes, fibres, powders, and films ranging from delicate biological samples to hard minerals (Stuart, 2004; Skoog et al., 2007). IR radiation spectrum is ranging from 12800 to 10 cm^{-1} wavenumbers and can be roughly divided into three spectral regions which are near IR, middle IR, and far IR regions as in table 3.3.

Table 3.3: Applications of IR Spectroscopy.

Region	Wavelengths (λ), μm	Wavenumbers (cm^{-1})	Measurement type	Analysis	Applicable samples
Near IR	0.8-2.5	12800-4000	Diffuse reflectance	Quantitative	Solid, liquid
			Absorption	Quantitative	Gaseous mixture
Mid IR	2.5-50.0	4000-200	Absorption	Qualitative	Pure solid, liquid, gas
				Quantitative	Solid, liquid, gas mixture
				Chromatographic	Solid, liquid, gas mixture
			Reflectance	Qualitative	Pure solid, liquid
			Emission	Quantitative	Atmospheric samples
Far IR	50.0-1000.0	200-10	Absorption	Qualitative	Inorganic, organometallic

Absorption, emission, and reflection spectra of IR occurred from the changes in the energy due to the vibrational and rotational energy of molecules. When IR ray is radiated to the samples, functional groups will absorb the radiation at the same wavenumbers range regardless the entire molecule's structure (Smith, 1998) and start to

vibrate. Molecular vibrational frequency is responsible for absorption process. The relationship of frequency and wavenumbers are

$$\text{Wavenumbers (cm}^{-1}) = \frac{1}{\text{Wavelength, } \lambda \text{ (}\mu\text{m)}} \times 10^4 (\mu\text{m cm}^{-1}) = \frac{\text{Frequency (Hz)}}{\text{Speed of light, c (cm s}^{-1})}$$

Correlation between the wavenumbers that being absorbed, band position, and molecular structures allows unknown molecule can be identified.
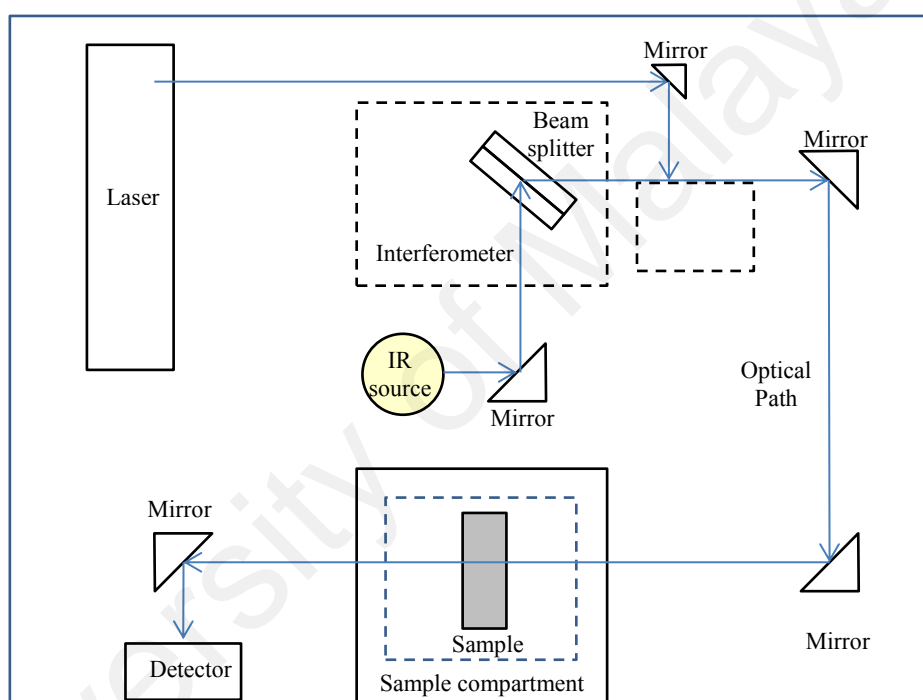
Figure 3.1: Basic diagram of Fourier Transform Infra-Red Spectroscopy (FTIR)

IR absorption can be measured by monochromator grating dispersive spectrophotometers, nondispersive photometers or Fourier transform spectrophotometers pairing with an interferometer (Skoog et al., 2007). Researchers widely use Fourier transform spectrophotometers due to the speed, reliability, signal-to-noise advantage, cheap, and user-friendly (Skoog et al., 2007; Rohman & Che Man, 2011; Depciuch et al., 2016). It is also a non-destructive technique involving a very small amount of sample. Figure 3.1 shows the schematic diagram of FTIR. IR source which is normally silicon carbide, metal carbide or metal filament radiates the

frequency into the interferometer after reflected by the mirror. Interferometers are used to modulate IR radiation from the IR source and red light from He-Ne laser to provide a reference signal for the detector. Modulated radiation is then reflected to the sample in the sample compartment. IR detector will detect the radiation and analysed by the data acquisition system.

IR spectroscopy measurements of fatty acids were analysed with Fourier Transform Infra-Red Spectroscopy (FTIR) Spectrum 400 (Perkin Elmer, USA) in Department of Chemistry, University of Malaya. One hundred µg of sample (0.2% w/w) was measured using AG245 Dual Range Analytical Balance (Mettler Toledo,USA) and added to potassium bromide (KBr) in the mortar and ground to homogeneous at room temperature (Zofka et al., 2013). The mixture was then carefully sandwiched in the 13 mm evacuable potassium bromide die (Perkin Elmer,USA) and transferred onto pistil of the manual hydraulic press (Specac, UK) followed with the manual pump until the pressure reached 10 tons to produce the sample disk of ~13 mm. After a minute, the pressure was released and the sample disk was transferred to IR sample holder. The disk was then scanned for sixteen scans per sample at room temperature within wavenumbers range of 400 to 4000 cm^{-1}. IR spectroscopy of sample was matched to the wavenumbers of every species.

3.2.2 Differential Scanning Calorimetry (DSC)

Differential Scanning Calorimetry (DSC) is a thermal analysis technique that being widely used to measure the temperature and heat flows associated with thermal transitions of the material due to its speed and ease of use (Skoog et al., 2007). DSC has three types of instrumentation which are power-compensated DSC, heat-flux DSC, and modulated DSC which extensively used in many fields including

pharmaceuticals, polymers, food, and electronics (Skoog et al., 2007; Zofka et al., 2013; de Matos et al., 2016; Duh et al., 2016).
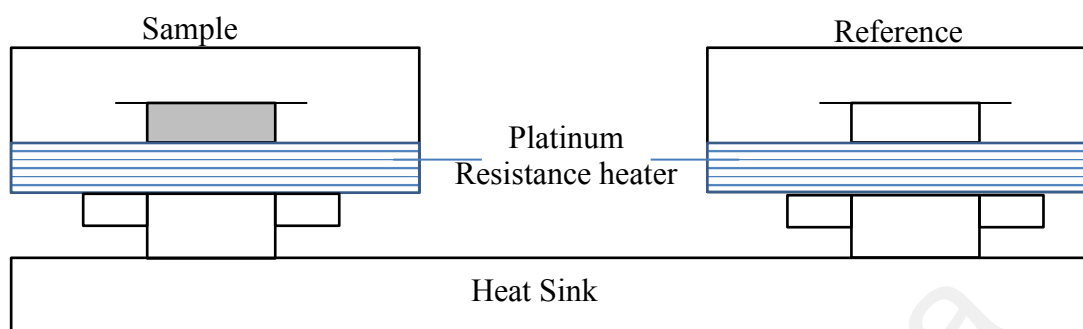
Figure 3.2: Basic diagram of Differential Scanning Calorimetry (DSC).

The sample can either be heated or cooled where the heat flow is recorded as a function of temperature and converted to thermogram. Thermogram or the plots of heat flow versus temperature is generated from the difference in the heat flow between samples and reference which is made from inert materials such as aluminium, platinum, graphite, or gold pan. Figure 3.2 exhibits the diagram of power compensate DSC where two independent units were used. The computerized system will generate the temperature program will control the temperature of sample and reference holders through platinum resistance heater simultaneously in pre-set atmospheric condition such as nitrogen, air, argon, or controlled mixed gas. DSC applying a constant pressure which makes the heat flow can be converted to enthalpy changes through the equation $(\frac{dq}{dt})p = \frac{dH}{dt}$, where $\frac{dH}{dt}$ is the heat flow in unit mcal sec. Hence, the heat flow difference can be positive or negative depends on either it is exothermic or endothermic which can be expressed as $\Delta \frac{dH}{dt} = \frac{dH}{dt} sample - \frac{dH}{dt} reference$. The difference in power needed to equalize the temperature of sample and reference to programmed temperature is converted to DSC signal as a thermogram. The plots in thermogram were further used to determine the changes in heat capacity, boiling point, melting point, glass transition, the stability of crystal, or crystallization temperature.

Thermal behaviour of the samples was analysed using DSC Q20 Difference Scanning Calorimetry (TA Instruments, USA) in Department of Chemistry, University of Malaya. About 5 mg of sample was weighed carefully into the 40 μL Tzero aluminium pans (Menon et al., 2015; Duh et al., 2016), covered with the Tzero Hermetic Lid, and sealed carefully using a Tzero sample press. An empty 40 μL Tzero pans covered with Tzero Hermetic Lids and sealed in the same manner was used as reference pan. Both sample and reference were then transferred onto the platform in the DSC cell. Nitrogen gas with flow rates of 50 mL min^{-1} was used as the atmospheric gas. The DSC was set to equilibrate at -30 °C for one minute with the aid of liquid nitrogen and ramping to 150 °C with ramping rates of 2 °C min^{-1}. Glass transition temperature of the samples was identified from the thermograms.

3.2.3 Acid-Base Titration

Titration curve of acid-base provides very useful information in determining the stoichiometric point of fatty acids (Atkins, 1994) where the amount of acid is the equivalence to the base in the system. Brønstead-Lowry explains an acid as a proton donor, $HA \rightarrow H^+ + A^-$ while a base as a proton acceptor, $B + H^+ \rightarrow BH^+$ (Atkins & de Paula, 2014). Acid and base can be classified as strong or weak depending on the ionization or protonation of the acid or base. A strong acid is a strong proton donor which it ionized completely while a strong base is a strong receptor which protonated completely in the solution.

Fatty acids are weak acid where they are not ionized completely in the solution, hence HA manipulating the solution. Titration of fatty acids with a strong base, NaOH, provides OH$^-$ to the system which contributes to the formation of hydronium ion, H$_3$O$^+$. Acidity constant, $K_a = \frac{[H_3O^+][Base]}{[Acid]}$, can be generated from the equilibrium equation, *Acid (aq) + H$_2$O (l) ⇌ H$_3$O$^+$ (aq) + Base (aq)*. However, acidity constant is more

convenient to be expressed in the logarithms where $pK_a = -\log K_a$. According to the Henderson-Hasselbalch equation, pH of the solution can be calculated from the equation $pH = pK_a - \log \left(\frac{[Acid]}{[Base]} \right)$. At the stoichiometric point of fatty acids, the molar concentration of acid and salt are equal, pH can be defined as pH = pK_a. In a pH curve plot, pK_a can be determined at the half from the neutralization end point (Teo et al., 2011; Chia & Misran, 2013).

In the aim of producing the pH curve, the fatty acid solution was firstly weighed using AA-160 Precision Balance (Denver Instrument, New York) and dissolved in the 0.05 mol dm^{-3} sodium hydroxide (NaOH) solution with stirring followed by bath sonication for one minute until all fatty acid was dissolved producing a colourless stock solution of ionized fatty acid. One mL of stock solution was then transferred into 14 mL glass vials. Various volume of 0.05 mol dm^{-3} hydrochloric acid (HCl) was then added into the different glass vials and marked up with deionized water to a total volume of 5 mL in order to form the solution with various pH. The mixtures were left stirred on a Harmony HTS-1003 Hotplate Stirrer (Laboratory & Medical Supplies, Japan) at room temperature for 24 hours. The pH was later measured by using a PC 510 pH and Conductivity bench meter (Eutech, USA) which was pre-calibrated with pH buffer solution pH 4, 7, and 10 (Mettler-Toledo, USA). The *pKa* of fatty acids was determined from the pH curve.

3.2.4   Tensiometer

The study on the interfacial phenomena plays a major role in determining the effectiveness, the efficiency of surfactant, wetting behaviour and decomposition of materials to be used in wide range of field from engineering to formulation of cosmetic products. Tensiometer provides the information of difference in the intermolecular force experienced by the molecules in the solution.

In a solution, molecules at the surface and molecules in the bulk solution faced a different intermolecular force (cohesive force) where molecules in the bulk faced cohesive force in all direction while molecules at the surface only experience the inward cohesive force (Figure 3.3). This phenomenon can be explained by surface Gibbs energy equation, G (σ) = G – [G (α) + G (β)] where α is a Gibbs energy in the gas phase and β is a Gibbs energy in liquid phase. For a dilute solution at a constant temperature, Gibbs equation for surface tension can be expressed as $\left(\frac{\partial \gamma}{\partial c}\right) T = -\frac{RT\Gamma_s}{c}$, where γ is the surface tension, Γ is a surface excess, T is a temperature, and R is a universal gas constant.
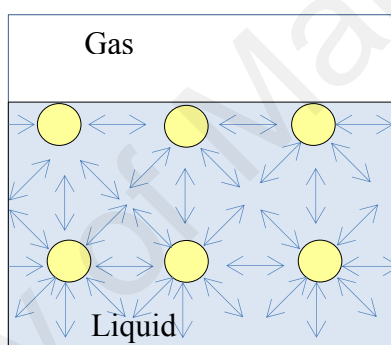
Figure 3.3: Cohesive force experienced by molecules in the solution.

Interfacial tension can be measured by tensiometer using various techniques such as Spinning Drop Tensiometer, Drop Volume Tensiometer, Bubble Pressure Tensiometer, and Force Sensor Tensiometer depends on the phase of the samples. In this research, Force Sensor Tensiometer coupled with Du Noüy ring was used. This tensiometer is suitable for measuring liquid-gas interfacial tension for the samples which have interfacial tension within the range of 1-100 mN m^{-1}.

K100 Force Sensor Tensiometer (Krüss, Germany) from Department of Chemistry, University of Malaya was employed to measure the interfacial tension of the fatty acid solution. Various amount of fatty acid was weighed using AA-160 Precision Balance (Denver Instrument, New York), dissolved in desired buffer solution by sonicating in

JAC 1505 ultrasonicator (JEOI Tech, Japan) for one minute, and stirred using Harmony HTS-1003 Hotplate Stirrer (Laboratory & Medical Supplies, Japan) for 24 hours to produce a homogenous solutions of fatty acid. Forty mL of fatty acid solution was poured into the SV20 fire-proof glass sample vessel (Krüss, Germany) and transferred into the heat-conductive metal aluminium thermostat jacket and leave to equilibrium at 30 °C. The platinum-iridium metal alloy RI01 Du Noüy ring (Krüss, Germany) was pre aligned with TO01 Tools (Krüss, Germany), rinsed with deionized water, followed by ethanol, and burned to red with blue flame Bunsen burner to remove the residue from the ring. The ring was then carefully clamped into the ring holder which located above the thermostat jacket. Detachment force of the ring from the solution was used to calculate the interfacial tension of the solution in ten replicates. The graph of interfacial tension against ln [concentration] was constructed and the inflection point of the graph was identified as the Critical Vesicle Concentration (CVC) point.

3.2.5   Preparation of Liposomes

Preparation of liposomes generally involves hydration of the thin lipid film or cake which later will agitate and self-closed to form a large vesicle entrapping the dispersion media followed with sizing the liposomes to the desired size. Table 3.4 shows the techniques that commonly used in preparing the liposomes (Barenholz & Lasic, 1996).

In this study, liposomes were prepared using pH adjustment technique with the aim of forming the unilamellar vesicle. Fatty acid and other ingredients were weighed using AA-160 Precision Balance (Denver Instrument, New York) and dissolved in 5 mL pharmaceutical grade chloroform ($CHCl_3$) with sonication using JAC 1505 ultrasonicator (JEOI Tech, Japan) for five minute to produce a homogenous mixture. One mL of the lipid mixture was transferred into 50 mL round bottom flask and

connected to R114 rotary evaporator (Büchi, USA) equipped with pre-set water bath of 45 °C to produce the thin lipid (Kanicky & Shah, 2002; Morigaki & Walde, 2007; Teo et al., 2011; Tan & Misran, 2013). When chloroform was completely removed from round bottom flask under reduced pressure, another mL of the lipid mixture was poured into round bottom flask. The step is repeated until all the lipid mixture was poured into the flask and chloroform was completely removed. European Medicines Agency set the guidelines for permitted daily exposure of chloroform is 0.6 mg per day (Bart & Pilz, 2011). Addition of 0.3 mL of 0.05 mol dm^{-3} NaOH, followed with 1 minute sonication ionized the thin lipid. Three mL of buffer solution was then added to the solution followed by adjusting the pH of liposomes solution to the desired pH using 0.05 mol dm^{-3} NaOH or 0.05 mol dm^{-3} HCl. The concentration of salt in the liposomes formulations were controlled to be less than 135-145 mmol L^{-1} which was the normal range of sodium in the blood (Daugirdas et al., 2007; Hale & Hovey, 2013). The liposomes solution was marked up to 5 mL with buffer solution and left for 24 hours prior to use.

Table 3.4: Preparation techniques of liposomes.

Method	Process	Products
Mechanical	Vortexing the phospholipids dispersion	MLV
	Extrusion through polycarbonate filter	OLV, UV
	Extrusion through French pressure cell	SUV
	Micro fluidizer	SUV
	High-pressure homogenization	SUV
	Gas bubbling	BSV
Organic solvent replacement	Removing organic solvent	MLV,OLV,SUV
	Water immiscible solvents	MLV,OLV,SUV
	Reverse-phase evaporation	LUV,OLV,MLV
Detergent removal	Spontaneous fusion	LUV, OLV, MLV
	Freeze-thawing, Freeze drying	MLV
	Dehydration	LUV,OLV,MLV
	Ion induced fusion	LUV,OLV,MLV
	Detergent-induced growth	LUV,OLV
pH adjustment	pH adjustment	SUV, LUV

Abbreviation: MLV= Multilamellar Vesicle (> 0.5 µm), OLV= Oligolamellar Vesicle (0.1-1 µm), UV= Unilamellar vesicle, SUV= Small Unilamellar Vesicle (20-100 nm), BSV= Bubblesomes, LUV= Large Unilamellar Vesicle
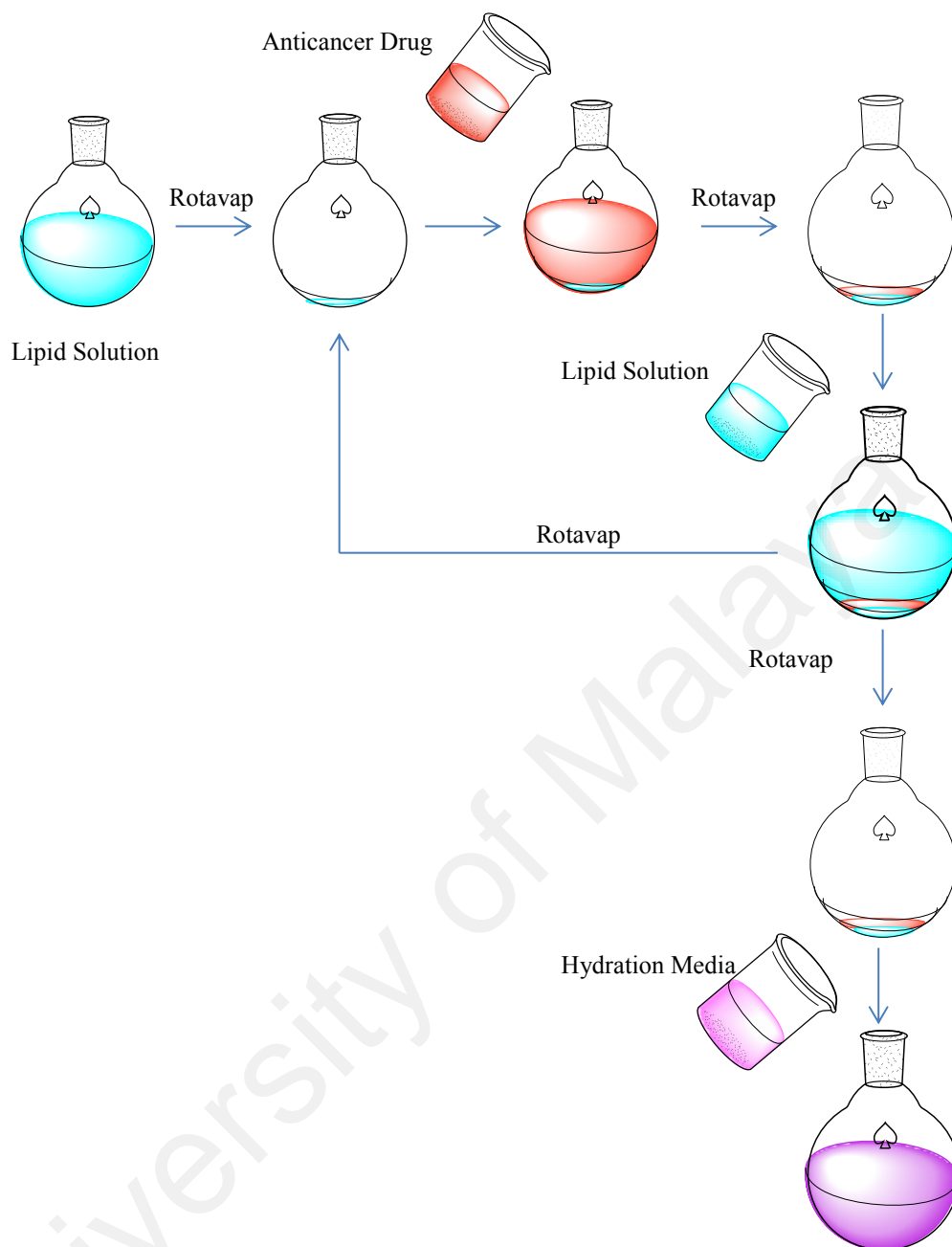
Figure 3.4: Preparation of liposomes encapsulating anticancer drug.

Figure 3.4 show the schematic diagram for preparation of liposomes encapsulating anticancer drug. Lipid and DOPEPEG2000 were mixed with chloroform, and homogenized using JAC 1505 ultrasonicator (JEOI Tech, Japan) for five minutes. Fifty µL of the lipid mixture was transferred into round bottom flask and the chloroform in the mixture was then discarded using R114 rotary evaporator (Büchi, USA) at temperature higher than the T_g of the lipid, forming a lipid thin layer at the wall of the flask. When chloroform was totally removed from the mixture, 50 µL of anticancer drug

solution was carefully inserted on top of lipid thin layer followed by the removal of chloroform. These procedures were repeated until all the lipid mixtures and anticancer drugs were layered, producing the lipid thin layer of many layers. Then, lipid layers were ionized with 50 µL of 0.05 mol dm^{-3} NaOH followed with the hydration medium which was PBS solution. The pH of liposomes solution was adjusted to pH 7.4 by using 0.05 mol dm^{-3} NaOH or HCl. The liposomes encapsulating anticancer drug solution was marked up to 5 mL with PBS and incubated for 24 hours prior to use.

3.2.6   Optical Polarizing Microscope

Polarized light is the light wave which the vibrations occurs in a single plane due to the light was polarized through transmission, reflection, refraction or scattering. Since the discovery of polarized light by Erasmus in 1669 (Goldstein & Goldstein, 2003), polarized light has been used broadly in many fields from astrophysics, chemistry, optics, microscopy (Goldstein-Dennis, 2016), to the production of the 3-D movie. The polarized microscope was previously known as petrographic microscope due to the early applications in mineralogy; however, its application was expanded to diverse fields such as biology, chemistry, and medicine.

Figure 3.5 shows the unpolarised light passing through polarizer A to the sample through the condenser. A sample which having a birefringent property is a perfect sample for polarizing microscope due to the ability to divide the single light to two daughter light through refraction. Birefringent structures in the sample will change the polarization by 90° as shown in the red line. The image of the sample will go through the objective lens to polarizer B and can be observed. The polarizing microscope can be viewed in dark field and light field mode which twisting the polarizer B to 90° will give the dark field mode.
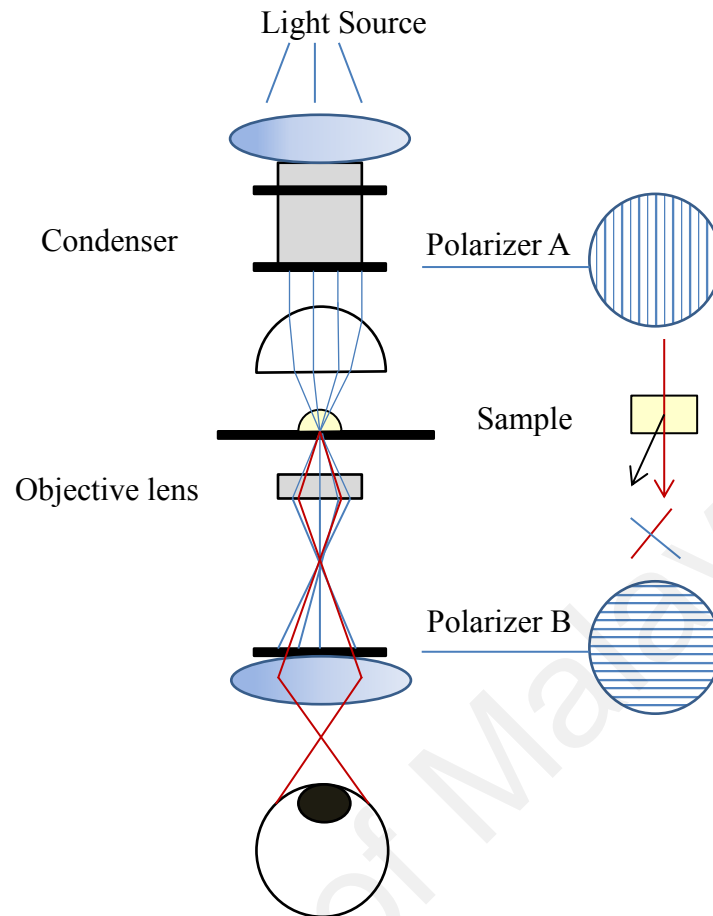
Figure 3.5: Schematic diagram of Optical Polarizing Microscope (OPM).

Polarizing micrograph of liposomes was obtained by employing DMxRP Optical Polarizing Microscope (Leica, USA) equipped with image analysis software Leica QWin (Leica, USA). A drop of liposomes solution was spiked onto clean one mm thick clear glass microscope slides (Sail, China), followed with a clean cover slip (Marienfeld, Germany), and a drop of immersion oil on top of the cover slip. The slide was then transferred to the stage of the polarizing microscope. The sample was viewed through built-in focusing plate dioptre-corrected eyepieces while the rotatable stage was adjusted to align with the optical path of the 50×objective lens (Teo et al., 2011; Tan & Misran, 2013) at 500 times magnification. A polarizer was then adjusted to control the direction of vibrated light. The intensity of light from LED illumination light was adjusted to light up the sample evenly.

3.2.7 High Resolution Transmission Electron Microscopy (HR-TEM)

Electrons can be described as ionizing radiation (Williams & Carter, 2009), which capable to remove the tightly bonded electron by transferring its energy to the atom of the sample and produced the secondary signals (Figure 3.6) that can be detected by most electron microscopy such as AEM, STEM, and HR-TEM. HR-TEM is a powerful instrument for direct imaging of samples up to atomic level. It is widely used to observe biological samples as well as non-biological samples such as semiconductors, graphene, and nanotubes (Williams & Carter, 2009; Tanaka & Iijima, 2014). HR-TEM micrograph provides very useful information on atomic structure up to 0.05 nm and the intensity of electrons at the particular site.
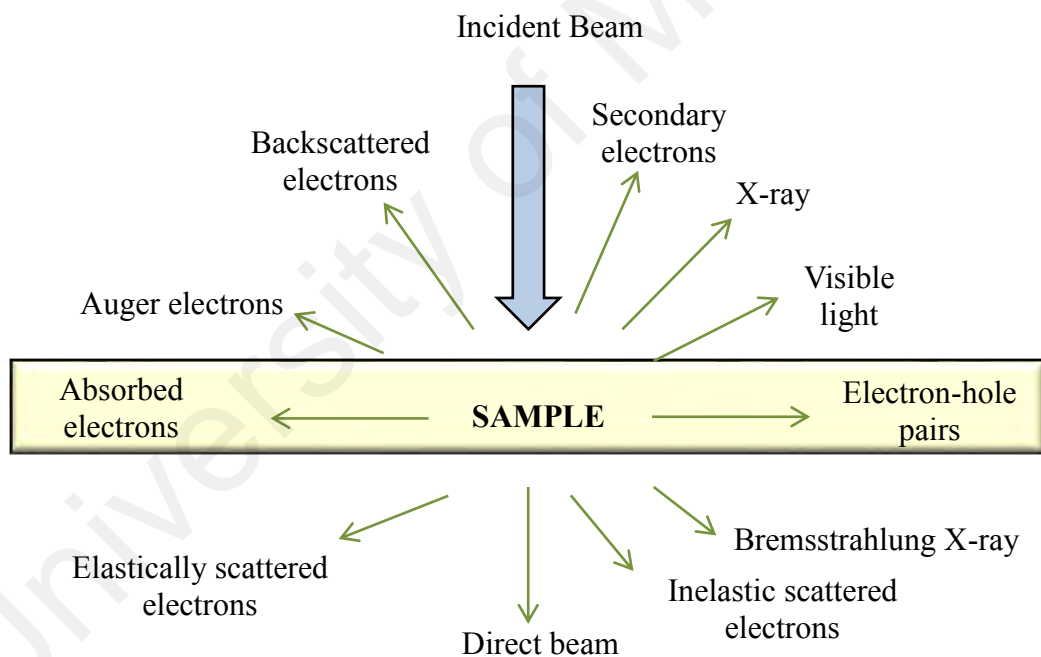
Figure 3.6: Generated signals due to the high energy incident beam.

The morphological structure of the liposomes was observed via computer controlled High Resolution-Transmission Electron Microscopy JEM2100F (JEOL, USA) in the Department of Physics, University of Malaya. One drop of 1 day old liposomes solution was slowly dropped onto a 400 mesh copper-coated carbon grid (Electron Microscopy Sciences, USA) using a disposable pipette and a clean filter paper for removing the

excess solution. A negative staining agent, 3% phosphotungstic acid, was added on to the grid and excess liquid was removed. The grid was air dried for 10 minutes and stored in the 28% humidity Digital Dry Cabinet (Weifo, Taiwan) for 24 hours to remove the excess moisture from the grid. The grid was then transferred onto Poseidon 510 in Situ Electrochemistry Flow Cell Holder (JEOL, USA), clamped, then loaded into goniometer stage, after the green light was lit up. Electron beam was generated at an accelerating voltage of 200 kV by ZrO/W Schottky electron emitter. Illumination and brightness of sample was optimized using condenser lens aperture. The micrograph was taken immediately after the satisfactory replica was observed to prevent liposomes from disintegrating due to exposure at high kV of energy source. Gatan software was used to analyse the micrograph (Gatan Inc,USA).

3.2.8   Zeta Potential and Particle Size

In the colloidal delivery system, evaluation of particle size and zeta potential is very crucial in order to study the precipitation, aggregation, sedimentation, uniformity, and viscosity of the system. Information from particle size and zeta potential analysis will explain the behavioural of the system and effect on the bioavailability of active ingredients.

There are many techniques that being selected by researchers in measuring the particle size of particles such as separation (size exclusion chromatography, centrifugation), microscopic technique (transmission electron microscopy, optical polarizing microscopy), and laser diffraction technique. However, dynamic light scattering (DLS) is the most used technique (Storey & Ymén, 2011) due to its ability to measure up to submicron size. In this approach, the diffusion speed change of laser intensity due to the scattering of Brownian particle can be explained by Stoke-Einstein's equation, $D=\frac{K_B T}{3\pi\eta d}$ where d is a diameter of particle, K_B is a Boltzmann's constant, T is

Kelvin's temperature, and η is dynamic viscosity of the solvent (Duzgunes & Düzgüneş, 2012; Rahman & Ahmed, 2012).

On the other hands, zeta potential also plays a massive role in understanding the colloidal dispersion. Dispersed particles are freely drifted while carrying solvent and a thin layer of ions separated by surface hydrodynamic shear (Figure 3.7). Zeta potential is the difference in potential at this surface and can be measured through the drifting velocity in the electric field. Zeta potential is measured using Laser Doppler Electrophoresis technique by applying the Henry equation, $U_E = \frac{2\varepsilon z f(ka)}{3\eta}$, where U_E is electrophoretic mobility, ε is dielectric constant, z is zeta potential, *f(ka)* is Henry's function while η is viscosity (Rahman & Ahmed, 2012).
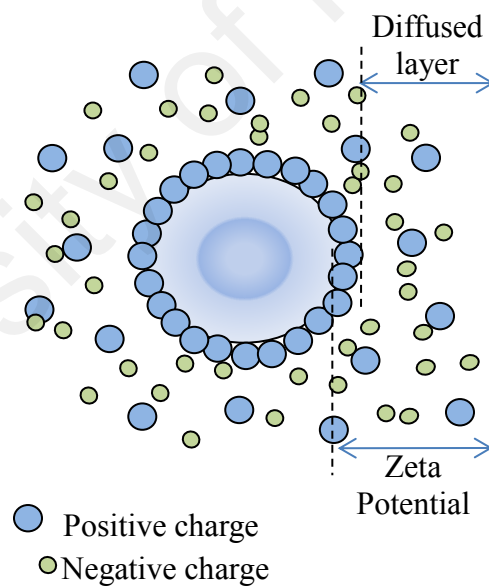
Figure 3.7: Zeta Potential of particles**.**

In this research, zeta potential and particle size of the liposomes were measured using Zetasizer NanoZS (Malvern Instruments Ltd., United Kingdom) in Department of Chemistry, University of Malaya. Liposomes solution was prepared as described earlier. Liposomes were transferred into 1 cm path length four-sided clear fluorescent quartz cuvette (Hellma Analytics, Germany), inserted carefully into the cell area, and analysed

using pre-set standard operation procedure (SOP) for DLS. The attenuator will control the laser beam generated by 4 mW He-Ne laser so that the beam passing through the sample was within the specific range. The scattered light will be detected by backscattered detector at 173° from scattering transmission to avoid the multiple scattering due to laser beam was not travel to entire sample and reduced the scattering of the dust particle. The intensity of scattered beam was then transferred to the correlator and processed with the software.

A DTS 1070 U-shape polycarbonate cell with gold plated electrodes (Malvern Instruments Ltd., United Kingdom) was used to measure the zeta potentials of the sample using their patented M3-PALS® technique that involved the application of phase analysis light scattering. Cell containing liposomes was transferred into cell area and measured using pre-set SOP. The laser beam emitted from 4 mW He-Ne laser was separated into the incident beam for illuminating the sample passing through attenuator and reference beam which will be modulated for undergoing Doppler effect. The scattered beam which forms from the incident beam that passes through the middle of the sample was directed to compensation optic at 17° from the scattering beam. An electric field was then introduced to the sample resulting in the fluctuation of the particle in the sample and drifted to opposite charge electrode. The detector will detect the fluctuation in the frequency of scattered beam and convey the information to the digital signal processor to be analysed by the software. All measurements were carried out in triplicates at 30±1 ºC.

The stability test was carried out by incubating the sample in the 30 °C BM400 incubator (Memmert, Germany) and brought out for measuring the zeta potential as well as particle size within the period of 30 days (Teo et al., 2011).

3.2.9   Ultraviolet-Visible Spectrophotometer

The Ultraviolet-visible spectrophotometer has generally been used in many fields for quantitative determination of organic, inorganic compounds, solvents, and functional groups (Skoog et al., 2007). It is applying the molecular absorption spectroscopy based on electromagnetic radiation within the wavelength of 190-800 nm, where the wavelength region for visible light (VIS) is 400-780 nm, and wavelength region for ultraviolet (UV) is 180-400 nm. The UV radiation can generally separate to three region which is UV-A (315-400 nm), UV-B (280-315 nm), and UV-C (180-280 nm) that is harmful to human health (Manickavasagan & Jayasuriya, 2014). Table 3.5 presents the colours of reflected and absorbed light at the range of UV-VIS range (Clark et al., 1993).

Table 3.5: Apparent colour of materials

Wavelength range (nm)	Colours of reflected light	Colours of absorbed light
400-465	Violet	Yellow-green
465-482	Blue	Yellow
482-487	Greenish blue	Orange
487-493	Blue-green	Red-orange
493-498	Bluish green	Red
498-530	Green	Red-purple
530-559	Yellowish green	Reddish-purple
559-571	Yellow-green	Purple
571-576	Greenish yellow	Violet
576-580	Yellow	Blue
580-587	Yellowish-orange	Blue
587-597	Orange	Greenish blue
597-617	Reddish-orange	Blue-green
617-780	Red	Blue-green

UV-VIS Spectrophotometer employing Beer's law (Skoog et al., 2007; Manickavasagan & Jayasuriya, 2014) in translating the power of the radiation into transmittance and absorbance. Transmittance can be calculated by using the equation, Transmittance, $T = \frac{P_{solution}}{P_{solvent}} \approx \frac{P}{P_0}$, where P and P_0 are the power of radiation passing through cells containing solvent and the analyte respectively. Furthermore,

absorbance (A) of the solution with the path length of b cm can be generated from the transmittance through the equation $A = -\log T = \log\frac{P_0}{P} = \varepsilon b c$, where ε is a molar absorptivity and c is the concentration of the absorber.

UV-VIS Spectroscopy of the samples in this research was obtained by Varians Cary 50 UV-VIS Spectrophotometer (Agilent Technologies, USA) in Department of Chemistry, University of Malaya. In order to calculate the encapsulation efficiency (%EE) of liposomes, UV-VIS spectroscopy technique was explored. Liposomes solution was prepared as mentioned earlier while anticancer drugs were incorporated during the hydration step. One mL of the liposomes encapsulating anticancer drug was then transferred into the Molecular Weight Cut off (MWCO) of 10 000 kDa patented Vivaspin centrifugal unit (Sartorius Stedim, Belgium). Then, Velocity 18R refrigerated centrifuge (Dynamica Scientific Ltd., UK) was used to discard the free drug by centrifugation at 1500 rpm for 15 minutes at 25±1 °C (Ohnishi et al., 2013) as liposomes encapsulating anticancer drug will be retained on top of the membrane. The eluent which was unencapsulated anticancer drugs was then collected, slowly poured into 2 mm internal width, 1 cm path length clear wall quartz Micro Cells 18/Q/10 (Starna Scientific, United Kingdom), and transferred into sample compartment. Quartz cell was very suitable for UV-VIS analysis due to their chemical resistant property and displays high UV transmission achieving 200 nm. The equipped Xenon flash lamp provided UV-VIS radiation of 200-1100 nm, detected by two silicon diode detector, and the UV absorbance of the samples was measured at 200-800 nm. Absorbance of the anticancer drugs was referred to the calibration curve of the drugs at varied concentration. The encapsulation efficiency (%EE) of anticancer drugs incorporated into liposomes can be expressed as $\%EE = [100 - \left(\frac{F}{T} \times 100\right)]$, where F is the amount of free drug while T is the total amount of drugs added.

3.2.10 Franz Diffusion Cell

One of the important key evaluations in drug development is the study of the drug release in the controlled environment. *In vitro* test is often used to verify the quality, stability as well as performance (Levin, 2001) of the product and it is being recognized by U.S. Food and Drug Administration (U.S. FDA) through their well-known Scale-Up and Post Approval Changes (SUPAC) (Shah et al., 2015). There are many apparatus and parameters that should be considerate to mimic *in vivo* condition such as the composition of medium, pH, particle size, and surface charge of drugs and carriers.

The static diffusion cell is one of the most common method that is used in evaluating the *in vitro* drug release (Ng et al., 2010; Shah et al., 2015). This is a simple method that involved two compartments, which are donor and receptor chamber (Figure 3.8). Water jacketed and water bath system was used to maintain the temperature conditioned to mimic site of delivery. Sample at receptor chamber will be collected at certain time point for analysis.
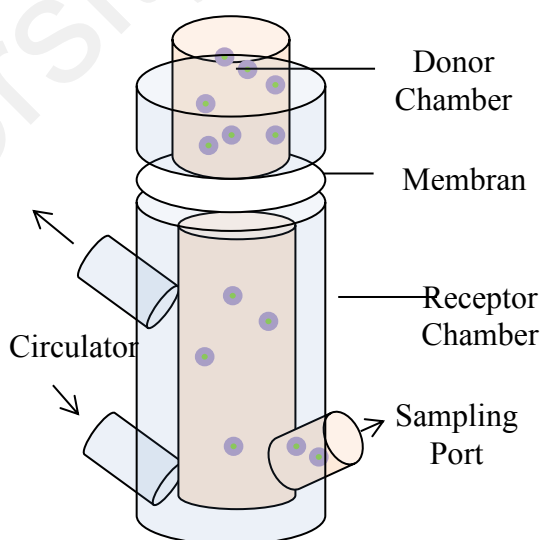
Figure 3.8: Basic diagram of Franz Diffusion Cell.

In this study, Automated Franz Diffusion Cell System (Hanson Research, USA) in Department of Chemistry was employed in order to observe the in vitro release of anticancer drugs encapsulated in the liposomes. Five kDa MWCO high permeable

cellulose dialysis membranes (The Nest Group Inc, USA) which is suitable to the particle size and molecular weight of liposomes and anticancer drugs, was cut to 25 mm diameter and pre-equilibrated in 0.01 mol dm^{-3} phosphate buffered saline (PBS) at room temperature for 24 hours before every experiment. The receptor chamber was filled with 0.01 mol dm^{-3} PBS, slowly covered with dialysis membrane to avoid the formation of bubbles, and wiped out the excess PBS using the delicate task wipers (Kimwipes, USA). The receptor chamber was then covered with donor chamber, sealed using C-shaped pinch clamp, and continuously stirred at 400 rpm with the controlled temperature of 37±1 ºC by a water bath (Polyscience, USA).

An amount of one mL of liposomes encapsulating anticancer drugs was transferred into the donor chamber using a pipette, covered tightly, and covered with aluminium foil to prevent the sample from degradation due to light. Franz diffusion cell was set to collect 1 mL of eluent from the receptor chamber into 1.5 mL amber glass short thread HPLC/GC certified vial and replaced with equal volume of pre-thermostated fresh PBS at 37±1 °C at intervals of 0.5, 1, 2, 4, 6, 8, 10, 12, 16, 20, and 24 hours. The sample collected from the Franz Diffusion Cell was then analysed directly using UV-VIS Spectrophotometer (Agilent Technologies, USA) as described above to prevent the degradation of anticancer drugs.

The release of anticancer drugs from liposomes was then fitted into 5 mathematical modelling which is zero order, first order, Higuchi, Korsmeyer-Peppas, and Gompertz dissolution models to measure physical parameters such as the drug diffusion coefficient, model fitting, then understands the factors affecting drug release kinetics (Costa & Lobo, 2001). Table 3.6 shows the equations that being used to evaluate and compare the dissolution profiles of liposomes encapsulating anticancer drugs.

Table 3.6: Equations for dissolution profiles modelling.

Dissolution Model	Equation	Remark
Zero Order	$Q_t = Q_0 + K_0 t$	Q_t = amount of anticancer drug dissolved in time t Q_0 = initial amount of anticancer drug in the solution (most times, Q_0=0) K_0 = zero order release constant expressed in units of concentration/time t= time
First Order	$log\, Q_t = log\, Q_0 + \dfrac{K_1 t}{2.303}$	Q_t = amount of anticancer drug dissolved in time t Q_0 = initial amount of anticancer drug in the solution (most times, Q_0=0) K_1 = first order release constant t= time
Higuchi	$f_t = K_H t^{\frac{1}{2}}$	K_H = Higuchi dissolution constant t = time
Korsmeyer-Peppas	$\dfrac{M_t}{M_\infty} = K t^n$	$\dfrac{M_t}{M_\infty}$ = fraction of anticancer drug released at time t K = release rate constant n = release for cylindrical shaped matrices *only 60% of first release data is used (Costa & Lobo, 2001)
Gompertz	$X(t) = X_{max} \exp[-\propto e^{\beta \log t}]$	$X(t)$ = percent dissolved at time t divided by 100 Xmax = maximum dissolution α = undissolved proportion at time t=1 and described as scale parameter β = dissolution rate per unit of time described as shape parameter t = time

3.2.11 Cell Culture

Cell culture can be described as growing of cells that have been removed from animal or plant in their favourable controlled artificial environment which is outside their natural environment. Cell culture research is practiced extensively throughout the globe and ignited various field of studies such as genetic engineering, protein chemistry

and chemical engineering. Cell culture technology has been evolved and successfully produced viral vaccines, cytokines, growth hormones, monoclonal antibodies (Langdon, 2004), as well as cell and gene therapy (Ozturk & Hu, 2005).

Cells can be divided into two major shapes which are fibroblast or epithelial (Adams, 1990), however, the shape is varied with the medium, density as well as the tissue source. They may exist as suspension or adherent to the substrate (Table 3.7). Generally, cell culture involves several important basic techniques such as sterilization, thawing and freezing, subculture, cloning, measuring cell growth, viability, and the starting primary culture.

Table 3.7: Comparison of adherent to suspension cell culture.

Adherent cell culture	Suspension cell culture
Suitable for most cell line including primary cell line	Suitable for non-adhesive cell line and the cell that adapted to suspension culture media
Requires periodic passaging	Easier to passage by diluting to encourage growth
Easy observation using inverted light microscope	Not easy to observe using inverted light microscope
Cells detached by mechanical or enzymatic detachment such as trypsin, dispase	Does not need any mechanical or enzymatic detachment techniques
Surface area limiting the cell growth	Concentration of cell limiting the cell growth
Need tissue culture treated vessel	Does not need tissue culture treated vessel, but have to shake or stir to get enough gas exchange

In this study, Homo sapiens lung carcinoma cell lines (A549), which obtained from ATCC, USA, was used. All equipment and solution were autoclave and disinfected with 70% ethanol. DMEM supplemented with 10% FBS and 1% Penicillin-Streptomycin-Glutamine were warmed up in the water bath at 37 °C and the cell culture hood was disinfected with 70% ethanol to maintain the sterility of the cell culture hood. Cells were thawed rapidly in water bath 37 °C until the whole content in the vial completely dissolved to avoid cell injury by ice crystal. The cryovial was then clean with

70% ethanol before opening the vials in culture hood to prevent contamination. The cells solution was transferred into 15 mL centrifuge tube and centrifuged at 1500 rpm for the period of 5 minutes. The culture media was carefully removed out from centrifuge tube using an aspirator to prevent the cell pellet from being disturbed. The cell pellet was then re-suspended with 1 mL culture medium using 5 mL disposable pipette. The cell was then immediately cultured into petri dish that contains pre-incubated 9 mL culture media, cover the lid, and incubated the petri dish in 5% CO_2 incubator at 37 °C to allow the cell to attached and spread. The petri dish was observed every 24 hours using an inverted light microscope. The culture media was changed every 48 hours and the confluent monolayer of the cell was detached using trypsinization method for sub culturing and cryopreservation.

3.2.12   Cytotoxic Assay

There is a rise in awareness to study the cytotoxicity effect of the product towards the cells due to this pre-screening steps can ensure that the products that were developed are effective and marketable. Cytotoxicity test involved the measure of the ability of the products such as drugs, detergents, cosmetics, or preservatives (Adams, 1990) to destroy the living cell either through the accident death (necrosis) or programmed death (apoptosis). Accurately measuring cell cytotoxicity of anticancer drugs towards cancerous cell will be a valuable tool to identify the dosage and drugs to be used in cancer therapy.

Generally, the procedure is exposing the cell to a range of different concentration of products and tested for a certain period. The number of cell survived or death which indicates cell cytotoxicity/viability is measured. Various approached has been used in order to determine the cytotoxicity assay by measuring the adenosine triphosphate (ATP) level (Riss et al., 2011; Sorichetti et al., 2014), co-enzyme secretion, nucleotide

uptake activity, protease biomarkers (Quail & Joyce, 2013), or application of vital dyes such as colony formation method using trypan blue and detection formation of formazan using WST or MTT assay (Riss et al., 2011; Stockert et al., 2012; Mullick-Chowdhury et al., 2013; Boeckel et al., 2014).

MTT (3-[4,5-dimethylthiazol-2-yl]-2,5-diphenyltetrazolium bromide) assay technique was employed to quantify the changes in a number of cells regarding the cytotoxicity of the medium (Sun et al., 2015; Yang et al., 2015). The cells density of 0.5×10^5 cells in 0.1 mL growth medium were seeded in 96 wells plate and allowed to attach for 24 hours in 5% CO_2 incubator at 37 °C. The cells then treated with 100 µL of various concentrations of liposomes, anticancer drugs, or liposomes encapsulating drugs. After 24 hours, cells were washed with 100 µL PBS using a micropipette, replaced with 100 µL fresh culture medium, and treated with 15 µL of 5 mg mL^{-1} of MTT in PBS solution in a dark culture hood. The 96 wells plate was then incubated in 5% CO_2 incubator at 37 °C for 4 hours. The metabolically active cell will reduce the MTT into blue formazan crystal. The formazan was dissolved with 100 µL of dimethyl sulfoxide (DMSO). The cells were further incubated for 12 hours and the UV absorbance of the cells treated with liposomes, anticancer drugs, liposomes encapsulating anticancer drugs, and control were measured using multi-mode microplate reader (SpectraMax®, USA) at the wavelength of 575 and 650 nm. The half maximal inhibitory concentration (IC_{50}) value towards A549 cells was determined. All experiments were carried out in Esco Airstream® Class II Biological Safety Cabinet.

CHAPTER 4: RESULTS AND DISCUSSION

4.1   Fourier Transform Infrared (FTIR) Spectroscopy

Vibrational spectroscopy such as infrared (IR) spectroscopy has been extensively used as a routine test in lipid analysis as compared to other vibrational techniques such as mass spectrometry (MS), Raman, and nuclear magnetic resonance (NMR) (Cross, 1998) due to their simplicity and straightforward interpretation of spectroscopy. Mid IR spectroscopy is mostly applied by lipid researchers regarding most organic and inorganic molecules absorbed the radiation within the wavelength range from 400 to 4000 cm^{-1}. It also provides information on "fingerprints" that can be explored for identification and quantification of functional groups in the lipids.
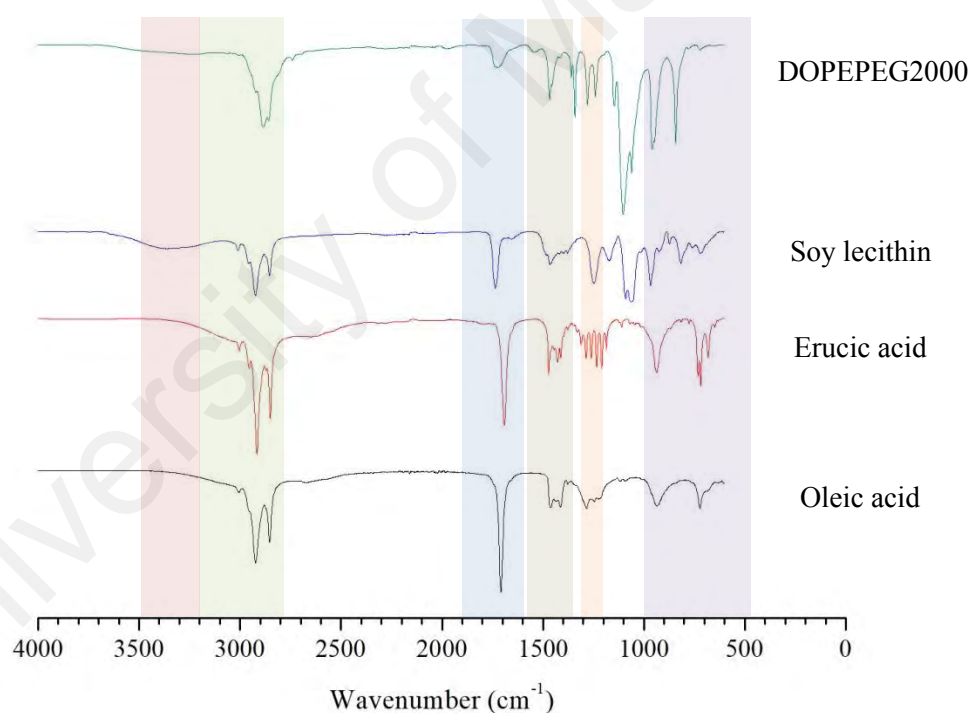
Figure 4.1: Comparison of FTIR spectra for oleic acid, erucic acid, soy lecithin, and DOPEPEG2000.

FTIR is normally employed to provide spectral details indicating some similarities from one to another during raw material analysis, quality control, characterization, and identification of extract product in the fats and oil industry. Figure 4.1 displays the FTIR spectrum of lipids that were used to prepare liposomes. The O-H stretch at 3200 to

3400 cm^{-1} was detected in soy lecithin and DOPEPEG2000. The sharp peak within 2800 to 3100 cm^{-1} in all samples was attributed to the stretching of C-H bond. The stretching of C=O and C-O bonds at 1600 to 1800 cm^{-1} and 1210-1320 cm^{-1}, respectively, was found in all samples. Multiple bands at 1400 to 1600 cm^{-1} in all samples were due to the stretching of C=C band. Several peaks around the wavenumbers ranging from 1000 to 500 cm^{-1} were due to the fingerprints region that generally not useful for the determination of functional groups.

Figure 4.2 (a) displays the FTIR spectroscopy of pure oleic acid. A peak at 722 cm^{-1} was attributed to the C-H groups of alkanes in oleic acid (Singh et al., 2016). The characteristic peaks at 1119 cm^{-1} was assigned to the stretching vibration of C-O in alcoholic C-O-H bond (Chylińska et al., 2016; Ma et al., 2016). The characteristic absorption at 1284 cm^{-1} was due to the C-O stretching (Tariq et al., 2011). Peak at 1461 cm^{-1} that attributed to the asymmetric COO^{-} was observed (Varga et al., 2013; Singh et al., 2016). The sharp peak at 1708 cm^{-1} was appeared corresponding to the stretching vibration of C=O in free COOH group (Ma et al., 2016; Singh et al., 2016) which normally used to measure the acid value (AV) of edible oils (Jiang et al., 2016). The peaks at 2853, 2922, and 3005 cm^{-1} were due to the symmetric and asymmetric stretching vibrations of C-H bands of a methylene group in oleic acid (Deygen & Kudryashova, 2016; Muthukumaran & Philip, 2016; Singh et al., 2016).

Figure 4.2 (b) shows spectroscopy from FTIR for erucic acid. The bending vibration of CH$_2$ was detected from the peaks 718 and 1208 cm^{-1} (Tariq et al., 2011). The peaks at 1044 and 1330 cm^{-1} indicated the vibration of C-O in C-O-H bond (Ma et al., 2016) for both symmetric and asymmetric axial stretch (Tariq et al., 2011), while the peaks at 1411 and 1427 cm^{-1} were appeared due to the stretching of C-O bond (Ma et al., 2016; Muthukumaran & Philip, 2016). Deformation bending vibration of O-H

(Chylińska et al., 2016) and C-H bond (Varga et al., 2013) were detected at peak 1691 and 1471 cm^{-1} respectively.
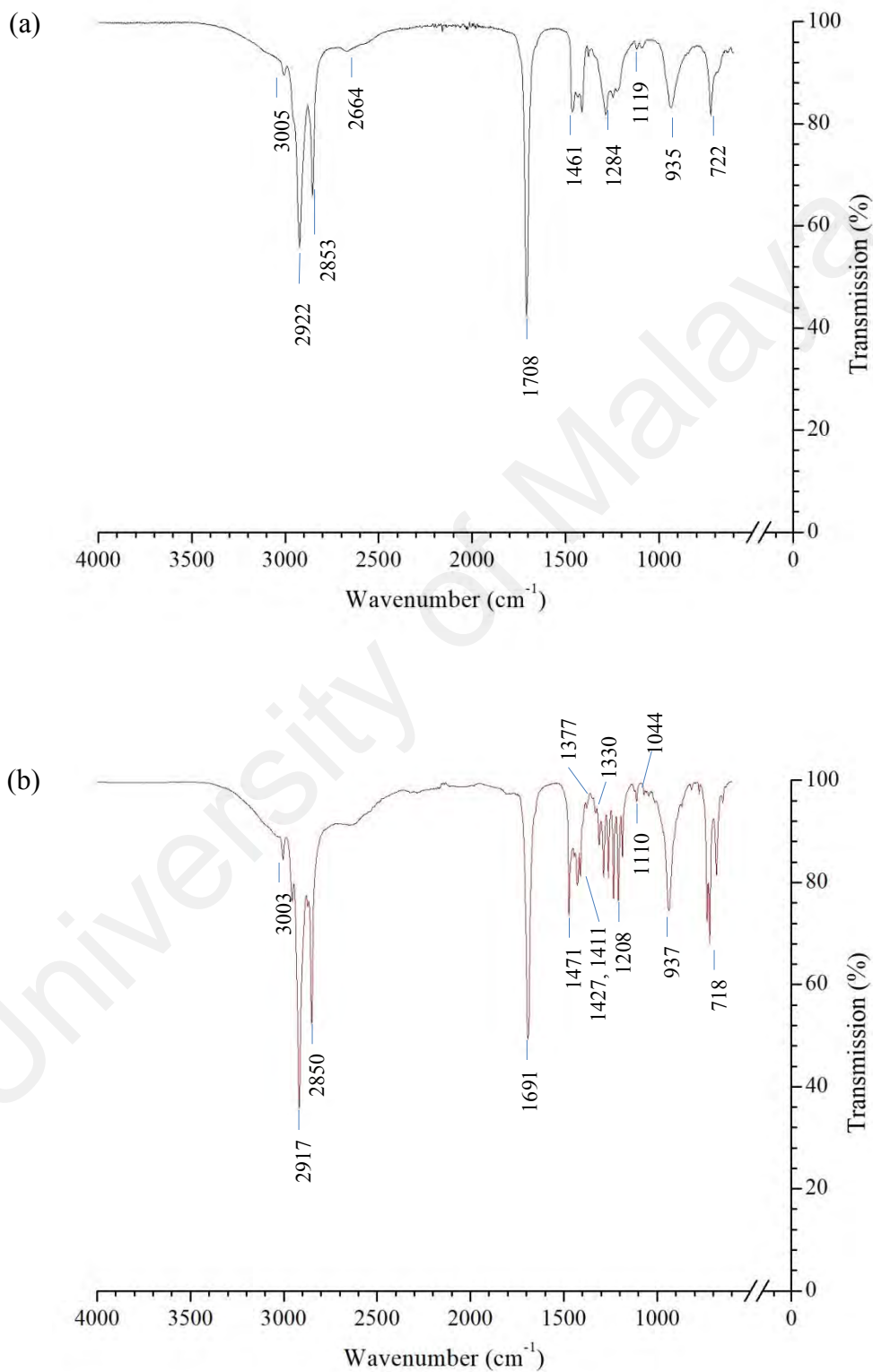
Figure 4.2: KBr-FTIR spectra of pure oleic acid (a) and erucic acid (b).

The peaks at 2917 and 2850 cm^{-1} in Figure 4.2 (b) were attributed to the stretching vibration at CH, CH$_2$ and CH$_3$ of 22 carbon atoms in the erucic acid chain (Tariq et al., 2011), while the vibration of the methylene group appeared at 1377 cm^{-1} (Deygen & Kudryashova, 2016). The peak at 3003 cm^{-1} was due to the symmetric and asymmetric stretching vibrations of C-H bands of the methylene group in erucic acid (Deygen & Kudryashova, 2016; Muthukumaran & Philip, 2016; Singh et al., 2016).

The bending vibrations of methylene group in soy lecithin at 719 and 1378 cm^{-1} were exposed in Figure 4.3 (Tariq et al., 2011; Deygen & Kudryashova, 2016). The stretching vibration of P=O and P-O group appeared at 924 cm^{-1} (Muthukumaran & Philip, 2016). The sharp peaks at 967 and 1061 cm^{-1} were attributed by the symmetric and asymmetric stretching vibration of C-O-C in addition to the alcoholic group of C-O and C-O-H (Varga et al., 2013; Chylińska et al., 2016; Ma et al., 2016). A C-H bending vibration of alkyl chain peak (Varga et al., 2013) was observed at 1463 cm^{-1} while O-H bending mode was observed at 1651 cm^{-1} (Yang et al., 2010; Chylińska et al., 2016). The absorption band of the carbonyl group was arising at the peak of 1735 cm^{-1} (Tariq et al., 2011; Varga et al., 2013) while the methylene peaks were observed at 3010, 2923, and 2853 cm^{-1} (Deygen & Kudryashova, 2016). Strong intramolecular hydrogen bonding in soy lecithin molecule was detected from the stretching vibration of O-H group at 3344 cm^{-1} (Ma et al., 2016; Singh et al., 2016).

FTIR spectroscopy of DOPEPEG2000 is presented in Figure 4.4, where the peak at 1102 cm^{-1} was the characteristic peak for stretching in C-C, C-O, and C=O bonds as well as bending vibration in C-C and C-O bonds (Tariq et al., 2011; Varga et al., 2013; Chylińska et al., 2016; Muthukumaran & Philip, 2016). The absorbance band at 1146 cm^{-1} was the main characteristic of polyethylene glycol (PEG) molecules (Deygen & Kudryashova, 2016), which can be further used for determination either it was related

to trans conformation or gauche conformation with respective to C-C bond (Varga et al., 2013).
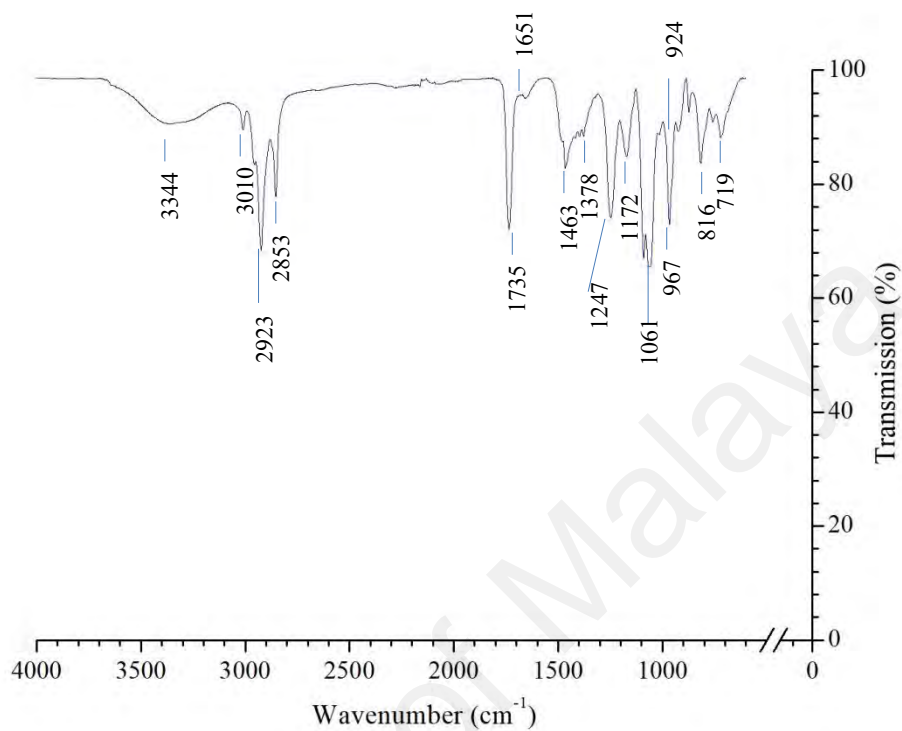
Figure 4.3: KBr-FTIR spectra of soy lecithin.
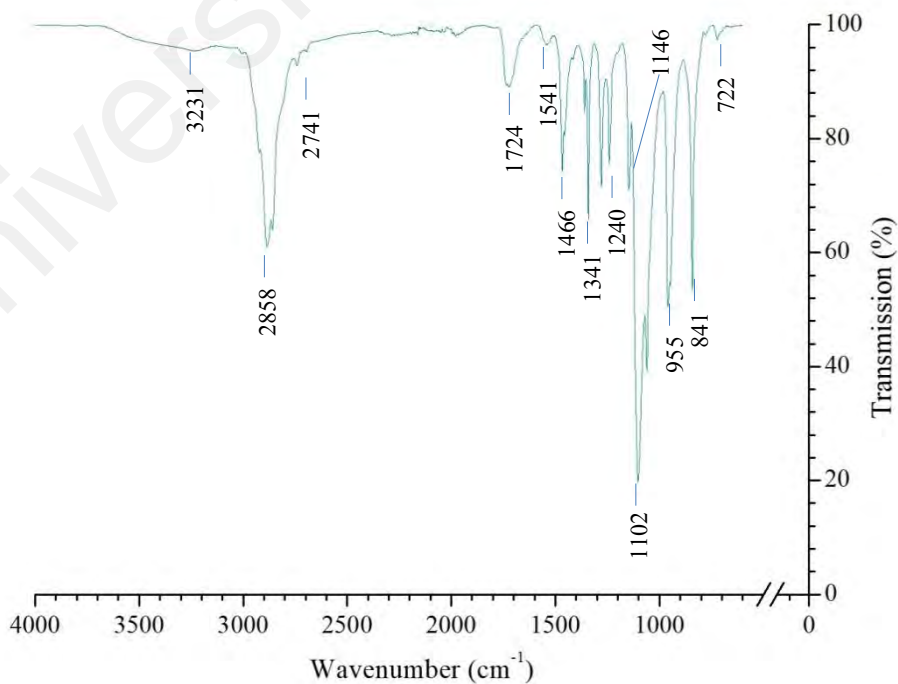
Figure 4.4: KBr-FTIR spectra of DOPEPEG2000.

The asymmetric PO_2^- stretching region can be detected from the peak at 1240 cm^{-1} (Varga et al., 2013; Muthukumaran & Philip, 2016), however, in the fully hydrated state, this peak was reported to shift to 1222 cm^{-1} (Varga et al., 2013). The strong peak at 1724 cm^{-1} was due to the stretching vibration of C=O bond in DOPEPEG2000 (Tariq et al., 2011; Varga et al., 2013; Singh et al., 2016). The peaks at 2741 and 2858 cm^{-1} were attributed to stretching vibration from the methylene group (Yang et al., 2010; Deygen & Kudryashova, 2016). The O-H group stretching vibration was shown with the presence of blunt peak at 3231 cm^{-1} (Ma et al., 2016; Singh et al., 2016).

4.2 Differential Scanning Calorimetry (DSC)

Over fifty years, it is known that differential scanning calorimetry (DSC) has an important role in lipid analysis in order to understand the heat related phenomena such for instance melting and crystallization (Chiavaro, 2014). DSC thermograms provide useful information on thermal properties of lipid and thermodynamic characteristics that can be applied in the quantitative and qualitative identification of lipid.

Table 4.1: Glass transition temperatures, T_g of lipids used to prepare the liposomes

Sample	Glass Transition Temperature, T_g (°C)				Melting Temperature
	T_g half extrapolated tangent	T_g inflection	T_g half height	T_g half width	Peak Temperature (°C)
Oleic acid	-	-8.7	-8.8	-8.8	18.6
Erucic acid	12.7	11.7	12.3	12.3	46.7
Soy Lecithin	69.9	77.5	75.0	75.1	-
DOPEPEG2000	-	-2.1	-1.5	-1.4	62.4

Figure 4.5 and 4.6 represent the thermogram for oleic acid, erucic acid, soy lecithin, and DOPE-PEG2000 measured at -20 to 120 °C. Glass transition temperature (T_g) of oleic acid, DOPEPEG2000, soy lecithin, and erucic acid are displayed in Table 4.1. At these temperatures, the samples lose their ordered glass-like properties (Crompton, 2006), where the hydrocarbon chains are fully extended and closely packed to become a disordered liquid crystalline phase, the hydrocarbon chains are randomly oriented, and fluid. During this transition, the stress relaxation where Young's and shear modulus,

specific heat, the coefficient of expansion, and dielectric constant were changed abruptly.

Inset figures show the melting point temperature, T_m, of oleic acid, erucic acid, and DOPEPEG2000 at 18.6, 46.7, and 62.4 °C, respectively. Unsaturated fatty acid, oleic acid has the T_m lower than the room temperature, hence it appeared as a viscous liquid at the room temperature. These sharp endothermic peaks were assigned to the melting of non-polar hydrocarbon tail of surfactants and forming a liquid crystal (Balanč et al., 2016). However, soy lecithin showed a blunt T_m peak at 85.0 °C due to the transition in the carbon-hydrogen in soy lecithin chain (Balanč et al., 2016), which was comparable with the result reported by Vijayakumar and co-researchers (Vijayakumar et al., 2016).

Determination of glass transition temperatures, T_g, for surfactants was very crucial for preparation of liposomes in order to produce the small unilamellar liposomes as the temperature that being used to prepare liposomes had to be higher than the T_g of the surfactants (Testa, 2001) due to the steric arrangement of surfactant in the bilayer was temperature-dependent. There are several factors which directly affect the phase transition temperature including hydrocarbon length, unsaturation, charge, and head group species.
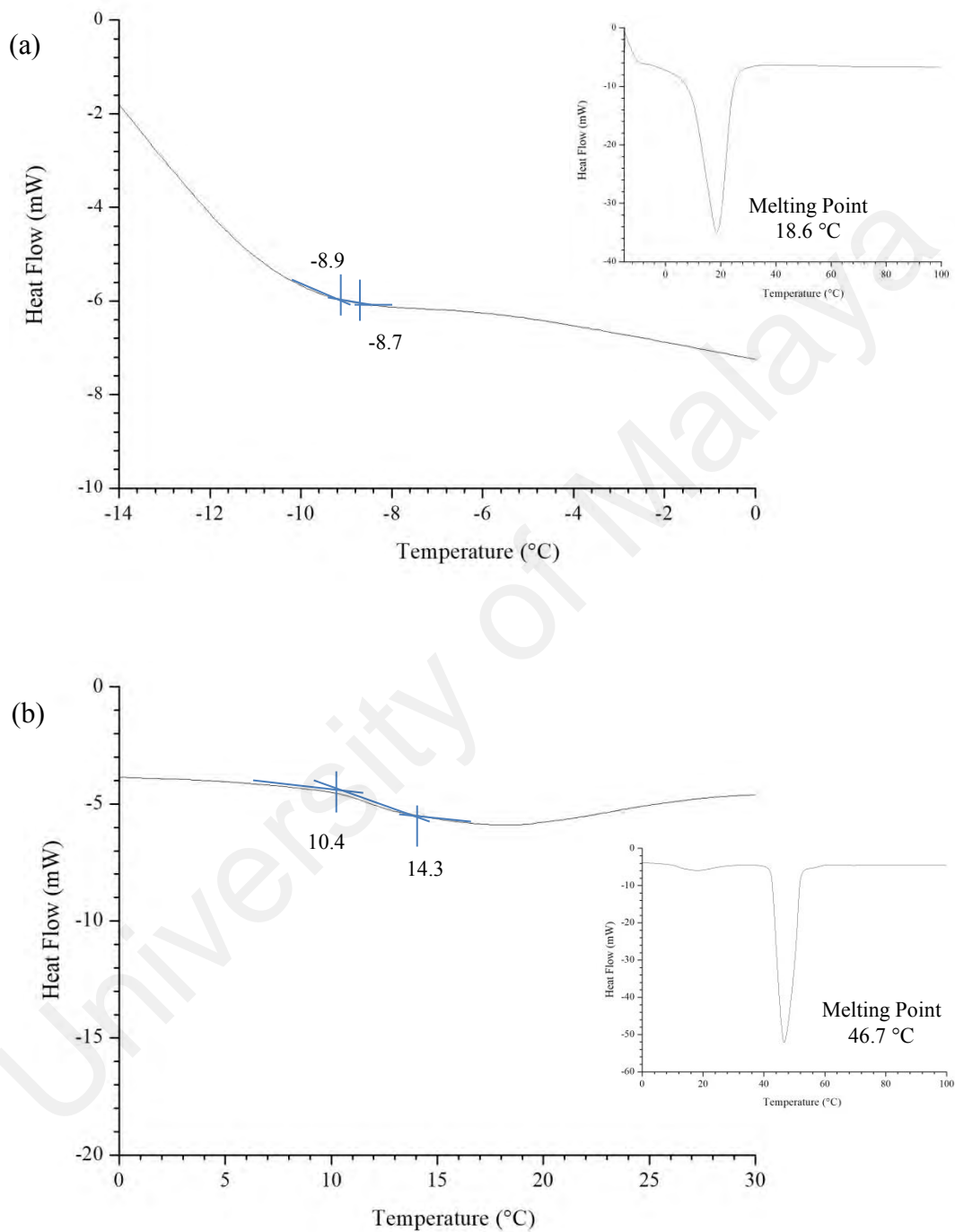
Figure 4.5: Differential scanning calorimetry (DSC) thermograms of oleic acid (a) and erucic acid (b).
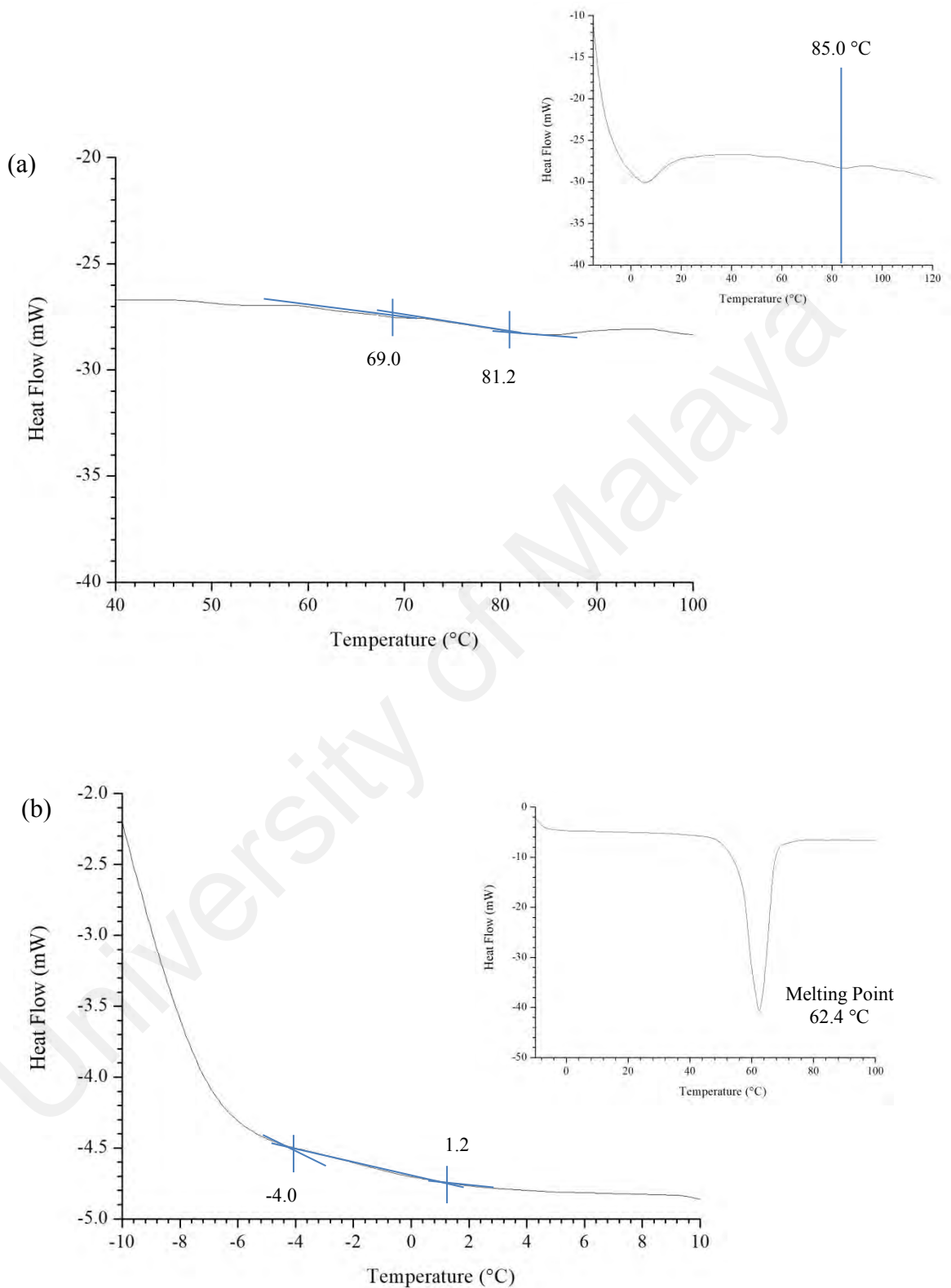
Figure 4.6: Differential scanning calorimetry (DSC) thermograms of soy lecithin (a) and DOPEPEG2000 (b).

4.3 Equilibrium Curve of Surfactant

Titration is the most convenient method for determining the formation of high water content liposomes (Gregoriadis, 2016). The pH adjustment technique is the popular technique that was employed by many researchers due to the simplicity and ability to produce a stable (Cistola et al., 1988), high curvature liposomes spontaneously (Kreuter, 1994) just by altering the protonation/ionization ratio of the OH-group (Fameau et al., 2014).

The experiment was carried out by introducing the hydrochloric acid into the fully ionized surfactant solution (Teo et al., 2011), left 24 hours at room temperature then the pH of the solution was measured using pre-calibrated pH meter. The mixture was left overnight due to the formation of liposomes consumed long time due to assembly and disassembly of molecules (Morigaki et al., 2003; Chen & Szostak, 2004; Rogerson et al., 2006), unless the introduction of external perturbation was done on to the solution (Morigaki et al., 2003). As 0.05 mol dm^{-3} hydrochloric acid (HCl) was added to the solution, an ionized surfactant solution was protonated and forming liposomes at the equal concentration of ionized and non-ionized species in the solution.

Figure 4.7 shows the equilibrium titration curve of oleic acid at room temperature. At pH higher than pH 11, the solution of ionized oleic acid was clear transparent colour due to the ionic repulsion between the adjacent ionized oleic acid head groups (Chen & Szostak, 2004). At high ionization energy of oleic acid, the spherical or worm like micelles (Fameau et al., 2014) were the dominating aggregate in the solution (Morigaki & Walde, 2007). Determination of critical micelle concentration (CMC) of oleic acid in NaOH had been done by measuring the absorbance at 612 nm from the various concentration of oleic acid solution containing 0.01 mmol dm^{-3} methylene blue.

The inflection point represented the formation of micelles in the solution which showed the CMC value of 1 mmol dm^{-3} at 30 °C.
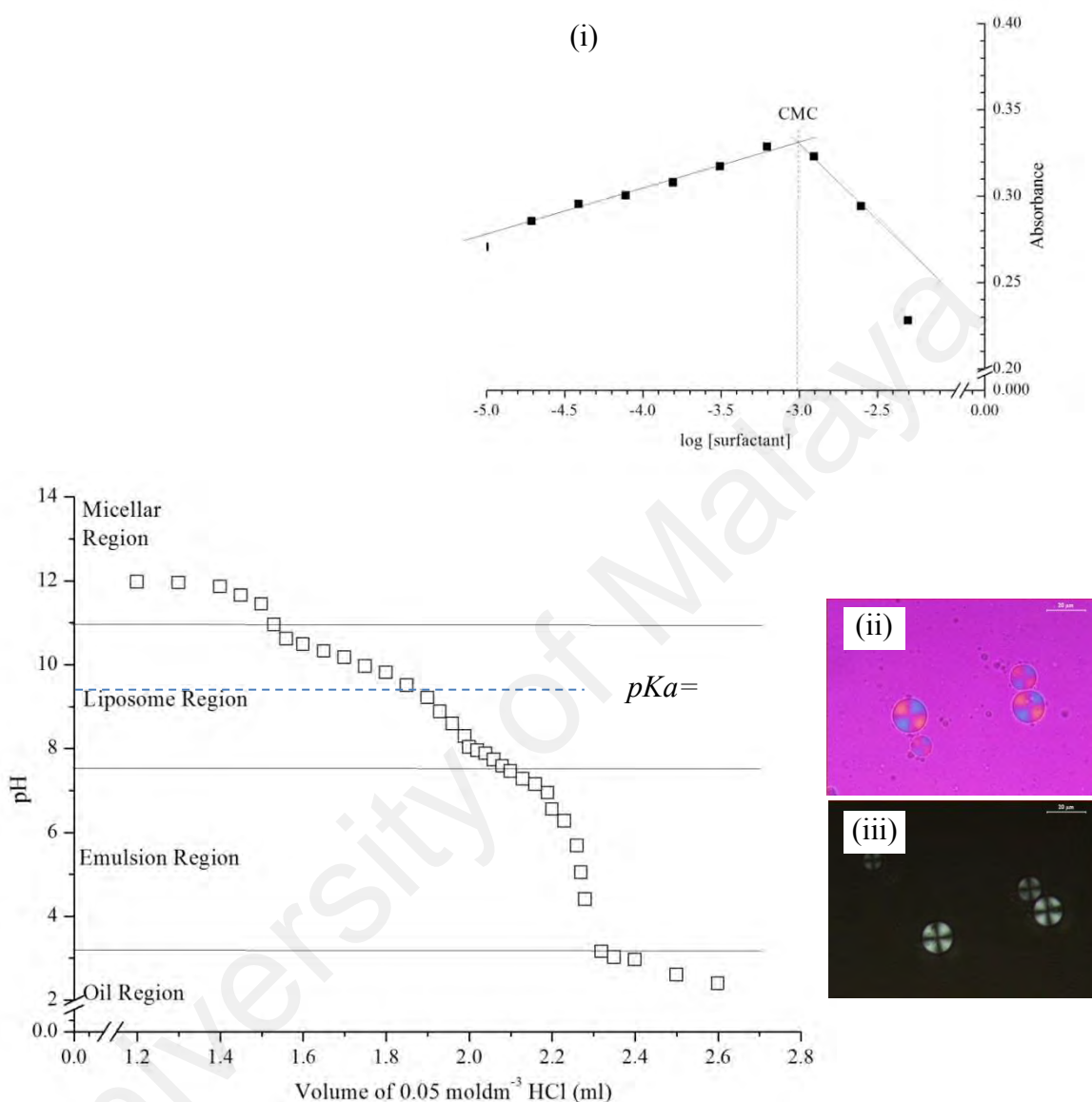
Figure 4.7: Equilibrium curve of oleic acid, as a function of added 0.05 mol dm^{-3} HCl. The insets were (i) the determination of critical micelle concentration and micrograph of liposomes as viewed in (ii) light and (iii) dark phase with 20 μm scale. All measurements were done at 30 °C.

The addition of HCl protonated the ionized oleic acid and reduced the pH of the solution. However, the pH was decrease and reaches a plateau at pH around 11, after addition of 1.30 mL 0.05 mol dm^{-3} HCl. Further protonating the oleic acid reduced the pH of the solution as a result of the protonated oleic acid which makes the oleic acid monolayer packed closer to each other (Kanicky & Shah, 2002). When the ionized and

non-ionized species of oleic acid in the solution were approaching equimolar, the cylindrical pseudo-double-chain amphiphile was formed through hydrogen bonding. This ionic pair had a smaller head group as compared to oleic acid monomer (Teo et al., 2011), hence they will spontaneously form the liposomes to minimize the energy. Further addition of HCl until 2.20 mL, ionized oleic acid was protonated which can be observed through the formation of oleic acid crystals and emulsion at pH 6.55. The pK_a of oleic acid calculated as the half from the neutralization endpoint was 9.21 (Kanicky & Shah, 2002), which was comparable to previous studies from various researchers (Kanicky & Shah, 2002; Teo et al., 2011).
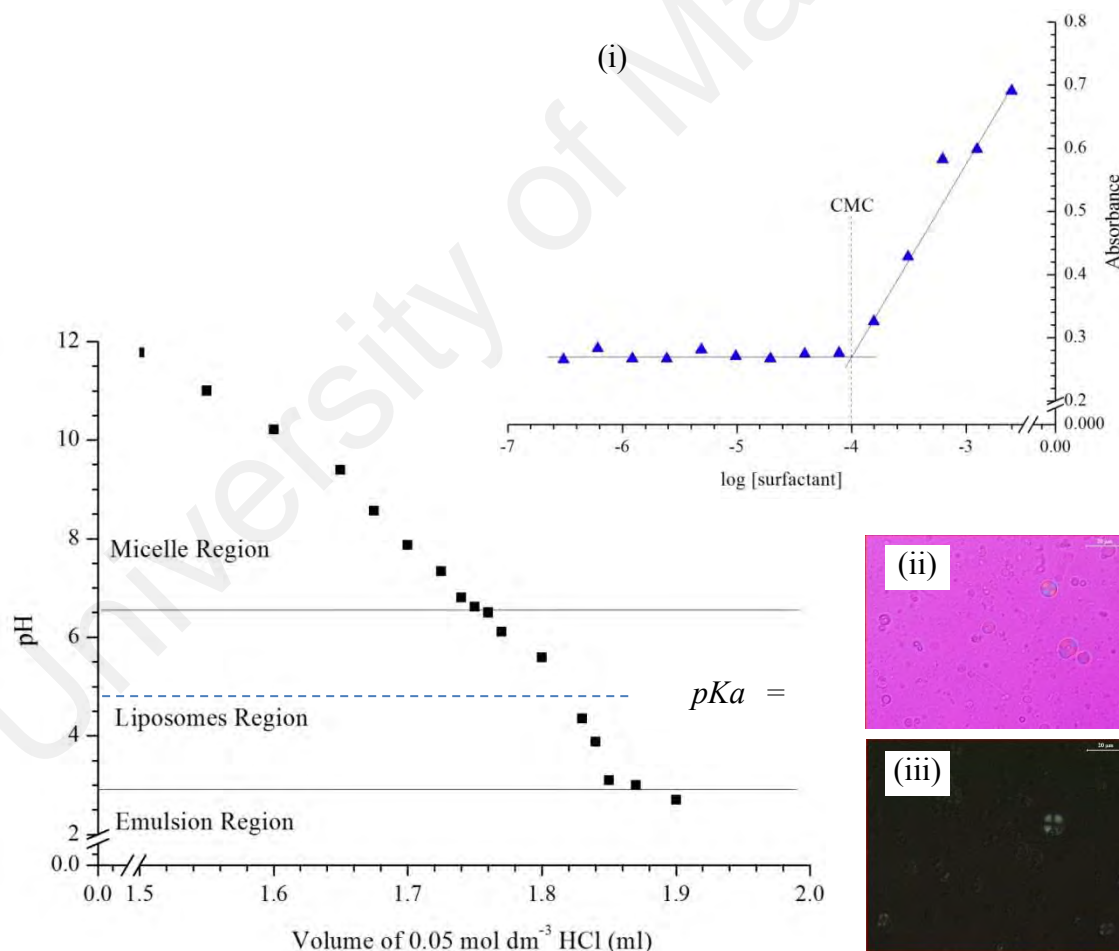
Figure 4.8: Equilibrium titration curve of erucic acid as a function of added HCl. The insets were (i) the determination of critical micelle concentration and micrograph of liposomes as viewed in (ii) light and (iii) dark phase with 20 μm scale. All measurements were done at 30 °C.

Figure 4.8 displays the phase transition of erucic acid concerning the volume of HCl added into the mixtures. Erucic acid is a pH-responsive surfactant which the effective area of head group can be microscopically modified by varying the pH of the solution. At high pH, the clear solution of sodium erucate was dominated by micelles (Chen & Szostak, 2004; Morigaki & Walde, 2007; Teo et al., 2011), due to the COO$^-$ group had a larger effective group area which tended to form worm-like micelles (Fameau et al., 2014). The inset figure displays the CMC at 30 °C of erucic in NaOH at 0.1 mmol dm^{-3}. As 0.05 mol dm^{-3} of HCl was introduced into the solution, the ionized carboxylate group in erucic acid was protonated. The pH of the solution fell slowly and buffered around pH 6.50. As approximately half of the COO$^-$ group was protonated, and bilayer membranes of erucic acid were formed spontaneously. The pK_a of erucic acid molecules was calculated through half of neutralization endpoint, which at pH 4.80 and can be used to determine the pH region, where erucic acid can be found (Fameau et al., 2014). The pH of the solutions started to experience the buffering at pH 3.10 where 1.87 mL of 0.05 mol dm^{-3} of HCl was added to the solution. As the pH of the solution was reduced progressively, the electrostatic repulsion of adjacent carboxylates groups was reduced (Chen & Szostak, 2004) until the total protonation of the carboxylates forming the insoluble oil droplets (Morigaki & Walde, 2007).

Equilibrium titration curve of soy lecithin as a function of the volume of HCl is presented in Figure 4.9. Phosphatidylcholine in soy lecithin is a zwitterionic surfactant with amphiphilic character. As the ratio of NaOH was high in the solution, the solution was colourless due to the soy lecithin was fully soluble and ionized in the solution. The CMC was determined to be at 0.71 mmol dm^{-3} at 30 °C. This aqueous solution contained uniformly distributed PO$_4^-$ and N$^+$(CH$_3$)$_3$ species due to the molecule has equimolar of PO$_4^-$ and N$^+$(CH$_3$)$_3$ species (Naumowicz & Petelska, 2016). As 2.6 mL of HCl was introduced into the solution, the group PO$_4^-$ was protonated and the pH of the

solution was started to reduce gradually until pH 8.77. Small buffering region can be observed around this pH, where 2.97 mL of 0.05 mol dm^{-3} of HCl make the solution turned cloudy. Liposomes can be observed when half of PO$_4^-$ in the solution was protonated. The region where only liposomes were present was determined by implementing Gibbs' phase order (Rogerson et al., 2006), which was found at pH 6.7 to 8.5. Protonation came to an end when 3.3 mL of 0.05 mol dm^{-3} of HCl was introduced into the solution and oil droplets begin to appear. The *pK$_a$* of soy lecithin where 50% of PO$_4^-$ had protonated (Kanicky & Shah, 2002) was calculated to be around pH 7.75 as agreed to other finding (Grauby-Heywang et al., 2016).
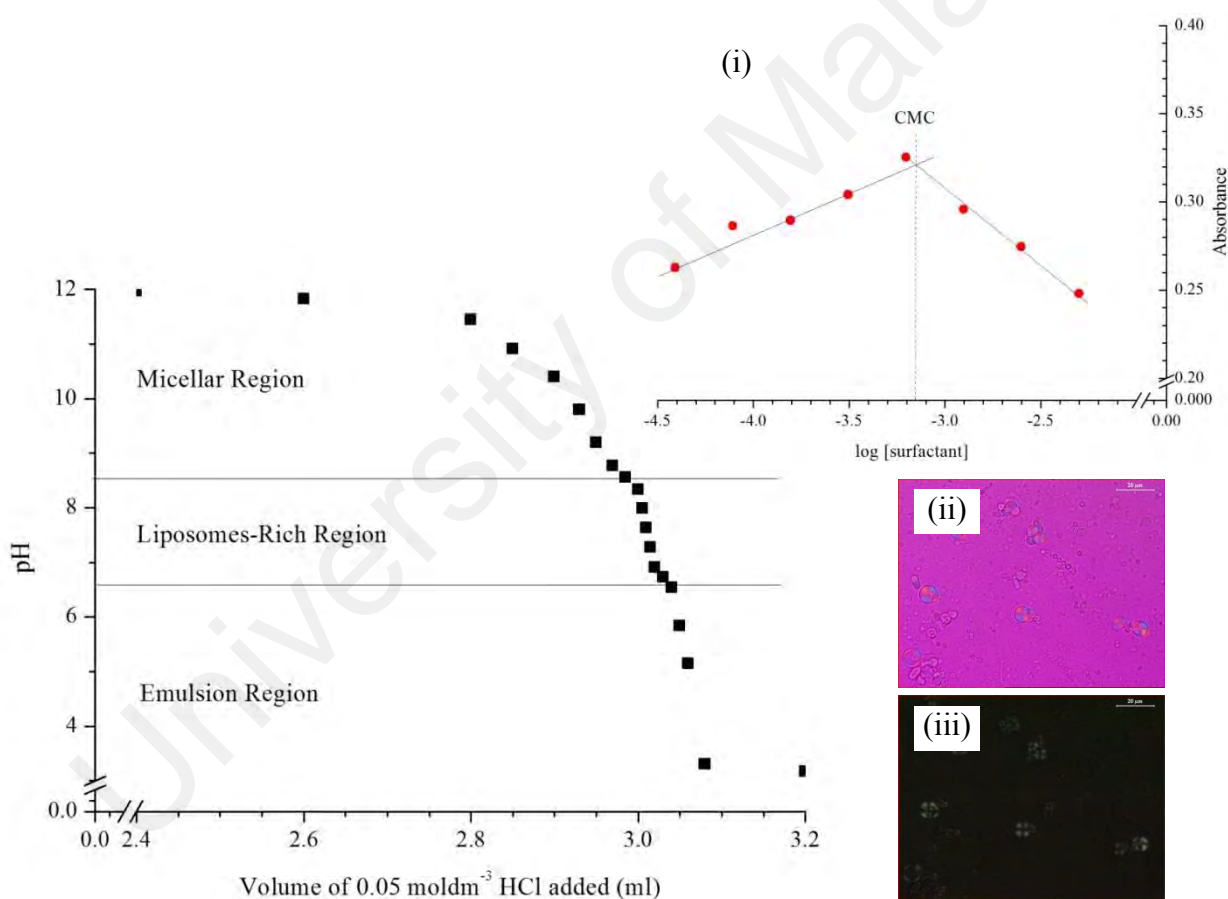
Figure 4.9: Equilibrium titration curve of soy lecithin, at room temperature as a function of added HCl 0.05 mol dm^{-3}. The insets were (i) the determination of critical micelle concentration and micrograph of liposomes as viewed in (ii) light and (iii) dark phase with 20 µm scale. All measurements were done at 30 °C.

Determination of pK_a and evaluation of equilibrium titration curve for surfactants provide the information on the pH region that liposomes formed spontaneously (Teo et al., 2011; Eh Suk & Misran, 2017), as well as their optimum pH before entering the emulsion, oil droplets (Morigaki & Walde, 2007; Fameau et al., 2014), or crystalline (Cistola et al., 1988; Kanicky & Shah, 2002) region. The liposomes-rich region was varied as a function of the surfactants pK_a, which is linked to their chemical nature (Fameau et al., 2014). The presence of liposomes in the solution was confirmed using the microscopy techniques such as an optical polarizing microscope (Chia & Misran, 2013; Tan & Misran, 2013) and high resolution-transmission electron microscopy (Morigaki & Walde, 2007; Salentinig et al., 2010).

4.4 Surface Active Agent Properties

In the presence of sufficient aqueous electrolyte solutions, most phospholipids and unsaturated fatty acids with undergo spontaneous aggregation to rearrange as lipid bilayer membranes in the form of liposomes (Petelska & Figaszewski, 2000). Phospholipids and unsaturated fatty acids structures comprised of the two distinctly molecular parts which are lyophobic (or hydrophobic) tail part and lyophilic (or hydrophilic) head part, which is similar to surfactant (surface active agent). It is a material that has an ability to adsorb at the interface and reduce the interfacial free energy (Rosen & Kunjappu, 2012) between the two immiscible systems. Interfacial free energy, γ, is a minimum work needed to create a boundary at the interface per unit area and is usually called as an interfacial tension for the liquid-liquid interface and the surface tension for the liquid-gas interface.The study of adsorption of surfactant monomers from the bulk solution to the interface can be conducted using the Du Nouy ring method (Shankar & Patnaik, 2007; Teo et al., 2011; Tan & Misran, 2013).
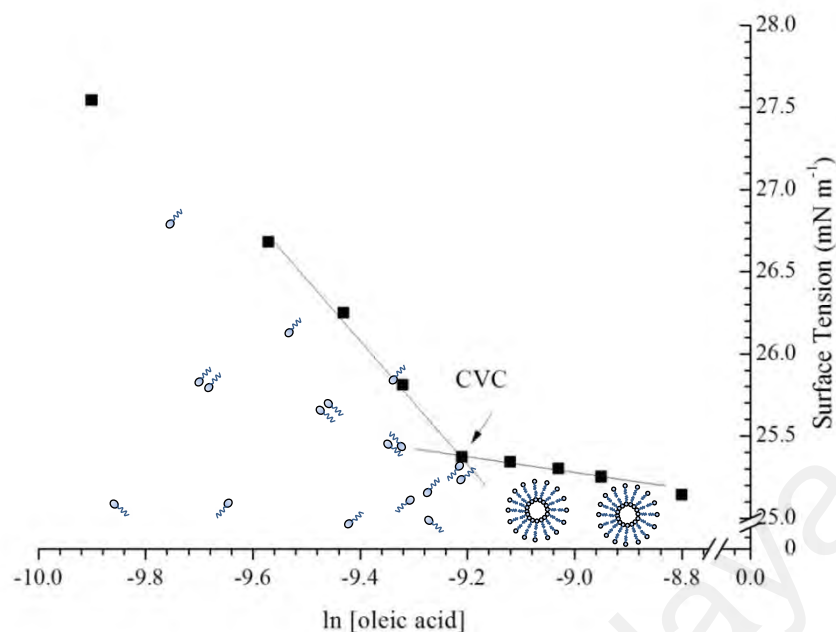
Figure 4.10: Surface tension of oleic acid in pH 8.5 at 30 °C.

Figure 4.10 presents the γ profile of one day old oleic acid solutions in pH 8.5 at 30 °C as oleic acid liposomes were abundantly present around this pH. At the low concentration of oleic acid in the solution, there were a few of oleic acid monomers were presence in the solution. The molecules were diffused from the bulk, concentrated and re-orientated so that their hydrophobic groups were directed away from the solution at the liquid-gas interface. This phenomenon reduced the interfacial free energy of water which was 71.2 mN m^{-1}. The high interfacial free energy at the low concentration of oleic acid may be due the appreciable amount of oleic acid molecules has not yet reached the liquid-gas interface. As the amount of oleic acid in the solution was increased gradually, the presence of the oleic acid monomers at the liquid-gas interface was proportionally increased, and reduced the interfacial free energy of the solution to 25.4 mN m^{-1}. Further addition of oleic acid in the solution was not affecting the interfacial free energy of the oleic acid solution due to the monomers were saturated at the liquid-gas interface as well as rearranged the oleic acid monomers to form oleic acid liposomes (Tan & Misran, 2013). Formation of oleic acid liposomes is an alternative mechanism to reduce the free energy of the system by removing hydrophobic groups

from contacts with the water. Critical vesicle concentration (CVC) which is the minimum concentration acquired for the oleic acid to form liposomes was obtained from the break of the plot which was 0.10 mmol dm^{-3} which agreed with the previous study by (Teo et al., 2011).
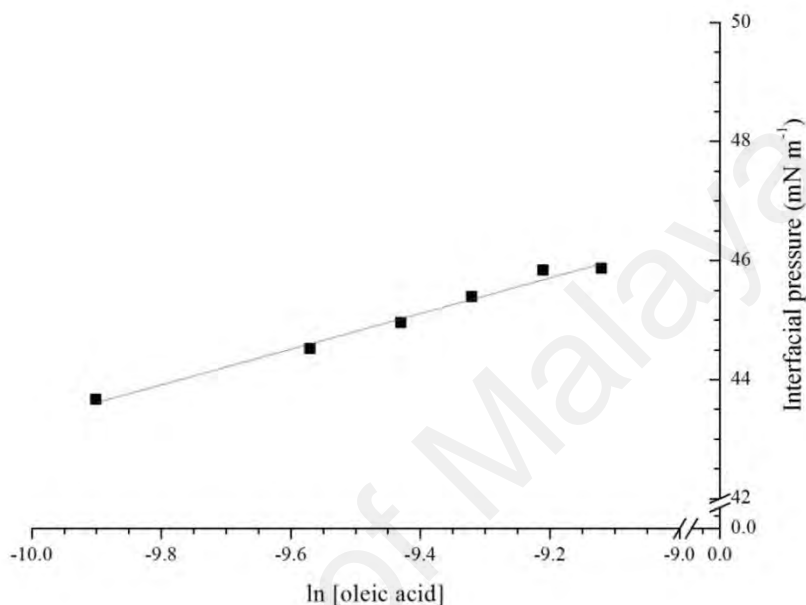
Figure 4.11: Interfacial pressure, Π, of oleic acid in pH 8.5 at 30 °C as a function of oleic acid concentration reported in mmol dm^{-3}. The linear equation was y=2.99x+73.244 with the regression coefficient, R^2 of 0.99.

The equilibrium interfacial tension profiles of the liquid-gas interface in the presence of oleic acid is exhibited in Figure 4.11 where the interfacial pressure, Π, was plotted against the natural logarithm concentration of oleic acid. Interfacial pressure, Π is the difference in γ of the given liquid-gas interface in the absence ($\gamma_{l/g}$) and in the presence of oleic acid ($\gamma_{l+o/g}$) which is related as $\Pi = \Delta\gamma = \gamma_{l/g} - \gamma_{l+o/g}$. The equilibrium interfacial profile presented that interfacial pressure, Π, was increased linearly with bulk oleic acid concentration indicated that oleic acid was adsorbed efficiently at the given liquid-gas interface. The data were then fitted into linear equation and yielded a straight line with a regression coefficient of 0.99, proving that oleic acid was relatively pure, probably because of the absence of any kind of surface-active impurities (Lunkenheimer et al., 1995).

Interfacial pressure, Π, and bulk surfactant concentration was related to the maximum adsorption density, Γ, which can be determined through Gibbs adsorption equation as $d\Pi/d\ln C = -nRT\Gamma$, where R is the universal gas constant, 8.3 Nm mol^{-1} K^{-1}, T is the absolute thermodynamic temperature, 303 K, n is number of mole, and $d\Pi/d\ln C$ was 2.99×10^{-3} Nm^2 mol^{-1}, which is the slope of equilibrium interfacial profile of oleic acid. This equation yielded the maximum desorption density, Γ of 3.41×10^{-6} mol m^{-2}. Next, the value of Γ can be related to the demand for minimum surface area per surfactant molecule, $A_{\min}$, by $A_{min}= 1/(N_A\Gamma)$ where N_A stands for Avogadro number. The calculation suggested that oleic acid molecules demanded a surface area of 48.7 Å^2 which is comparable with the value reported by other researchers (Kanicky & Shah, 2002). Determination of area per surfactant molecule is very important in understanding the orientation of surfactant at the interface.
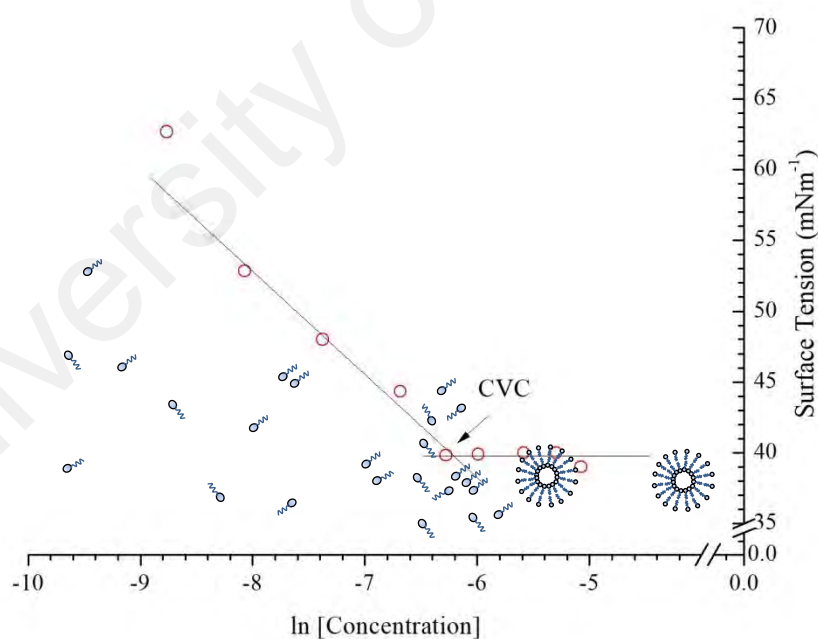
Figure 4.12: Surface tension against amount of erucic acid in mmol dm^{-3} in pH 7.4 at 30 °C.

Figure 4.12 displays the surface tension of erucic acid with respect to the concentration of erucic acid at pH 7.4. Surface tension of solution at 30 °C was decreasing gradually with the increase in the amount of erucic acid in the solution and

achieved a plateau region at 39.9 mN m^{-1} at the concentration of erucic acid in PBS buffer pH 7.4 was 1.88 mmol dm^{-3}. This concentration is comparable to the report by other researchers that reporting the formation of self-assembly aggregates of erucic acid vesicles, vesicle micelles, spherical micelles, or worm-like micelles depending on their pH solution in order to reduce the free energy of the system (Markus & J., 2010; Qiu et al., 2018).
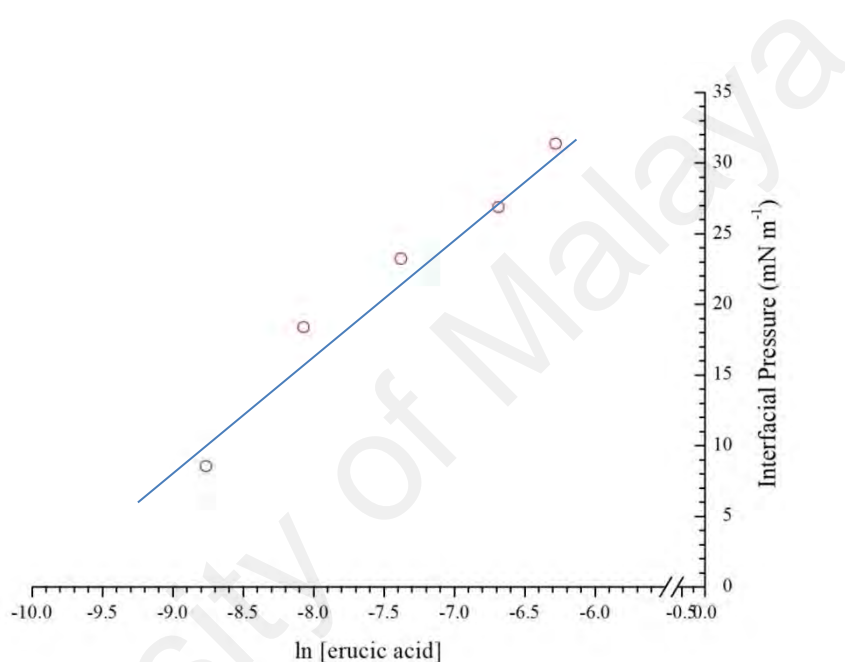
Figure 4.13: Interfacial pressure, Π, of erucic acid concentration in mmol dm^{-3} in pH 7.4 (○) at 30 °C.

The interfacial pressure, Π, of erucic acid was increased with the amount of erucic acid in the bulk concentration as displays in the equilibrium interfacial tension profile in the Figure 4.13, which indicated that the molecules were adsorbed efficiently at the liquid-gas interface. The plot yielded a straight line with the linear equation of y=8.5328x+85.11 with a regression coefficient of 0.97. The Gibbs adsorption equation was employed to calculate the maximum adsorption density, Γ, of 3.37×10^{-6} mol m^{-2} in pH 7.4. The minimum surface area per surfactant molecule, A_{min}, in pH 7.4 was calculated as 49.1 Å^2, which was slightly higher as compared to the values reported by Feng and co-workers, where the experiment has been done in pure water (Feng et al.,

2012). The calculated minimum surface area per surfactant molecule for erucic acid at pH 7.4 was found to be higher, which may be due to the presence of Na$^+$ ions interlayers from PBS (Altin et al., 1999) that affecting the diffusion of the monomers to the liquid-gas interface (Theander & Pugh, 2001).
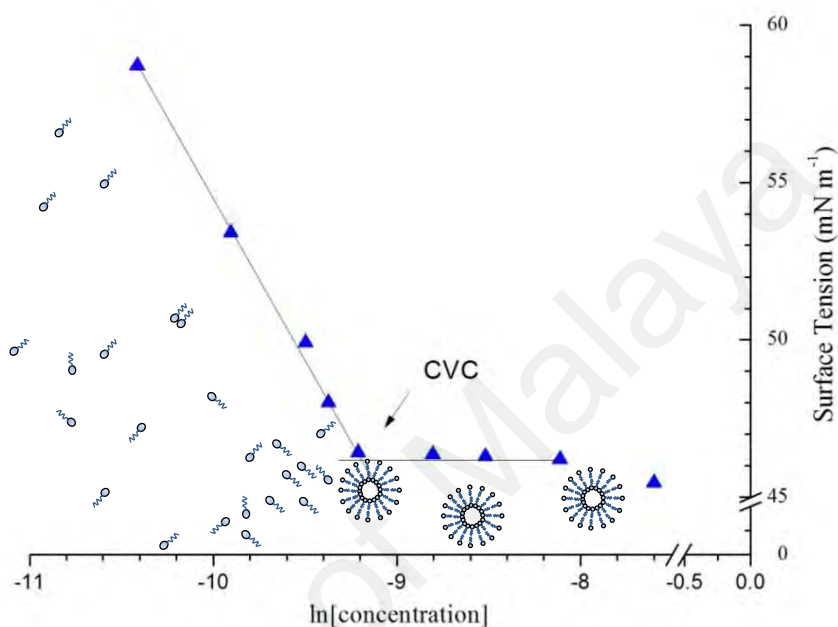
Figure 4.14: Surface tension against concentration of soy lecithin in mmol dm^{-3} in pH 7.4 at 30 °C.

The surface activity of soy lecithin was investigated with a surface tensiometer using Du Nuoy ring method at 30 °C in pH 7.4 as displays in the Figure 4.14 (Teo et al., 2011; Tan & Misran, 2013). The surface tension, γ, of the solution is directly related to the accumulation and adsorption of the surfactant mass at the liquid-gas interface. In the solution, soy lecithin molecules diffused from the bulk to the interface, concentrated at the surface, and oriented such that their hydrophobic groups were directed away from the solution (Rosen & Kunjappu, 2012). As the solution concentration increased, γ decreased as the hydrophobic groups at the interface was increased and concentrated at the surface hence minimizing the free energy of the solution (Rosen & Kunjappu, 2012). However, the reduction in surface tension was then reached an optimum value when the molecules at the liquid-gas interface and in the bulk solution were in

thermodynamic equilibrium (Burlatsky et al., 2013), and the plateau region was reached at 45.0 mN m^{-1} after which they spontaneously form the liposomes. The critical vesicle concentration (CVC) of soy lecithin was 0.10 mmol dm^{-3} as calculated from the inflection point of the plots, which was comparable to the values obtained by Menon and co-workers (Menon et al., 2015).
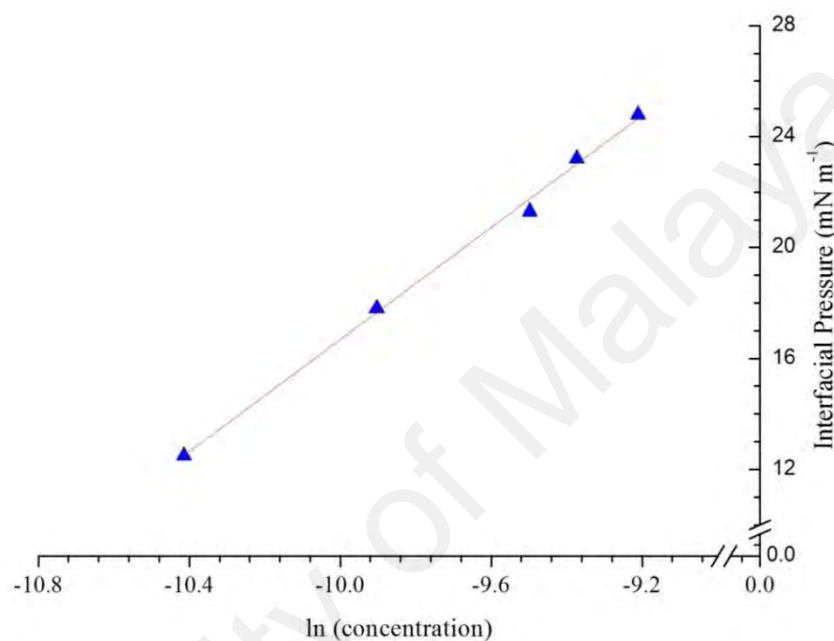
Figure 4.15: Interfacial pressure, Π, in pH 7.4 at 30 °C as a function of soy lecithin concentration in mmol dm^{-3}. The linear equation was y=10.101x+117.69 with the regression coefficient, R^2 of 0.99.

The equilibrium interfacial tension profile of soy lecithin which presented in Figure 4.15 displayed that the interfacial pressure, Π, was increased perpendicularly with the amount of soy lecithin in the bulk concentration. This phenomenon indicated that soy lecithin molecules were adsorbed efficiently at the liquid-gas interface. The plot yielded a straight line, which yielded a linear equation of y = 10.101x + 117.69 with the slope of equilibrium interfacial profile was 10.101×10^{-3} Nm^2 mol^{-1} and regression coefficient of 0.99. The maximum adsorption density, Γ, of 4.01×10^{-6} mol m^{-2}, was calculated by using Gibbs adsorption equation, while the minimum surface area per surfactant molecule, A_{min}, was calculated to be 41.4 Å^2, which was agreeable with other researchers (Shah & Schulman, 1967; Petelska & Figaszewski, 2011). Surface area per surfactant molecule

of lecithin can achieved up to 96 Å^2 depending to the binding of cations to the phosphate group, length, conformation, and degree of unsaturation of the hydrocarbon chains (Petelska & Figaszewski, 2011).

4.5 Morphological Studies

Information on size, shape, and dynamic properties of liposomes can be observed through various microscopy techniques that had been designed up to submicron scale. Every technique required a specific sample preparation depending on the capabilities and limitations of the technique that being chosen. In this study, optical polarizing microscope (OPM) and high resolution-transmission electron microscope (HR-TEM) were used to observe the presence as well as the morphology of the liposomes.

4.5.1 Optical Polarizing Microscope (OPM)

Due to the fact that liposomes are anisotropic aggregates (Bibi et al., 2011; Placzek & Kosela, 2016), which have the ordered, concentric arrangement of phospholipid layers, they are capable to divide the light rays into two orthogonal components resulting in liquid crystalline characteristics of their bilayers (Leitmannova-Liu, 2006; Placzek & Kosela, 2016). The optical polarizing microscope is a suitable microscopy technique to confirm the presence of liposomes. Micrograph was generated from the interaction of plane-polarized light against an anisotropic specimen from the diffraction, interference, and existence of ordered molecular arrangements in the liposomes bilayer (Bibi et al., 2011). In the microscopic image, "maltese cross" textures were detected when the polarized rays pass through the lamellar layers that arranged perpendicularly to the polarization plane. However, if a birefringent plate located in the way of polarized rays, additive interference colours, which appear more vivid, such as first-order, blue, yellow, and red can be observed. Polarization microscopy is also used to detect the

liposomes present in emulsion systems, because oil drops, in contrast to phospholipid vesicles, do not possess optically active properties (Placzek & Kosela, 2016).
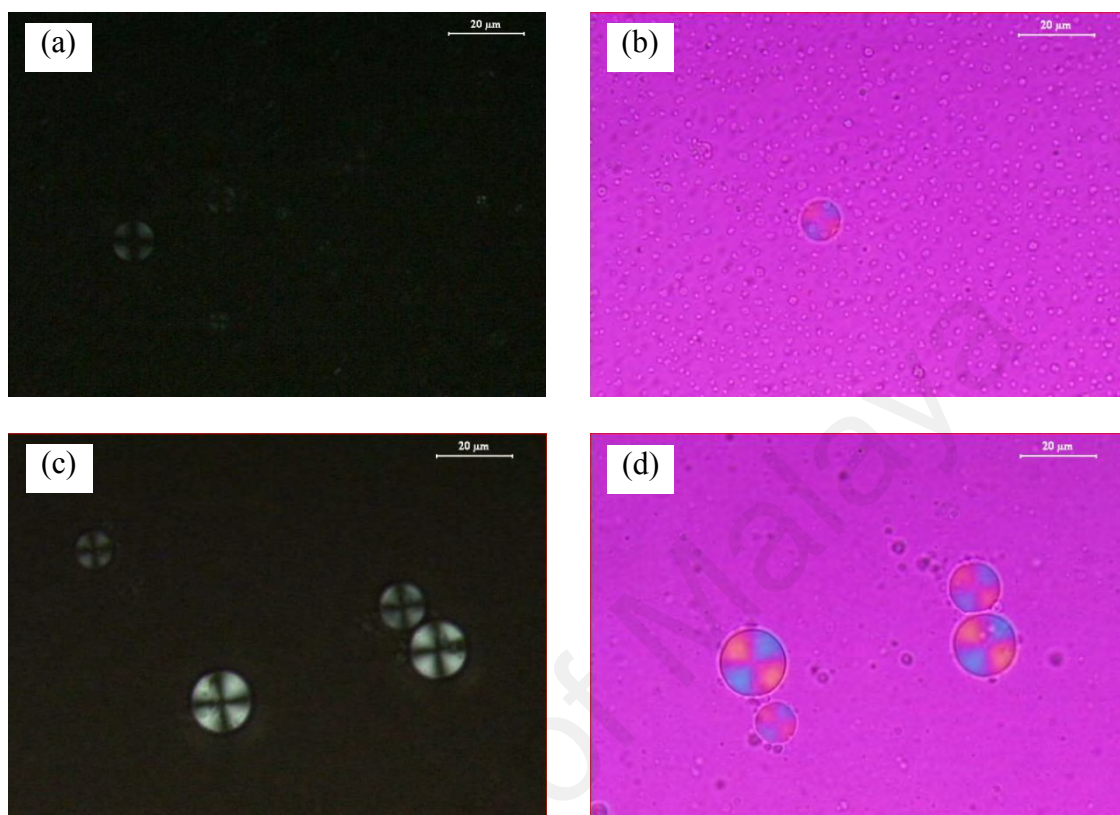
.
Figure 4.16: Optical polarizing microscope (OPM) micrograph of one day old oleic acid liposomes prepared in pH 7.4 (a and b) and pH 8.5 (c and d), where a and c were viewed under dark field and b and were viewed under light field at room temperature. The scales were 20 μm.

Figure 4.16 shows the presence of oleic acid liposomes in pH 8.5 and 7.4 in the dark field. As the perpendicularly polarized rays passing through the bilayers, "Maltese cross" could be clearly observed in the micrographs (a) and (c). During the light field mode, the polarized light was further interfered by the white polarized light through the rotational lambda plate, resulting from the formation of vivid first-order blue, yellow, and red (Bibi et al., 2011) which is known as birefringent effect as in micrographs (b) and (d). This phenomenon occurred due to the difference in the speed of two orthogonal components of light (ordinary and extraordinary waves) at different refractive indices. The intensity of the colours observed was related to the coordination of the material in

the light path. The presence of emulsion can be visibly detected in the oleic acid liposomes pH 7.4. This has come to an agreement with Figure 4.7 which shows that liposomes still can be found in the early emulsion region.

Incorporation of DOPEPEG2000 into oleic acid liposomes displayed a significantly reduced in size as presented in Figure 4.17 and 4.18. The distribution of liposomes in pH 7.4 (Figure 4.18) was lower as compared to liposomes pH 8.5 (Figure 4.17), as emulsion started to form at pH 7.4 where the emulsion droplet could be detected within this region. The Maltese cross and birefringent effect were clearly expressed in all formulations. In figure 4.17 and 4.18, at the molar ratio of 0.01:1, DOPEPEG2000-oleic acid liposomes formed an individual structures ((a) and (b)), and started to aggregate at the ratio of 0.02:1 as presented in (c) and (d). The addition of DOPEPEG2000 in the preparation had increased the aggregation of DOPEPEG2000 as showed in (e) and (f) as shown in figure 4.17 and 4.18, where the ratio of DOPEPEG2000: oleic acid was 0.05:1. The same phenomenon was also detected in the DOPEPEG2000-oleic acid liposomes prepared at pH 7.4. Although a less vivid micrograph was obtained due to the liposomes-rich emulsion solution was more turbid as compared to liposomes at pH 8.5, the liposomes still express a significant birefringent effect because emulsion did not possess optically active properties (Placzek & Kosela, 2016) as compared to liposomes.
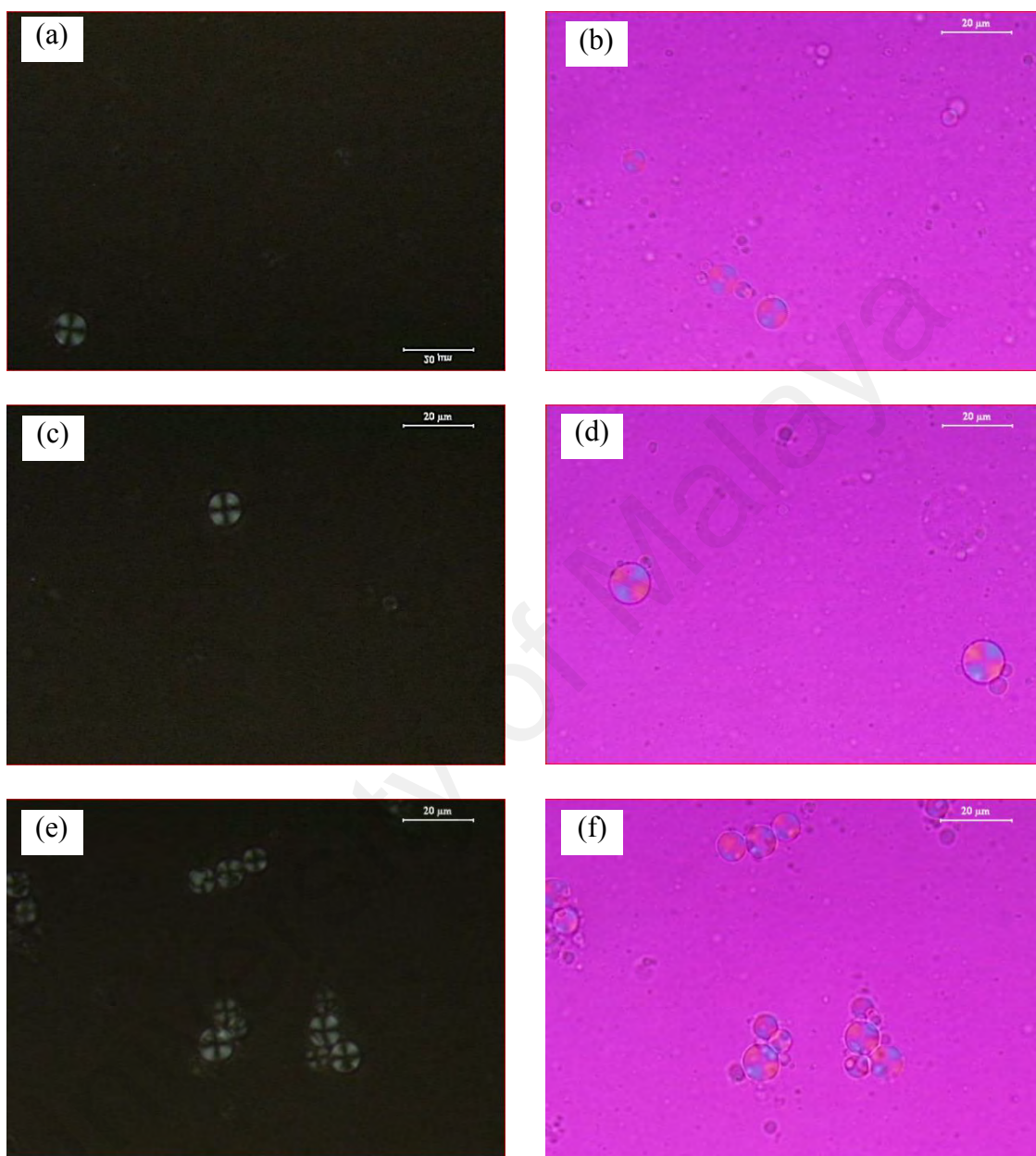
Figure 4.17: Optical polarizing microscope (OPM) micrograph of one day old DOPEPEG2000-oleic acid liposomes prepared in pH 8.5 with the molar ratio of DOPEPEG2000:oleic acid of 0.01:1 (a and b), 0.02:1 (c and d), and 0.04:1 (e and f) at room temperature. The scales were 20 μm.
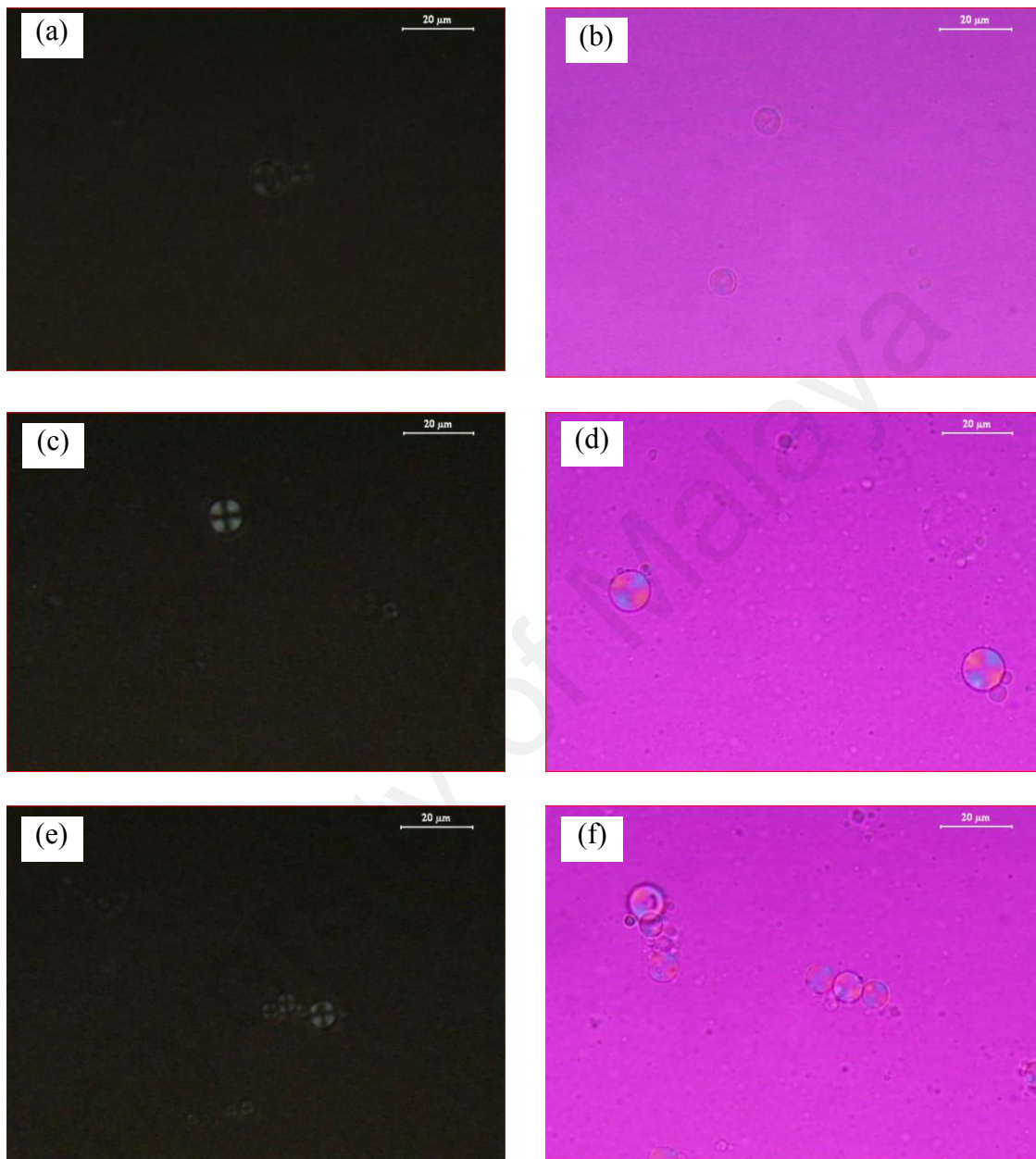
Figure 4.18: Optical polarizing microscope (OPM) micrograph of one day old DOPEPEG2000-oleic acid liposomes prepared in pH 7.4 with the molar ratio of DOPEPEG2000:oleic acid of 0.01:1 (a and b), 0.02:1 (c and d) and 0.04:1 (e and f) at room temperature. The scales were 20 μm.

Figure 4.19 presents the micrograph of DOPEPEG2000-oleic acid-erucic acid liposomes in pH 7.4 at room temperature. The presence of liposomes was obviously seen through the formation of Maltese cross during the dark phase. The blue and yellow birefringent occurrences were also discovered during the light field mode. Formation of small single liposomes can be observed in micrograph c and d while micrograph (a), (b), (e), and (f) shows the aggregation of large size liposomes in the solution.
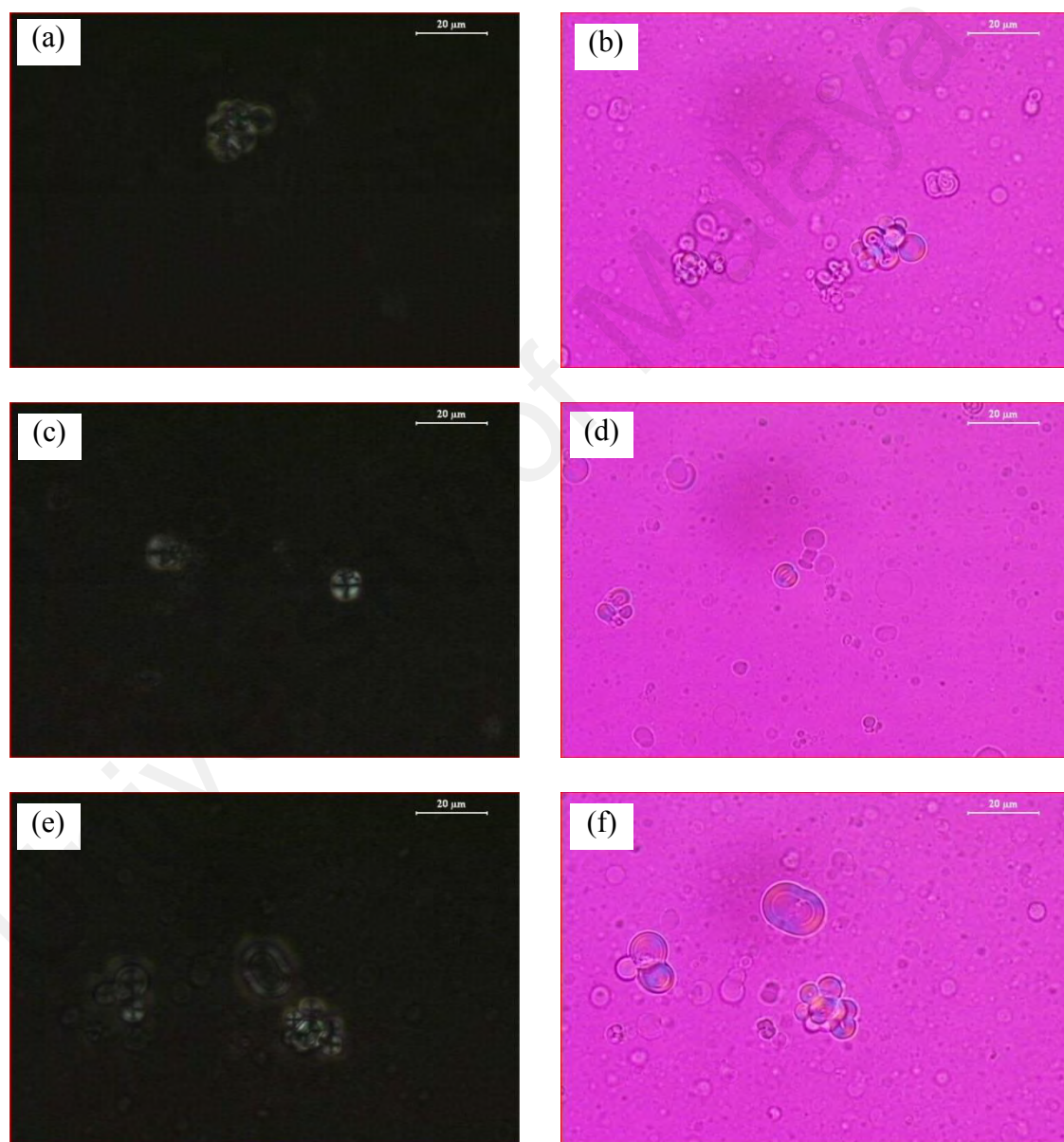
Figure 4.19: Optical polarizing microscope (OPM) micrograph of one day old DOPEPEG2000-oleic acid-erucic acid liposomes prepared in pH 7.4 with the molar ratio of erucic acid to DOPEPEG2000-oleic acid of 0.125:1 (a and b), 1:1 (c and d), and 4:1 (e and f) at room temperature. The scales were 20 μm.
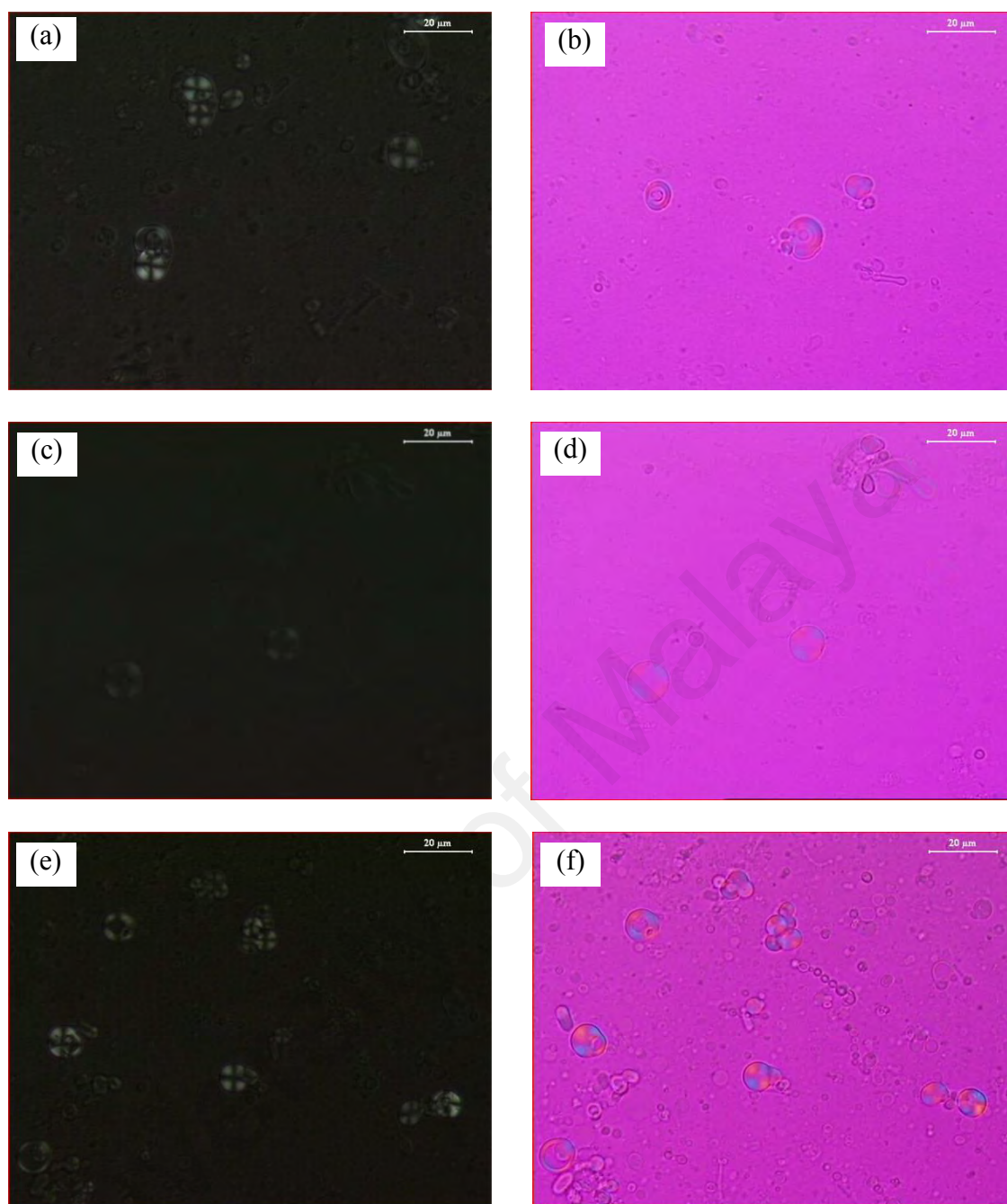
Figure 4.20: Optical polarizing microscope (OPM) micrograph of one day old DOPEPEG2000-oleic acid-soy lecithin liposomes prepared in pH 7.4 with the molar ratio of soy lecithin to DOPEPEG2000-oleic acid of 0.125:1 (a and b), 1:1 (c and d), and 4:1 (e and f) at room temperature. The scales were 20 μm.

Micrographs of DOPEPEG2000-oleic acid-soy lecithin liposomes are displays in Figure 4.20. In the dark field mode, the presence of liposomes could be detected through the formation of Maltese cross while a birefringence phenomenon was observed during the light field mode. The micrograph showed that DOPEPEG2000-oleic acid-soy lecithin liposomes had a high tendency to form multi lamellar liposomes

(micrograph (a) and (b)). However, when the ratio of soy lecithin to DOPEPEG2000-oleic acid was increased to 1:1, more independent single lamellar liposomes can be observed in the solution. Further incorporation of soy lecithin in the formulation promoted the formation of liposomes as displayed in micrograph (d) and (e). However, the liposomes were aggregated to each other.

4.5.2 High Resolution-Transmission Electron Microscopy (HR-TEM)

High Resolution-Transmission Electron Microscopy employed the interaction of energetic electrons at the surface of the specimen to provide the information on the morphological, compositional, and crystallographic arrangement of the sample beyond the resolution achieved by conventional light microscopy up to atomic-scale. A good staining agent ensured the quality of micrographs. In this study, negative staining method using phosphotungstic acid to bind with the phosphate group of phospholipids which enabled the analysis of liposomes through the formation of light or dark halos around the structures of liposomes. The uncorrected aberration mode was employed to avoid the presence of fringe lattices (House et al., 2016), hence improved the contrast as well as visibility of liposomes.

Figure 4.21 displays the micrograph of oleic acid liposomes in the different pH conditions. HR-TEM offered a higher magnification and resolution microscopy, which allowed the smaller size of liposomes can be detected easily. The liposomes were spherical in shape with the light halos formed surrounding the structures (Placzek & Kosela, 2016). A higher density of smaller size liposomes can be found in pH 8.5 as oleic acid has a higher tendency to form liposomes in pH 8.5, but starts to form a larger size emulsion at pH 7.4. Furthermore, oleic acid liposomes in pH 7.4 formed less spherical structures as compared to oleic acid liposomes pH 8.5 which may be due to the surface tension forces, growth of electrolyte volume at the surface of liposomes

from the phosphotungstic acid (Kim & Honma, 2003) or the high vacuum in the microscope chamber that subsidized to sample drying (Placzek & Kosela, 2016).
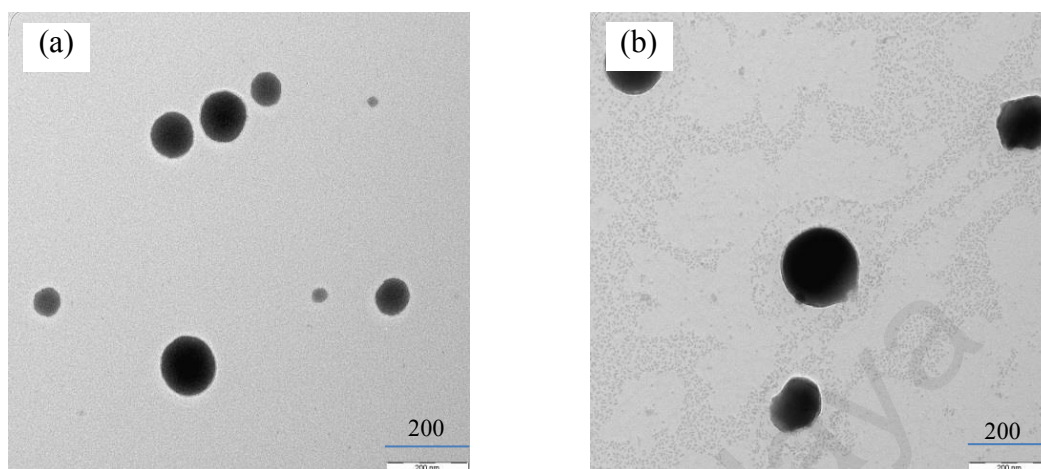
Figure 4.21: High resolution-transmission electron micrograph of one day old oleic acid liposomes prepared in pH 8.5 (a) and pH 7.4 (b) at room temperature. The scales were 200 nm.

The micrographs of oleic acid liposomes incorporated with DOPEPEG2000 are shown in Figure 4.22. The round structures liposomes of various diameters were clearly observed. At molar ratio of DOPEPEG2000: oleic acid at 0.01:1 and 0.02:1, liposomes was single structures with various diameters from 75 to 300 nm. Slightly aggregate can be viewed in plate (d) where the molar ratios of DOPEPEG2000: oleic acid was 0.02:1 at pH 7.4. However, aggregation of liposomes could be detected in the plate (e) and (f), where the molar ratios of DOPEPEG2000 to oleic acid was 0.04:1 in both pH 7.4 and 8.5. This showed that incorporation of excess DOPEPEG2000 into the formulation was promoted the inter-particle attractive interaction of DOPEPEG2000-oleic acid liposomes.
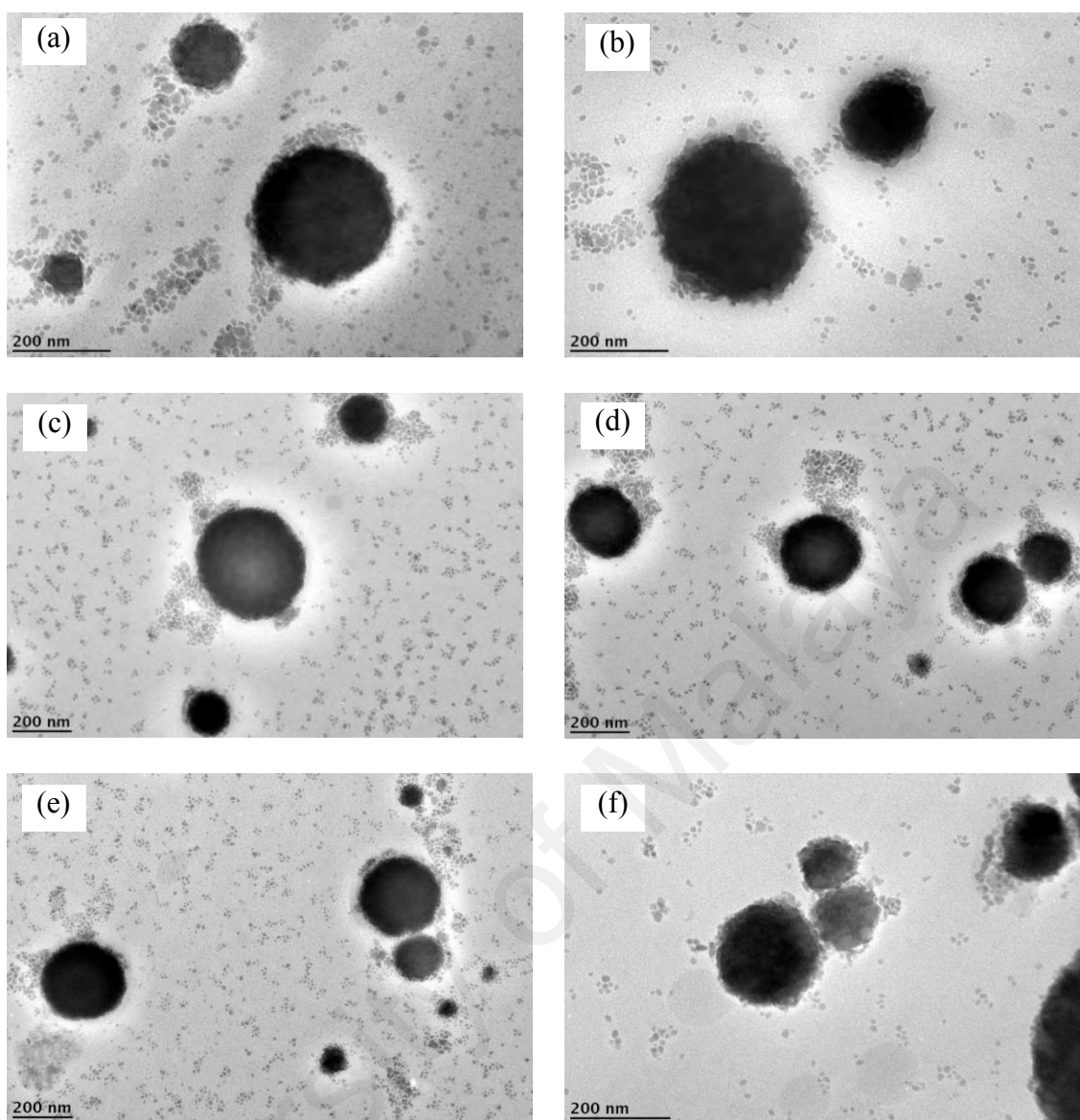
Figure 4.22: High resolution-transmission electron micrograph of one day old oleic acid liposomes prepared in pH 8.5 (a, c, and e) and 7.4 (b, d, and f) at 30 °C. Micrograph a and b were DOPEPEG2000-oleic acid liposomes of 0.01:1, c and d were 0.02: 1, while e and f were 0.04:1. The scales were 200 nm.

In pH 7.4, erucic acid formed an irregular round structure as shown in Figure 4.23(a), due to the pH of the medium which was slightly higher than the pH of its liposomes-rich region which is within pH 3 to 7. Incorporation of DOPEPEG2000-oleic acid into the formulation increased the distribution of black spherical structures with light halo of liposomes. Figure 4.23(b) showed the smallest independent DOPEPEG2000-oleic acid-erucic acid liposomes of molar ratio of 1:1, where DOPEPEG2000: oleic acid was 0.02:1. However, as the amount of erucic acid was raised, aggregation started to build up as shown in Figure 4.23(c), when the molar ratio of DOPEPEG2000-oleic acid to

erucic acid was 1:2. Figure 4.23 (d) displayed the large aggregated DOPEPEG2000-oleic acid-erucic liposomes. This may due to the aggregation of liposomes, which lead to the fusion of liposomes.
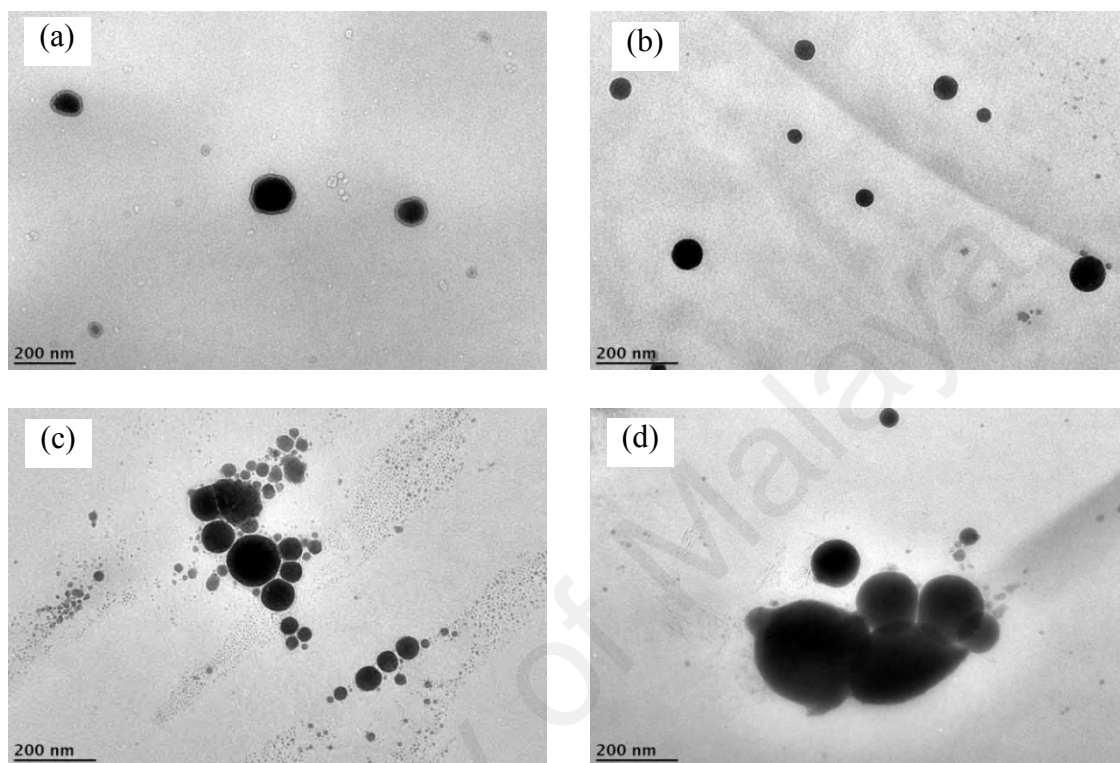
Figure 4.23: High resolution-transmission electron micrograph of one day old DOPEPEG2000-oleic acid-erucic acid liposomes prepared in pH 7.4 at room temperature. The scales were 200 nm. Plate (a), (b), (c), and (d) are micrograph for DOPEPEG2000-oleic acid- erucic acid liposomes with molar ratio of 0:0:1, 0.02:1:1, 0.02:1:2, and 0.02:1:4, respectively.

DOPEPEG2000-oleic acid- soy lecithin liposomes also showed spherical structures with light surrounding halo of liposomes characteristics as shown in the Figure 4.24. At low amount of soy lecithin in the formulation, liposomes appeared as a single spherical structure. Figure 4.24 (a) shows soy lecithin liposomes with average size exceeding 1 μm, while Figure 4.24 (b), (c) and (d) show the effect of incorporating of soy lecithin into the formulation. Amount of DOPEPEG2000 to oleic acid was fixed to be 0.05:1 and reported as single unit. The molar ratios of DOPEPEG2000-oleic acid to soy lecithin of 1:1 in (b) showed the smallest size of the single independent structure of the liposomes. As the amount of soy lecithin in the formulation was increased such as in

(c) (1:2) and (d) (1:4), liposomes tended to aggregate and clumped to each other forming a large liposomes aggregates.
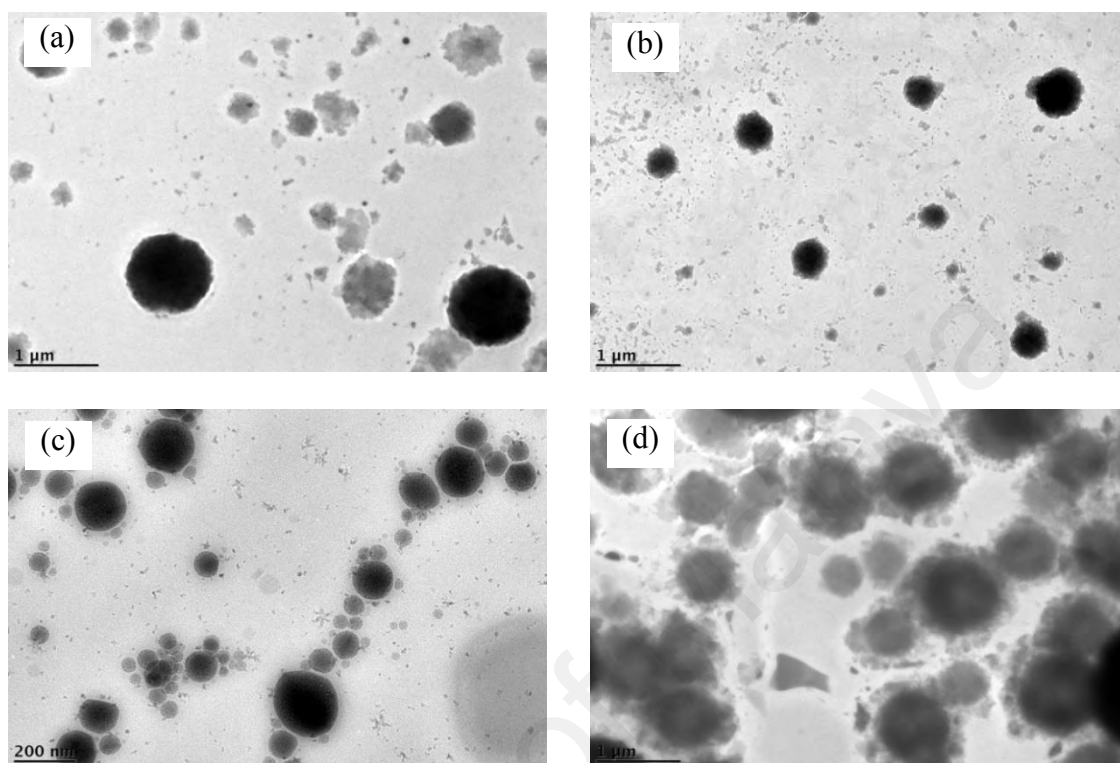
Figure 4.24: High resolution-transmission electron micrograph of one day old DOPEPEG2000- oleic acid -soy lecithin liposomes prepared in pH 7.4 at room temperature. Plate (a), (b), (c), and (d) are DOPEPEG2000-oleic acid-soy lecithin liposomes with molar ratio of 0:0:1, 0.02:1:1, 0.02:1:2, and 0.02:1:4, respectively. The scales were 1 μm for plate a, b, and d, while 200 nm for plate c.

Application of HR-TEM in observing the morphology of liposomes gave an advantage in detecting the smaller size liposomes due to the higher degree of magnification as compared to OPM. However, many precaution steps need to be taken into consideration such as staining agent which may affect the structure of liposomes (Placzek & Kosela, 2016), drying of liposomes and the high vacuum as well as high kV of HR-TEM will alter the morphology of liposomes (Eh Suk & Misran, 2017).

4.6   Zeta Potential

Evaluating the electrical charge of the particles provides an important information in defining the properties of a colloidal suspension such as flotation, flocculation and stability of suspended particles (Hunter et al., 2013). The zeta potential is the estimated

value of surface charge of particles in aqueous medium at a certain temperature. It was measured from the potential between Stern layer, which is the strongly bound inner region and the diffuse layer, which is the weakly bound outer region. This is due to the distribution of ions surrounding the particles resulting in the increased of the counter ions close to the surface which formed the electrical double layer around the particle.

In most cases, fatty acid liposomes bear a negative charge (Ciani et al., 2007) due to their ionized species of fatty acid (Fameau et al., 2014). The zeta potential value of 10 mmol dm^{-3} oleic acid liposomes at 30 °C, prepared in phosphate buffer pH 8.5 and 7.4 were -72 and -63 mV, respectively. This is expected to have a good compatibility with cell membrane, which mostly bears a negative charge (Ciani et al., 2007). However, the strong negative charge will enhance the clearance of liposomes in the blood system (Levchenko et al., 2002). The magnitude of zeta potential was shifted to less negative with the reduced in the pH may be due to the differences in the affinity of the two phases towards H^{+} ions in the buffer solution and ionization of charged surface (Hunter et al., 2013). The buffer of pH 8.5 contains more H^{+} ions in the system, which results in the higher potential between the surface of the particle and the bulk solution.

Figure 4.25 displays the effect of DOPEPEG2000 on the zeta potential of DOPEPEG2000-oleic acid liposomes. The magnitude was sloped dramatically with the increases of DOPEPEG2000 in the formulation, attributable to the long and bulky polyethylene glycol anchored lipid attaching to the liposomal membrane that screening the net charge of DOPEPEG2000-oleic acid liposomes. However, the zeta potential value of DOPEPEG2000-oleic acid liposomes was levelling off at the when the ratios of DOPEPEG2000 to oleic acid was 0.02:1. At this region, DOPEPEG2000-oleic acid liposomes are expected to be compatible with the cell membranes and close to the zeta potential of the red blood cells which is around -15 mV (Ciani et al., 2007).

Agglomeration and intravascular coagulation which lead to the blood clearance may occur if the zeta potential deviated beyond the zeta potential of the blood.
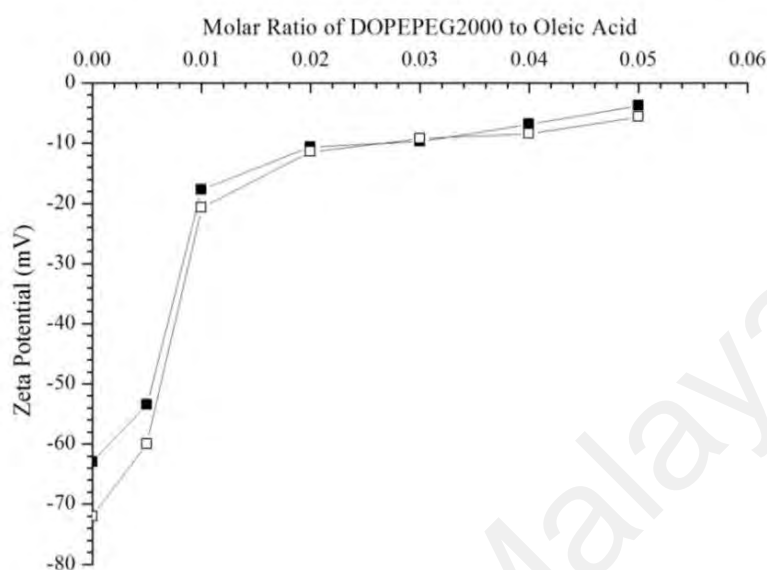
Figure 4.25: Zeta Potential values of one day old DOPEPEG2000-oleic acid liposomes with standard deviation less than 0.5 at pH 8.5 (□) and pH 7.4 (■) at 30 °C.

The stability of DOPEPEG2000-oleic acid liposomes in term of zeta potential was monitored over a period of 28 days at 30 °C. Figure 4.26 (a) and (b) shows that the formulation with the ratios of oleic acid to DOPEPEG2000 of 1:0.02, 1:0.03, 1:0.04, and 1:0.05 displayed a small variation of zeta potential as compared to other formulations. These were within the acceptable range proving that DOPEPEG2000 was successfully sterically stabilizing the oleic acid liposomes so that the clearance by the macrophages can be delayed hence the lifetimes of liposomes can be extended (Holland et al., 1996; Song et al., 2002; Okamoto et al., 2016; Jøraholmen et al., 2017). DOPEPEG2000-oleic acid liposomes with the molar ratios of 0.02:1 at pH 7.4 and 8.5 were chosen to further study with other materials due to their zeta potential values fall within that of red blood cell and stable throughout the incubation period of 28 days.
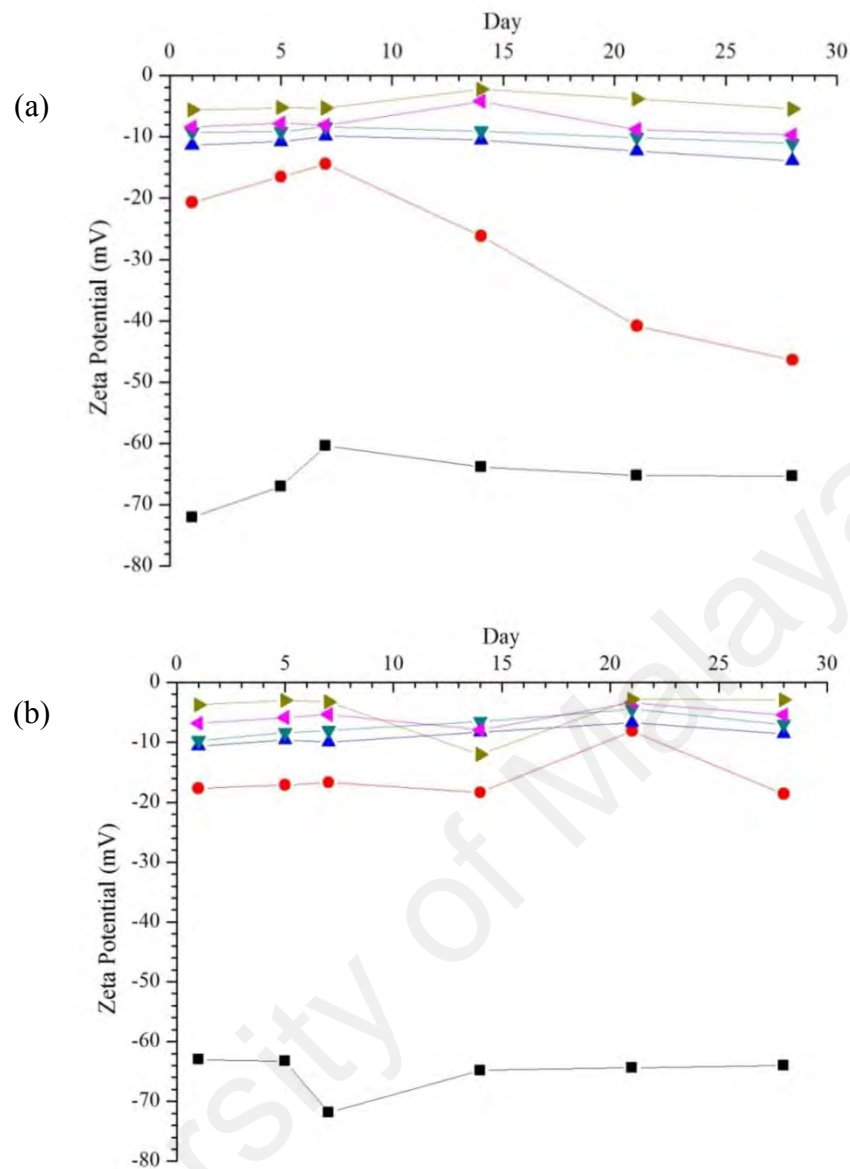
Figure 4.26: Zeta Potential of DOPEPEG2000-oleic acid liposomes with the molar ratio of DOPEPEG2000 to oleic acid of 0:1, (■), 0.01:1, (●), 0.02:1, (▲), 0.03:1, (▼), 0.04:1, (◀), and 0.05:1 (▶) in (a) pH 8.5 and (b) 7.4 with standard deviation less than 0.5 as incubated at 30 °C for 28 days.

Analysis for zeta potential of DOPEPEG2000-oleic acid-erucic acid liposomes with respect to the amount of erucic acid incorporated gave a reduction of zeta potential as shown in Figure 4.27. The ionized and non-ionized species of erucic acid, oleic acid, and DOPEPEG2000 interacted by lateral hydrogen bonding to build the bilayer of DOPEPEG2000-oleic acid-erucic acid liposomes. The magnitude of the zeta potential of liposomes was moved to more negative with the addition of erucic acid in the formulations as the zeta potential of erucic acid liposomes in pH 7.4 was -26.3 mV.
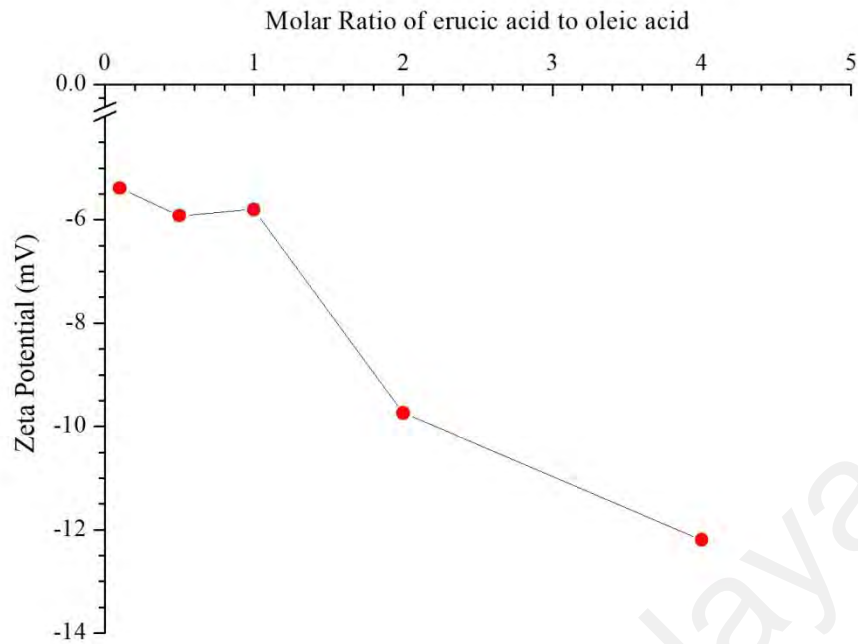
Figure 4.27: Zeta Potential of one day old DOPEPEG2000-oleic acid-erucic acid liposomes at pH 7.4 at 30 ºC with standard deviation less than 0.5. The ratio of DOPEPEG2000 to oleic acid in formulation was fixed at 0.02:1.
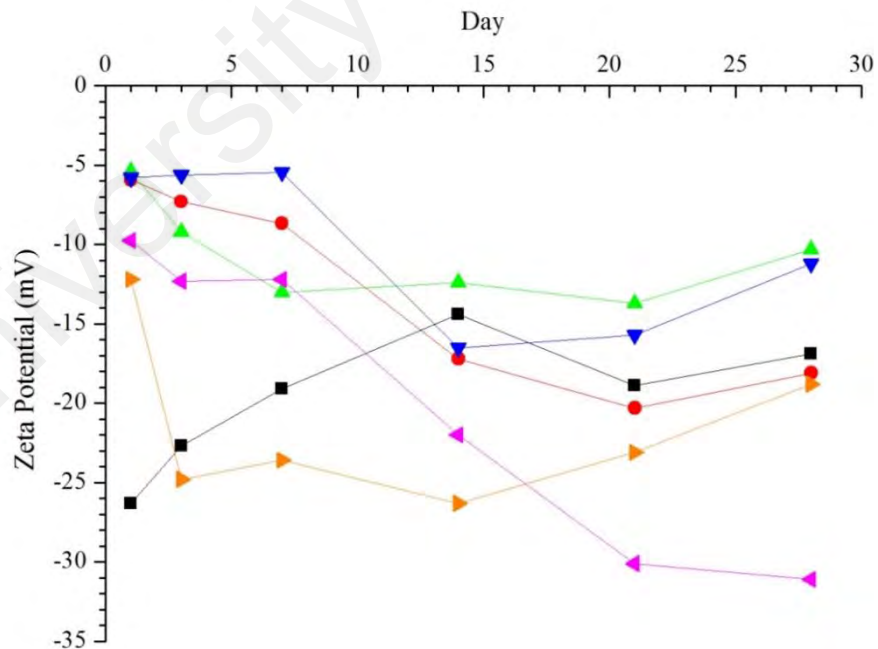
Figure 4.28: Zeta Potential of erucic acid liposomes (■) and DOPEPEG2000-oleic acid- erucic acid liposomes with standard deviation less than 0.5 and the molar ratios of erucic acid to oleic acid of 0.1:1, (●) , 0.5:1, (▲), 1:1, (▼),2:1, (◄), and 4:1(►), as incubated at 30 °C for 28 days. The ratio of DOPEPEG2000 to oleic acid was fixed at 0.02:1.

DOPEPEG2000-oleic acid-erucic acid liposomes were then further incubated in incubator at 30 °C and zeta potential was measured with the aim of monitoring the stability of liposomes for 28 days. Over incubation period, the zeta potential of DOPEPEG2000-oleic acid-erucic acid liposomes became more negative as shown in Figure 4.28, which may be due to the oxidation of ionized species at the bilayer of liposomes. The ratio of DOPEPEG2000 to oleic acid was fixed to 0.02:1 and reported as a single unit. DOPEPEG2000-oleic acid-erucic acid liposomes with the ratio of 0.5:1 and 1:1 display the least fluctuation and stable over 28 days as compared to other formulations. The stability of liposomes highly depended on the ratio of protonation/ionization ratio which affected the formation of hydrogen bonds at their carboxylic acid terminal (Fameau et al., 2014).
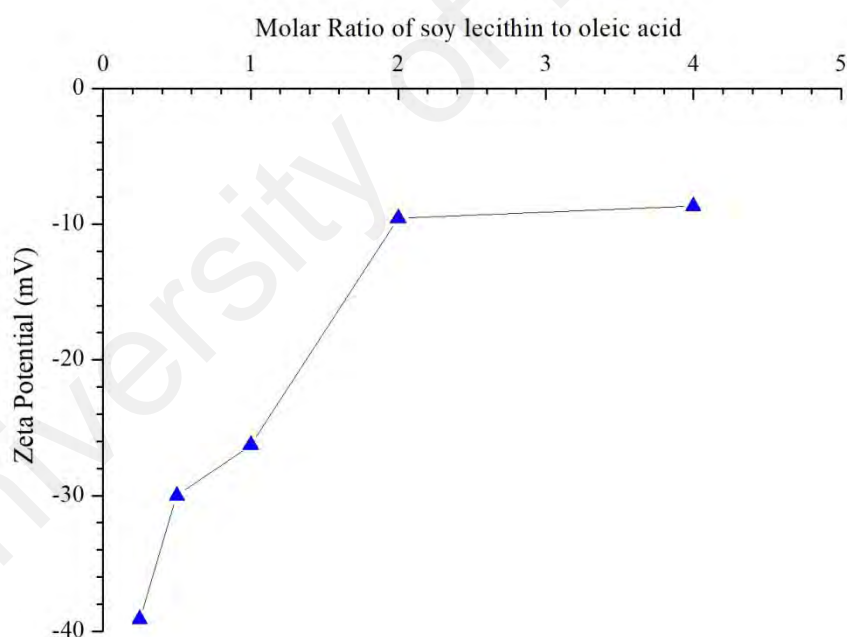
Figure 4.29: Zeta Potential of one day old DOPEPEG2000-oleic acid-soy lecithin liposomes at pH 7.4 with standard deviation less than 0.5 as a function of the molar ratio of soy lecithin to DOPEPEG2000-oleic acid at 30 °C. The ratio of DOPEPEG2000 to oleic acid was fixed at 0.02:1 and reported as single component.

Figure 4.29 shows the effect of incorporating soy lecithin in the formulation on the zeta potential of DOPEPEG2000-oleic acid liposomes indicating that the zeta potential values of DOPEPEG2000-oleic acid-soy lecithin liposomes became less negative with

the addition of soy lecithin in the formulation as compared to -7.4 mV in soy lecithin liposomes. This phenomenon was occurred due to the shielding of anionic charge from soy lecithin (Zhang et al., 2012). The attractive van der Waals forces was increased inversely with the zeta potential values until the electrical double layer repulsive forces were overcame, which forced liposomes to contact to each other, adhered, then aggregated (Crooke, 2007).

Table 4.2 showed that combination 1, 2, and 3 became less negative with respected to incubating period due to the rapid transfer of oleic acid from oleic acid liposomes to soy lecithin liposomes through an aqueous phase (Rogerson et al., 2006). This promoted the degradation of lipid components via oxidation, hydrolysis, collision, or unification. However, the slower kinetic transfer of soy lecithin to oleic acid liposomes affected combination 4 to 6 to become more negative, which increased the repulsive electrical double layer of liposomes and reduced the collision frequency among liposomes (Crooke, 2007).

Table 4.2: Zeta Potential of DOPEPEG2000-oleic acid-soy lecithin liposomes with standard deviation less than 0.5 at 30 ºC

Combination	Ratio of Soy Lecithin to DOPEPEG2000-Oleic Acid	Zeta Potential (mV)	
		Day 1	Day 28
1	0.25: 0.02: 1.00	-39.1	-14.8
2	0.50: 0.02: 1.00	-30.0	-17.4
3	1.00: 0.02: 1.00	-26.3	-17.5
4	2.00: 0.02: 1.00	-9.6	-16.9
5	4.00: 0.02: 1.00	-8.7	-9.7
6	1.00: 0.00: 0.00	-7.4	-10.4

The stability of liposomes in term of zeta potential is very important in designing the drug carrier in order to make sure that the designed liposomes will be stable in the desired site of the target without bursting and flooding the system with the encapsulated ingredient because this may cause toxicity to the system.

4.7   Particle Size

Dynamic light scattering is the most popular (Storey & Ymén, 2011) and the most established technique (Anderson et al., 2013) to measure the hydrodynamic size of the particles up to submicron. Controlling the size of liposomes is very crucial due to the size of liposomes has to be less than 4000 nm to be compatible with the size of blood capillary (Zhang et al., 2011), in order to control the uptake by macrophage, phagocytic, and non-phagocytic cells (He et al., 2010).
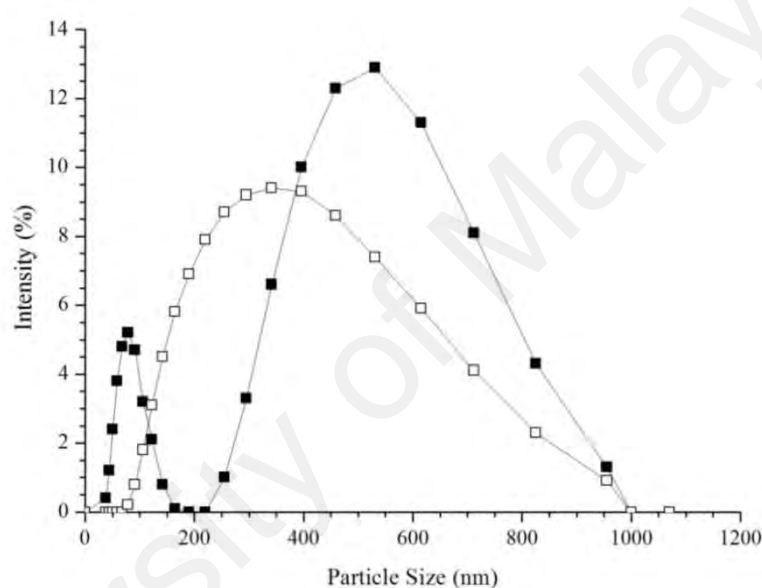
Figure 4.30: Particle size of one day old oleic acid liposomes with standard deviation less than 0.5 at pH 8.5 (□) and pH 7.4 (■) at 30 °C.

Figure 4.30 presents the average particle size of 10 mmol dm^{-3} oleic acid liposomes at pH 7.4 and pH 8.5 without the input of any external energy or mechanical procedure. In pH 8.5, the most liposomes have the size of 531.2 nm. However, peak at 78.8 nm showed that liposomes have a wide range of size may be due to the aggregation of oleic acid liposomes. The large size of liposomes is due to the aggregation of liposomes as well as the formation of multilamellar liposomes as shown in Figure 4.16 and 4.17. On the other hands, oleic acid liposomes pH 7.4 showed a broad peak with the highest intensity was at 342.0 nm. The size of liposomes can be controlled using extruder, sonication or filtering using a syringe filter.

Incorporation of DOPEPEG2000 into oleic acid liposomes formulation reduced the average particle size of DOPEPEG2000-oleic acid liposomes in both pH 7.4 and 8.5 as displays in Figure 4.31 (a) and (b). DOPE formed a conical structure due to the greater lipophilic tail part as compared to its head part (Holland et al., 1996). As a result, the curvature of the outer and inner surfaces of the DOPEPEG2000-oleic acid liposomes was increased which reduced the average particle size of DOPEPEG2000-oleic acid liposomes in both pH 7.4 and 8.5. Continuous addition of DOPEPEG2000 into formulation further reduced the size of DOPEPEG2000-oleic acid liposomes to the minimum size of 125.3 and 136.6 nm in pH 8.5 and 7.4, respectively. The molar ratio of DOPEPEG2000 to oleic acid at the smallest size of DOPEPEG2000-oleic acid formed was 0.03:1 in both pH 8.5 and 7.4. The average particle size of DOPEPEG2000-oleic acid was increased after this molar ratio due to the aggregation of liposomes as the DOPEPEG2000 was saturated at the surface of liposomes (Zhang et al., 2012).

The DOPEPEG2000-oleic acid liposomes were then incubated and the changes in the particle size were monitored for the period of 28 days at 30 °C. Both figures display the same trend of the growth of the mean particle size of DOPEPEG2000-oleic acid liposomes through the incubation period of 28 days due to the aggregation of the liposomes. A small increment in the mean particle size exposed that DOPEPEG2000-oleic acid liposomes were stable during the tested period. However, over the incubation period, oleic acid liposomes showed the aggregation as early as 5th days in pH 8.5 and 7th days in pH 7.4 then underwent reduction in the particle size may be due to the oxidation of the membrane which leads to the rupture of liposomal bilayer membrane. The presence of DOPEPEG2000 delayed the aggregation of liposomes which enhance the stability of liposomes. DOPEPEG2000-oleic acid liposomes with the molar ratio of 0.02:1 showed the most stable particle size through the maturation period and this ratio was used to mix with soy lecithin and erucic acid.
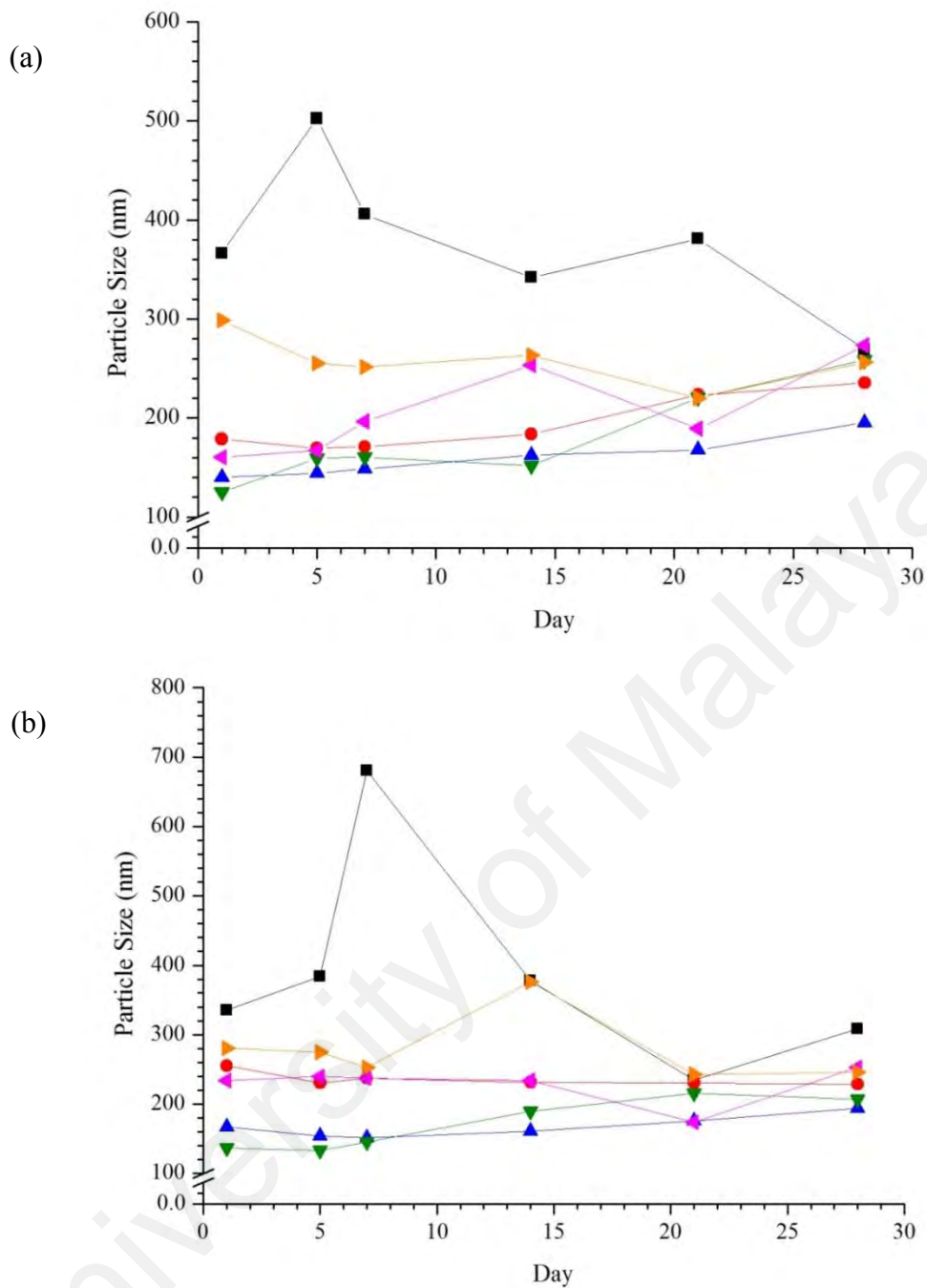
Figure 4.31: Particle size of DOPEPEG2000-oleic acid liposomes with standard deviation less than 0.5 and the molar ratio of DOPEPEG2000 to oleic acid of 0:1, (■), 0.01:1, (●), 0.02:1, (▲), 0.03:1, (▼), 0.04:1, (◄), and 0.05:1 (►) as incubated at 30 °C for 28 days at (a) pH 8.5 and (b) 7.4.

The hydrodynamic size of one day old 10 mmol dm^{-3} erucic liposomes at pH 7.4 was 740.0 nm. Incorporation of DOPEPEG2000-oleic acid into formulation reduced the average particle size of DOPEPEG2000-oleic acid-erucic acid liposomes as shown in the Figure 4.32. Incorporation of DOPEPEG2000-oleic acid into the preparation reduced the average particle size of the prepared liposomes. The drop in particle size

achieved its maximum at the molar ratio of DOPEPEG2000-oleic acid to erucic acid at 1:1, where the average particle size was 276.3 nm. However, as the amount of erucic acid was further introduced into the formulation, the average particle size of liposomes is found to be larger due to the aggregation among liposomes.
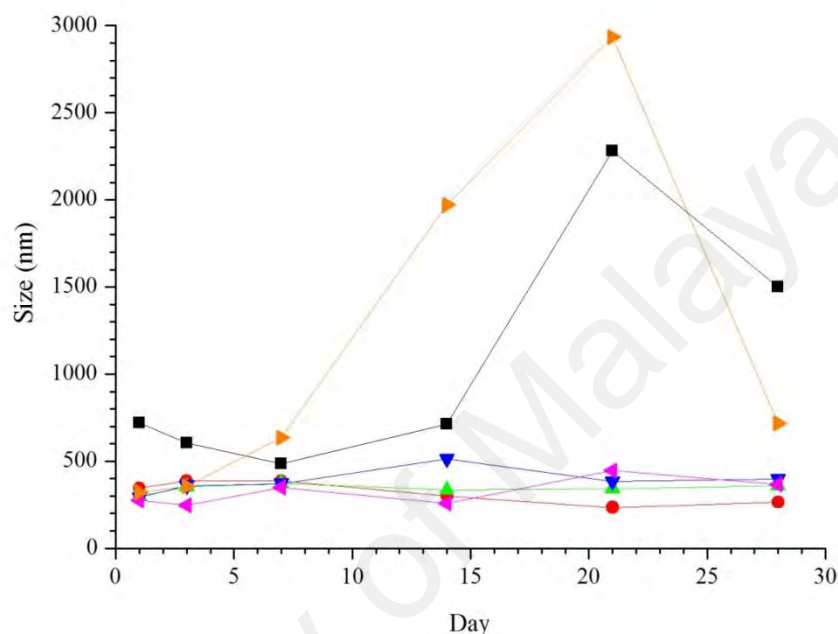
Figure 4.32: Particle Size with standard deviation less than 0.5 of erucic acid liposomes (■) and DOPEPEG2000-oleic acid- erucic acid liposomes with the molar ratios of erucic acid to oleic acid of 0.1:1, (●) , 0.5:1, (▲), 1:1, (▼), 2:1, (◄), and 4:1(►), to DOPEPEG2000-oleic acid as incubated at 30 °C for 28 days. The ratio of DOPEPEG2000 to oleic acid in the formulation was fixed at 0.02:1.

Incubation of DOPEPEG2000-oleic acid-erucic acid liposomes at 30 °C for 28 days showed the growth in the average particle size which may vary due to the aggregation, collision and fusion of liposomes. DOPEPEG2000-oleic acid-erucic of the molar ratio of DOPEPEG2000-oleic acid to erucic of 1:1 exhibited the least changes in the particle size, proving the stability of that formulation. As compared to erucic acid liposomes, incorporation of DOPEPEG2000-oleic acid strongly increase the stability of erucic acid liposomes.

Soy lecithin liposomes had a very large hydrodynamic diameter of 3572 nm as compared to DOPEPEG2000-oleic acid liposomes due to the mixture of phospholipids

and the esterified sugar groups that attached to glycolipids were incorporated within the liposomes bilayer (Zhao et al., 2015), that developing the multilamellar liposomes (Imran et al., 2015). Mixed oleic acid-soy lecithin liposomes were designed to engineer the properties of the mixed oleic acid-soy lecithin liposomes membrane by rationing the soy lecithin against oleic acid with the presence of DOPEPEG2000. As the soy lecithin was added to the formulations, the average particle size of DOPEPEG2000-oleic acid-soy lecithin liposomes was significantly reduced to 288 nm at the ratio of DOPEPEG2000-oleic acid to soy lecithin of 1 to 1 (Figure 4.33) as oleic acid increased the mean curvature of the bilayer (Godoy et al., 2015). The formation rate of oleic acid liposomes was slower as compared to the interaction rate between the oleic acid and phosphatidylcholine in soy lecithin (Lonchin et al., 1999), making the membrane of soy lecithin liposomes was governed by soy lecithin and perturbed by the addition of oleic acid in the formulation (Kleinfeld et al., 1997). Also, incorporation of DOPEPEG2000 reduced the particle size of DOPEPEG2000-oleic acid- soy lecithin liposomes by promoting the curvature at the surface of the liposomes (Teo et al., 2011; Zhang et al., 2012). However, further addition of soy lecithin into DOPEPEG2000-oleic acid-soy lecithin liposomes increased the average particle size of liposomes due to the formation of multilamellar, multivesicular, and aggregations of liposomes (Zhang et al., 2012). The slow phospholipids exchange rate between liposomes leaves a metastable oleate that eventually formed the liposomes (Rogerson et al., 2006), resulting in the decrement of the particle size of DOPEPEG2000-oleic acid-soy lecithin liposomes at day 7 of incubation. The small transformation in particle size at day 7 to day 28 further proved that stable DOPEPEG2000-oleic acid-soy lecithin liposomes were successfully formulated.
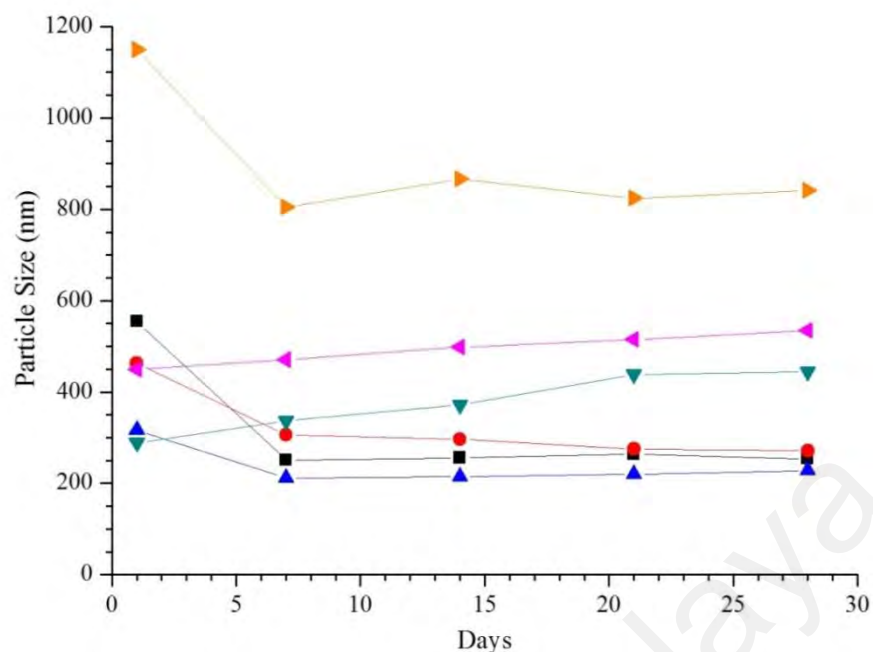
Figure 4.33: Hydrodynamic diameter with the standard deviation less than 0.5 of the different molar ratio of soy lecithin to oleic acid for 0.125:1(■), 0.25:1 (●), 0.5:1 (▲), 1:1 (▼), 2:1 (◄), and 4:1(►) at 30 °C. The ratio of DOPEPEG2000 to oleic acid in the formulation was fixed at 0.02:1.

In summary, most of the formulations had an increase in particle size over the incubation period. These were due to the abstraction of the hydrogen atom from the lipid chain that catalysed by the radiation or sonication. Furthermore, the double bond in the lipid chains was promoting the oxidation of the lipid. The presence of oxygen would further be developed to form aldehydes, chain scissions or lipid hydro-peroxides.

4.8   Cell Viability Assay

4.8.1   Cell Culture

Since the first use of human cancer cell lines (HeLa) in biomedical research industry, the cell culture technologies have evolved, resulting to the derivation of more than thousands of cancerous cell lines (Langdon, 2004). Development in cell culture technology allows scientist to understand and overcome the previously unforeseen problems such as genetically and phenotypically instability (Freshney, 2015). Current technologies allow excellent control on the cellular environment that regulates the physicochemical and physiological aspects of cell growth. These technologies are applied not only in biology and pathology, but also in immunology, microelectronics, astrophysics, and even nuclear engineering areas (Masters, 2000).

Human epithelial lung cancer cells A549 were seeded in 96 wells plate and the confluency of the cells were recorded (Figure 4.34). From the growth curve, the lag phase of cell proliferation can be observed within 48 hours at the seeding density of 0.25×10^5 and 0.125×10^5 cells mL^{-1}. During this period, the cells were adapting to the medium conditions with less increase in cell number (Banfalvi, 2013), attached to the wall of plate, and preparing for cell division (Martin, 1994). The cells growth were then started to accelerate extensively from day 2 to day 7, which marked the exponential phase of cells growth as shown by the rapid increase in the confluency. However, the cell growth was limited by the nutrients in the medium during the plateau stationary phase from day 4 to day 5, where the confluency was constant and the cell viability started to reduce, which can be observed in the deceleration of growth curve at day 5 (Martin, 1994; Masters, 2000; Banfalvi, 2013).
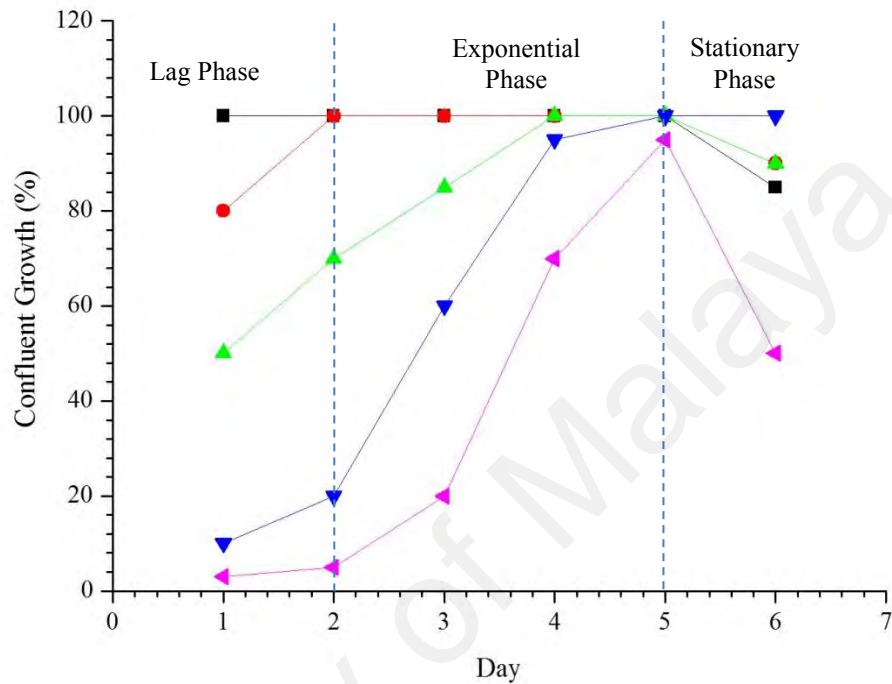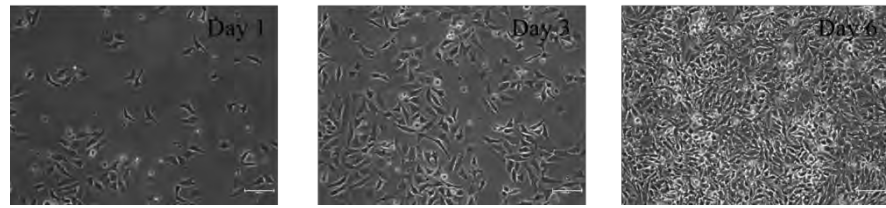
Figure 4.34: Growth curve of human epithelial lung cancer cells A549 grown in DMEM supplemented with 10% FBS and 1% penicillin streptomycin at 37 °C with 5% CO_2 where the seeded density at 2×10^5(■), 1×10^5 (●), 0.5×10^5 (▲), 0.25×10^5 (▼), and 0.125×10^5 (◄) cells mL^{-1}.

Determination of the growth curve was important in determining the incubation period for the sub-culturing process to maintain the logarithmic of the growth as well as the density of the seeded cells. The seeding density of 0.5×10^5 cells mL^{-1} was chosen for further experiments because it yielded a confluency of more than 70% after 48 hours, which was suitable for cells sensitivity test.

4.8.2   Cell Viability Assay

Phospholipids such as phosphatidylcholine, phosphatidylethanolamine (PE), sterols, sphingolipids and fatty acids are essential in cell proliferation (Currie et al., 2013). They have the ability to accumulate at the cell membrane (Yenuganti et al., 2016) and to store

the energy that can stimulate the production of cells membrane (Buckland, 2013) and the production of signalling molecules (Currie et al., 2013).

Pre-clinical screening of fatty acid liposomes is important to evaluate the potential therapeutic effect as well as safety indication (Frazier, 1992). Cell viability assay is one of the most common phenotypic assays (Holenz et al., 2016) used to evaluate the *in vitro* compatibility of fatty acid liposomes to the cells (Masters, 2000; Sun et al., 2015; Yenuganti et al., 2016).
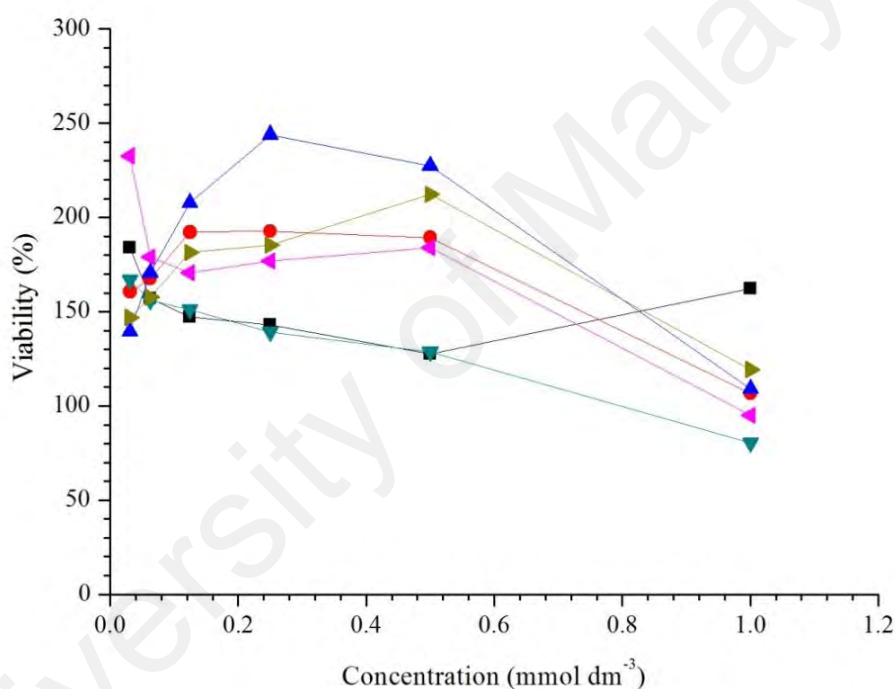
Figure 4.35: Growth (%) of human epithelial lung cancer cell A549 in the presence of DOPEPEG2000-oleic acid liposomes with the molar ratio DOPEPEG2000 to oleic acid of 0:1(■), 0.005:1(●), 0.01:1 (▲), 0.02:1 (▼), 0.03:1 (◄), and 0.04:1 (►) at 37 °C. Data is the mean of three replicates with standard deviation less than 0.2.

The effect of unsaturated oleic acid liposomes to the growth of cells was evaluated by observing the reduction of water soluble tetrazolium salt from MTT (3-[4,5-dimethylthiazol-2-yl]-2,5-diphenyltetrazolium bromide) through the mitochondrial activities, cellular metabolism, and enzymatic activities within the cell. The growth of human epithelial lung cancer cell A549 was affected by the amount of unsaturated fatty acid in the formulations (Figure 4.35, 4.36, and 4.37). The growth of cell was high at the

concentration lower than the CVC of oleic acid liposomes as the free fatty acid was abundance in the medium (Kaminogawa et al., 2012). These fatty acids were mainly utilized in the membrane, storage, signalling lipids, or oxidized to carbon dioxide as an energy source (Buckland, 2013; Currie et al., 2013). Formation of liposomes will reduce the free fatty acid in the environment that can reduce the proliferation of A549 cells, as observed in the experiment.

Incorporation of DOPEPEG2000 in the formulation enhanced the formation of sterically stable DOPEPEG2000-oleic acid liposomes which inhibited the growth of the cell through reduction of free fatty acid (Holland et al., 1996; Gjetting et al., 2010). The hydrophilic DOPEPEG2000 acted as a steric barrier at the surface of liposomes to prevent the fusion of liposomes with the cell membranes (Song et al., 2002), liposomes will stay longer within the cells and in the blood (Song et al., 2002; Yang et al., 2007; Zhang et al., 2012; Hsu et al., 2014; Pachauri et al., 2015).

As a result, fatty acid liposomes that carrying anticancer drugs can maximize the delivery of anticancer drugs to the sites through passive extravasation and accumulation in both tumour and inflamed tissues (Song et al., 2002). These liposomes showed possible cytocompatibility with cells, indicating its potential utility in drug delivery applications.
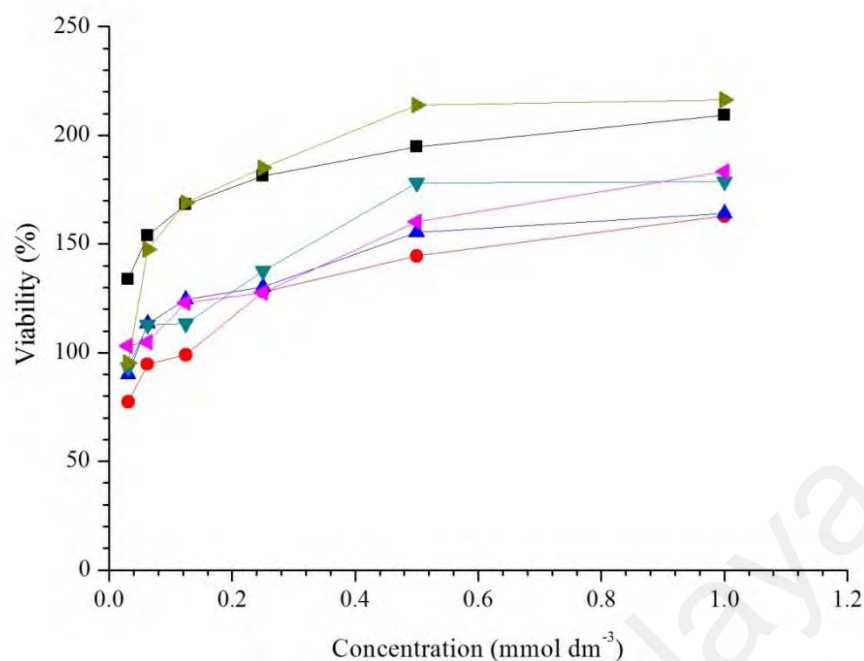
Figure 4.36: Growth (%) of human epithelial lung cancer cell A549 in the presence of DOPEPEG2000-oleic acid-erucic acid liposomes with the molar ratio of erucic acid to DOPEPEG2000-oleic acid of 1:0(■), 0.125:1(●), 0.25:1 (▲), 0.5:1 (▼), 1:1 (◄), and 1:2 (►) at 37 °C. Data is the mean of three replicates with standard deviation less than 0.2.
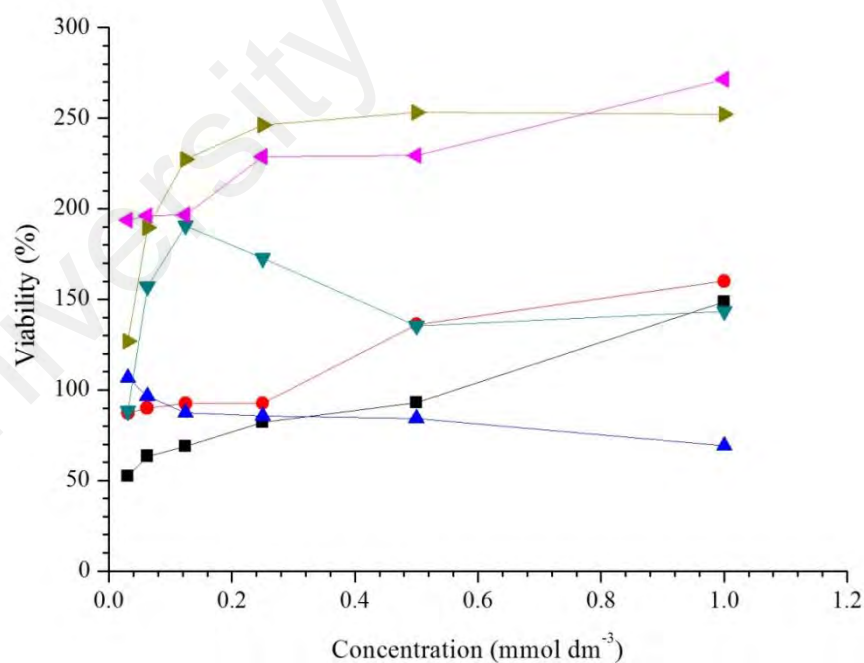
Figure 4.37: Growth (%) of human epithelial lung cancer cell A549 in the presence of DOPEPEG2000-oleic acid-soy lecithin liposomes with the molar ratio of soy lecithin to DOPEPEG2000-oleic acid of 1:0(■), 0.125:1(●), 0.25:1 (▲), 0.5:1 (▼), 1:1 (◄), and 1:2 (►) at 37 °C. Data is the mean of three replicates with standard deviation less than 0.2.

4.9   Encapsulation Efficiency

Liposomes are known to be a competent vehicle to ensure the optimum carrier, enhance specific targeting and reduce the toxicity of anticancer drugs. The unique biphasic morphology of liposomes enables them to carry both lipophilic and hydrophilic molecules in a wide range of solubility (Eloy et al., 2014; Koudelka et al., 2015). The solubility of anticancer drugs is very important in observing the diffusion of active ingredients through the lipid bilayers (Hacker et al., 2009).

In this study, four anticancer drugs were selected based on their log P value ranging from -3 to +3 at pH 7.4, which were folinic acid calcium salt, methotrexate, doxorubicin hydrochloride, and irinotecan hydrochloride that has log P of -2.7, -0.5, +0.5, and +2.8 respectively. They were individually incorporated into liposomes during thin lipid hydration. The positive value of log P indicated that the anticancer drugs were more soluble in the lipid, or known as lipophilic. Oppositely, the negative log P represented the anticancer drugs which were soluble in water and known as hydrophilic. Anticancer drugs that have zero log P value showed that they are equally soluble in both lipid bilayer and the aqueous core of liposomes. Log P value is very important in predicting the location of anticancer drugs, either encapsulated in the aqueous core or within the lipid bilayer of liposomes. The strongly polar anticancer drugs which have a positive log P were located within the lipid bilayer, while the strongly non-polar anticancer drugs which have a negative log P value were located in the aqueous core of liposomes. The pH where the log P was measured is important as the pH conditions will determine the ionization of a molecule to form a hydrophilic anion or cation, which determined the partitioning behaviour of that molecule. In this study, hydrophilic drugs, folinic acid calcium salt and methotrexate were predicted to locate in the aqueous part of liposomes, while lipophilic drugs, doxorubicin and irinotecan hydrochloride were

entrapped within the bilayer of liposomes (Figure 4.38) (Gulati et al., 1998; Hacker et al., 2009).
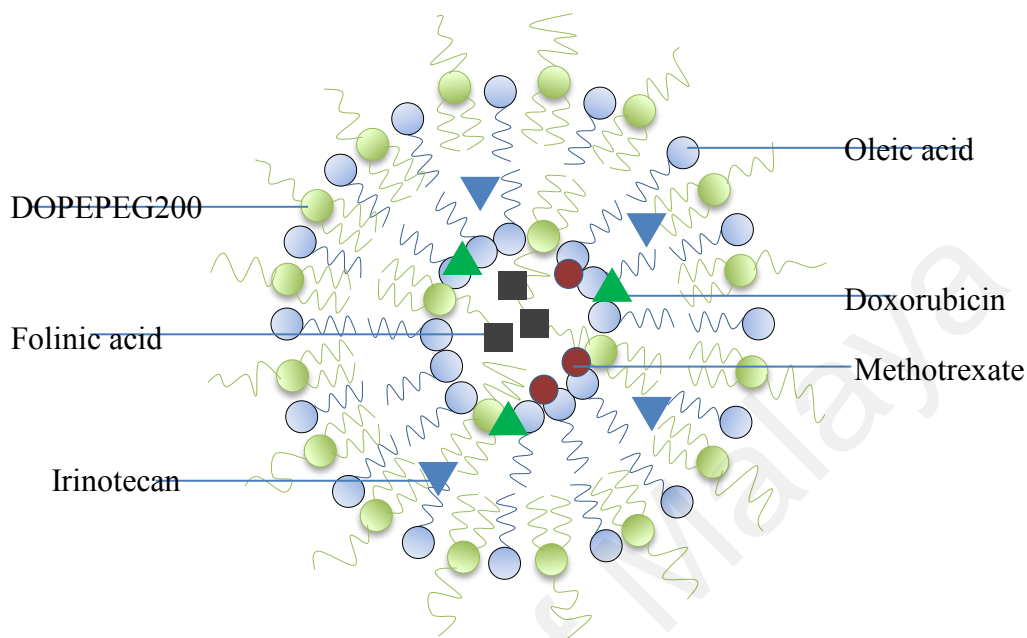
Figure 4.38: Schematic diagram of DOPEPEG2000-oleic acid liposomes and predicted site of anticancer drugs incorporating into liposomes.

Figure 4.39 exposes the encapsulation efficiency of varied anticancer drugs in oleic acid liposomes, both in pH 7.4 and 8.5 as calculated from the centrifugal technique as described in section 3.2.9. More than 70% of anticancer drugs were successfully encapsulated in the oleic acid liposomes. The repeated loading method, which layering the lipids and anticancer drugs for several times yielded significantly higher encapsulation efficiency for both hydrophilic and hydrophobic molecules as compared to the previous study (Teo et al., 2011), which was 4.4 and 61.2% for hydrophilic and lipophilic molecules, respectively. As shown in Figure 4.39, the encapsulation efficiency of hydrophilic drugs was lower than hydrophobic drugs due to the solubility of hydrophilic anticancer drugs in the medium of liposomes that ease the transport of hydrophilic anticancer drugs across the lipid bilayer (Gulati et al., 1998). This diffusion of drugs through the membrane causes leakage of drugs from the liposomes to the environment which affected the encapsulation ability of oleic acid liposomes.

Doxorubicin showed high encapsulation efficiency due to their molecules that can be located in both aqueous and within bilayers. Encapsulation efficiency of most anticancer drugs was higher in oleic acid liposomes pH 7.4 than in oleic acid liposomes pH 8.5 due to the presence of emulsion in the system as well as the larger particle size that capable in loading a larger amount of anticancer drugs.
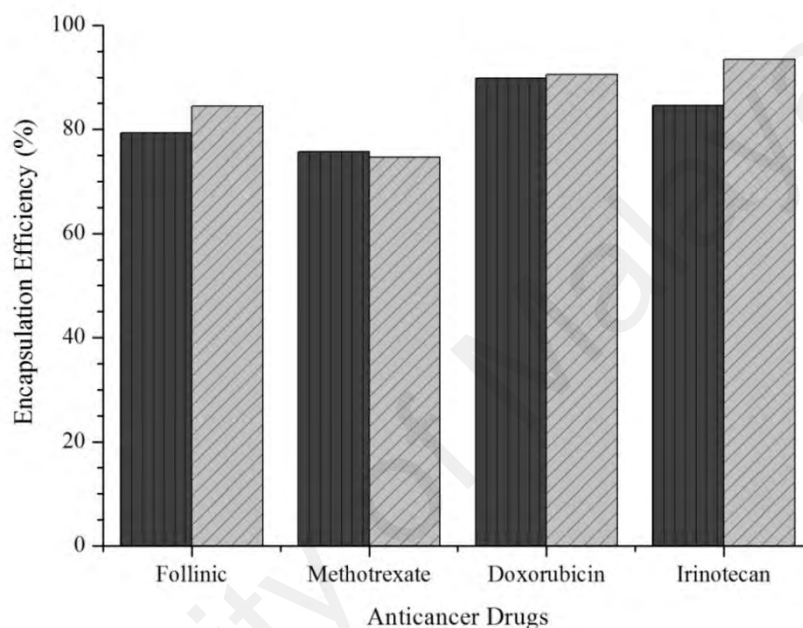
Figure 4.39: Percentage of encapsulation efficiency with standard deviation less than 1 for folinic acid, methotrexate, doxorubicin and irinotecan in oleic acid liposomes pH 7.4 (▨) and 8.5 (▥) at 30 $^{\circ}$C.

Figure 4.40 displays the effect of incorporating DOPEPEG2000 into the oleic acid liposomes formulation, where the encapsulation efficiency of DOPEPEG2000 has followed the same trend as displays in Figure 4.39. This figure shows that encapsulation efficiency of folinic acid calcium salt, doxorubicin hydrochloride, and irinotecan hydrochloride is increased with the raised of DOPEPEG2000 in the formulation which is in contrast to methotrexate which showed reduced in the encapsulation efficiency. However, encapsulation efficiency of folinic acid calcium salt, methotrexate, doxorubicin hydrochloride, and irinotecan hydrochloride reach optimum, where the molar ratio of DOPEPEG2000 to oleic acid was 0.02:1 in both pH 7.4 and 8.5.
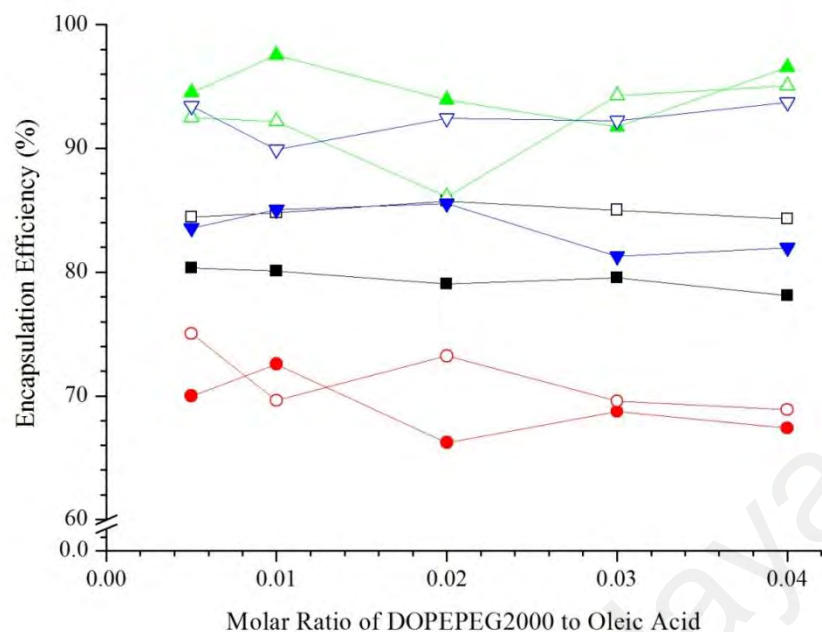
Figure 4.40: Encapsulation efficiency (%) with the standard deviation less than 1, of DOPEPEG2000-oleic acid liposomes in pH 8.5 and 30 °C for folinic acid (■), methotrexate (●), doxorubicin (▲), and irinotecan (▼). The opened symbols represented the DOPEPEG2000-oleic acid liposomes in pH 7.4.
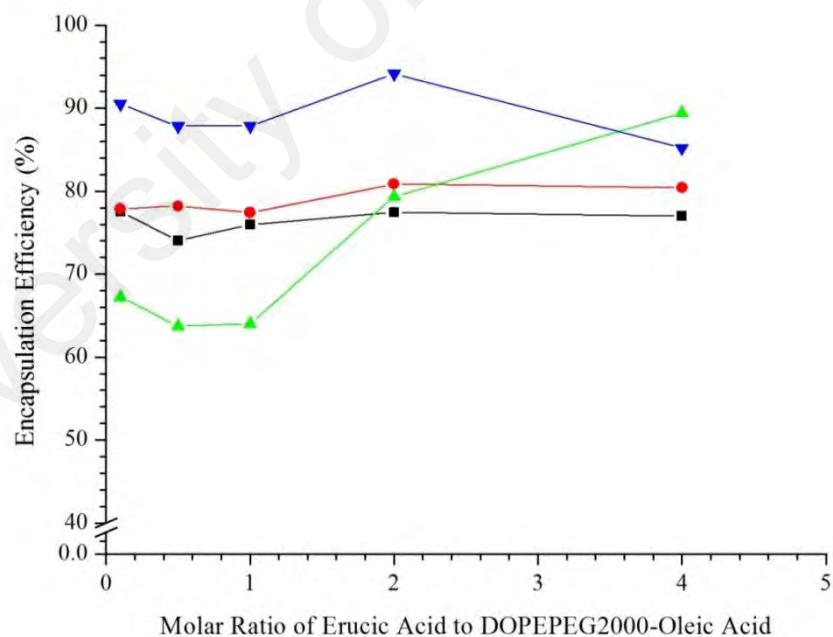
Figure 4.41: Encapsulation efficiency (%) with standard deviation less than 1, of DOPEPEG2000-oleic acid-erucic acid liposomes for folinic acid (■), methotrexate (●), doxorubicin (▲), and irinotecan (▼) in pH 7.4 at 30 °C. The ratio of DOPEPEG2000 to oleic acid was fixed at 0.02:1and reported as a single component.

Encapsulation efficiency with the standard deviation less than 1 of folinic acid,

methotrexate, doxorubicin, and irinotecan in erucic acid liposomes were 76.6, 79.9,

99.5, and 77.8%, respectively. Figure 4.41 indicates that encapsulation efficiency of all anticancer drugs encapsulated in DOPEPEG2000-oleic acid-erucic acid liposomes was greater than 60%. The encapsulation efficiency of folinic acid, methotrexate, and irinotecan was the highest in DOPEPEG2000-oleic acid-erucic acid liposomes at a molar ratio of erucic acid to the DOPEPEG2000-oleic acid of 2:1. Encapsulation efficiency of folinic acid and methotrexate was achieving 75% and 80%, respectively and it was almost the same for all formulation which could be influenced by the volume of the aqueous phase entrapped in the core of DOPEPEG2000-oleic acid-erucic acid liposomes during their formation (Eloy et al., 2014). The hydrophobic irinotecan gave out 94% encapsulation efficiency due to its hydrophobicity and the tendency to locate within bilayer instead of diffusing to the surrounding media (Paini et al., 2015). Encapsulation efficiency of doxorubicin was increasing perpendicularly with the amount of erucic acid in the formulation, achieving the highest encapsulation efficiency of 89.4%. Erucic acid has a long hydrocarbon tail that will increase the thickness of lipid bilayer, which favouring the encapsulation of hydrophobic drugs as compared to hydrophilic drugs such as folinic acid and methotrexate. This was agreeable with the increasing in hydrodynamic size of DOPEPEG2000-oleic acid-erucic acid liposomes as the erucic acid was further introduced to the system. However, biphasic properties of doxorubicin allowed a better encapsulation both in the lipid bilayer and internal aqueous core which yielded higher encapsulation efficiency as compared to hydrophobic irinotecan.

Figure 4.42 displays that encapsulation efficiency of DOPEPEG2000-oleic acid-soy lecithin liposomes was improved with the presence of DOPEPEG2000-oleic acid in the formulation. As compared to pure soy lecithin liposomes, encapsulation efficiency of DOPEPEG2000-oleic acid-soy lecithin liposomes was significantly higher.
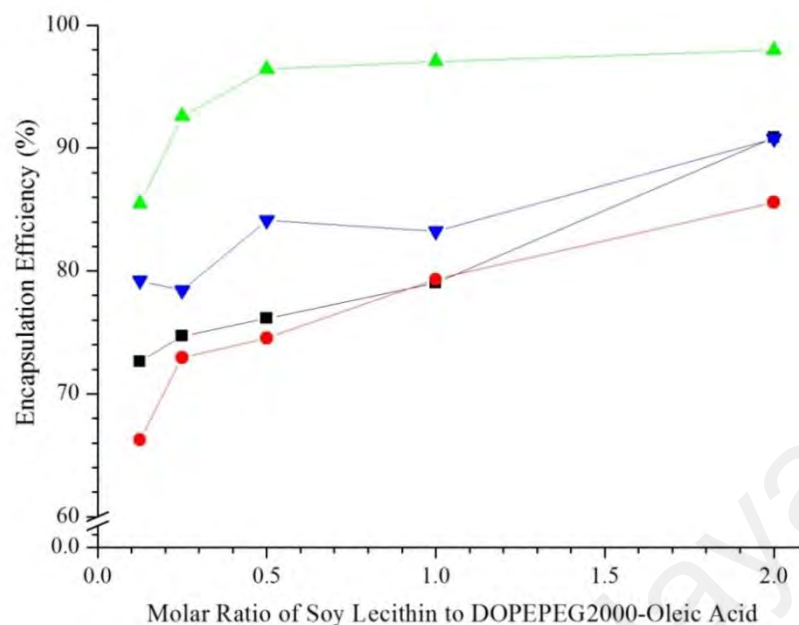
Figure 4.42: Encapsulation efficiency (%) with standard deviation less than 1 of DOPEPEG2000-oleic acid-soy lecithin liposomes for folinic acid (■), methotrexate (●), doxorubicin (▲), and irinotecan (▼) in pH 7.4 at 30 °C. The ratio of DOPEPEG2000 to oleic acid was fixed at 0.02:1 and reported as a single component.

Encapsulation efficiency with standard deviation less than 1 of folinic acid, methotrexate, doxorubicin, and irinotecan for soy lecithin liposomes were 65.5, 64.4, 65.8, and 24.2%, respectively. As the amount of soy lecithin was increased in the formulation, there was a higher probability of entrapment of the all anticancer drugs in the DOPEPEG2000-oleic acid-soy lecithin liposomes, thus raising the encapsulation efficiency of the drugs. This was consistent with the hydrodynamic size of DOPEPEG2000-oleic acid-soy lecithin liposomes which grew larger with the addition of soy lecithin in the formulation. The low surface charge of DOPEPEG2000-oleic acid-soy lecithin liposomes promoted the aggregation or flocculation that increased the encapsulation efficiency values of liposomes (Li-Zhiyu et al., 2015). The increase in the encapsulation efficiency of DOPEPEG2000-oleic acid-soy lecithin liposomes was optimum at the molar ratio of DOPEPEG2000-oleic acid to soy lecithin of 1:0.5 for doxorubicin and irinotecan. However, encapsulation efficiency of hydrophilic drugs namely folinic acid and methotrexate was increasing with the addition of soy lecithin.

The finding has been demonstrated that exploring the formulation of liposomes was known to alter the thickness, fluidity, and polarity of liposomes which then affecting the partitioning and encapsulation of the anticancer drugs (Eloy et al., 2014). These four anticancer drugs with different log P could be further used as a model for encapsulating a wide range of anticancer drugs within the designated mixed oleic acid liposomes.

4.10 Cytotoxicity Assay

In vitro toxicology test is important to establish the safety limit of exposure to anticancer drugs (Frazier, 1992). The LDH leakage assay (Han et al., 2011), a protein assay (Wakuri et al., 2017), the neutral red, and the MTT assay (Stockert et al., 2012; Boeckel et al., 2014; Yang et al., 2015) are *in vitro* toxicology studies that widely used for the detection of cytotoxicity or cell viability following exposure to toxic substances (Fotakis & Timbrell, 2006), hence, evaluate efficacy of the drugs or formulations against the desired effect.

Antitumor potential of various liposomes formulations encapsulating anticancer drugs namely folinic acid, methotrexate, doxorubicin, and irinotecan were evaluated in human lung cancer cell using MTT assay. It is a simple technique to measure the cellular oxidative metabolism, indicating activity of viable cells through spectrometry (Yadav & Tyagi, 2008; Stockert et al., 2012). The 3-[4,5-dimethylthiazol-2-yl]-2,5-diphenyltetrazolium bromide (MTT) is a water-soluble tetrazolium salt that transforms into formazan by succinate dehydrogenase within the mitochondria, which accumulates at the healthy viable cells (Fotakis & Timbrell, 2006). The absorbance of the purple formazan was then quantified using UV-VIS spectrophotometer.

The A549 cells were exposed to the increasing concentration of folinic acid, methotrexate, doxorubicin, and irinotecan in order to evaluate the half maximal inhibitory concentration (IC_{50}) values towards A549 cells (Table 4.3). The toxicity of

anticancer drugs in cells is determined by the cancer cells sensitivity, the amount of anticancer drugs, exposure time, as well as the metabolism, elimination, and binding of the anticancer drugs to the target molecules. Generally, the IC_{50} values of free anticancer drugs were reduced with increasing exposure time of anticancer drugs, indicating that the cell viability was decreased with the incubation time. Liposomes encapsulating anticancer drugs showed the reduction in IC_{50} as compared to free drugs, suggesting that these liposomal formulations were remarkably effective in inhibiting the cell growth (Ishida et al., 2001; Sun et al., 2015). This may due to the enhanced accumulation of liposomes formulation at the targeted sites, increased permeability, and release of the anticancer drugs into the cancer cells.

Table 4.3: The half maximal inhibitory concentration (IC_{50}) values for A549 cells with the exposure to various anticancer drugs and liposomes encapsulating anticancer drugs based on the dose-response curve derived from MTT assay.

Samples	$IC_{50} \pm < 0.2$ (mmol dm^{-3})		
	24 hours	48 hours	72 hours
Folinic acid	3.4	3.3	3.1
in DOPEPEG2000:oleic acid (0.02:1)	2.1	2.9	3.5
in DOPEPEG2000: oleic acid: erucic acid (0.02:1:1)	1.6	2.8	1.9
in DOPEPEG2000: oleic acid: soy lecithin (0.02:1:1)	1.9	3.5	2.5
Methotrexate	3.4	3.3	2.9
in DOPEPEG2000:oleic acid (0.02:1)	1.7	2.4	2.9
in DOPEPEG2000: oleic acid: erucic acid (0.02:1:1)	2.1	2.6	2.9
in DOPEPEG2000: oleic acid: soy lecithin (0.02:1:1)	1.9	2.2	2.5
Doxorubicin	0.9	2.3	2.2
in DOPEPEG2000:oleic acid (0.02:1)	0.9	2.2	2.7
in DOPEPEG2000: oleic acid: erucic acid (0.02:1:1)	1.0	2.6	3.5
in DOPEPEG2000: oleic acid: soy lecithin (0.02:1:1)	1.9	3.3	3.8
Irinotecan	3.8	3.1	1.5
in DOPEPEG2000:oleic acid (0.02:1)	1.1	2.5	3.0
in DOPEPEG2000: oleic acid: erucic acid (0.02:1:1)	1.9	3.6	2.8
in DOPEPEG2000: oleic acid: soy lecithin (0.02:1:1)	1.8	2.3	3.2

4.11   *In vitro* Release Study

Adequate drug bioavailability in the cancerous tissue is depending on drug release from the liposomes (Andresen et al., 2005). *In vitro* diffusion of the liposomes encapsulating drug studies provided abundant information whether the prepared liposomes can be permeated through the membrane and released the active ingredients at the controlled time. Franz diffusion cell is a most widely used system (Kielhorn et al., 2006) to study the release of nanoparticles through the membrane which is suitable for *in vitro* release studies as they are not rate-limiting barriers as well as a support to the system (Modi, 2014). The receptor fluid under the membrane was automatically collected by removing the aliquots for analysis using UV spectrophotometer.
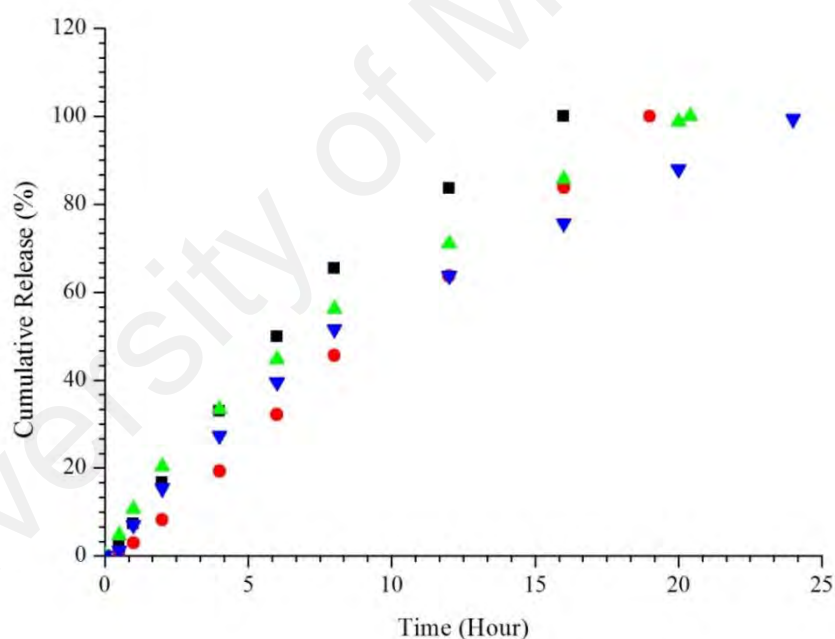
Figure 4.43: Cumulative release (%) with standard deviation less than 1, at 37 $^{\circ}$C of folinic acid (■), methotrexate (●), doxorubicin (▲), and irinotecan (▼).

Figure 4.43 represents the *in vitro* release of four anticancer drugs with log P ranging from -3 to +3, which were folinic acid (-2.7), methotrexate (-0.5), doxorubicin (+0.5), and irinotecan (+2.8). Folinic acid which was the most hydrophilic drug that was used showed the fastest released as compared to other anticancer drugs. The release of

anticancer drugs achieved 100% for folinic acid, methotrexate, doxorubicin, and irinotecan were 16, 19, 20.4, and 23.6 hours respectively.

The dissolution profiles showed that the regression coefficient (R^2) value that analysed using zero order dissolution models as displayed in Table 4.4 was highest in irinotecan which compatible to their nature that was the most hydrophobic as compared to other anticancer drugs (Dash et al., 2010). The lowest *SME* values showed that irinotecan was fitted most to the zero order dissolution models. Oppositely, in the first order, Higuchi, and Gompertz dissolution models, folinic acid showed the highest R^2 values which were explainable by their highest solubility in water (Dash et al., 2010).

Table 4.4: Rate of release, *K*, regression coefficient, R^2, and standard median error (*SME*) values of folinic acid, methotrexate, doxorubicin, and irinotecan at 37 °C

Kinetic Model		Molar ratio of DOPEPEG2000 to oleic acid			
		Folinic Acid	**Methotrexate**	**Doxorubicin**	**Irinotecan**
Zero Order	K_0	5.2085	4.6188	6.0521	5.1948
(n=10)	R^2	0.9249	0.9347	0.9493	0.9978
	SME	7.7552	4.2348	1.0796	1.0544
First Order	K_1	0.0914	0.1151	0.1436	0.0967
(n=10)	R^2	0.984	0.9607	0.8947	0.886
	SME	1.8937	5.5276	22.4051	21.6720
Higuchi	K_H	20.9464	18.5042	24.1325	20.1291
(n=10)	R^2	0.957	0.9415	0.9289	0.8505
	SME	6.0425	6.9394	15.1247	28.4238
Korsmeyer-Peppas	K_{KP}	12.972	10.6515	12.7178	5.5179
(n=6)	R^2	0.9980	0.9922	0.9917	0.9979
	SME	3.2385	10.3739	19.8544	4.3982
Gompertz	$K_{G\alpha}$	7.0333	48.451	7.327	32.815
(n=10)	$K_{G\beta}$	2.753	4.7998	3.1127	5.2297
	R^2	0.9562	0.9155	0.9121	0.8926
	SME	5.8468	18.0783	13.9000	25.7191

4.11.1 *In vitro* Release Study of DOPEPEG2000-oleic acid Liposomes

Oleic acid liposomes encapsulating folinic acid, methotrexate, doxorubicin, and irinotecan were diffused through five kDa MWCO cellulose dialysis membranes via osmotic gradient force (Gillet et al., 2009). Figure 4.44 displays the cumulative released of various anticancer drugs from oleic acid liposomes within 24 hours.
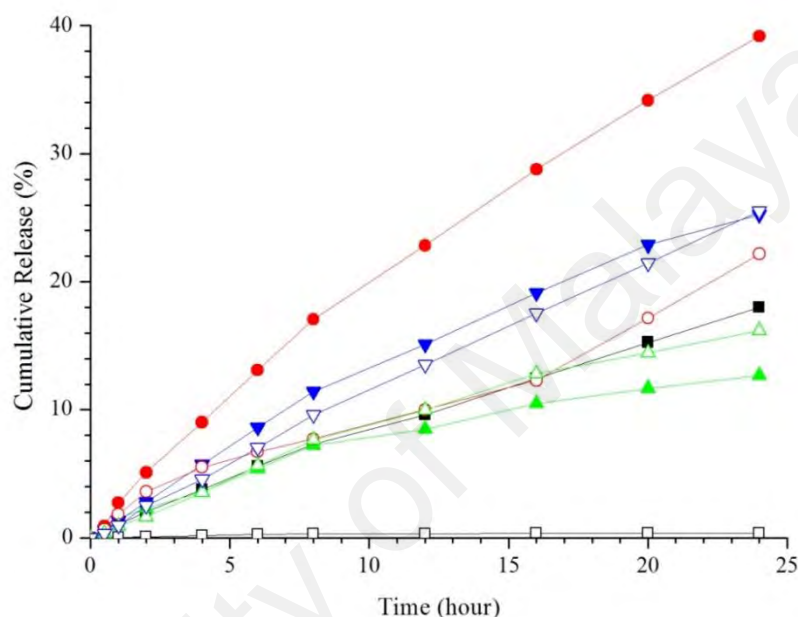
Figure 4.44: Cumulative release percentage (%) with standard deviation not more than 1 of folinic acid (■), methotrexate (●), doxorubicin (▲), and irinotecan (▼) from oleic acid liposomes in pH 8.5 at 37 °C. The opened symbols represented the cumulative release (%) of respective anticancer drugs from oleic acid liposomes in pH 7.4.

Generally, oleic acid liposomes both in pH 8.5 and 7.4 displayed a slow released property where less than 40% of anticancer drugs were released after 24 hours. In oleic acid liposomes pH 8.5, methotrexate released the highest after 24 hours which was 39.1% followed by irinotecan, folinic acid, and doxorubicin which were 25.2, 18.0, and 12.7%, respectively. Hydrophilic drug methotrexate released the most of the loaded drug as compared to other anticancer drugs due to the intermediate log P of methotrexate that entrapped in both aqueous and membrane phase was easily leaked out of the liposomes into the environment (Gulati et al., 1998). The diffusion rate of methotrexate from oleic acid liposomes into the environment was the greatest as

compared to the other anticancer drugs. A positively intermediate log P doxorubicin showed an opposite phenomenon where the cumulative released was the lowest at 12.7% after 24 hours. Slightly hydrophobic doxorubicin associated with the bilayers had a potentially longer life in vivo as compared to other hydrophilic drugs.

Oleic acid liposomes pH 7.4 showed a different release phenomenon as compared to those in pH 8.5 due to the presence of oleic acid emulsion in the pH 7.4. Hydrophobic anticancer drug irinotecan released the most at 25.5% followed by methotrexate, doxorubicin, and folinic acid at 22.2, 16.2, and 0.4%, respectively. The presence of emulsion in the sample promoted the released of irinotecan into the environment. In contrast, folinic acid showed a very low release of 0.4% in all formulations due to the liposomes-rich emulsion environment was not favoured by their hydrophilicity behaviour.

The dissolution profiles of various anticancer drugs released from oleic acid liposomes pH 7.4 and 8.5 were evaluated by using five dependent methods, which were zero-order, first-order, Higuchi, Korsmeyer-Peppas, and Gompertz dissolution model as shown in Table 4.5. The linear regression values were used to determine the suitable anticancer drug release kinetic model. The release of folinic acid from oleic acid liposomes pH 7.4 and doxorubicin from oleic acid liposomes of both pH was best fitted to Gompertz dissolution model due to the sharp increase in the earlier stage of release, then turned slowly to the asymptotic maximal dissolution. These models were suitable for the drugs with good solubility having an intermediate release rate in PBS 7.4 such as folinic acid and doxorubicin (Dash et al., 2010). Irinotecan from oleic acid liposomes pH 8.5 and methotrexate from oleic acid liposomes pH 7.4 and 8.5 had the highest R^2 in the Korsmeyer-Peppas model. The R^2 value of folinic acid, methotrexate, doxorubicin, and irinotecan released from oleic acid liposomes pH 8.5 and 7.4 gave out more than

0.9, which can be explained by the release that happened due to the erosion of oleic acid liposomes (Gad, 2008), that releasing the anticancer drugs into the environment. In oleic acid liposomes pH 7.4, the release of lipophilic irinotecan was best fitted to first-order dissolution model, which was suitable for the drug that released directly proportional to the amount of the drug loaded (De et al., 2013) from porous liposomes to the surrounding media (Dash et al., 2010). The lipophilic behaviour promoted the diffusion of irinotecan from entrapping within the bilayer membrane of liposomes to the emulsion environment.

Table 4.5: Regression Coefficient, R^2, values of various anticancer drugs release from oleic acid liposomes pH 7.4 and 8.5.

| Kinetic Model | Regression Coefficient, R^2 | | | | | | | |
| | Folinic acid | | Methotrexate | | Doxorubicin | | Irinotecan | |
	pH 8.5	pH 7.4	pH 8.5	pH 7.4	pH 8.5	pH 7.4	pH 8.5	pH 7.4
Zero	0.9902	0.5681	0.9779	0.9553	0.8992	0.9694	0.9762	0.9973
First	0.9952	0.5694	0.9962	0.9541	0.9173	0.9802	0.9902	0.9995
Higuchi	0.8932	0.9105	0.9144	0.8564	0.9554	0.9087	0.9084	0.8693
Korsmeyer-Peppas	0.9989	0.9112	0.9989	0.9596	0.9890	0.9924	0.9960	0.9993
Gompertz	0.9920	0.9269	0.9893	0.9203	0.9954	0.9985	0.9972	0.9926

Figure 4.45 displays the effect of DOPEPEG2000 in the formulation to the release of folinic acid from DOPEPEG2000-oleic acid liposomes pH 8.5 and 7.4. The release of anticancer drugs through the membrane was increased with the addition of DOPEPEG2000 in the system due to the PEG was capable to increase fluidity and permeability of DOPEPEG2000-oleic acid liposomes through the membrane (Suzuki et al., 2012). Less than 25% of loaded folinic acid in all formulations of DOPEPEG2000-oleic acid liposomes pH 8.5 and less than 20% from DOPEPEG2000-oleic acid liposomes pH 7.4 were released into the media within 24 hours, showing a good property of slow release carrier as described in Figure 4.45. Although the fluidity of DOPEPEG2000-oleic acid liposomes pH 8.5 and 7.4 was increased with the amount of DOPEPEG2000 in the formulations, the formulation with the highest DOPEPEG2000

showed a decreased in the release of folinic acid from the DOPEPEG2000-oleic acid liposomes pH 8.5. This may be due to the aggregation of liposomes which make folinic acid entrapped between the liposomes and released to the media slower as compared to the other formulations.

The rate of release from DOPEPEG2000-oleic acid liposomes pH 8.5 was high within the first 8 hours of the experiment but reduced slightly as shown in the plots. In DOPEPEG2000-oleic acid liposomes pH 7.4, the rate of release which is the amount of anticancer drugs being released over time among the molar ratio of 0.005:1, 0.01:1, 0.02:1, and 0.03:1 were similar, showing that there was no significant effect on the rate of release as all the release data are similar. This was due to the formation of the emulsion in the DOPEPEG2000-oleic acid liposomes pH 7.4 systems which hindered the release of hydrophobic folinic acid to the system.

Figure 4.45: Cumulative release (%) with standard deviation not more than 1 of folinic acid from DOPEPEG2000-oleic acid liposomes (a) pH 8.5 and (b) pH 7.4 with the molar ratio DOPEPEG2000 to oleic acid of 0:1(■), 0.005:1(●), 0.01:1 (▲), 0.02:1 (▼), 0.03:1 (◄), and 0.04:1 (►) at 37 °C.

Table 4.6: Rate of release, K, Regression Coefficient, R^2, and standard median error (*SME*) values of folinic acid released from DOPEPEG2000 oleic acid liposomes pH 8.5 and 7.4.

pH	Kinetic Model		Molar ratio of DOPEPEG2000 to oleic acid					
			0:1	0.005:1	0.010:1	0.020:1	0.030:1	0.040:1
8.5	Zero Order (n=10)	K_0	0.7777	1.0483	1.0523	1.1419	1.1797	0.9347
		R^2	0.9902	0.9751	0.9771	0.9526	0.9429	0.9749
		SME	0.3722	1.6863	1.5787	3.6080	4.6393	1.3610
	First Order (n=10)	K_1	0.0084	0.0117	0.0118	0.0130	0.0135	0.0103
		R^2	0.9952	0.9883	0.9895	0.9739	0.9673	0.9867
		SME	0.1797	0.7902	0.7199	1.9906	2.6551	0.7213
	Higuchi (n=10)	K_H	3.0551	4.1414	4.1527	4.5485	4.7079	3.6913
		R^2	0.8932	0.9066	0.9034	0.9267	0.9274	0.9049
		SME	4.0391	6.3255	6.6465	5.5811	5.9054	5.1520
	Korsmeyer-Peppas (n=6)	K_{KP}	1.1496	1.8085	1.7720	2.3514	2.5216	1.6020
		R^2	0.9989	0.9947	0.9947	0.9921	0.9882	0.9940
		SME	0.0472	0.4012	0.4121	0.6765	1.0811	0.3668
	Gompertz (n=10)	$K_{G\alpha}$	5.4862	5.0718	5.1339	4.5892	4.5044	5.1245
		$K_{G\beta}$	0.8225	0.8922	0.9042	0.8519	0.8539	0.8471
		R^2	0.9920	0.9985	0.9985	0.9989	0.9991	0.9990
		SME	0.3393	0.1115	0.1133	0.0957	0.0805	0.0601
7.4	Zero Order (n=10)	K_0	0.0199	0.8709	0.8565	0.8379	0.8606	0.6310
		R^2	0.5681	0.9748	0.9707	0.9676	0.9680	0.9910
		SME	0.0078	1.2063	1.3237	1.3923	1.4431	0.2376
	First Order (n=10)	K_1	0.0199	0.8709	0.8565	0.8379	0.8606	0.6310
		R^2	0.5694	0.9856	0.9826	0.9800	0.9807	0.9951
		SME	0.0078	0.6893	0.7856	0.8597	0.8716	0.1308
	Higuchi (n=10)	K_H	0.0833	3.4369	3.3884	3.3182	3.4088	2.4674
		R^2	0.9105	0.9025	0.9093	0.9114	0.9128	0.8776
		SME	0.0016	4.6616	4.0922	3.8046	3.9299	3.2367
	Korsmeyer-Peppas (n=6)	K_{KP}	0.0870	1.4766	1.5271	1.5279	1.5760	0.8554
		R^2	0.9112	0.9929	0.9933	0.9925	0.9932	0.9962
		SME	0.0018	0.3807	0.3405	0.3624	0.3425	0.1144
	Gompertz (n=10)	$K_{G\alpha}$	7.1266	5.1591	5.0597	5.0228	4.9985	5.8424
		$K_{G\beta}$	0.1856	0.8212	0.7978	0.7824	0.7898	0.7935
		R^2	0.9269	0.9994	0.9993	0.9993	0.9991	0.9991
		SME	0.0015	0.0301	0.0342	0.0326	0.0446	0.0270

Table 4.6 presented the regression coefficient of the plots as fitted to various kinetic

models. The release of folinic acid from DOPEPEG2000-oleic acid liposomes pH 8.5

and 7.4 were most fitted to Gompertz model with the regression coefficient over 0.99. The standard mean error (*SME*) for this model was the lowest, which less than 0.35 in both samples and agreeable with the fact that this model was more suitable for an active ingredient with intermediate release rate such as folinic acid (Arias, 2014). The release fitted to Korsmeyer-Peppas model showed a high regression coefficient of more than 0.99 with *SME* of less than 0.37, attributed to the polymeric incorporation of DOPEPEG2000 in the liposomes. The regression coefficient achieving 0.99 while the *SME* was less than 2.00 in the first-order model can be related to the nature of water-soluble folinic acid that released from porous matrices as described by the first-order dissolution model (Dash et al., 2010).

Figure 4.46 shows that methotrexate gave out the highest cumulative release in DOPEPEG2000-oleic acid liposomes pH 8.5 at the molar ratio of DOPEPEG2000 to oleic acid at 0.04:1 at 48.2%. The release of methotrexate from DOPEPEG2000-oleic acid liposomes pH 8.5 and 7.4 were increased with the addition of DOPEPEG2000 into the formulation. However, the release of methotrexate was optimum at the molar ratio of DOPEPEG2000 to oleic acid was 0.03:1 in both samples. This high cumulative release may be due to the ability of methotrexate to entrap in both lipid bilayer and in the core of liposomes. The sharp release of methotrexate during the first 8 hours may be due to the methotrexate at the core of DOPEPEG2000-oleic acid liposomes being immediately diffused into the environment followed with those that entrapped within the bilayer of liposomes (Gulati et al., 1998).

The regression coefficient of dissolution models in Table 4.6 shows that the release was the most fitted to the model described by Gompertz (Dash et al., 2010) in both samples where the R^2 values were more than 0.99 and *SME* of less than 0.34. The presence of DOPEPEG2000 in the formulation was also give rise in Korsmeyer-Peppas.
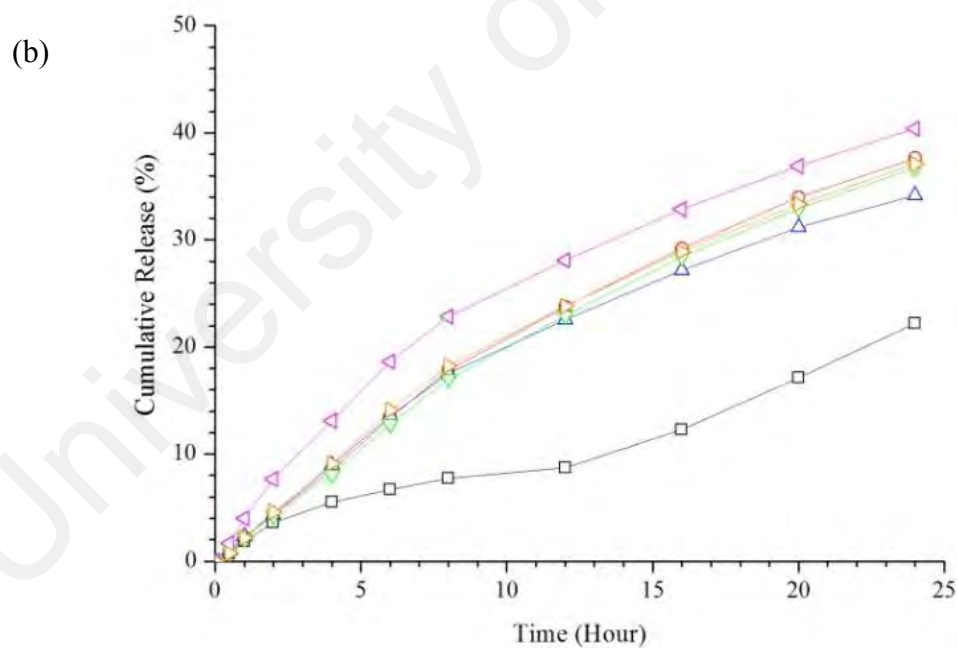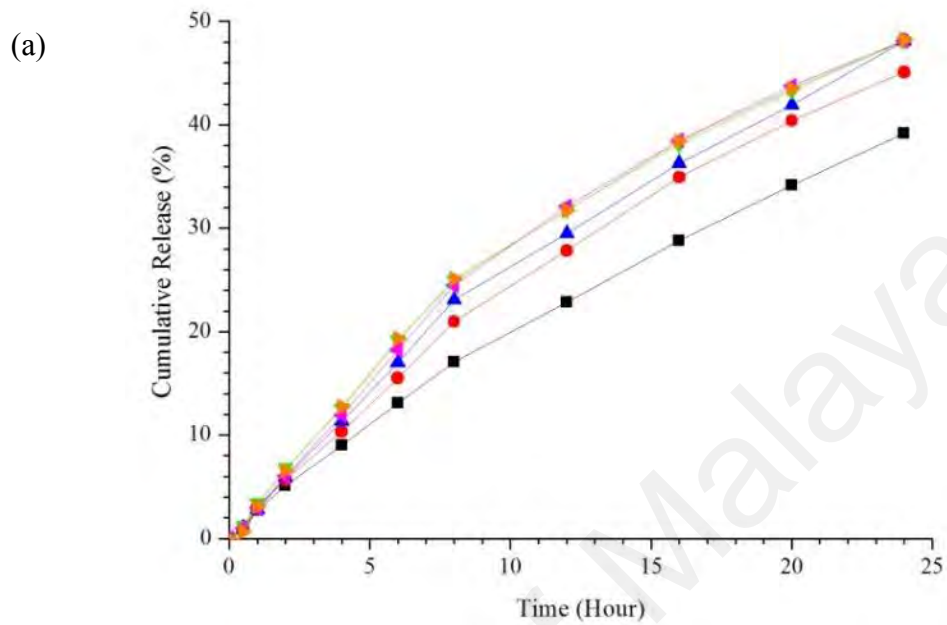
Figure 4.46: Cumulative release (%) with standard deviation not more than 1 of methotrexate from DOPEPEG2000-oleic acid liposomes (a) pH 8.5 and (b) pH 7.4, with the molar ratio of DOPEPEG2000 to oleic acid of 0:1(■), 0.005:1(●), 0.01:1(▲), 0.02:1 (▼), 0.03:1(◄), and 0.04:1(►) at 37 ºC.

Table 4.7: Rate of release, *K*, Regression Coefficient, R^2, and standard median error (*SME*) values of methotrexate released from DOPEPEG2000-oleic acid liposomes pH 8.5 and 7.4.

pH	Kinetic Model		Molar ratio of DOPEPEG2000 to oleic acid					
			0:1	0.005:1	0.010:1	0.020:1	0.030:1	0.040:1
8.5	Zero Order (n=10)	K_0	1.7518	2.0712	2.1871	2.2671	2.2705	2.2759
		R^2	0.9779	0.9690	0.9645	0.9368	0.9470	0.9375
		SME	4.0296	7.8863	10.0454	18.2245	15.9379	18.4623
	First Order (n=10)	K_1	0.0213	0.0264	0.0284	0.0300	0.0300	0.0301
		R^2	0.9962	0.9958	0.9207	0.9850	0.9892	0.9850
		SME	0.6863	1.0619	1.5768	4.3358	3.2606	4.4386
	Higuchi (n=10)	K_H	6.9302	8.2117	8.6838	9.0744	9.0531	9.1033
		R^2	0.9144	0.9176	0.9207	0.9381	0.9266	0.9349
		SME	15.6132	20.9829	22.4329	17.8397	22.0664	19.2301
	Korsmeyer-Peppas (n=6)	K_{KP}	3.0835	3.8517	4.2003	5.1299	4.7680	5.0857
		R^2	0.9989	0.9958	0.9948	0.9915	0.9897	0.9899
		SME	0.2168	1.1913	1.6541	2.7521	3.4960	3.3523
	Gompertz (n=10)	$K_{G\alpha}$	4.9479	4.9488	4.8050	4.2716	4.5901	4.3023
		$K_{G\beta}$	1.1662	1.2936	1.3139	1.2468	1.3106	1.2570
		R^2	0.9996	0.9974	0.9966	0.9940	0.9924	0.9927
		SME	2.2048	2.1524	2.3678	1.5264	1.1435	1.1936
7.4	Zero Order (n=10)	K_0	0.8747	1.7386	1.6158	1.6872	1.9613	1.7261
		R^2	0.9553	0.9659	0.9409	0.9699	0.8742	0.9543
		SME	2.0778	6.1891	8.7584	5.1862	24.1516	7.9643
	First Order (n=10)	K_1	0.0095	0.0212	0.0195	0.0204	0.0250	0.0211
		R^2	0.9541	0.9909	0.9751	0.9923	0.9418	0.9847
		SME	2.1347	1.6461	3.6841	1.3204	11.1729	2.6594
	Higuchi (n=10)	K_H	3.4364	6.8947	6.4586	6.6811	7.9566	6.8733
		R^2	0.8564	0.9161	0.9344	0.9127	0.9666	0.9262
		SME	6.6730	15.2161	9.7169	15.0290	6.4102	12.8492
	Korsmeyer-Peppas (n=6)	K_{KP}	1.1883	3.5630	3.2582	3.0627	5.6849	3.5257
		R^2	0.9596	0.9937	0.9912	0.9943	0.9905	0.9927
		SME	2.1128	1.2955	1.4701	1.1023	2.0428	1.4340
	Gompertz (n=10)	$K_{G\alpha}$	5.3583	4.8169	4.3243	4.9163	3.5316	4.5188
		$K_{G\beta}$	0.8486	1.1412	1.0020	1.1377	0.9663	1.0827
		R^2	0.9203	0.9967	0.9982	0.9965	0.9975	0.9977
		SME	4.1641	0.6723	0.2984	0.6690	0.5426	0.4591
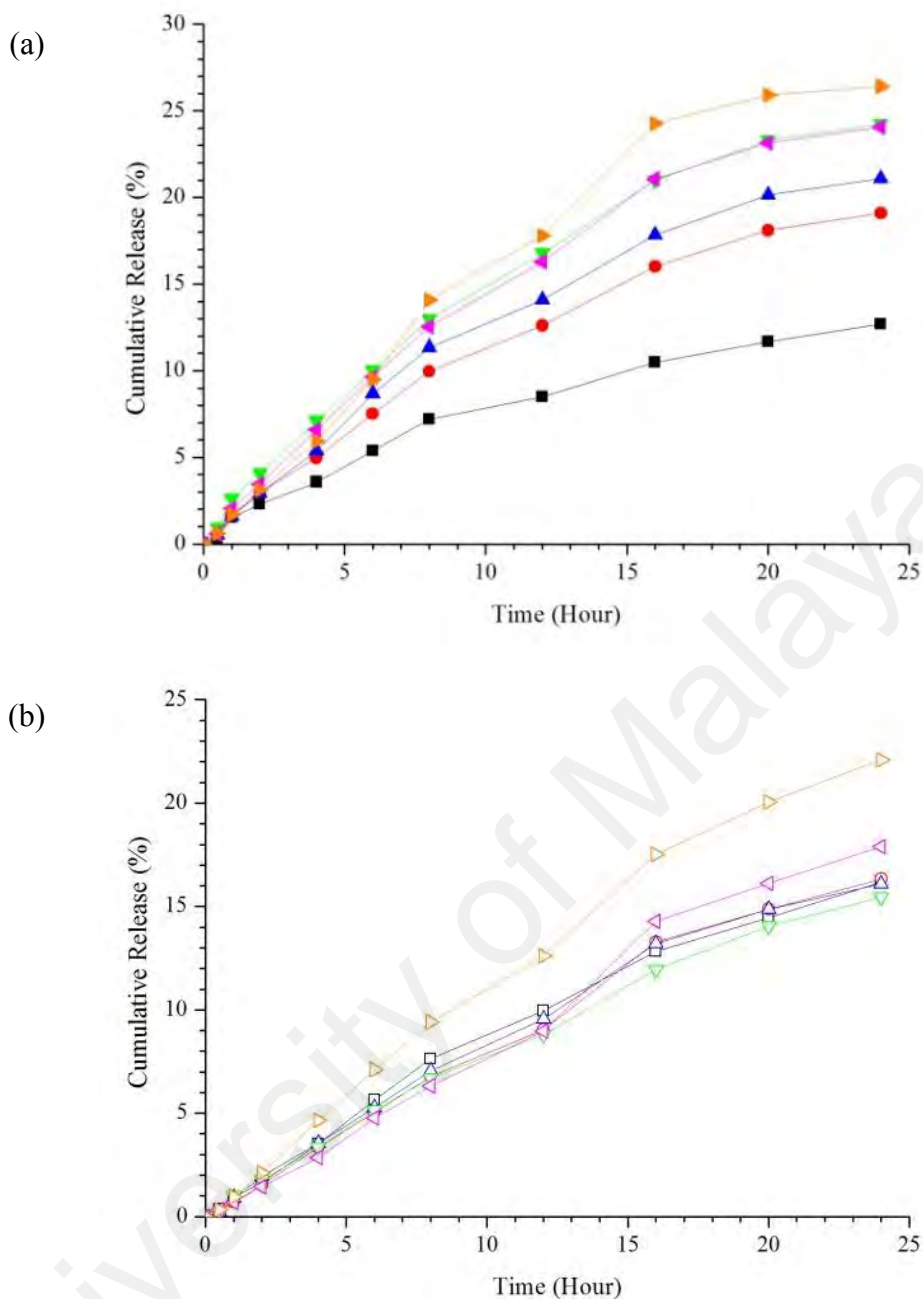
Figure 4.47: Cumulative release (%) with standard deviation not more than 1 of doxorubicin from DOPEPEG2000-oleic acid liposomes (a) pH 8.5 and (b) pH 7.4. The molar ratios of DOPEPEG2000 to oleic acid were 0:1(■), 0.005:1(●), 0.01:1 (▲), 0.02:1 (▼), 0.03:1 (◄) and 0.04:1 (►) at 37 °C.

On the other hand, the positively intermediate log P doxorubicin gave a lower cumulative released as compared to negatively intermediate log P methotrexate due to opposite site of dissociation as displays in Figure 4.47 (Gulati et al., 1998). The DOPEPEG2000-oleic acid liposomes with the molar ratio of 0.04:1 in pH 8.5 and 7.4

released the most of the loaded doxorubicin after 24 hours up to 26.4 and 22.1% respectively. In pH 8.5, the cumulative release was directly proportional to the amount of DOPEPEG2000 in the formulation due to the enhancement in fluidity by PEG. Oppositely, in pH 7.4, incorporation of DOPEPEG2000 was significantly affecting the release of doxorubicin to the environment. The release profile can be divided into two mechanisms of release, which was 0 to 12 and 12 to 24 hours due to the release of doxorubicin from a different site of incorporation. The release profile at first 12 hours may be attributed to the release of doxorubicin at the core while the latter was from the bilayer liposomes.

The dissolution profiles of doxorubicin from DOPEPEG2000-oleic acid liposomes pH 8.5 and 7.4 gave out the regression coefficient of more than 0.98, as presented by the model dependent in Table 4.8. The regression coefficient was highest in the Gompertz model which explained the intermediate release of doxorubicin as well as the diffusion of media-soluble part of doxorubicin. However, the R^2 from the curve fitting to Gompertz showed an inversely proportional value with the amount of DOPEPEG2000, which may be due to the increase of doxorubicin entrapped within the bilayer of liposomes.

Table 4.8: Rate of release, K, Regression Coefficient, R^2, and standard median error (*SME*) values of doxorubicin released from DOPEPEG2000-oleic acid liposomes pH 8.5 and 7.4.

pH	Kinetic Model		Molar ratio of DOPEPEG2000 to oleic acid					
			0:1	0.005:1	0.010:1	0.020:1	0.030:1	0.040:1
8.5	Zero Order (n=10)	K_0	0.6128	0.9220	1.0257	1.1945	1.1805	1.3069
		R^2	0.8992	0.9362	0.9314	0.9124	0.9306	0.9392
		SME	1.9656	3.0298	4.0988	6.6347	5.4638	6.3473
	First Order (n=10)	K_1	0.0066	0.0102	0.0115	0.0137	0.0135	0.0151
		R^2	0.9173	0.9573	0.9555	0.9457	0.9585	0.9645
		SME	1.6127	2.0295	2.6607	4.1139	3.2635	3.7036
	Higuchi (n=10)	K_H	2.4738	3.6898	4.1052	4.8079	4.7260	5.1956
		R^2	0.9554	0.9365	0.9326	0.9490	0.9331	0.9039
		SME	0.8686	3.0175	4.0294	3.8636	5.2646	10.0333
	Korsmeyer-Peppas (n=6)	K_{KP}	1.6279	2.0780	2.3185	3.0034	2.6784	2.5914
		R^2	0.9890	0.9903	0.9862	0.9893	0.9861	0.9741
		SME	0.2405	0.5183	0.9278	0.9163	1.2270	3.0424
	Gompertz (n=10)	$K_{G\alpha}$	4.5088	4.5289	4.4697	4.1424	4.3893	4.7660
		$K_{G\beta}$	0.5686	0.7383	0.7775	0.7895	0.8324	0.9575
		R^2	0.9911	0.9925	0.9890	0.9915	0.9888	0.9774
		SME	0.1005	0.1893	0.2359	0.4287	0.4267	1.3339
7.4	Zero Order (n=10)	K_0	0.7450	0.7428	0.7459	0.7020	0.7895	1.0053
		R^2	0.9694	0.9833	0.9756	0.9812	0.9890	0.9829
		SME	1.0383	0.6051	0.8468	0.5708	0.4809	1.1118
	First Order (n=10)	K_1	0.0081	0.0080	0.0081	0.0076	0.0085	0.0112
		R^2	0.9802	0.9893	0.9846	0.9887	0.9900	0.9920
		SME	0.6737	0.3871	0.5343	0.3423	0.4368	0.5200
	Higuchi (n=10)	K_H	2.9476	2.9113	2.9422	2.7673	3.0603	3.9496
		R^2	0.9087	0.8799	0.8996	0.9015	0.8434	0.8895
		SME	3.0997	4.3421	3.4796	2.9957	6.8674	7.1722
	Korsmeyer-Peppas (n=6)	K_{KP}	1.3313	1.0675	1.2404	1.1438	0.8474	1.5301
		R^2	0.9924	0.9909	0.9921	0.9962	0.9893	0.9935
		SME	0.2907	0.3705	0.3061	0.1313	0.5292	0.4747
	Gompertz (n=10)	$K_{G\alpha}$	5.1531	5.6652	5.3181	5.3678	6.5007	5.4158
		$K_{G\beta}$	0.7547	0.8315	0.7810	0.7641	0.9691	0.9264
		R^2	0.9985	0.9944	0.9955	0.9959	0.9904	0.9964
		SME	0.0568	0.2279	0.1770	0.1415	0.4711	0.2599

The release of hydrophobic irinotecan from DOPEPEG2000-oleic acid liposomes pH 8.5 showed an opposite pattern where incorporation of DOPEPEG2000 reduced the

amount of irinotecan released to the environment as displays in Figure 4.48. The cumulative release of irinotecan from DOPEPEG2000-oleic acid liposomes pH 8.5 was lowest at the molar ratio of DOPEPEG2000 to oleic acid at 0.02:1 then increased to 23.9% after 24 hours at 0.03:1 and 0.04:1. However, in the presence of emulsion in the surrounding of DOPEPEG2000-oleic acid liposomes in pH 7.4, the release of irinotecan from the bilayer of liposomes to the environment was promoted with the presence of more than 0.01 molar ratio of DOPEPEG2000 in the formulation.

Table 4.9 shows the coefficient regressions from the release profile of irinotecan using various model dependent methods. The zero-order and first-order dissolution models showed a high coefficient regression due to the hydrophobic nature of irinotecan that released slowly from the liposomes. In the Table 4.9, more than 0.99 regression is shown in Gompertz model with *SME* of less than 0.8 that agreed with the intermediate release rate of irinotecan from porous matrices (first-order) which were less than 25.0% released after 24 hours (Dash et al., 2010). The polymeric system of DOPEPEG2000 (Dash et al., 2010) and the release mechanism that involved multiple steps also resulted in a high regression in Korsmeyer-Peppas model (Costa & Lobo, 2001).
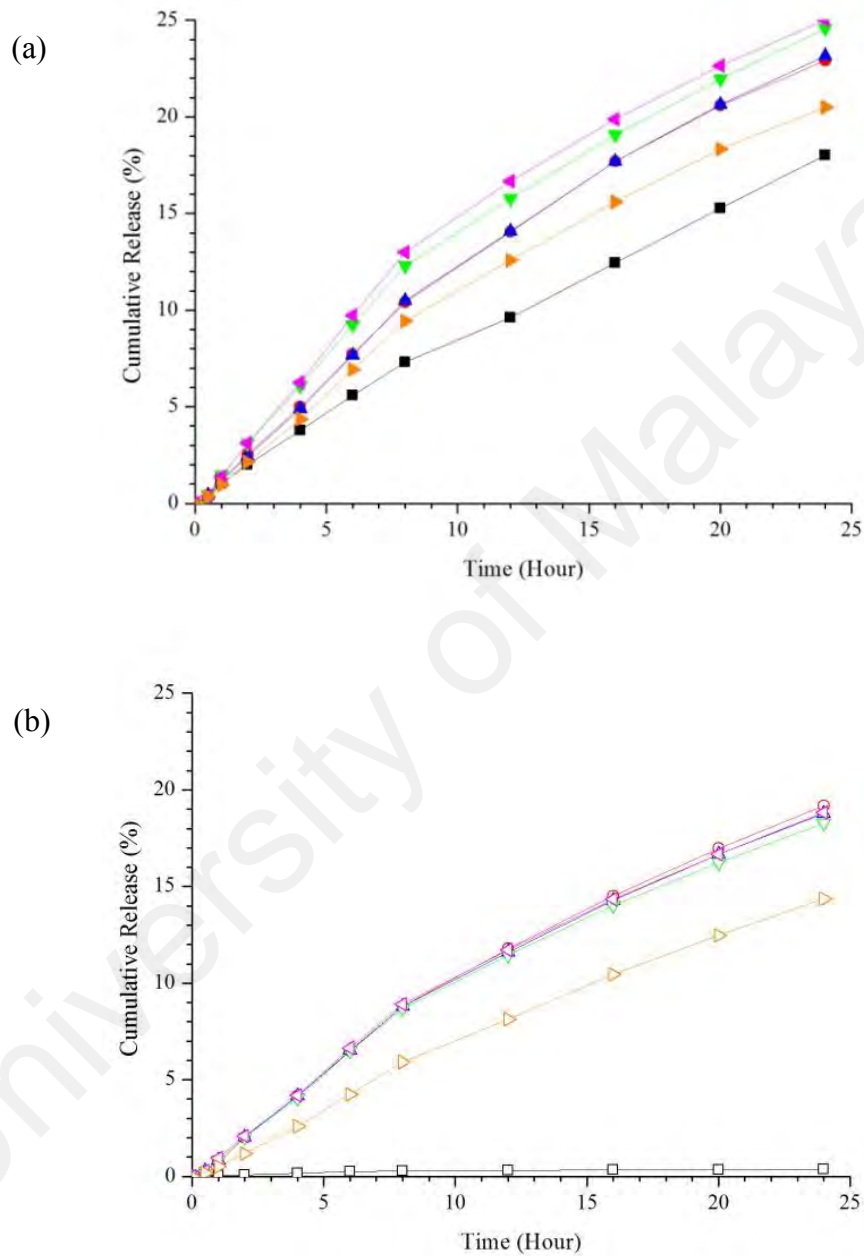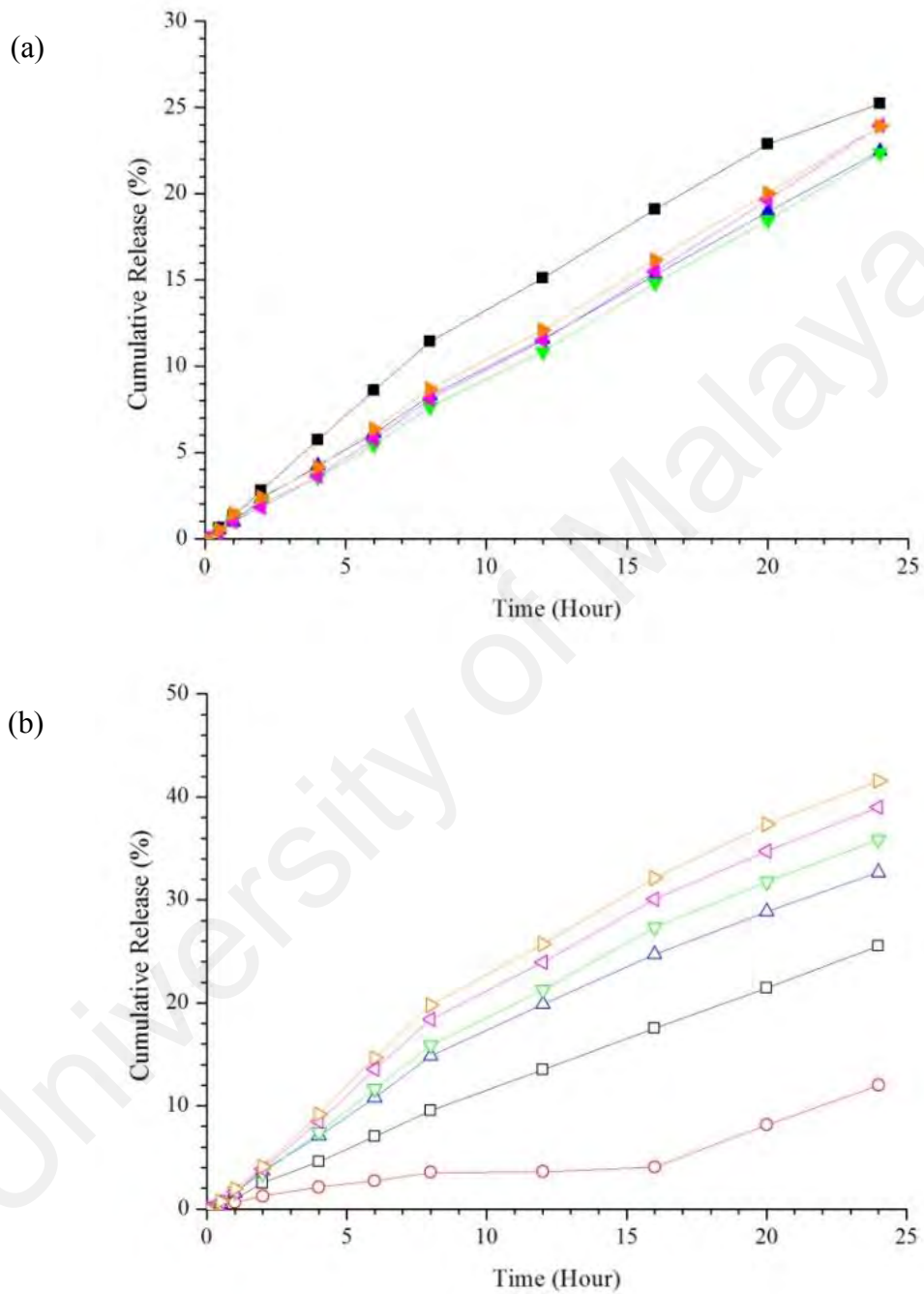
Figure 4.48: Cumulative release (%) with standard deviation not more than 1 of irinotecan from DOPEPEG2000-oleic acid liposomes (a) pH 8.5 and (b) pH 7.4. The molar ratios of DOPEPEG2000 to oleic acid were 0:1(■), 0.005:1(●), 0.01:1(▲), 0.02:1 (▼), 0.03:1 (◄), and 0.04:1 (►) at 37 °C.

Table 4.9: Rate of release, K, Regression Coefficient, R^2, and standard median error (*SME*) values of irinotecan released from oleic acid liposomes pH 8.5 and 7.4.

pH	Kinetic Model		0:1	0.005:1	0.010:1	0.020:1	0.030:1	0.040:1
			Molar ratio of DOPEPEG2000 to oleic acid					
8.5	Zero Order (n=10)	K_0	1.1510	1.2083	0.9530	0.9262	0.9838	1.0077
		R^2	0.9762	0.9870	0.9979	0.9996	0.9992	0.9985
		SME	1.9259	1.2680	0.1275	0.0258	0.0563	0.1004
	First Order (n=10)	K_1	0.0130	0.0138	0.0105	0.0102	0.0109	0.0112
		R^2	0.9902	0.9970	0.9995	0.9974	0.9956	0.9990
		SME	0.7953	0.3581	0.0297	0.1523	0.2989	0.0706
	Higuchi (n=10)	K_H	4.5484	4.7498	3.7159	3.5871	3.7995	3.9233
		R^2	0.9084	0.8892	0.8700	0.8466	0.8379	0.8644
		SME	7.4103	0.3046	7.7748	9.0724	11.1041	9.1100
	Korsmeyer-Peppas (n=6)	K_{KP}	1.9906	1.8475	1.1555	0.9162	0.9043	1.1640
		R^2	0.9960	0.9979	0.9997	0.9996	0.9995	0.9995
		SME	0.3668	0.3046	0.0181	0.0287	0.0402	0.0365
	Gompertz (n=10)	$K_{G\alpha}$	5.0238	5.3776	5.9925	6.6508	6.8893	6.1783
		$K_{G\beta}$	0.9307	1.0122	0.9834	1.0558	1.1126	1.0343
		R^2	0.9762	0.9870	0.9979	0.9996	0.9992	0.9985
		SME	0.2521	0.4564	0.6476	0.7304	0.7954	0.8806
7.4	Zero Order (n=10)	K_0	1.0865	0.4118	1.4801	1.6190	1.7838	1.9107
		R^2	0.9973	0.8899	0.9762	0.9810	0.9710	0.9692
		SME	0.2118	1.4654	3.2206	3.1495	5.7227	6.9288
	First Order (n=10)	K_1	0.0122	0.0043	0.0174	0.0194	0.0219	0.0238
		R^2	0.9995	0.8839	0.9932	0.9961	0.9929	0.9933
		SME	0.0407	1.5451	0.9205	0.6529	1.4101	1.5060
	Higuchi (n=10)	K_H	4.2345	1.5798	5.8452	6.3743	7.0516	7.5592
		R^2	0.8693	0.7179	0.9062	0.8970	0.9063	0.9083
		SME	10.3008	3.7554	12.6976	17.1031	18.5017	20.6389
	Korsmeyer-Peppas (n=6)	K_{KP}	1.3235	0.1693	2.5339	2.5892	3.1325	3.4143
		R^2	0.9993	0.9054	0.9951	0.9948	0.9923	0.9921
		SME	0.0630	1.4163	0.7394	0.9700	1.7148	1.9996
	Gompertz (n=10)	$K_{G\alpha}$	5.9918	8.3514	5.0382	5.3074	5.0326	5.0214
		$K_{G\beta}$	1.0463	0.9340	1.0739	1.1743	1.1965	1.2448
		R^2	0.9926	0.8615	0.9969	0.9968	0.9975	0.9971
		SME	0.6528	2.0740	0.4652	0.6001	0.5494	0.7282

4.11.2 *In vitro* Release Study of DOPEPEG2000-oleic acid-erucic acid Liposomes

The therapeutic activity and toxicity of active ingredients from DOPEPEG2000-oleic acid-erucic acid liposomal drug delivery system were studied through the *in vitro* release using Franz diffusion cell. The dissolution model methods were used to understand the release kinetic and mechanism of anticancer drugs encapsulated in the liposome as well as the effect of the erucic acid on their dissolution profiles.

Figure 4.49: Cumulative release (%) with standard deviation not more than 1 of folinic acid from one day old DOPEPEG2000-oleic acid-erucic acid liposomes for 24 hours in pH 7.4. The molar ratios of erucic acid to DOPEPEG2000-oleic acid were 0:1(■), 0.25:1(●), 0.5:1 (▲), 1:1 (▼), and 2:1 (◄) at 37 ºC. The ratio of DOPEPEG2000 to oleic acid was fixed at 0.02:1and reported as a single component.

Figure 4.49 shows the cumulative release of folinic acid from DOPEPEG2000-oleic acid-erucic acid liposomes for 24 hours. Generally, the cumulative release was reduced with the addition of erucic acid in the formulation. Cumulative release of DOPEPEG2000-oleic acid-erucic acid liposomes with the equimolar ratio of erucic acid and DOPEPEG2000-oleic acid at 1:1 displayed the lowest cumulative release of 21.9%, which was 8.6% lower than erucic acid liposomes. The rate of release was faster within the first eight hours of the experiment.

Table 4.10: Rate of release, K, Regression Coefficient, R^2, and standard median error (*SME*) values of folinic acid released from one day old DOPEPEG2000-oleic acid-erucic acid liposomes at 37°C. The ratio of DOPEPEG2000 to oleic acid was fixed at 0.02:1and reported as a single component.

Kinetic Model		Molar ratio of erucic acid to DOPEPEG2000-oleic acid				
		1:0	0.25:1	0.5:1	1:1	2:1
Zero Order	K_0	1.3990	1.4193	1.3714	0.9798	1.2997
(n=10)	R^2	0.9698	0.9705	0.9704	0.9859	0.9837
	SME	3.6081	3.6285	3.4223	0.8608	1.7543
First Order	K_1	0.0163	0.0166	0.0160	0.0109	0.0150
(n=10)	R^2	0.9889	0.9895	0.9889	0.9944	0.9953
	SME	1.3286	1.2873	1.2822	0.3415	0.5021
Higuchi	K_H	5.5383	5.6182	5.4256	3.8501	5.1109
(n=10)	R^2	0.9117	0.9119	0.9094	0.8930	0.8941
	SME	10.5629	10.8188	10.4788	6.5566	11.4283
Korsmeyer-Peppas	K_{KP}	2.5297	2.5610	2.4486	1.4936	2.0192
(n=6)	R^2	0.9938	0.9942	0.9932	0.9966	0.9956
	SME	0.8344	0.7995	0.8803	0.2339	0.5365
Gompertz	$K_{G\alpha}$	4.8711	4.8739	4.9218	5.3896	5.3205
(n=10)	$K_{G\beta}$	1.0124	1.0212	1.0097	0.9101	1.0436
	R^2	0.9983	0.9978	0.9986	0.9979	0.9978
	SME	0.2243	0.3061	0.1766	0.1434	0.2623

Table 4.10 displays the release rate of folinic acid from DOPEPEG2000-oleic acid-erucic acid liposomes as fitted into five dissolution models. The average release rate in all dissolution models was slower with the addition of erucic acid in the DOPEPEG2000-oleic acid-erucic acid liposomes preparation. This was happened because of erucic acid that incorporated within the bilayer of liposomes forming a compact structure due to the longer C22 chains as compared to C18 in oleic acid. The regression coefficient values showed that the release was fitted to Korsmeyer-Peppas and Gompertz dissolution model with the *SME* of less than 1. These models were used to explain the dissolution of folinic acid that having a negative log P value and intermediate release rate (Dash et al., 2010; Jain & Jain, 2016).
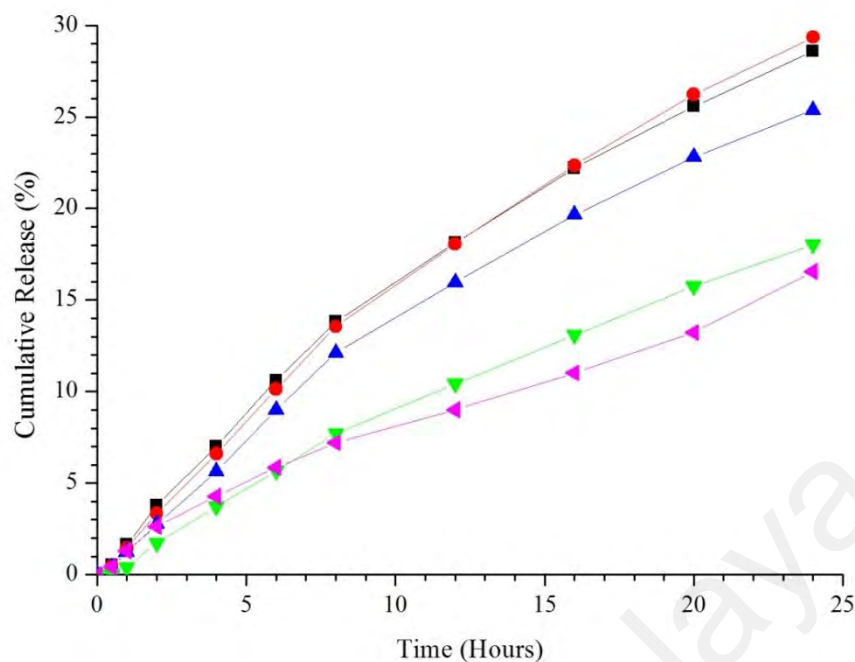
Figure 4.50: Cumulative release (%) with standard deviation not more than 1 of methotrexate from one day old DOPEPEG2000-oleic acid-erucic acid liposomes for 24 hours in pH 7.4. The molar ratios of erucic acid to DOPEPEG2000-oleic acid were 0:1(■), 0.25:1(●), 0.5:1 (▲), 1:1 (▼), and 2:1 (◄) at 37 °C. The ratio of DOPEPEG2000 to oleic acid was fixed at 0.02:1and reported as a single component.

The release of methotrexate from DOPEPEG2000-oleic acid-erucic acid liposomes is presented in the Figure 4.50. Incorporation of erucic acid in the formulation hindered the release of methotrexate into the diffusate of Franz diffusion cell. Erucic acid liposomes released 28.6% of methotrexate after incubation at 37 °C for 24 hours while only 16.6% methotrexate was release from DOPEPEG2000-oleic acid-erucic acid liposomes with the amount of erucic acid was two folded of DOPEPEG2000. The fast release of methotrexate within the first eight hours incubation was reduced with the addition of erucic acid in the preparation showed that erucic acid promoted the sustained release of methotrexate from DOPEPEG2000-oleic acid-erucic acid liposomes.

The kinetic dissolution models which were zero-order, first-order, Higuchi, Korsmeyer-Peppas, and Gompertz dissolution models showed a decrease in the release rate of methotrexate from DOPEPEG2000-oleic acid-erucic acid liposomes with the

increasing amount of erucic acid in the formulation as displays in Table 4.11. As the release was fitted into different dissolution models, the coefficient regression values from the curve fitting showed that the dissolution was most fitted to Gompertz and Korsmeyer-Peppas dissolution model where the R^2 values were more than 0.99 while the *SME* values were less than 0.8. This indicated that the release route of methotrexate from DOPEPEG2000-oleic acid-erucic acid liposomes which were ruled by the nature of methotrexate which having an intermediate release rate and good solubility in pH 7.4 at 37 °C (Dash et al., 2010).

Table 4.11: Rate of release, *K,* Regression Coefficient, R^2, and standard median error (*SME*) values of methotrexate released from one day old DOPEPEG2000-oleic acid-erucic acid liposomes at 37°C. The ratio of DOPEPEG2000 to oleic acid was fixed at 0.02:1and reported as a single component.

Kinetic Model		Molar ratio of erucic acid to DOPEPEG2000-oleic acid				
		1:0	0.25:1	0.5:1	1:1	2:1
Zero Order	K_0	1.3242	1.3407	1.1699	0.7993	0.7103
(n=10)	R^2	0.9580	0.9723	0.9669	0.9862	0.9593
	SME	4.3129	3.0415	2.7695	0.5760	1.1474
First Order	K_1	0.0154	0.0155	0.0133	0.0087	0.0077
(n=10)	R^2	0.9809	0.9898	0.9841	0.9928	0.9688
	SME	1.9648	1.1193	1.3342	0.3025	0.8804
Higuchi	K_H	5.2687	5.3043	4.6335	3.1361	2.8266
(n=10)	R^2	0.9255	0.9109	0.9114	0.8877	0.9262
	SME	7.6457	9.7708	7.4091	4.6936	2.0825
Korsmeyer-Peppas	K_{KP}	2.6596	2.3891	2.1406	1.1822	1.4192
(n=6)	R^2	0.9940	0.9948	0.9922	0.9952	0.9927
	SME	0.6899	0.6392	0.7378	0.2263	0.2330
Gompertz	$K_{G\alpha}$	4.5881	4.9149	4.8873	5.4953	4.8218
(n=10)	$K_{G\beta}$	0.9307	0.9951	0.9170	0.8364	0.6783
	R^2	0.9983	0.9979	0.9990	0.9986	0.9821
	SME	0.1998	0.2604	0.0949	0.0651	0.5677

Figure 4.51 represents the release of doxorubicin from DOPEPEG2000-oleic acid-erucic acid liposomes. Doxorubicin is an anticancer drug having the log P value of +0.5, which tends to incorporate more in the lipid bilayer than in the aqueous core of

liposomes. Erucic acid liposomes released 30.2% of doxorubicin after incubated for 24 hours. The release profile showed that the amount of erucic acid in the formulation was significantly affecting the cumulative release of doxorubicin. Doxorubicin released the most in the formulation with the molar ratio of erucic acid to the DOPEPEG2000-oleic acid of 0.25:1 which was 52.6% while it was lowest in the formulation with the molar ratio of 2:1 with the cumulative release of 10.2%. The slope of the plot became continuous with the addition of erucic acid in the formulation, proving that incorporation of erucic acid in the formulation promoted the sustained release of doxorubicin. In the formulation with the molar ratio of erucic acid less than 1, the fast release can be observed within the first 4 hours of incubation and the magnitude was slightly reduced after the fourth hours due to the doxorubicin located at the aqueous core was released first followed by those incorporated within the lipid bilayer.

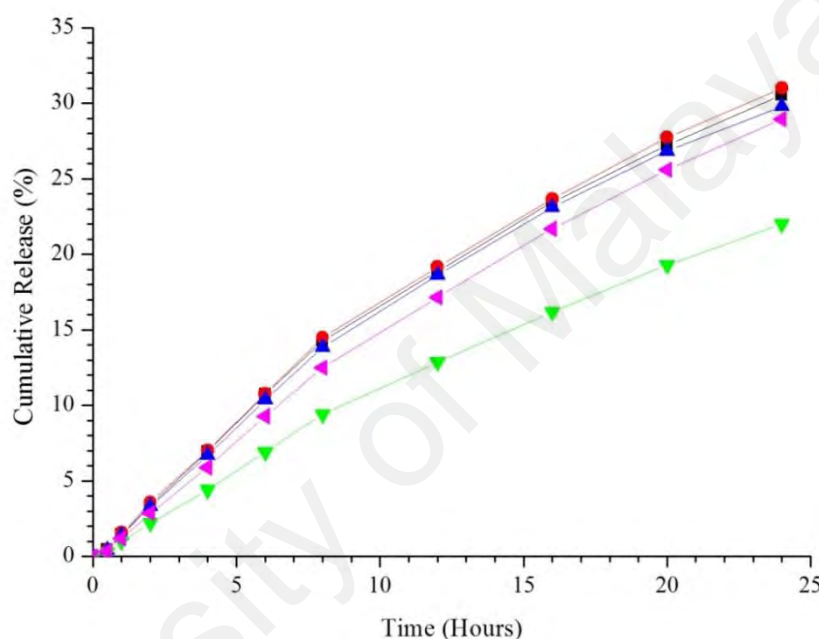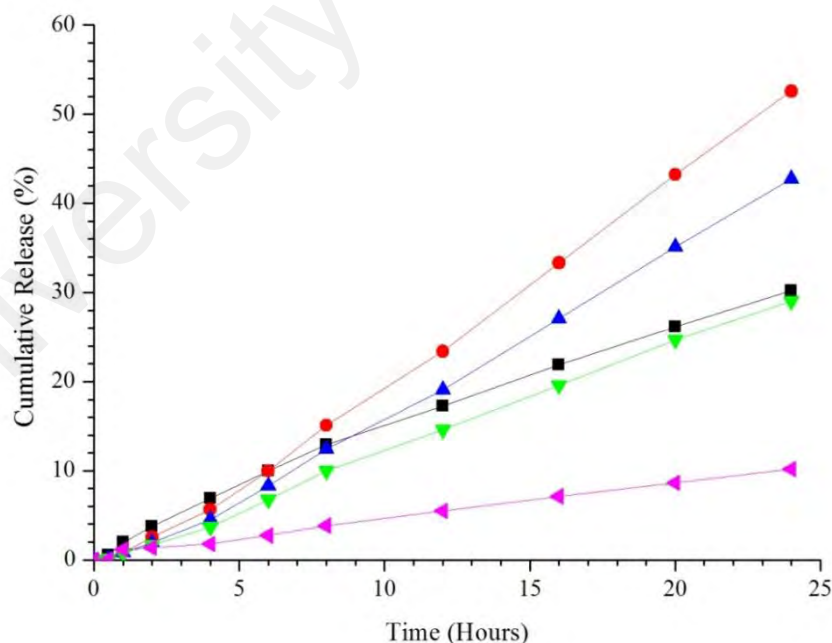**Figure 4.51:** Cumulative release (%) with standard deviation not more than 1 of doxorubicin from one day old DOPEPEG2000-oleic acid-erucic acid liposomes for 24 hours in pH 7.4. The molar ratios of erucic acid to DOPEPEG2000-oleic acid were 0:1(■), 0.25:1(●), 0.5:1 (▲), 1:1 (▼), and 2:1 (◄) at 37 °C. The ratio of DOPEPEG2000 to oleic acid was fixed at 0.02:1and reported as a single component.

Table 4.12: Rate of release, K, Regression Coefficient, R^2, and standard median error (*SME*) values of doxorubicin released from one day old DOPEPEG2000-oleic acid-erucic acid liposomes at 37°C. The ratio of DOPEPEG2000 to oleic acid was fixed at 0.02:1and reported as a single component.

Kinetic Model		Molar ratio of erucic acid to DOPEPEG2000-oleic acid				
		1:0	0.25:1	0.5:1	1:1	2:1
Zero Order	K_0	1.3400	2.1035	1.7108	1.2151	0.4381
(n=10)	R^2	0.9814	0.9898	0.9903	0.9969	0.9898
	SME	2.0179	3.5913	2.2417	0.3430	0.1235
First Order	K_1	0.0155	0.0261	0.0203	0.0137	0.0046
(n=10)	R^2	0.9946	0.9623	0.9708	0.9920	0.9919
	SME	0.5832	13.2935	6.7708	0.8800	0.0983
Higuchi	K_H	5.2921	8.0012	6.5113	4.6746	1.7162
(n=10)	R^2	0.9096	0.7883	0.7902	0.8268	0.8791
	SME	9.7884	74.5794	48.7078	18.9438	1.4627
Korsmeyer-Peppas	K_{KP}	2.2677	1.2400	1.0289	1.0555	0.5907
(n=6)	R^2	0.9990	0.9993	0.9993	0.9977	0.9946
	SME	0.1222	0.2649	0.1949	0.2833	0.0741
Gompertz	$K_{G\alpha}$	5.0067	12.3786	10.4453	7.3568	6.0560
(n=10)	$K_{G\beta}$	1.0084	2.0677	1.7690	1.2736	0.6962
	R^2	0.9917	0.9857	0.9894	0.9958	0.9862
	SME	1.0097	5.6817	2.7695	0.5210	0.1877

The average release rate of doxorubicin was indirectly proportional with the amount of erucic acid in the DOPEPEG2000-oleic acid-erucic acid liposomes as displayed in Table 4.12. From five release kinetic models that being evaluated, the release of doxorubicin from liposomes was most fitted to Korsmeyer-Peppas model with the regression coefficient of more than 0.99 and *SME* of less than 0.3 in all of the combinations due to the release mechanism involving several steps from aqueous core to the environment through the bilayer membrane (Costa & Lobo, 2001).

The cumulative release of hydrophobic irinotecan from erucic acid liposomes after 24 hours was 38.0% as showed in Figure 4.52 and was increased with the amount of erucic acid in the DOPEPEG2000-oleic acid-erucic acid liposomes up to 47.5% in the formulation where the molar ratio of erucic acid to DOPEPEG2000-oleic acid was 1:1.

Irinotecan which having the log P of +2.78 was incorporated within the bilayer of liposomes. However, the cumulative release was significantly dropped to 33.5%, when the amount of erucic acid was doubled of the amount of DOPEPEG2000-oleic acid. The release magnitude was reduced after 8 hours of incubation period in the formulation where the molar ratio of erucic acid was greater than 1.
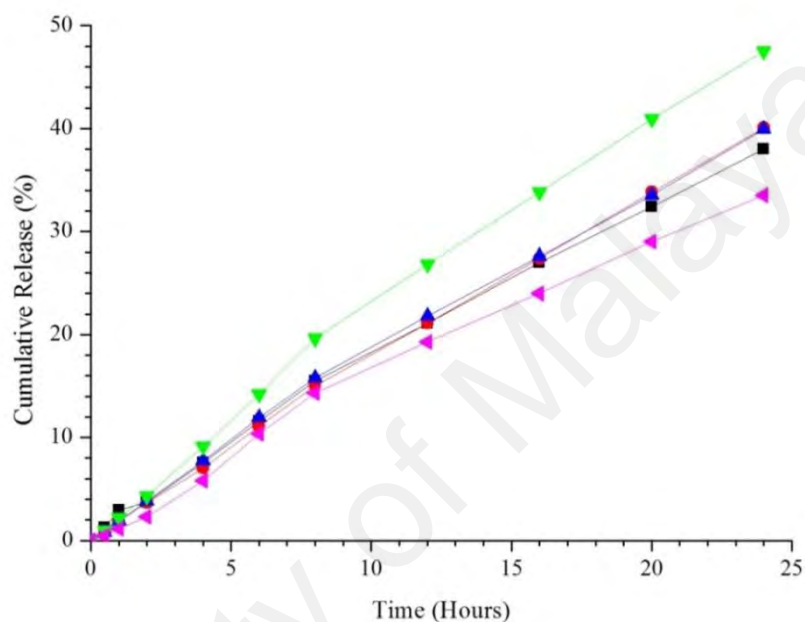
Figure 4.52: Cumulative release (%) with standard deviation not more than 1 of irinotecan from one day old DOPEPEG2000-oleic acid-erucic acid liposomes for 24 hours in pH 7.4. The molar ratios of erucic acid to DOPEPEG2000-oleic acid were 0:1(■), 0.25:1(●), 0.5:1 (▲), 1:1 (▼), and 2:1 (◄) at 37 °C. The ratio of DOPEPEG2000 to oleic acid was fixed at 0.02:1and reported as a single component.

The kinetic release rate of irinotecan from DOPEPEG2000-oleic acid-erucic acid liposomes with the molar ratio of 0.25:1 and 0.5:1 was less significant to the release rate of naked erucic acid liposomes as displayed in Table 4.13, when evaluated using five dissolution models. The release rate was the highest in equimolar of erucic acid and DOPEPEG2000-oleic acid and the lowest in the DOPEPEG2000-oleic acid-erucic acid liposomes with the molar ratio of erucic acid to DOPEPEG2000-oleic acid of 2:1. The R^2 values of more than 0.99 with *SME* of less than 1 in were obtained from Korsmeyer-Peppas model followed with first and zero-order. The high regression coefficient with low *SME* in these models were best to describe the released of less soluble irinotecan

(zero-order) from the porous liposomes (first-order) through many release phenomenon
(Korsmeyer-Peppas) (Costa & Lobo, 2001; Dash et al., 2010).

Table 4.13: Rate of release, *K*, Regression Coefficient, R^2, and standard median error (*SME*) values of irinotecan released from one day old DOPEPEG2000-oleic acid-erucic acid liposomes at 37°C. The ratio of DOPEPEG2000 to oleic acid was fixed at 0.02:1and reported as a single component.

Kinetic Model		Molar ratio of erucic acid to DOPEPEG2000-oleic acid				
		1:0	0.25:1	0.5:1	1:1	2:1
Zero Order	K_0	1.6558	1.7065	1.7178	2.0787	1.4737
(n=10)	R^2	0.9897	0.9976	0.9932	0.9911	0.9880
	SME	1.7442	0.4613	1.2860	2.4803	1.7342
First Order	K_1	0.0199	0.0205	0.0207	0.0263	0.0173
(n=10)	R^2	0.9987	0.9980	0.9990	0.9987	0.9960
	SME	0.2208	0.3801	0.1841	0.3494	0.5772
Higuchi	K_H	6.5060	6.6513	6.7274	8.1450	1.3680
(n=10)	R^2	0.8935	0.8689	0.8840	0.8849	0.9073
	SME	18.1001	25.3524	22.0328	32.1425	0.3728
Korsmeyer-Peppas	K_{KP}	2.4629	2.0680	2.3702	2.9341	2.0380
(n=6)	R^2	0.9989	0.9995	0.9989	0.9978	0.9939
	SME	0.2077	0.1124	0.2267	0.6782	0.9891
Gompertz	$K_{G\alpha}$	5.5841	6.3806	5.8051	6.0766	5.7333
(n=10)	$K_{G\beta}$	1.2291	1.3603	1.2863	1.4684	1.1792
	R^2	0.9874	0.9877	0.9886	0.9903	0.9967
	SME	2.4176	2.6843	2.4336	3.0536	0.5375

4.11.3 *In vitro* **Release Study of DOPEPEG2000-oleic acid-soy lecithin Liposomes**

The study on the release of methotrexate, irinotecan, folinic acid, and doxorubicin from DOPEPEG2000-oleic acid-soy lecithin liposomes provided the information on dosage and exposure time in order to minimize harm to non-targeted tissues (Stevenson-Abouelnasr et al., 2007).

The cumulative drug release of folinic acid from DOPEPEG2000-oleic acid-soy lecithin liposomes after 24 hours were increased with the amount of soy lecithin added into the formulations as showed in Figure 4.53. However, at the highest amount of soy

lecithin in the formulations, the cumulative release was lower as compared to soy lecithin liposomes. This was agreeable with the largest average particle size of liposomes which may prevent the liposomes from passing through the membrane. The release rate of all formulations was high within the first 8 hours of the experiment.

Figure 4.53: Cumulative release (%) with standard deviation not more than 1 of folinic acid from DOPEPEG2000-oleic acid-soy lecithin liposomes in pH 7.4 at 37 °C .The molar ratios of soy lecithin to DOPEPEG2000-oleic acid were 1:0 (■), 0.125:1(●), 0.25:1 (▲), 0.5:1 (▼), 1:1 (◄), and 2:1 (►). The ratio of DOPEPEG2000 to oleic acid was fixed at 0.02:1and reported as a single component.

Five kinetics models were explored to study the release mechanism of folinic acid from DOPEPEG2000-oleic acid-soy lecithin liposomes as displays in table 4.14. The regression coefficient value was highest in Gompertz dissolution model with R^2 values of more than 0.99 in all formulations of DOPEPEG2000-oleic acid-soy lecithin liposomes. The *SME* values were lowest in this model, which was less than 0.9. This was accurate to the application of Gompertz model (Dash et al., 2010), which was suitable with the folinic acid that have a good solubility and poses intermediate release rate. Incorporation of polymeric DOPEPEG2000 in the formulations contributed to the

high R^2 values with *SME* less than 3.3 in Kor*SME*yer-Peppas model and was suitable to describe the release from the polymeric system.

Table 4.14: Rate of release, *K*, Regression Coefficient, R^2, and standard median error (*SME*) values of folinic acid released from one day old DOPEPEG2000-oleic acid-soy lecithin liposomes in PBS pH 7.4 at 37 °C. The ratio of DOPEPEG2000 to oleic acid was fixed at 0.02:1and reported as a single component.

Kinetic Model		Molar ratio of soy lecithin to DOPEPEG2000-oleic acid					
		1:0	0.125:1	0.25:1	0.5:1	1:1	2:1
Zero Order (n=10)	K_0	0.8912	1.6089	1.7391	1.7570	1.1419	0.5524
	R^2	0.9829	0.9595	0.9759	0.9682	0.9526	0.9156
	SME	0.8111	6.1935	4.4829	5.9207	3.6080	1.4085
First Order (n=10)	K_1	0.0098	0.0193	0.0212	0.0215	0.0130	0.0059
	R^2	0.9915	0.9860	0.9954	0.9922	0.9739	0.9304
	SME	0.4023	2.1459	0.8577	1.4554	1.9906	1.1607
Higuchi (n=10)	K_H	3.5191	6.3961	6.8707	6.9630	4.5485	2.2213
	R^2	0.9094	0.9227	0.9075	0.9151	0.9267	0.9456
	SME	4.2898	11.8097	17.2090	15.7997	5.5811	0.9080
Korsmeyer-Peppas (n=6)	K_{KP}	1.4922	3.1785	3.0004	3.2477	2.3514	1.3640
	R^2	0.9995	0.9934	0.9955	0.9944	0.9921	0.9882
	SME	0.0256	1.1270	0.9455	1.1743	0.6765	0.2219
Gompertz (n=10)	$K_{G\alpha}$	5.1400	4.6132	5.0703	4.8367	4.5892	4.7293
	$K_{G\beta}$	0.8264	1.0530	1.1838	1.1517	0.8519	0.5715
	R^2	0.9912	0.9977	0.9959	0.9966	0.9989	0.9985
	SME	0.4708	0.3944	0.8587	0.7198	0.0957	0.0273

Figure 4.54 shows the cumulative release of methotrexate from DOPEPEG2000-oleic acid-soy lecithin liposomes at 37 °C. Cumulative release after 24 hours was highest in the DOPEPEG2000-oleic acid-soy lecithin liposomes with the molar ratio of soy lecithin to DOPEPEG2000-oleic acid were at 0.125:1, which was 51.6%. The incorporation of soy lecithin in the formulations reduced the diffusion of intermediate log P methotrexate to the environment. *In vitro* model dependent profiles show that the release mechanism of methotrexate was most fitted to Korsmeyer-Peppas model with the *SME* less than 1.5 as showed in Table 4.15, that agreed with the presence of DOPEPEG2000 in the formulations (Dash et al., 2010), as well as the morphology of

DOPEPEG2000-oleic acid-soy lecithin liposomes, which had a high tendency to form a

multivesicular liposomes (Jain & Jain, 2016).
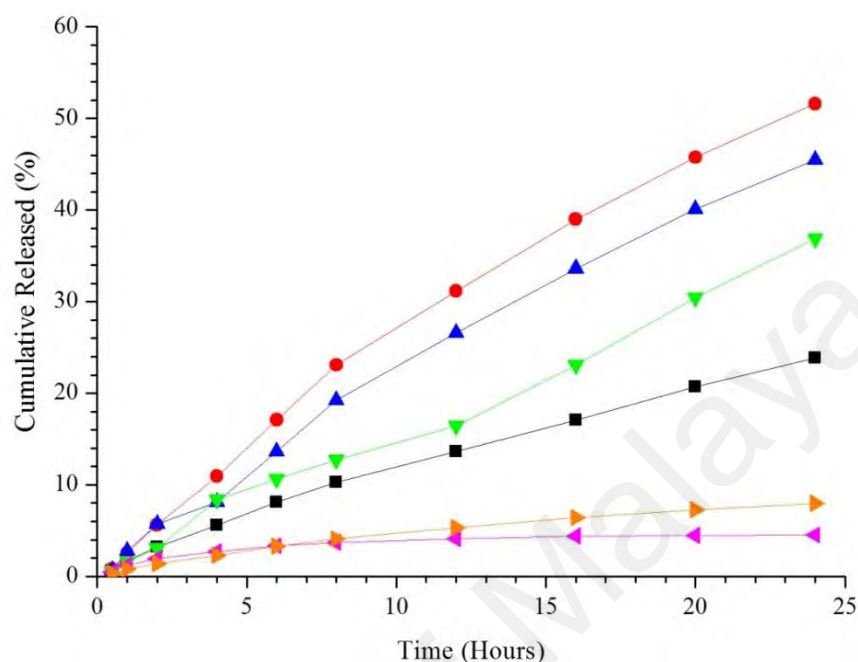
Figure 4.54: Cumulative release (%) with the standard deviation not more than 1 for methotrexate from DOPEPEG2000-oleic acid-soy lecithin liposomes in pH 7.4 at 37 °C. The molar ratios of soy lecithin to DOPEPEG2000-oleic acid were 1:0 (■), 0.125:1 (●), 0.25:1 (▲), 0.5:1 (▼), 1:1 (◄), and 2:1 (►). The ratio of DOPEPEG2000 to oleic acid was fixed at 0.02:1and reported as a single component.

Table 4.15: Rate of release, *K*, Regression Coefficient, R^2, and standard median error (*SME*) values of methotrexate released from one day old DOPEPEG2000-oleic acid-soy lecithin liposomes in PBS pH 7.4 at 37 °C. The ratio of DOPEPEG2000 to oleic acid was fixed at 0.02:1 and reported as a single component.

Kinetic Model		Molar ratio of soy lecithin to DOPEPEG2000-oleic acid					
		1:0	0.125:1	0.25:1	0.5:1	1:1	2:1
Zero Order	K_0	1.0584	2.3353	2.0261	1.5136	0.2566	0.3807
(n=10)	R^2	0.9775	0.9785	0.9864	0.9908	0.1312	0.9179
	SME	1.4801	7.2934	3.5229	1.4135	1.8100	0.6174
First Order	K_1	0.0119	0.0308	0.0255	0.0177	0.0026	0.0040
(n=10)	R^2	0.9895	0.9989	0.9980	0.9867	0.1587	0.9281
	SME	0.6897	0.3814	0.5152	2.0358	1.7526	0.5406
Higuchi	K_H	4.1891	9.2136	7.9598	5.8920	1.0970	1.5327
(n=10)	R^2	0.9162	0.9035	0.8913	0.8569	0.8759	0.9571
	SME	5.5213	32.6930	28.2180	21.8856	0.2584	0.3228
Korsmeyer-	K_{KP}	1.8789	3.9067	3.0428	1.7018	1.5224	0.9656
Peppas	R^2	0.9992	0.9955	0.9962	0.9914	0.9370	0.9961
(n=6)	*SME*	0.0628	1.7091	1.1037	1.4821	0.1477	0.0326
Gompertz	$K_{G\alpha}$	4.9212	5.5485	5.8771	6.1557	4.2488	4.9847
(n=10)	$K_{G\beta}$	0.8701	1.4940	1.4199	1.2491	0.2505	0.4930
	R^2	0.9914	0.9923	0.9886	0.9656	0.9580	0.9994
	SME	0.6387	2.9394	3.3316	5.9123	0.0985	0.0053

The release profiles of positively intermediate log P doxorubicin from DOPEPEG2000-oleic acid-soy lecithin liposomes are exhibited in the Figure 4.55. The cumulative release after 24 hours gave out a lower amount of doxorubicin released, when more than 0.5:1 molar ratio of soy lecithin to DOPEPEG2000-oleic acid. The release rate was high during the first 8 hours of the experiment and was reduced to a slower rate of release.

The results from the analysis using model dependent methods in Table 4.16 shows that the release of doxorubicin from DOPEPEG2000-oleic acid-soy lecithin liposomes was most fitted to Korsmeyer-Peppas model with regression coefficient values of more than 0.99 and *SME* of less than 0.3 in most of the formulations. The R^2 values were found to be high in Gompertz and first-order model, however, the *SME* values in

Gompertz model were approaching 5.7 and 13.3 in first order dissolution model showing that the suitable mechanism to explain the kinetic release of doxorubicin from DOPEPEG2000-oleic acid-soy lecithin liposomes was Korsmeyer-Peppas dissolution model.
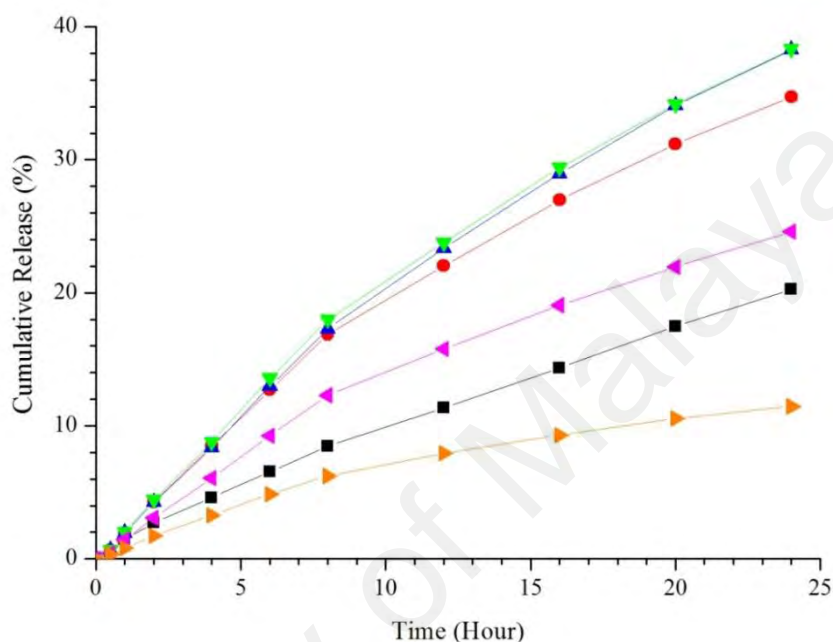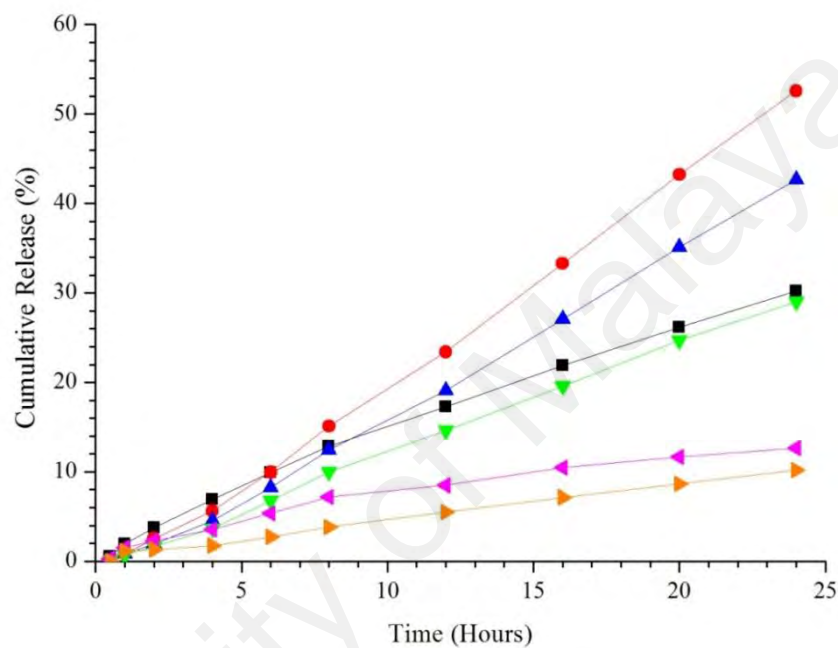

Figure 4.55: Cumulative release (%) with standard deviation not more than 1 for doxorubicin from DOPEPEG2000-oleic acid-soy lecithin liposomes in pH 7.4 at 37 °C. The molar ratios of soy lecithin to DOPEPEG2000-oleic acid were 1:0 (■), 125:1(●), 0.25:1 (▲), 0.5:1 (▼), 1:1 (◄), and 2:1(►). The ratio of DOPEPEG2000 to oleic acid was fixed at 0.02:1and reported as a single component.

Table 4.16: Rate of release, *K*, Regression Coefficient, R^2, and standard median error (*SME*) values of doxorubicin released from released from one day old DOPEPEG2000-oleic acid-soy lecithin liposomes in PBS pH 7.4 at 37 °C. The ratio of DOPEPEG2000 to oleic acid was fixed at 0.02:1and reported as a single component.

Kinetic Model		Molar ratio of soy lecithin to DOPEPEG2000-oleic acid					
		1:0	0.125:1	0.25:1	0.5:1	1:1	2:1
Zero Order	K_0	1.3400	2.1035	1.7108	1.2151	0.6128	0.4381
(n=10)	R^2	0.9814	0.9898	0.9903	0.9969	0.8992	0.9898
	SME	2.0179	3.5913	2.2417	0.3430	1.9656	0.1235
First Order	K_1	0.0155	0.0261	0.0203	0.0137	0.0066	0.0046
(n=10)	R^2	0.9946	0.9623	0.9708	0.9920	0.9173	0.9919
	SME	0.5832	13.2935	6.7708	0.8800	1.6127	0.0983
Higuchi	K_H	5.2921	8.0012	6.5113	4.6746	2.4738	1.7162
(n=10)	R^2	0.9096	0.7883	0.7902	0.8268	0.9554	0.8791
	SME	9.7884	74.5794	48.7078	18.9438	0.8686	1.4627
Korsmeyer-	K_{KP}	2.2677	1.2400	1.0289	1.0555	1.6279	0.5907
Peppas	R^2	0.9990	0.9993	0.9993	0.9977	0.9890	0.9946
(n=6)	*SME*	0.1222	0.2649	0.1949	0.2833	0.2405	0.0741
Gompertz	$K_{G\alpha}$	5.0067	12.3786	10.4453	7.3568	4.5088	6.0560
(n=10)	$K_{G\beta}$	1.0084	2.0677	1.7690	1.2736	0.5686	0.6962
	R^2	0.9917	0.9857	0.9894	0.9958	0.9954	0.9862
	SME	1.0097	5.6817	2.7695	0.5210	0.1005	0.1877

Figure 4.56 displays the cumulative release of hydrophobic irinotecan from DOPEPEG2000-oleic acid-soy lecithin liposomes in pH 7.4. At the equimolar of DOPEPEG2000-oleic acid to soy lecithin, a sustain release was achieve after the eighth hour of incubation. However, in the excess amount of soy lecithin in the formulation, the release was raised and approaching 50% in the formulation with the ratio of DOPEPEG2000-oleic acid to soy lecithin at 0.5:1. This is due to the hydrophilic irinotecan is favour to release in the lipid rich environment. The curve fitting into different dissolution models shows the highest regression coefficient of more than 0.99 in first-order and Korsemeyer-Peppas dissolution models as shown in Table 4.17. The first-order dissolution model described the release of irinotecan through the porous structure of the DOPEPEG2000-oleic acid-soy lecithin liposomes with *SME* values of

2.3. In the Korsemeyer-Peppas dissolution model, the release of active ingredients through the polymeric system was explained to involve many steps of release, gave out the *SME* values of less than 1.
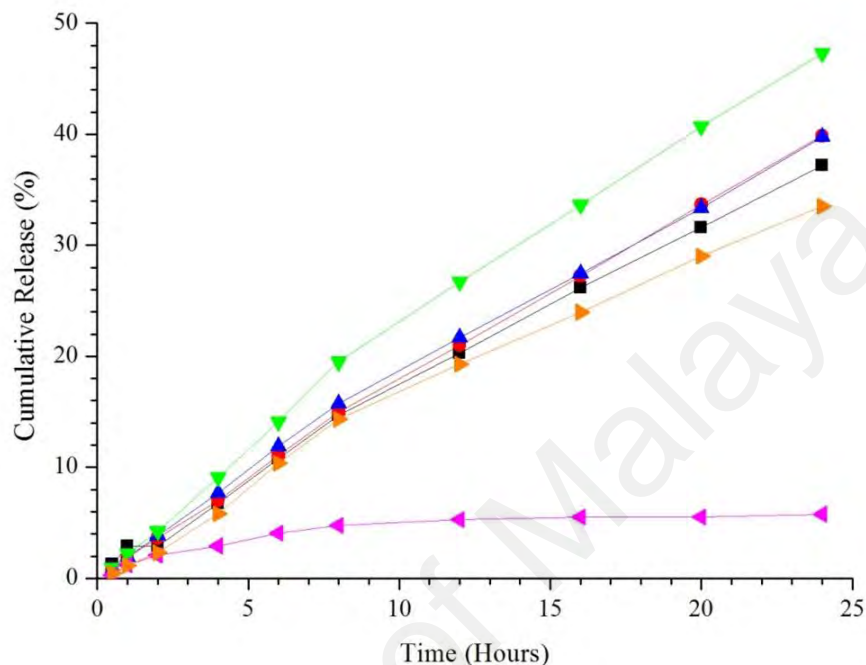
Figure 4.56: Cumulative release (%) with standard deviation not more than 1 of irinotecan from DOPEPEG2000-oleic acid-soy lecithin liposomes in pH 7.4 at 37 °C for 24 hours. The molar ratio of DOPEPEG2000-oleic acid to soy lecithin liposomes were 1:0 (■), 125:1 (●), 0.25:1 (▲), 0.5:1 (▼), 1:1 (◄), and 2:1(►) of soy lecithin to DOPEPEG2000-oleic acid. The ratio of DOPEPEG2000 to oleic acid was fixed at 0.02:1and reported as a single component.

Table 4.17: Rate of release, *K*, Regression Coefficient, R^2, and standard median error (*SME*) values of irinotecan released from released from one day old DOPEPEG2000-oleic acid-soy lecithin liposomes in PBS pH 7.4 at 37 °C. The ratio of DOPEPEG2000 to oleic acid was fixed at 0.02:1and reported as a single component.

Kinetic Model		Molar ratio of soy lecithin to DOPEPEG2000-oleic acid					
		1:0	0.125:1	0.25:1	0.5:1	1:1	2:1
Zero Order	K_0	1.6066	1.6974	1.7087	2.0676	0.3215	1.4737
(n=10)	R^2	0.9932	0.9976	0.9932	0.9911	0.3946	0.9880
	SME	1.1186	0.4563	1.2723	2.4539	2.4082	1.7342
First Order	K_1	0.0191	0.0204	0.0206	0.0261	0.0033	0.0173
(n=10)	R^2	0.9982	0.9981	0.9990	0.9988	0.4215	0.9960
	SME	0.3034	0.3682	0.1804	0.3382	2.3011	0.5772
Higuchi	K_H	6.2874	6.6157	6.6914	8.1014	1.3607	5.7658
(n=10)	R^2	0.8799	0.8689	0.8840	0.8849	0.9073	0.8777
	SME	19.8264	25.0819	21.7978	31.7996	0.3688	17.6751
Korsmeyer-	K_{KP}	2.1593	2.0570	2.3576	2.9184	1.6488	2.0380
Peppas	R^2	0.9980	0.9995	0.9989	0.9978	0.9233	0.9939
(n=6)	*SME*	0.3740	0.1112	0.2243	0.6709	0.3433	0.9891
Gompertz	$K_{G\alpha}$	5.9947	6.3738	5.8000	6.0646	4.2072	5.7333
(n=10)	$K_{G\beta}$	1.2687	1.3558	1.2819	1.4623	0.3052	1.1792
	R^2	0.9881	0.9877	0.9887	0.9904	0.9486	0.9967
	SME	2.2018	2.6396	2.3924	2.9957	0.2301	0.5375

Figure 4.57 shows the proposed general release mechanism of various anticancer drugs from liposomes to the site of action, which involving multiple release phenomenon crossing the bilayer membrane to the polyethylene glycol coating layer, before being released into the site of action. The release of anticancer drugs from polyethylene glycol coatings to the environment explained why most of the release mechanisms were fitted to Korsmeyer-Peppas dissolution model as shown in Table 4.18. This is due to the polyethylene glycol that presence in the formulation becomes the release determinant for anticancer drugs from the stealth mixed oleic acid liposomes.
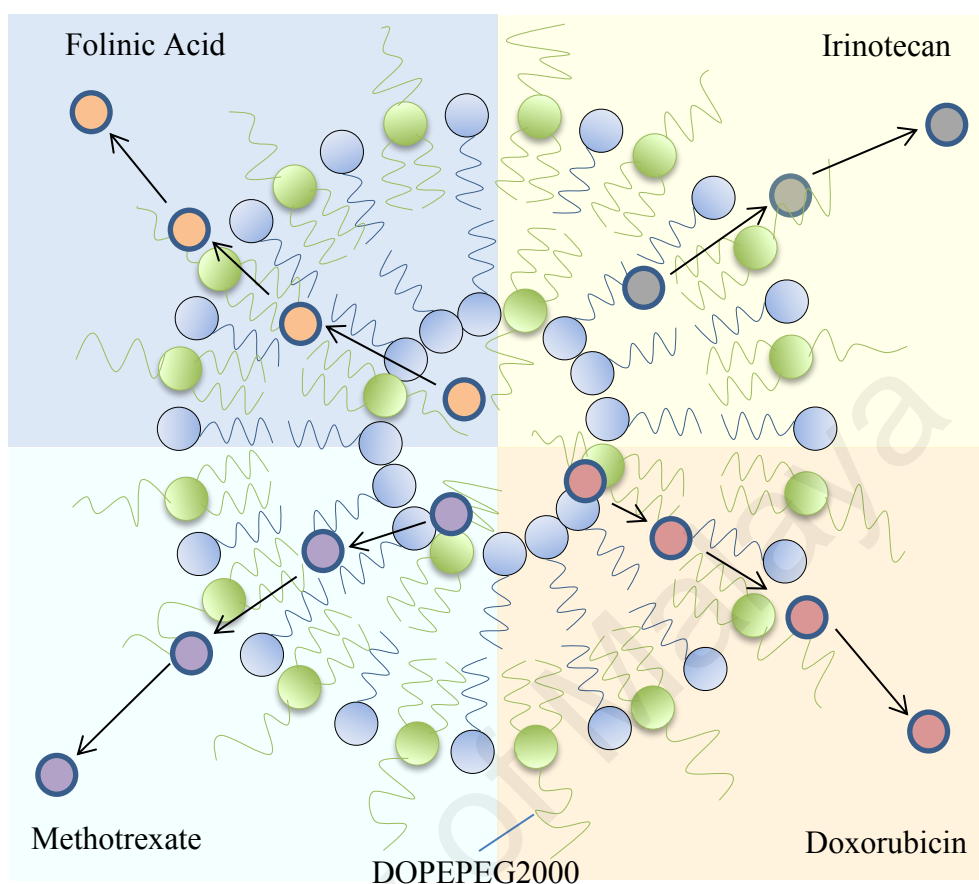
Figure 4.57: Proposed released mechanism of various anticancer drugs to the site of action.

Table 4.18: Drug dissolution model of anticancer drugs release from liposomes.

Liposomes	Drug Dissolution Model				
	Zero Order	First Order	Higuchi	Kosmeyer-Peppas	Gompertz
Oleic acid pH 8.5		F,M		F,M,D,I	D,I
Oleic acid pH 7.4	I	M		F,M,D,I	F,D
DOPEPEG2000-oleic acid pH7.4		I		F,M,D,I	F,M,D
DOPEPEG2000-oleic acid- erucic acid pH7.4	D	F,I		F,M,D,I	M
DOPEPEG2000-oleic acid- soy lecithin pH7.4				F,M,D,I	F,M,D,I
Abbreviations: F= folinic acid, M= methotrexate, D= doxorubicin, and I= irinotecan					

CHAPTER 5: CONCLUSIONS

5.1   Conclusions

Through more than sixty years of drug delivery technology (Bae et al., 2013), many mechanisms of controlled drug delivery have been achieved and well established. Nanotechnology is currently one of the most rapidly developing branches of science that being applied in tailoring the carrier of various active ingredient for the treatment of various life-threatening diseases. Liposomes is one of the nanocarriers that being proposed by the scientist as potential delivery systems for a variety of chemotherapeutic compounds. However, due to many obstacles, many of liposomal based chemotherapy remain at the stage of early preclinical development.

In this study, liposomes from various mixture of oleic acid with erucic acid and soy lecithin were prepared by using thin lipid hydration techniques. The pH jump technique was employed to determine the pH region where the liposomes were abundantly present. The critical vesicular concentration (CVC), which is the minimum concentration of oleic acid, erucic acid, or soy lecithin needed to form liposomes, was evaluated using surface tension technique. The glass transition temperature obtained from the thermogram, that generated by differential scanning calorimetry provides the suitable temperature for the formation of liposomes.

The presence of liposomes was verified using two microscopy technique, which is Optical Polarizing Microscope (OPM) and High Resolution-Transmission Electron Microscope (HR-TEM). Under the light field of polarized light, liposomes displayed birefringence properties where vibrant yellow-blue spherical particles were present due to the refraction of light passing the membrane of liposomes (Bibi et al., 2011). Also, the dark field mode OPM micrograph, Maltese cross effect phenomenon can be observed which indicates the presence of liposomes.

The membrane of liposomes was decorated with lipid anchored PEG, namely DOPEPEG2000 (1,2-dioleoyl-sn-glycerol-3-phosphoethanolamide-N- [methoxy(poly ethylene glycol) -2000]) to achieve the stealth properties in the term of technological, chemical, and biological stability to the liposomal system as has been reported in the literature (Pasut et al., 2015). Incorporation of DOPEPEG2000 in the oleic acid liposomes formulations significantly reduced the average particle size down to 200 nm at the molar ratios of DOPEPEG2000 to oleic acid at 0.02:1. The zeta potential of all formulations was altered with the presence of DOPEPEG2000. Formulations with a stable particle size and zeta potential were identified from the stability in term of particle size and zeta potential within 28 days.

Biphasic character of liposomes which can act as a carrier for both hydrophilic and hydrophobic molecules is explored in the aim to encapsulate chemotherapeutic compounds. Four anticancer drugs from various log P ranging from -3 to +3 namely folinic acid, methotrexate, doxorubicin, and irinotecan were tested. High encapsulation efficiency is achieved in most formulations. The solubility and partitioning characteristics of anticancer drugs determined the site of incorporation in the liposomes whether in the aqueous core or within the membrane of liposomes. This is directly affecting the entrapment and release properties of drugs from liposomes.

In vitro release of folinic acid, methotrexate, doxorubicin, and irinotecan from liposomes were evaluated using automated Franz diffusion cell. Most of the formulations gave out the cumulative release of anticancer drugs after 24 hours less than 40% indicating slow and delayed release properties. The data collected were fitted into five kinetic modelling which is Zero order, First order, Higuchi, Korsmeyer-Peppas, and Gompertz dissolution model. Polyethylene glycol in the formulation is affecting the

release properties which gave out Korsemeyer-Peppas dissolution model as the most fitted kinetic model to describe the release of drugs from the prepared stealth liposomes.

The application of stealth liposomal strategy to assist anticancer drug delivery has provenly improved the chemotherapy procedure. Generally, stealth liposomal formulations comprised of DOPEPEG2000, oleic acid, erucic acid, and soy lecithin showed comparable results and exhibited a promising alternative for a cost effective anticancer drugs nanocarriers in the aim to improve the chemotherapeutic treatment that leads to great benefit in the patient's response and outcome.

5.2 Future Prospects

The development of stealth liposomes as carriers for chemotherapeutic molecules is an ever-growing research area. This study presents the successful preparation and characterization of stealth liposomes using cheaper alternatives which are oleic acid, erucic acid, and soy lecithin, as compared to conventional phospholipids. Specifically targeted liposomes can be achieved by functionalizing the stealth fatty acid liposomes with specific targeting molecules such as antibodies, peptides, growth factors, and receptors. By this, the tailored specific targeting stealth fatty acid liposomes will enhance the therapeutic efficacy of liposomal chemotherapy.

REFERENCES

Adams, R. L. P. (1990). *Cell Culture for Biochemists*. Amsterdam: Elsevier Science.

Ahmad, N., Muhammad, R., Tajuddin, H. A., & Misran, M. (2014). Effect of glycolipids on the stability and electrophoretic mobility of decanoic acid vesicles. *Colloids and Surfaces A: Physicochemical and Engineering Aspects, 443*, 96-101.

Akbarzadeh, A., Rezaei-Sadabady, R., Davaran, S., Joo, S. W., Zarghami, N., Hanifehpour, Y., Samiei, M., Kouhi, M., & Nejati-Koshki, K. (2013). Liposome: classification, preparation, and applications. *Nanoscale Research Letters, 8*(1), 102.

Akbarzadeh, A., Samiei, M., Joo, S. W., Anzaby, M., Hanifehpour, Y., Nasrabadi, H. T., & Davaran, S. (2012). Synthesis, characterization and in vitro studies of doxorubicin-loaded magnetic nanoparticles grafted to smart copolymers on A549 lung cancer cell line. *Journal of Nanobiotechnology, 10*(1), 46.

Alavi, S., Haeri, A., & Dadashzadeh, S. (2017). Utilization of chitosan-caged liposomes to push the boundaries of therapeutic delivery. *Carbohydrate Polymers, 157*, 991-1012.

Allen, T. M., & Martin, F. J. (2004). Advantages of liposomal delivery systems for anthracyclines. *Seminars in Oncology, 31*(6 Suppl 13), 5-15.

Altin, O., Özbelge, H. Ö., & Dogu, T. (1999). Effect of pH in an Aqueous Medium on the Surface Area, Pore Size Distribution, Density, and Porosity of Montmorillonite. *Journal of Colloid and Interface Science, 217*(1), 19-27.

Anabousi, S., Bakowsky, U., Schneider, M., Huwer, H., Lehr, C.-M., & Ehrhardt, C. (2006). In vitro assessment of transferrin-conjugated liposomes as drug delivery systems for inhalation therapy of lung cancer. *European Journal of Pharmaceutical Sciences, 29*(5), 367-374.

Anderson, W., Kozak, D., Coleman, V. A., Jämting, Å. K., & Trau, M. (2013). A comparative study of submicron particle sizing platforms: Accuracy, precision and resolution analysis of polydisperse particle size distributions. *Journal of Colloid and Interface Science, 405*, 322-330.

Andresen, T. L., Jensen, S. S., & Jørgensen, K. (2005). Advanced strategies in liposomal cancer therapy: Problems and prospects of active and tumor specific drug release. *Progress in Lipid Research, 44*(1), 68-97.

Arias, J. L. (2014). *Nanotechnology and Drug Delivery, Volume One: Nanoplatforms in Drug Delivery*. Florida: CRC Press.

Atkins, P. (1994). *Physical Chemistry Fifth Edition*. Virginia: W.H. Freeman.

Atkins, P., & de Paula, J. (2014). *Atkins' Physical Chemistry*. Oxford: OUP Oxford.

Bae, Y. H., Mrsny, R. J., & Park, K. (2013). *Cancer Targeted Drug Delivery: An Elusive Dream*. New York: Springer New York.

Balanč, B., Trifković, K., Đorđević, V., Marković, S., Pjanović, R., Nedović, V., & Bugarski, B. (2016). Novel resveratrol delivery systems based on alginate-sucrose and alginate-chitosan microbeads containing liposomes. *Food Hydrocolloids, 61*, 832-842.

Banfalvi, G. (2013). *Homeostasis - Tumor - Metastasis*. Netherlands: Springer Science & Business Media.

Bangham, A. D., & Horne, R. W. (1964). Negative staining of phospholipids and their structural modification by surface-active agents as observed in the electron microscope. *Journal of Molecular Biology, 8*(5), 660-IN610.

Bansal, D., Gulbake, A., Tiwari, J., & Jain, S. K. (2016). Development of liposomes entrapped in alginate beads for the treatment of colorectal cancer. *International Journal of Biological Macromolecules, 82*, 687-695.

Barenholz, Y., & Lasic, D. D. (1996). *Handbook of Nonmedical Applications of Liposomes*. Florida: CRC Press.

Bart, H. J., & Pilz, S. (2011). *Industrial Scale Natural Products Extraction*. Germany: Wiley.

Beaglehole, R., Bonita, R., & Magnusson, R. (2011). Global cancer prevention: An important pathway to global health and development. *Public Health, 125*(12), 821-831.

Berginc, K., Suljaković, S., Škalko-Basnet, N., & Kristl, A. (2014). Mucoadhesive liposomes as new formulation for vaginal delivery of curcumin. *European Journal of Pharmaceutics and Biopharmaceutics, 87*(1), 40-46.

Bhatia, S. (2016). Microbial Polysaccharides as Advance Nanomaterials *Systems for Drug Delivery: Safety, Animal, and Microbial Polysaccharides* (pp. 29-54). Cham: Springer International Publishing.

Bibi, S., Kaur, R., Henriksen-Lacey, M., McNeil, S. E., Wilkhu, J., Lattmann, E., Christensen, D., Mohammed, A. R., & Perrie, Y. (2011). Microscopy imaging of liposomes: From coverslips to environmental SEM. *International Journal of Pharmaceutics, 417*(1–2), 138-150.

Boakye, C. H. A., Patel, K., & Singh, M. (2015). Doxorubicin liposomes as an investigative model to study the skin permeation of nanocarriers. *International Journal of Pharmaceutics, 489*(1–2), 106-116.

Boeckel, D. G., Shinkai, R. S. A., Grossi, M. L., & Teixeira, E. R. (2014). *In vitro* evaluation of cytotoxicity of hyaluronic acid as an extracellular matrix on OFCOL II cells by the MTT assay. *Oral Surgery, Oral Medicine, Oral Pathology and Oral Radiology, 117*(6), e423-e428.

Bray, F., & Shield, K. D. (2017). Cancer: Global Burden, Trends, and Projections A2 - Quah, Stella R *International Encyclopedia of Public Health (Second Edition)* (pp. 347-368). Oxford: Academic Press.

Buckland, B. C. (2013). *Cell Culture Engineering IV: Improvements of Human Health*. USA: Springer Netherlands.

Buckley, A., McQuaid, S., Johnson, P., Buggy, D. J., & Hemmings, H. C. (2014). Effect of anaesthetic technique on the natural killer cell anti-tumour activity of serum from women undergoing breast cancer surgery: a pilot study. *BJA: British Journal of Anaesthesia, 113*(suppl_1), i56-i62.

Burlatsky, S. F., Atrazhev, V. V., Dmitriev, D. V., Sultanov, V. I., Timokhina, E. N., Ugolkova, E. A., Tulyani, S., & Vincitore, A. (2013). Surface tension model for surfactant solutions at the critical micelle concentration. *Journal of Colloid and Interface Science, 393*, 151-160.

Cagel, M., Grotz, E., Bernabeu, E., Moretton, M. A., & Chiappetta, D. A. (2017). Doxorubicin: nanotechnological overviews from bench to bedside. *Dru Discovery Today, 22*(2), 270-281.

Candiotti, K. A., Sands, L. R., Lee, E., Bergese, S. D., Harzman, A. E., Marcet, J., Kumar, A. S., & Haas, E. (2014). Liposome Bupivacaine for Postsurgical Analgesia in Adult Patients Undergoing Laparoscopic Colectomy: Results from Prospective Phase IV Sequential Cohort Studies Assessing Health Economic Outcomes. *Current Therapeutic Research, 76*, 1-6.

Celia, C., Ferrati, S., Bansal, S., van de Ven, A. L., Ruozi, B., Zabre, E., Hosali, S., Paolino, D., Sarpietro, M. G., Fine, D., Fresta, M., Ferrari, M., & Grattoni, A. (2014). Sustained zero-order release of intact ultra-stable drug-loaded liposomes from an implantable nanochannel delivery system. *Advanced Healthcare Materials, 3*(2), 230-238.

Chen, I. A., & Szostak, J. W. (2004). A Kinetic Study of the Growth of Fatty Acid Vesicles. *Biophysical Journal, 87*(2), 988-998.

Chia, S. W., & Misran, M. (2013). Flow Behavior of Oleic Acid Liposomes in Sucrose Ester Glycolipid Oil-in-Water Emulsions. *Journal of Surfactants and Detergents, 17*(1), 1-10.

Chiavaro, E. (2014). *Differential Scanning Calorimetry: Applications in Fat and Oil Technology*. Florida: Taylor & Francis.

Chun, S. G., Skinner, H. D., & Minsky, B. D. (2017). Radiation Therapy for Locally Advanced Esophageal Cancer. *Surgical Oncology Clinics of North America, 26*(2), 257-276.

Chylińska, M., Szymańska-Chargot, M., & Zdunek, A. (2016). FT-IR and FT-Raman characterization of non-cellulosic polysaccharides fractions isolated from plant cell wall. *Carbohydrate Polymers, 154*, 48-54.

Ciani, L., Ristori, S., Bonechi, C., Rossi, C., & Martini, G. (2007). Effect of the preparation procedure on the structural properties of oligonucleotide/cationic liposome complexes (lipoplexes) studied by electron spin resonance and Zeta potential. *Biophysical Chemistry, 131*(1–3), 80-87.

Cistola, D. P., Hamilton, J. A., Jackson, D., & Small, D. M. (1988). Ionization and phase behavior of fatty acids in water: application of the Gibbs phase rule. *Biochemistry, 27*(6), 1881-1888.

Clark, B. J., Frost, T., & Russell, M. A. (1993). *UV Spectroscopy: Techniques, instrumentation and data handling*. London: Chapman&Hall.

Cortesi, R. (1999). Preparation of liposomes by reverse-phase evaporation using alternative organic solvents. *Journal of Microencapsulation, 16*(2), 251-256.

Costa, P., & Lobo, J. M. S. (2001). Modeling and comparison of dissolution profiles. *European Journal of Pharmaceutical Sciences, 13*(2), 123-133.

Crompton, T. R. (2006). *Polymer Reference Book*: Rapra Technology Limited.

Crooke, S. T. (2007). *Antisense Drug Technology: Principles, Strategies, and Applications, Second Edition*. Florida: CRC Press.

Cross, J. (1998). *Anionic Surfactants: Analytical Chemistry, Second Edition*. New York: Marcel Dekker Inc.

Currie, E., Schulze, A., Zechner, R., Walther, Tobias C., & Farese Jr, Robert V. (2013). Cellular Fatty Acid Metabolism and Cancer. *Cell Metabolism, 18*(2), 153-161.

Dan, T., & Williams, N. L. (2017). Management of Stage I Lung Cancer with Stereotactic Ablative Radiation Therapy. *Surgical Oncology Clinics of North America, 26*(3), 393-403.

Dash, S., Murthy, P. N., Nath, L., & Chowdhury, P. (2010). Kinetic modeling on drug release from controlled drug delivery systems. *Acta Poloniae Pharmaceutica-Drug Research, 67*(3), 217-223.

Daugirdas, J. T., Blake, P. G., & Ing, T. S. (2007). *Handbook of Dialysis*. Philadelphia: Lippincott Williams & Wilkins.

De, A., Bose, R., Kumar, A., & Mozumdar, S. (2013). *Targeted Delivery of Pesticides Using Biodegradable Polymeric Nanoparticles*. New Delhi: Springer.

de Martel, C., Ferlay, J., Franceschi, S., Vignat, J., Bray, F., Forman, D., & Plummer, M. (2012). Global burden of cancers attributable to infections in 2008: a review and synthetic analysis. *The Lancet Oncology, 13*(6), 607-615.

de Matos, F. C., da Costa, M. C., Meirelles, A. J. d. A., & Batista, E. A. C. (2016). Binary solid–liquid equilibrium systems containing fatty acids, fatty alcohols and trilaurin by differential scanning calorimetry. *Fluid Phase Equilibria, 423*, 74-83.

Depciuch, J., Sowa-Kućma, M., Nowak, G., Dudek, D., Siwek, M., Styczeń, K., & Parlińska-Wojtan, M. (2016). Phospholipid-protein balance in affective disorders: Analysis of human blood serum using Raman and FTIR spectroscopy. A pilot study. *Journal of Pharmaceutical and Biomedical Analysis, 131*, 287-296.

Deygen, I. M., & Kudryashova, E. V. (2016). New versatile approach for analysis of PEG content in conjugates and complexes with biomacromolecules based on FTIR spectroscopy. *Colloids and Surfaces B: Biointerfaces, 141*, 36-43.

Dollinger, M., Tempero, M., & Mulvihill, S. (2002). *Everyone's Guide to Cancer Therapy; 4th Edition: How Cancer Is Diagnosed, Treated, and Managed Day to Day*. Kansas: Andrews McMeel Publishing.

Dua, J., Rana, A., & Bhandari, A. (2012). Liposome: methods of preparation and applications. *International Journal of Pharmaceutical Studies and Research, 3*, 14-20.

Duh, Y.-S., Lee, C.-Y., Chen, Y.-L., & Kao, C.-S. (2016). Characterization on the exothermic behaviors of cathode materials reacted with ethylene carbonate in lithium-ion battery studied by differential scanning calorimeter (DSC). *Thermochimica Acta, 642*, 88-94.

Duzgunes, N., & Düzgüneş, N. (2012). *Nanomedicine: Cancer, Diabetes, and Cardiovascular, Central Nervous System, Pulmonary and Inflammatory Diseases*. San Diego: Academic Press/Elsevier.

Dwiastuti, R., Radifar, M., Marchaban, M., Noegrohati, S., & Istyastono, E. P. (2016). Molecular Dynamics Simulations and Empirical Observations on Soy Lecithin Liposome Preparation. *Indonesian Journal of Chemistry, 16*(2), 222-228.

Eh Suk, V. R., & Misran, M. (2017). Preparation, characterization and physicochemical properties of DOPE-PEG2000 stabilized oleic acid-soy lecithin liposomes (POLL). *Colloids and Surfaces A: Physicochemical and Engineering Aspects*, *513*, 267-273.

Eloy, J. O., Claro de Souza, M., Petrilli, R., Barcellos, J. P. A., Lee, R. J., & Marchetti, J. M. (2014). Liposomes as carriers of hydrophilic small molecule drugs: Strategies to enhance encapsulation and delivery. *Colloids and Surfaces B: Biointerfaces, 123*, 345-363.

Fameau, A.-L., Arnould, A., & Saint-Jalmes, A. (2014). Responsive self-assemblies based on fatty acids. *Current Opinion in Colloid & Interface Science, 19*(5), 471-479.

Feng, D., Zhang, Y., Chen, Q., Wang, J., Li, B., & Feng, Y. (2012). Synthesis and Surface Activities of Amidobetaine Surfactants with Ultra-long Unsaturated Hydrophobic Chains. *Journal of Surfactants and Detergents, 15*(5), 657-661.

Feng, Z., Wen, H., Bi, R., Yang, W., & Wu, X. (2016). Prognostic impact of the time interval from primary surgery to intravenous chemotherapy in high grade serous ovarian cancer. *Gynecologic Oncology, 141*(3), 466-470.

Fotakis, G., & Timbrell, J. A. (2006). In vitro cytotoxicity assays: Comparison of LDH, neutral red, MTT and protein assay in hepatoma cell lines following exposure to cadmium chloride. *Toxicology Letters, 160*(2), 171-177.

Frazier, J. M. (1992). *In-Vitro Toxicity Testing: Applications to Safety Evaluation*. New York: CRC Press.

Freshney, R. I. (2015). *Culture of Animal Cells: A Manual of Basic Technique and Specialized Applications*. Canada: John Wiley & Son.

Gad, S. C. (2008). *Preclinical Development Handbook: ADME and Biopharmaceutical Properties*. New Jersey: John Wiley & Sons.

Ge, L., Möhwald, H., & Li, J. (2003). Phospholipid liposomes stabilized by the coverage of polyelectrolyte. *Colloids and Surfaces A: Physicochemical and Engineering Aspects, 221*(1–3), 49-53.

Gillet, A., Grammenos, A., Compère, P., Evrard, B., & Piel, G. (2009). Development of a new topical system: Drug-in-cyclodextrin-in-deformable liposome. *International Journal of Pharmaceutics, 380*(1–2), 174-180.

Gilman, A. (1963). The initial clinical trial of nitrogen mustard. *The American Journal of Surgery, 105*(5), 574-578.

Giodini, L., Re, F. L., Campagnol, D., Marangon, E., Posocco, B., Dreussi, E., & Toffoli, G. (2017). Nanocarriers in cancer clinical practice: a pharmacokinetic issue. *Nanomedicine: Nanotechnology, Biology and Medicine, 13*(2), 583-599.

Gjetting, T., Arildsen, N. S., Christensen, C. L., Poulsen, T. T., Roth, J. A., Handlos, V. N., & Poulsen, H. S. (2010). *In vitro* and *in vivo* effects of polyethylene glycol (PEG)-modified lipid in DOTAP/cholesterol-mediated gene transfection. *International Journal of Nanomedicine, 5*, 371-383.

Godoy, C. A., Valiente, M., Pons, R., & Montalvo, G. (2015). Effect of fatty acids on self-assembly of soybean lecithin systems. *Colloids and Surfaces B: Biointerfaces, 131*, 21-28.

Goldstein-Dennis, H. (2016). *Polarized Light, Third Edition*. Florida: CRC Press.

Goldstein, D., & Goldstein, D. H. (2003). *Polarized Light, Revised and Expanded* (Second ed.). New York: CRC Press.

Goodman, L. S., Wintrobe, M. M., Dameshek, W., Goodman, M. J., Gilman, A., & McLennan, M. T. (1984). Nitrogen mustard therapy: Use of methyl-bis(beta-chloroethyl)amine hydrochloride and tris(beta-chloroethyl)amine hydrochloride for hodgkin's disease, lymphosarcoma, leukemia and certain allied and miscellaneous disorders. *JAMA, 251*(17), 2255-2261.

Grauby-Heywang, C., Moroté, F., Mathelié-Guinlet, M., Gammoudi, I., Faye, N. R., & Cohen-Bouhacina, T. (2016). Influence of oxidized lipids on palmitoyl-oleoyl-phosphatidylcholine organization, contribution of Langmuir monolayers and Langmuir–Blodgett films. *Chemistry and Physics of Lipids, 200*, 74-82.

Gregoriadis, G. (2016). *Liposome Technology: Liposome Preparation and Related Techniques*. Florida: CRC Press.

Gregoriadis, G., Swain, C. P., Wills, E. J., & Tavill, A. S. (1974). Drug-Carrier Potential of Liposomes in Cancer Chemotherapy. *The Lancet, 303*(7870), 1313-1316.

Gulati, M., Grover, M., Singh, S., & Singh, M. (1998). Lipophilic drug derivatives in liposomes. *International Journal of Pharmaceutics, 165*(2), 129-168.

Guo, H., & Kim, J.-C. (2016). Reduction-responsive release property of egg phosphatidylcholine liposomes incorporating benzyl disulfide. *Journal of Industrial and Engineering Chemistry, 44*, 105-111.

Gupta, M., Sharma, V., & Chauhan, N. S. (2017). Chapter 16 - Nanotechnology for oral delivery of anticancer drugs: an insight potential A2 - Andronescu, Ecaterina. In A. M. Grumezescu (Ed.), *Nanostructures for Oral Medicine* (pp. 467-510): Elsevier.

Hacker, M., Messer, W. S., & Bachmann, K. A. (2009). *Pharmacology: Principles and Practice*. Oxford: Academic Press.

Hale, A., & Hovey, M. J. (2013). *Fluid, Electrolyte, and Acid-Base Imbalances: Content Review Plus Practice Questions*. Philadelphia: F. A. Davis Company.

Hamilton, R. L., & Guo, L. S. S. (1984). Liposomes preparation methods. *Journal of Clinical Biochemistry and Nutrition, 7*, 175.

Han, X., Gelein, R., Corson, N., Wade-Mercer, P., Jiang, J., Biswas, P., Finkelstein, J. N., Elder, A., & Oberdörster, G. (2011). Validation of an LDH assay for assessing nanoparticle toxicity. *Toxicology, 287*(1), 99-104.

Hasan, M., Belhaj, N., Benachour, H., Barberi-Heyob, M., Kahn, C. J. F., Jabbari, E., Linder, M., & Arab-Tehrany, E. (2014). Liposome encapsulation of curcumin: Physico-chemical characterizations and effects on MCF7 cancer cell proliferation. *International Journal of Pharmaceutics, 461*(1), 519-528.

He, C., Hu, Y., Yin, L., Tang, C., & Yin, C. (2010). Effects of particle size and surface charge on cellular uptake and biodistribution of polymeric nanoparticles. *Biomaterials, 31*(13), 3657-3666.

Heshmat, M., & Eltawil, A. (2017). A new sequential approach for chemotherapy treatment and facility operations planning. *Operations Research for Health Care*, In Press.

Himeno, T., Konno, Y., & Naito, N. (2017). Chapter 31 - Liposomes for Cosmetics *Cosmetic Science and Technology* (pp. 539-549). Amsterdam: Elsevier.

Hoekman, J. D., Srivastava, P., & Ho, R. J. Y. (2014). Aerosol-Stable Peptide-Coated Liposome Nanoparticles: A Proof-of-Concept Study with Opioid Fentanyl in Enhancing Analgesic Effects and Reducing Plasma Drug Exposure. *Journal of Pharmaceutical Sciences, 103*(8), 2231-2239.

Holenz, J., Mannhold, R., Kubinyi, H., & Folkers, G. (2016). *Lead Generation, Volume 68: Methods and Strategies*. Germany: Wiley.

Holland, J. W., Cullis, P. R., & Madden, T. D. (1996). Poly(ethylene glycol)−Lipid Conjugates Promote Bilayer Formation in Mixtures of Non-Bilayer-Forming Lipids. *Biochemistry, 35*(8), 2610-2617.

Hosseini, M., Tirgari, B., Forouzi, M. A., & Jahani, Y. (2016). Guided imagery effects on chemotherapy induced nausea and vomiting in Iranian breast cancer patients. *Complementary Therapies in Clinical Practice, 25*, 8-12.

House, S. D., Bonifacio, C. S., Grieshaber, R. V., Li, L., Zhang, Z., Ciston, J., Stach, E. A., & Yang, J. C. (2016). Statistical analysis of support thickness and particle size effects in HRTEM imaging of metal nanoparticles. *Ultramicroscopy, 169*, 22-29.

Hsu, W.-H., Liu, S.-Y., Chang, Y.-J., Chang, C.-H., Ting, G., & Lee, T.-W. (2014). The PEGylated liposomal doxorubicin improves the delivery and therapeutic efficiency of 188Re-Liposome by modulating phagocytosis in C26 murine colon carcinoma tumor model. *Nuclear Medicine and Biology, 41*(9), 765-771.

Hu, Y., Rip, J., Gaillard, P. J., de Lange, E. C. M., & Hammarlund-Udenaes, M. (2017). The Impact of Liposomal Formulations on the Release and Brain Delivery of Methotrexate: An in vivo Microdialysis Study. *Journal of Pharmaceutical Sciences*, 2606-2613.

Hudiyanti, D., Radifar, M., Raharjo, T. J., Narsito, N., & Noegrohati, S. (2014). A Coarse-Grained Molecular Dynamics Simulation Using NAMD Package to Reveal Aggregation Profile of Phospholipids Self-Assembly in Water. *Journal of Chemistry, 2014*, 6.

Hunter, R. J., Ottewill, R. H., & Rowell, R. L. (2013). *Zeta Potential in Colloid Science: Principles and Applications*. London: Academic Press.

Immordino, M. L., Franco, D., & Cattel, L. (2006). Stealth liposomes: review of the basic science, rationale, and clinical applications, existing and potential. *International Journal of Nanomedicine, 1*(3), 297-315.

Imran, M., Revol-Junelles, A.-M., Paris, C., Guedon, E., Linder, M., & Desobry, S. (2015). Liposomal nanodelivery systems using soy and marine lecithin to encapsulate food biopreservative nisin. *LWT - Food Science and Technology, 62*(1, Part 1), 341-349.

Ishida, T., Kirchmeier, M. J., Moase, E. H., Zalipsky, S., & Allen, T. M. (2001). Targeted delivery and triggered release of liposomal doxorubicin enhances cytotoxicity against human B lymphoma cells. *Biochimica et Biophysica Acta (BBA) - Biomembranes, 1515*(2), 144-158.

Jain, A., & Jain, S. K. (2016). In vitro release kinetics model fitting of liposomes: An insight. *Chemistry and Physics of Lipids, 201*, 28-40.

Jiang, X., Li, S., Xiang, G., Li, Q., Fan, L., He, L., & Gu, K. (2016). Determination of the acid values of edible oils via FTIR spectroscopy based on the OH stretching band. *Food Chemistry, 212*, 585-589.

Jøraholmen, M. W., Basnet, P., Acharya, G., & Škalko-Basnet, N. (2017). PEGylated liposomes for topical vaginal therapy improve delivery of interferon alpha. *European Journal of Pharmaceutics and Biopharmaceutics, 113*, 132-139.

Joshi, J. R., & Patel, R. P. (2012). Role of biodegradable polymers in drug delivery. *International Journal of Current Pharmaceutical Research, 4*(4), 74-81.

Kaminogawa, S., Ametani, A., & Hachimura, S. (2012). *Animal Cell Technology: Basic & Applied Aspects: Proceedings of the Fifth International Meeting of the Japanese Association for Animal Cell Technology, Omiya, Japan, November 30–December 4, 1992*. Netherland: Springer Netherlands.

Kanicky, J. R., & Shah, D. O. (2002). Effect of Degree, Type, and Position of Unsaturation on the pKa of Long-Chain Fatty Acids. *Journal of Colloid and Interface Science, 256*(1), 201-207.

Kielhorn, J., Melching-Kollmuss, S., & Mangelsdorf, I. (2006). *Dermal Absorption*. Geneva: World Health Organization.

Kim, J.-D., & Honma, I. (2003). Proton conducting polydimethylsiloxane/zirconium oxide hybrid membranes added with phosphotungstic acid. *Electrochimica Acta, 48*(24), 3633-3638.

Kleinfeld, A. M., Chu, P., & Romero, C. (1997). Transport of Long-Chain Native Fatty Acids across Lipid Bilayer Membranes Indicates That Transbilayer Flip-Flop Is Rate Limiting. *Biochemistry, 36*(46), 14146-14158.

Koudelka, S., Turanek Knotigova, P., Masek, J., Prochazka, L., Lukac, R., Miller, A. D., Neuzil, J., & Turanek, J. (2015). Liposomal delivery systems for anti-cancer analogues of vitamin E. *Journal of Controlled Release, 207*, 59-69.

Koutsoulas, C., Pippa, N., Demetzos, C., & Zabka, M. (2014). Preparation of liposomal nanoparticles incorporating terbinafine in vitro drug release studies. *Journal of Nanoscience and Nanotechnology, 14*(6), 4529-4533.

Kreuter, J. (1994). *Colloidal Drug Delivery Systems*. New York: Marcel Dekker,Inc.

Langdon, S. P. (2004). *Cancer Cell Culture: Methods and Protocols*. New Jersey: Humana Press Inc.

Lasic, D. D. (1998). Novel applications of liposomes. *Trends in Biotechnology, 16*(7), 307-321.

Leitmannova-Liu, A. (2006). *Advances in Planar Lipid Bilayers and Liposomes* (Volume 3). Massachusetts: Academic Press.

Levchenko, T. S., Rammohan, R., Lukyanov, A. N., Whiteman, K. R., & Torchilin, V. P. (2002). Liposome clearance in mice: the effect of a separate and combined presence of surface charge and polymer coating. *International Journal of Pharmaceutics, 240*(1–2), 95-102.

Levin, M. (2001). *Pharmaceutical Process Scale-Up*. Florida: CRC Press.

Lewis, H. L., & Bloomston, M. (2016). Hepatic Artery Infusional Chemotherapy. *Surgical Clinics of North America, 96*(2), 341-355.

Li-Zhiyu, Paulson, A. T., & Gill, T. A. (2015). Encapsulation of bioactive salmon protein hydrolysates with chitosan-coated liposomes. *Journal of Functional Foods, 19, Part A*, 733-743.

Li, R., Deng, L., Cai, Z., Zhang, S., Wang, K., Li, L., Ding, S., & Zhou, C. (2017). Liposomes coated with thiolated chitosan as drug carriers of curcumin. *Materials Science and Engineering: C, 80*, 156-164.

Liu, W., Liu, W., Ye, A., Peng, S., Wei, F., Liu, C., & Han, J. (2016). Environmental stress stability of microencapsules based on liposomes decorated with chitosan and sodium alginate. *Food Chemistry, 196*, 396-404.

Liu, W., Tian, M., Kong, Y., Lu, J., Li, N., & Han, J. (2017). Multilayered vitamin C nanoliposomes by self-assembly of alginate and chitosan: Long-term stability

and feasibility application in mandarin juice. *LWT - Food Science and Technology, 75*, 608-615.

Lonchin, S., Luisi, P. L., Walde, P., & Robinson, B. H. (1999). A Matrix Effect in Mixed Phospholipid/Fatty Acid Vesicle Formation. *The Journal of Physical Chemistry B, 103*(49), 10910-10916.

Lunkenheimer, K., Czichocki, G., Hirte, R., & Barzyk, W. (1995). Novel results on the adsorption of ionic surfactants at the air/water interface — sodium-n-alkyl sulphates. *Colloids and Surfaces A: Physicochemical and Engineering Aspects, 101*(2), 187-197.

Ma, Q., Hu, D., Wang, H., & Wang, L. (2016). Tara gum edible film incorporated with oleic acid. *Food Hydrocolloids, 56*, 127-133.

Manickavasagan, A., & Jayasuriya, H. (2014). *Imaging with Electromagnetic Spectrum: Applications in Food and Agriculture*. Berlin: Springer Berlin Heidelberg.

Markus, D., & J., S. H. (2010). Surfactants from oleic, erucic and petroselinic acid: Synthesis and properties. *European Journal of Lipid Science and Technology, 112*(1), 122-136.

Marsanasco, M., Márquez, A. L., Wagner, J. R., del V. Alonso, S., & Chiaramoni, N. S. (2011). Liposomes as vehicles for vitamins E and C: An alternative to fortify orange juice and offer vitamin C protection after heat treatment. *Food Research International, 44*(9), 3039-3046.

Martin, B. M. (1994). *Tissue Culture Techniques: An Introduction*. USA: Birkhäuser Boston.

Martinez-Pastor, B., & Mostoslavsky, R. (2012). Sirtuins, Metabolism, and Cancer. *Frontiers in Pharmacology, 3*(22).

Masters, J. R. W. (2000). *Animal Cell Culture: A Practical Approach* (Third ed.). USA: Oxford University Press.

Menon, P., Yin Yin, T., & Misran, M. (2015). Preparation and characterization of liposomes coated with DEAE-Dextran. *Colloids and Surfaces A: Physicochemical and Engineering Aspects, 481*, 345-350.

Merkow, R. P., Bentrem, D. J., Cohen, M. E., Paruch, J. L., Weber, S. M., Ko, C. Y., & Bilimoria, K. Y. (2013). Effect of Cancer Surgery Complexity on Short-Term Outcomes, Risk Predictions, and Hospital Comparisons. *Journal of the American College of Surgeons, 217*(4), 685-693.

Modi, P. (2014). Development of in vitro release test for capsaicin topical gel formulations by Rusing Franz diffusion cell. *International Journal of Pharma and Bio Sciences, 5*, 285-293.

Monroig, Ó., Navarro, J. C., Amat, F., & Hontoria, F. (2007). Enrichment of Artemia nauplii in vitamin A, vitamin C and methionine using liposomes. *Aquaculture, 269*(1), 504-513.

Morigaki, K., & Walde, P. (2007). Fatty acid vesicles. *Current Opinion in Colloid & Interface Science, 12*(2), 75-80.

Morigaki, K., Walde, P., Misran, M., & Robinson, B. H. (2003). Thermodynamic and kinetic stability. Properties of micelles and vesicles formed by the decanoic acid/decanoate system. *Colloids and Surfaces A: Physicochemical and Engineering Aspects, 213*(1), 37-44.

Moussa, Z., Chebl, M., & Patra, D. (2017). Interaction of curcumin with 1,2-dioctadecanoyl-sn-glycero-3-phosphocholine liposomes: Intercalation of rhamnolipids enhances membrane fluidity, permeability and stability of drug molecule. *Colloids and Surfaces B: Biointerfaces, 149*, 30-37.

Mozafari, M. R. (2005). Liposomes: an overview of manufacturing techniques. *Cellular & Molecular Biology Letters, 10*, 711-719.

Mufamadi, M. S., Pillay, V., Choonara, Y. E., Du Toit, L. C., Modi, G., Naidoo, D., & Ndesendo, V. M. (2011). A review on composite liposomal technologies for specialized drug delivery. *journal of drug delivery, 2011*, 939851.

Mullick-Chowdhury, S., Lalwani, G., Zhang, K., Yang, J. Y., Neville, K., & Sitharaman, B. (2013). Cell specific cytotoxicity and uptake of graphene nanoribbons. *Biomaterials, 34*(1), 283-293.

Muthukumaran, T., & Philip, J. (2016). Effect of phosphate and oleic acid capping on structure, magnetic properties, and thermal stability of iron oxide nanoparticles. *Journal of Alloys and Compounds, 689*, 959-968.

Naumowicz, M., & Petelska, A. D. (2016). Physicochemical modelling of the surface-active phospholipid bilayer relative to acid-base equilibria. *Journal of Electroanalytical Chemistry, 782*, 233-240.

Nayak, D., Boxi, A., Ashe, S., Thathapudi, N. C., & Nayak, B. (2017). Stavudine loaded gelatin liposomes for HIV therapy: Preparation, characterization and in vitro cytotoxic evaluation. *Materials Science and Engineering: C, 73*, 406-416.

Ng, S.-F., Rouse, J. J., Sanderson, F. D., Meidan, V., & Eccleston, G. M. (2010). Validation of a Static Franz Diffusion Cell System for In Vitro Permeation Studies. *Journal of the American Association of Pharmaceutical Scientists, 11*(3), 1432-1441.

Noyes, A. A., & Whitney, W. R. (1897). The rate of solution of solid substances in their own solutions. *Journal of the American Chemical Society, 19*(12), 930-934.

Ohnishi, N., Yamamoto, E., Tomida, H., Hyodo, K., Ishihara, H., Kikuchi, H., Tahara, K., & Takeuchi, H. (2013). Rapid determination of the encapsulation efficiency of a liposome formulation using column-switching HPLC. *International Journal of Pharmaceutics, 441*(1–2), 67-74.

Okamoto, Y., Taguchi, K., Yamasaki, K., Sakuragi, M., Kuroda, S. i., & Otagiri, M. (2016). Effect of PEGylation on the physicochemical and pharmacokinetic characteristics of bovine serum albumin-encapsulated liposome. *Asian Journal of Pharmaceutical Sciences, 11*(1), 112-113.

Ozturk, S., & Hu, W. S. (2005). *Cell Culture Technology for Pharmaceutical and Cell-Based Therapies*. Florida: CRC Press.

Pachauri, M., Gupta, E. D., & Ghosh, P. C. (2015). Piperine loaded PEG-PLGA nanoparticles: Preparation, characterization and targeted delivery for adjuvant breast cancer chemotherapy. *Journal of Drug Delivery Science and Technology, 29*, 269-282.

Paini, M., Daly, S. R., Aliakbarian, B., Fathi, A., Tehrany, E. A., Perego, P., Dehghani, F., & Valtchev, P. (2015). An efficient liposome based method for antioxidants encapsulation. *Colloids and Surfaces B: Biointerfaces, 136*, 1067-1072.

Park, S. N., Jo, N. R., & Jeon, S. H. (2014). Chitosan-coated liposomes for enhanced skin permeation of resveratrol. *Journal of Industrial and Engineering Chemistry, 20*(4), 1481-1485.

Pasut, G., Paolino, D., Celia, C., Mero, A., Joseph, A. S., Wolfram, J., Cosco, D., Schiavon, O., Shen, H., & Fresta, M. (2015). Polyethylene glycol (PEG)-dendron phospholipids as innovative constructs for the preparation of super stealth liposomes for anticancer therapy. *Journal of Controlled Release, 199*, 106-113.

Patil, Y. P., & Jadhav, S. (2014). Novel methods for liposome preparation. *Chemistry and Physics of Lipids, 177*, 8-18.

Petelska, A. D., & Figaszewski, Z. A. (2000). Effect of pH on the interfacial tension of lipid bilayer membrane. *Biophysical Journal, 78*(2), 812-817.

Petelska, A. D., & Figaszewski, Z. A. (2011). The equilibria of phosphatidylcholine–fatty acid and phosphatidylcholine–amine in monolayers at the air/water interface. *Colloids and Surfaces B: Biointerfaces, 82*(2), 340-344.

Placzek, M., & Kosela, M. (2016). Microscopic methods in analysis of submicron phospholipid dispersions. *Acta Pharmaceutica, 66*(1), 1-22.

Popov, M., Abu Hammad, I., Bachar, T., Grinberg, S., Linder, C., Stepensky, D., & Heldman, E. (2013). Delivery of analgesic peptides to the brain by nano-sized bolaamphiphilic vesicles made of monolayer membranes. *European Journal of Pharmaceutics and Biopharmaceutics, 85*(3), 381-389.

Qiu, L., Shen, Y., & Wang, C. (2018). pH- and KCl-induced formation of worm-like micelle viscoelastic fluids based on a simple tertiary amine surfactant. *Journal of Petroleum Science and Engineering, 162*, 158-165.

Quail, D. F., & Joyce, J. A. (2013). Microenvironmental regulation of tumor progression and metastasis. *Nature Medicine, 19*(11), 1423-1437.

Rahman, S., & Ahmed, J. (2012). *Handbook of Food Process Design*. New Jersey: John Wiley & Sons.

Raschi, E., Vasina, V., Ursino, M. G., Boriani, G., Martoni, A., & De Ponti, F. (2010). Anticancer drugs and cardiotoxicity: Insights and perspectives in the era of targeted therapy. *Pharmacology & Therapeutics, 125*(2), 196-218.

Riaz, M. (1996). Liposome preparation method. *Pakistan Journal of Pharmaceutical Sciences, 9*(1), 62-77.

Riss, T. L., Moravec, R. A., & Niles, A. L. (2011). Cytotoxicity Testing: Measuring Viable Cells, Dead Cells, and Detecting Mechanism of Cell Death. In M. J. Stoddart (Ed.), *Mammalian Cell Viability: Methods and Protocols* (pp. 103-114). Totowa, NJ: Humana Press.

Rogerson, M. L., Robinson, B. H., Bucak, S., & Walde, P. (2006). Kinetic studies of the interaction of fatty acids with phosphatidylcholine vesicles (liposomes). *Colloids and Surfaces B: Biointerfaces, 48*(1), 24-34.

Rohman, A., & Che Man, Y. B. (2011). Determination of Sodium Fatty Acid in Soap Formulation Using Fourier Transform Infrared (FTIR) Spectroscopy and Multivariate Calibrations. *Journal of Surfactants and Detergents, 14*(1), 9-14.

Röntgen, W. C. (1896). On a new kind of rays. *Science, 3*(59), 227-231.

Rosen, M. J., & Kunjappu, J. T. (2012). *Surfactants and Interfacial Phenomena* (Fourth ed.). New Jersey: John Wiley & Sons.

Saengkrit, N., Saesoo, S., Srinuanchai, W., Phunpee, S., & Ruktanonchai, U. R. (2014). Influence of curcumin-loaded cationic liposome on anticancer activity for cervical cancer therapy. *Colloids and Surfaces B: Biointerfaces, 114*, 349-356.

Sala, M., Miladi, K., Agusti, G., Elaissari, A., & Fessi, H. (2017). Preparation of liposomes: A comparative study between the double solvent displacement and the conventional ethanol injection—From laboratory scale to large scale. *Colloids and Surfaces A: Physicochemical and Engineering Aspects, 524*, 71-78.

Salentinig, S., Sagalowicz, L., & Glatter, O. (2010). Self-assembled structures and pKa value of oleic acid in systems of biological relevance. *Langmuir, 26*(14), 11670-11679.

Sercombe, L., Veerati, T., Moheimani, F., Wu, S. Y., Sood, A. K., & Hua, S. (2015). Advances and Challenges of Liposome Assisted Drug Delivery. *Frontiers in Pharmacology, 6*(286).

Shah, D. O., & Schulman, J. H. (1967). The ionic structure of lecithin monolayers. *Journal of Lipid Research, 8*(3), 227-233.

Shah, V., Maibach, H. I., & Jenner, J. (2015). *Topical Drug Bioavailability, Bioequivalence, and Penetration*. New York: Springer

Shankar, B. V., & Patnaik, A. (2007). pH-Dependent Chiral Vesicles from Enantiomeric Sodium 2,3-Bis(decyloxy) Succinate in Aqueous Solution. *Langmuir, 23*(7), 3523-3529.

Siepmann, J., & Siepmann, F. (2013). Mathematical modeling of drug dissolution. *International Journal of Pharmaceutics, 453*(1), 12-24.

Singh, V. K., Pandey, P. M., Agarwal, T., Kumar, D., Banerjee, I., Anis, A., & Pal, K. (2016). Development of soy lecithin based novel self-assembled emulsion hydrogels. *Journal of the Mechanical Behavior of Biomedical Materials, 55*, 250-263.

Skoog, D. A., Holler, F. J., & Crouch, S. R. (2007). *Principles of Instrumental Analysis* (6 ed.). California: Thomson Brooks/Cole.

Smith, B. C. (1998). *Infrared Spectral Interpretation: A Systematic Approach*. Florida: CRC Press.

Song, L. Y., Ahkong, Q. F., Rong, Q., Wang, Z., Ansell, S., Hope, M. J., & Mui, B. (2002). Characterization of the inhibitory effect of PEG-lipid conjugates on the intracellular delivery of plasmid and antisense DNA mediated by cationic lipid liposomes. *Biochimica et Biophysica Acta (BBA) - Biomembranes, 1558*(1), 1-13.

Sorichetti, R. J., McLaughlin, J. T., Creed, I. F., & Trick, C. G. (2014). Suitability of a cytotoxicity assay for detection of potentially harmful compounds produced by freshwater bloom-forming algae. *Harmful Algae, 31*, 177-187.

Stevenson-Abouelnasr, D., Husseini, G. A., & Pitt, W. G. (2007). Further investigation of the mechanism of Doxorubicin release from P105 micelles using kinetic models. *Colloids and Surfaces B: Biointerfaces, 55*(1), 59-66.

Stockert, J. C., Blázquez-Castro, A., Cañete, M., Horobin, R. W., & Villanueva, Á. (2012). MTT assay for cell viability: Intracellular localization of the formazan product is in lipid droplets. *Acta Histochemica, 114*(8), 785-796.

Storey, R. A., & Ymén, I. (2011). *Solid State Characterization of Pharmaceuticals*. New York: John Wiley & Sons.

Stuart, B. H. (2004). *Infrared Spectroscopy: Fundamentals and Applications*. West Sussex: John Wiley & Sons.

Sun, B., Taha, M. S., Ramsey, B., Torregrosa-Allen, S., Elzey, B. D., & Yeo, Y. (2016). Intraperitoneal chemotherapy of ovarian cancer by hydrogel depot of paclitaxel nanocrystals. *Journal of Controlled Release, 235*, 91-98.

Sun, L., Zhou, D.-S., Zhang, P., Li, Q.-H., & Liu, P. (2015). Gemcitabine and γ-cyclodextrin/docetaxel inclusion complex-loaded liposome for highly effective combinational therapy of osteosarcoma. *International Journal of Pharmaceutics, 478*(1), 308-317.

Suzuki, T., Ichihara, M., Hyodo, K., Yamamoto, E., Ishida, T., Kiwada, H., Ishihara, H., & Kikuchi, H. (2012). Accelerated blood clearance of PEGylated liposomes containing doxorubicin upon repeated administration to dogs. *International Journal of Pharmaceutics, 436*(1–2), 636-643.

Swenson, C. E., Perkins, W. R., Roberts, P., & Janoff, A. S. (2001). Liposome technology and the development of Myocet™ (liposomal doxorubicin citrate). *The Breast, 10*, 1-7.

Tacar, O., Sriamornsak, P., & Dass, C. R. (2013). Doxorubicin: an update on anticancer molecular action, toxicity and novel drug delivery systems. *Journal of Pharmacy and Pharmacology, 65*(2), 157-170.

Takayama, F., Wu, Z., Ma, H. M., Okada, R., Hayashi, Y., & Nakanishi, H. (2013). Possible involvement of aiPLA2 in the phosphatidylserine-containing liposomes induced production of PGE2 and PGD2 in microglia. *Journal of Neuroimmunology, 262*(1), 121-124.

Takeuchi, H., Matsui, Y., Yamamoto, H., & Kawashima, Y. (2003). Mucoadhesive properties of carbopol or chitosan-coated liposomes and their effectiveness in the oral administration of calcitonin to rats. *Journal of Controlled Release, 86*(2), 235-242.

Tan, H. W., & Misran, M. (2013). Polysaccharide-anchored fatty acid liposome. *International Journal of Pharmaceutics, 441*(1-2), 414-423.

Tanaka, K., & Iijima, S. (2014). *Carbon Nanotubes and Graphene*. Amsterdam: Elsevier Science.

Tariq, M., Ali, S., Ahmad, F., Ahmad, M., Zafar, M., Khalid, N., & Khan, M. A. (2011). Identification, FT-IR, NMR (1H and 13C) and GC/MS studies of fatty acid methyl esters in biodiesel from rocket seed oil. *Fuel Processing Technology, 92*(3), 336-341.

Teo, Y. Y., Misran, M., Low, K. H., & Zain, S. M. (2011). Effect of Unsaturation on the Stability of C18Polyunsaturated Fatty Acids Vesicles Suspension in Aqueous Solution. *Bulletin of the Korean Chemical Society, 32*(1), 59-64.

Testa, B. (2001). *Pharmacokinetic Optimization in Drug Research: Biological, Physicochemical, and Computational Strategies*. Zürich: Verlag Helvetic Chimica Acta.

Theander, K., & Pugh, R. J. (2001). The Influence of pH and Temperature on the Equilibrium and Dynamic Surface Tension of Aqueous Solutions of Sodium Oleate. *Journal of Colloid and Interface Science, 239*(1), 209-216.

Torchilin, V., & Weissig, V. (2003). *Liposomes: A Practical Approach* (Second ed.). Oxford: Oxford University Press.

Varga, Z., Mihály, J., Berényi, S., & Bóta, A. (2013). Structural characterization of the poly(ethylene glycol) layer of sterically stabilized liposomes by means of FTIR spectroscopy. *European Polymer Journal, 49*(9), 2415-2421.

Vijayakumar, M. R., Kosuru, R., Vuddanda, P. R., Singh, S. K., & Singh, S. (2016). Trans resveratrol loaded DSPE PEG 2000 coated liposomes: An evidence for prolonged systemic circulation and passive brain targeting. *Journal of Drug Delivery Science and Technology, 33*, 125-135.

Vineis, P., & Wild, C. P. (2014). Global cancer patterns: causes and prevention. *The Lancet, 383*(9916), 549-557.

Vlasova, M. A., Rytkönen, J., Riikonen, J., Tarasova, O. S., Mönkäre, J., Kovalainen, M., Närvänen, A., Salonen, J., Herzig, K.-H., Lehto, V.-P., & Järvinen, K. (2014). Nanocarriers and the delivered drug: Effect interference due to intravenous administration. *European Journal of Pharmaceutical Sciences, 63*, 96-102.

Vorbeck, C. S., Vogelius, I. R., Banner-Voigt, M. L. V. C., Mathiesen, H. F., & Mirza, M. R. (2017). Survival and failure types after radiation therapy of vulvar cancer. *Clinical and Translational Radiation Oncology, 5*, 20-27.

Wacker, M. (2013). Nanocarriers for intravenous injection—The long hard road to the market. *International Journal of Pharmaceutics, 457*(1), 50-62.

Wakuri, S., Yamakage, K., Kazuki, Y., Kazuki, K., Oshimura, M., Aburatani, S., Yasunaga, M., & Nakajima, Y. (2017). Correlation between luminescence intensity and cytotoxicity in cell-based cytotoxicity assay using luciferase. *Analytical Biochemistry, 522*, 18-29.

Wang, L., Hu, X., Shen, B., Xie, Y., Shen, C., Lu, Y., Qi, J., Yuan, H., & Wu, W. (2015). Enhanced stability of liposomes against solidification stress during freeze-drying and spray-drying by coating with calcium alginate. *Journal of Drug Delivery Science and Technology, 30*, 163-170.

Wang, L., Yang, G., Xing, W., & Xu, N. (2008). Mathematic model of the yield for diafiltration processes. *Separation and Purification Technology, 59*(2), 206-213.

Wang, M. T. M., Cho, I., Jung, S. H., & Craig, J. P. (2017). Effect of lipid-based dry eye supplements on the tear film in wearers of eye cosmetics. *Contact Lens and Anterior Eye, 40*(4), 236-241.

Williams, D. B., & Carter, C. B. (2009). *Transmission Electron Microscopy: A Textbook for Materials Science*. New York: Springer.

Wu, X. Z. X. J. B. (2013). *New Concept and New Way of Treatment of Cancer*. Indiana: AuthorHouse.

Yadav, P. R., & Tyagi, R. (2008). *Biotechnology of Animal Tissues*. New Delhi: Discovery Publishing House Pvt. Limited.

Yang, K., Peng, H., Wen, Y., & Li, N. (2010). Re-examination of characteristic FTIR spectrum of secondary layer in bilayer oleic acid-coated Fe_3O_4 nanoparticles. *Applied Surface Science, 256*(10), 3093-3097.

Yang, T., Cui, F.-D., Choi, M.-K., Cho, J.-W., Chung, S.-J., Shim, C.-K., & Kim, D.-D. (2007). Enhanced solubility and stability of PEGylated liposomal paclitaxel: In vitro and in vivo evaluation. *International Journal of Pharmaceutics, 338*(1–2), 317-326.

Yang, Y., Lu, X., Liu, Q., Dai, Y., Zhu, X., Wen, Y., Xu, J., Lu, Y., Zhao, D., Chen, X., & Li, N. (2017). Palmitoyl ascorbate and doxorubicin co-encapsulated liposome for synergistic anticancer therapy. *European Journal of Pharmaceutical Sciences, 105*, 219-229.

Yang, Y., Lu, Y., Wu, Q.-Y., Hu, H.-Y., Chen, Y.-H., & Liu, W.-L. (2015). Evidence of ATP assay as an appropriate alternative of MTT assay for cytotoxicity of secondary effluents from WWTPs. *Ecotoxicology and Environmental Safety, 122*, 490-496.

Yenuganti, V. R., Viergutz, T., & Vanselow, J. (2016). Oleic acid induces specific alterations in the morphology, gene expression and steroid hormone production of cultured bovine granulosa cells. *General and Comparative Endocrinology, 232*, 134-144.

Yom, S. S. (2015). Radiation Treatment of Head and Neck Cancer. *Surgical Oncology Clinics of North America, 24*(3), 423-436.

Zasada, K., Łukasiewicz-Atanasov, M., Kłysik, K., Lewandowska-Łańcucka, J., Gzyl-Malcher, B., Puciul-Malinowska, A., Karewicz, A., & Nowakowska, M. (2015). 'One-component' ultrathin multilayer films based on poly(vinyl alcohol) as stabilizing coating for phenytoin-loaded liposomes. *Colloids and Surfaces B: Biointerfaces, 135*, 133-142.

Zeb, A., Qureshi, O. S., Yu, C.-H., Akram, M., Kim, H.-S., Kim, M.-S., Kang, J.-H., Majid, A., Chang, S.-Y., Bae, O.-N., & Kim, J.-K. (2017). Enhanced anti-rheumatic activity of methotrexate-entrapped ultradeformable liposomal gel in adjuvant-induced arthritis rat model. *International Journal of Pharmaceutics, 525*(1), 92-100.

Zhang, L., Han, L., Sun, X., Gao, D., Qin, J., & Wang, J. (2012). The use of PEGylated liposomes to prolong the circulation lifetime of salvianolic acid B. *Fitoterapia, 83*(4), 678-689.

Zhang, T., Li, Y., & Mueller, A. (2011). Phase structure of liposome in lipid mixtures. *Chemistry and Physics of Lipids, 164*(8), 722-726.

Zhang, Y., Mintzer, E., & Uhrich, K. E. (2016). Synthesis and characterization of PEGylated bolaamphiphiles with enhanced retention in liposomes. *Journal of Colloid and Interface Science, 482*, 19-26.

Zhao, L., Temelli, F., Curtis, J. M., & Chen, L. (2015). Preparation of liposomes using supercritical carbon dioxide technology: Effects of phospholipids and sterols. *Food Research International, 77, Part 1*, 63-72.

Zofka, A., Board, N. R. C. T. R., & Program, S. S. H. R. (2013). *Evaluating Applications of Field Spectroscopy Devices to Fingerprint Commonly Used Construction Materials*. Washington, D.C.: Transportation Research Board.

LIST OF PUBLICATIONS AND PAPERS PRESENTED

PUBLICATIONS

1) Khalid, K., Zain, S. M., **Eh Suk, V. R.,** & Khan, M. N. (2017). Microscopic Evidence for the Correlation of Micellar Structures and Counterion Binding Constant for Flexible Nanoparticle Catalyzed Piperidinolysis of PS− in Colloidal System. *Tenside Surfactants Detergents*, *54*(3), 224-229.

2) **Eh Suk, V. R.**, & Misran, M. (2017). Preparation, characterization and physicochemical properties of DOPE-PEG2000 stabilized oleic acid-soy lecithin liposomes (POLL). *Colloids and Surfaces A: Physicochemical and Engineering Aspects*, *513*, 267-273.

3) **Eh Suk, V. R.**, & Misran, M. (2017). Development and Characterization of DOPEPEG2000 Coated Oleic Acid Liposomes Encapsulating Anticancer Drugs. *Journal of Surfactants and Detergents*, *20*(2), 321-329.

4) Naeem, S., Kiew, L. V., Chung, L. Y., **Eh Suk, V. R.**, Mahmood, A., & Misran, M. B. (2016). Optimization of phospholipid nanoparticle formulations using response surface methodology. *Journal of Surfactants and Detergents, 19*(1), 67-74.

ORAL PRESENTATION IN CONFERENCE

1) **Eh Suk, V. R.**, Chung, I., & Misran, M. (2018). PEGylated oleic acid- lecithin liposomes (POLL) for the treatment of lung cancer A549. *1st UTM-Emerging Scientists Conference,* Pulai Spring Resorts, Johor, Malaysia.

2) **Eh Suk, V. R.**, & Misran, M. (2015). Encapsulation of different log p anticancer drugs in 1,2-dioleoyl-sn-glycero -3-phosphoethanolamine- n-[methoxy (polyethyleneglycol) -2000 (DOPE-PEG2000) -oleic acid liposome. *5th Polymer Thai Conference*, Bangkok, Thailand.

3) **Eh Suk, V. R.**, & Misran, M. (2013). Effect of DOPE-PEG 2000 on oleic and linoleic fatty acid liposomes. *International Post Graduate Conference on Science and Mathematics,* UPSI, Perak, Malaysia.

MEDALS

1) Silver Medal, Malaysia Technology Expo 2014

2) Silver Medal Invention& Innovation Awards: Malaysia Technology Expo 2013

3) Silver Medal, International Conference and exposition on Inventions of Institution of Higher Learning (Pecipta) 2013